

**Design, synthesis and characterisation of ruthenium complexes
as medicinal therapeutic agents**

Pablo Caramés Méndez

Submitted in accordance with the requirements for the degree of
Doctor of Philosophy

The University of Leeds
School of Chemistry

April 2019

The candidate confirms that the work submitted is his own and that appropriate credit has been given where reference has been made to the work of others.

This copy has been supplied on the understanding that it is copyright material and that no quotation from the thesis may be published without proper acknowledgement.

The right of Pablo Caramés Méndez to be identified as Author of this work has been asserted by him in accordance with the Copyright, Designs and Patents Act 1988.

© 2019 The University of Leeds and Pablo Caramés Méndez

Acknowledgements

First of all, I would love to thank my father who suddenly passed away earlier this year for raising me as I am. You taught me there is always an A, B, C procedure in life, and that working hard, with passion and dedication will take me to unexpected places. Thank you with all my heart. Even though we were different, I hope that wherever you are, you are happy. You were always concerned about how I was, so, don't worry, I am fine, and I will be better. I miss you and I wish I could have said one more time that I love you.

Paddy! Where do you get the patience to deal with me? Thank you, thank you and thank you. You taught me lots of things I cannot even list them all! Thank you for the opportunity you gave me. I will always remember the first meeting we had (ruthenium, isomers and hypoxia) three words were enough and your 50th Birthday! You are such an awesome man and role-model. Thank you for your guidance, scientific suggestions and support throughout these years.

Team Huddersfield! Such an experience, almost three years doing so much biology, I loved it! Professor Roger Phillips, thanks for adopting me and for your guidance, I have learnt as much as I could, and I hope to keep that connection in the future. Simon, thank you for sharing your knowledge. Sam, two days in cell culture and it felt like we knew each other for a long time. Thank you for the training, the long hours in the lab, the coffee breaks and I am so happy you are a mum! That child will be pipetting next to you very soon! Thank you all.

Team King's College London! Dr. Rama, it was awesome being part of your group for three months! (Thanks RSC for funding) I was surprised how quickly I got on with your group, I miss you all! I started when all the chaos with my father's dead and it was hard, although being at KCL really helped me. Kristine! You are absolutely amazing, and I miss you a lot. Loved the coffee breaks, long hours in the lab, talking about anything and the girls. I will always be here for you.

Now, Team Leeds! Starting from Chris and all his knowledge, literally, so much knowledge and help, thank you. I remember the day you came to the office showing my first crystal structure after two long years, I literally cried! Laura Gandhi, you are my crazy friend, we must go to watch Rocky Horror (again) as we need to drag together! And cheese, we can eat lots of cheese, and dance to the rhythm of 'head, chin, shoulder, shoulder, shoulder'. Ceciiiiiiiilia, you are braking my heart (now, all together) you are my beloved friend who cared so much for me. Loved to see you every morning and we could talk about real life stuff and what made me love you, your honesty. Mateo (Matt), like the brother I never had, full of joy! I loved every single second of our bromance, I genially think you would be the man of my life, and as far we are concerned, better to keep the

bromance than dealing with me 24/7. Rianne, meeting you was such a joy. Talking to you always encourages me to carry on in research. Even though there are hard times in life, you showed there are other perspectives and I will always admire you. Sarah, you made these years particularly good, moving in together, living a great time, walking to uni, demonstrating together, playing overcooked (I promise I will learn how to distinguish between a tomato and an onion). Going out, eating, cleaning together, haha lots of things we have done together! And more that the future will bring!

Lauren and Abi. I love you both to pieces. I see you as my daughters, you pushed me so hard with your projects and that helped me to figure out what I want to do in the future. I wish you the best of the best in the future, you work really hard and you have beautiful minds and personalities. We always stand up, with energy, enthusiasm and we do our very best. To the other lot of master students, you brought so many different personalities to the office, and I really loved it.

Office 1.25, thank you for just being how you are. Communication is what keeps the best relationships and I wish you all a great future. Izar, it was nice to spend the last weeks together writing the thesis. Namrah, you started as a master student and it was nice to see how much progress you have made! Kay, 'first ligands, second complexes and then world domination'. Heba, you taught me we never lose hope. Frances, you started in the office 1.25! never forget that, thank you for being my conference buddy, and for the coffee in the last week!

Compostelanos, you made me feel loved every single day. My mood swings like a hundred times a day but you stayed with me, in the good times and the bad times, you supported me a lot, and you are my family. I love you. I think the next book I write should be about our 11 years of friendship! Looking forward to seeing you all, to hug you and to celebrate we keep counting years.

My jammers! Listen, there is a connection between all of you and this thesis. You helped to finish this PhD. Yes! your energy in classes kept me going every day (literally). My Jam muse, Naomi, thank you for being there and for being a great friend. Keep yourself sane to finish the degree in Law. Alena and Lin, you are always welcome to wherever I am! Bodyjam joined us together and the PhD craziness kept us till the end. We made it! Liz, love seeing your face when you count in the Bodyjam classes, but I loved even more listening to your research experiences and sharing them with me.

Caine, you saw the best and the worst of me throughout these years, so thank you for the beautiful trips that helped us to relax from chaos. My Guuuurls, Will, Cam, Pier and Juanpa, thank you for keeping me sane in the gayest possible ways.

Annica, my dear, our love started very slowly and when I realised you became such an important person in my life. I am going to miss you a lot and our coffee Tuesdays. I know we will keep in touch, but I have never thought I would connect with someone like I do with you, and I love it. Every single second I spend with you it is like a treasure in my little heart. Jaaaamba Jamba! You taught me how to get on and get over with a bunch of stuff. Thank you for being as you are, from the toes to your sweaty face in Zumba haha. I love you.

Dear family, thank you for being supportive with all what I have done, Haidong gumdo, Taekwondo, Championships, degrees and most important when I came out as a gay man. That gave me courage to show everybody who I am, and even though times are changing, it is still hard, but I will apply what you told me, I should do what makes me happy and my soul energised.

My sisters, Cris and Raquel, dad wanted us to be warriors for the right reasons. Another lesson he taught us is, we need to forgive and let the pass behind. Life is too short. We are still suffering but step up, he wants us to move on and create our own lives. There are some dark times, yes, and we learned from them. I love you. Xandre and Teo, my two little nephews, I love you and I am here for you two. Thank you for making me the happiest uncle on Earth.

Mum, you put up with so much. I could write a book (best seller) about you. You made the right decisions in life and you were worried so much about how I was going to end. I am who I am thanks to you. To your advice, to your constant support even when I thought about giving up. You told me once, 'I want you to be free' and I am. I don't know how to express how grateful I am for having you. So many ups and downs, and you were there for me without any doubts. I love you with all my soul. Thank is not even enough.

Abstract

This thesis is concerned with the design, synthesis and characterisation of a series of *trans*-dichloride bis-quinaldamide ruthenium (III) complexes. The anti-cancer, anti-bacterial and anti-fungal properties were investigated, with the lead compounds undergoing further chemical and biological mechanistic studies.

Chapter 1 presents an overview of metal complexes as therapeutic agents, their interaction with DNA and project aims.

Chapter 2 discusses the synthesis and characterisation of the novel quinaldamide ligands.

Chapter 3 is focused on the synthesis and characterisation of the *trans*-dichloride ruthenium (III) complexes that displayed promising anti-cancer results.

Chapter 4 discusses the biological evaluation of the ruthenium complexes under normoxia conditions. Lead compounds are analysed to a wider panel of cell lines and hypoxia conditions. Two outperforming compounds were taken for further mechanistic studies. Anti-bacterial and anti-fungal properties are also discussed.

Chapter 5 contains the chemical investigations (hydrolysis and hydrophobicity) of selected compounds.

Chapter 6 contains experimental details and characterisation data for all the compounds described in Chapters 2 and 3. All the protocols for the studies discussed in Chapter 4, and all experimental details of Chapter 5.

Chapter 7 summaries this thesis and the future work.

Appendix includes a summary of the x-ray crystallographic data for the crystalline compounds found in this work.

Table of Contents

List of Abbreviations	XIV
Glossary	XVII
List of Figures	XIX
List of Schemes	XXV
List of Tables	XXVI
Chapter 1 Introduction and objectives	
1.1 Introduction	- 2 -
1.1.1 Structure and role of DNA	- 2 -
1.1.2 Structure of DNA and its participation in cellular recognition	- 3 -
1.1.3 Gene Expression	- 4 -
1.2 Interactions of small molecules with DNA	- 5 -
1.3 Cancer	- 8 -
1.4 First Generation of Platinum Based Anti-Cancer Compounds	- 9 -
1.5 Second Generation Platinum Anti-Cancer Compounds	- 11 -
1.6 Introduction of Ruthenium into Medicine	- 12 -
1.6.1 NAMI and NAMI-A	- 14 -
1.6.2 KP418, KP1019 and NKP1019	- 15 -
1.6.3 'Piano-Stool' Complexes	- 16 -
1.7 Trans-dihalide Metal Complexes as Novel Anti-cancer Agents	- 18 -
1.8 Biological Assays	- 20 -
1.9 Objectives	- 23 -
Chapter 2 Synthesis of functionalised quinaldamide ligands	
2.1 Background	- 33 -
2.2 Synthesis of quinaldamide ligands	- 34 -
2.3 Characterisation of functionalised quinaldamide ligands	- 37 -
2.3.1 IR spectrum for ligand 2.3	- 38 -
2.3.2 NMR spectra for ligand 2.3	- 38 -

2.3.3 X-Ray structure for ligand 2.3	- 41 -
2.3.4 X-Ray structure for ligand 2.30	- 43 -
2.3.5 X-Ray structure for ligand 2.37	- 45 -
2.4 Conclusion	- 47 -
2.5 References	- 48 -
Chapter 3 Ruthenium (III) dichloride bis-quinaldamide complexes	
3.1 Background	- 50 -
3.2 Rationale behind Ru(Cl) ₂ (L) ₂ type complexes	- 51 -
3.3 Synthesis of the neutral trans-dichloride bisquinaldamide ruthenium (III) complexes	- 52 -
3.4 Characterisation of bis-quinaldamide trans-dichloride Ru (III) complexes	- 54 -
3.5 Ruthenium Complex 3.1	- 55 -
3.5.1 Infrared Spectroscopy of the complex 3.1	- 55 -
3.5.2 High Resolution Mass Spectrometry of the complex 3.1	- 56 -
3.5.3 General trends in X-ray Crystallography for the complexes and X-ray single crystal diffraction of complex 3.1	- 57 -
3.5.4 X-ray powder diffraction of complex 3.1	- 61 -
3.6 Ruthenium complex 3.18	- 62 -
3.6.1 X-ray single crystal diffraction of complex 3.18	- 62 -
3.7 Ruthenium complex 3.23	- 66 -
3.7.1 X-ray single crystal diffraction for complex 3.23	- 66 -
3.8 Ruthenium complex 3.29	- 69 -
3.8.1 X-ray single crystal diffraction of complex 3.29	- 69 -
3.8.2 X-ray powder diffraction	- 72 -
3.9 Ruthenium complex 3.32	- 73 -
3.9.1 X-ray single crystal diffraction of complex 3.32	- 73 -
3.10 Ruthenium complex 3.38	- 77 -

3.10.1	X-ray single crystal diffraction of complex 3.38	- 77 -
3.11	Side product when using basic conditions: Complex 3.25a	- 80 -
3.12	Side product of the base free reaction: complex 3.33a	- 82 -
3.13	Compound fragmentation, complex 3.15a	- 85 -
3.14	Conclusion	- 87 -
3.15	Further work	- 88 -
3.16	References	- 88 -
Chapter 4 Biological Investigations on the neutral trans-dichloride bisquinaldamide Ruthenium (III) complexes		
4.1	Introduction to the Drug Discovery Process	- 90 -
4.2	Cytotoxicity: MTT assay	- 90 -
4.3	Normoxia cytotoxic studies of trans-dichloride bisquinaldamide Ruthenium complexes	- 91 -
4.3.1	Rationale behind the cell lines studied	- 91 -
4.3.2	Normoxia cytotoxic results and discussion	- 92 -
4.3.3	Selectivity of the ruthenium complexes	- 102 -
4.3.4	Expansion of the cancer cell panel	- 108 -
4.3.5	Gene Preference of the ruthenium metal complexes	- 111 -
4.3.6	Summary of the normoxia cytotoxicity cell work	- 115 -
4.4	Hypoxia cytotoxic studies of trans-dichloride bisquinaldamide Ruthenium complexes	- 117 -
4.4.1	Hypoxia cytotoxic results	- 119 -
4.4.2	Hypoxia Cytotoxicity Ratio	- 122 -
4.4.3	Hypoxia Enhancement Ratio	- 123 -
4.4.4	Summary of the hypoxia cytotoxicity cell work	- 124 -
4.5	Cell recovery	- 124 -
4.6	Cell viability and cycle analysis	- 131 -
4.6.1	Summary of Cell viability and Cell cycle assay	- 145 -

4.7	Anti-bacterial activity	- 147 -
4.8	Anti-fungal activity	- 156 -
4.9	Conclusions	- 159 -
4.10	References	- 160 -

Chapter 5 Structure-Activity Relationships of the bis-quinaldamide trans-dichloride ruthenium complexes

5.1	Introduction	- 164 -
5.2	Hydrolysis Studies	- 164 -
5.3	Hydrophobicity	- 170 -
5.4	References	- 173 -

Chapter 6 Experimental

6.1	General Experimental Procedures	- 176 -
6.2	Characterisation techniques and Instrumentation	- 176 -
6.2.1	IR spectroscopy	- 176 -
6.2.2	Mass spectrometry	- 176 -
6.2.3	NMR spectroscopy	- 176 -
6.2.4	Elemental Analysis	- 176 -
6.2.5	Magnetic Susceptibility	- 177 -
6.2.6	X-Ray Crystallography	- 177 -
6.3	Preparation of Arene Functionalised Quinaldamide Ligands	- 178 -
6.3.1	N-(2,4-dimethoxyphenyl)quinoline-2-carboxamide, (2.3)	- 178 -
6.3.2	N-(2,5-dimethoxyphenyl)quinoline-2-carboxamide, (2.4)	- 179 -
6.3.3	N-(2,4-difluorophenyl)quinoline-2-carboxamide, (2.26)	- 180 -
6.3.4	N-(2,5-difluorophenyl)quinoline-2-carboxamide, (2.27)	- 181 -
6.3.5	N-(2,4-dichlorophenyl)quinoline-2-carboxamide, (2.31)	- 182 -
6.3.6	N-(2,5-dichlorophenyl)quinoline-2-carboxamide, (2.32)	- 183 -
6.3.7	N-(2,4-dibromophenyl)quinoline-2-carboxamide, (2.36)	- 184 -

6.3.8 N-(2,5-dibromophenyl)quinoline-2-carboxamide, (2.37)	- 185 -
6.3.9 N-(2-iodophenyl)quinoline-2-carboxamide, (2.38)	- 186 -
6.3.10 N-(3-iodophenyl)quinoline-2-carboxamide, (2.39)	- 187 -
6.3.11 N-(2-methoxy-4-nitrophenyl)quinoline-2-carboxamide, (2.41)	- 188 -
6.3.12 N-(2-methoxy-5-nitrophenyl)quinoline-2-carboxamide, (2.42)	- 189 -
6.3.13 N-(4-methoxy-2-nitrophenyl)quinoline-2-carboxamide, (2.43)	- 190 -
6.4 Preparation of trans-dichloride bis-quinaldamide ruthenium (III) neutral complexes	- 191 -
6.4.1 Synthesis and Characterisation of trans-dichloride bis-quinaldamide ruthenium (III) complexes	- 191 -
6.4.2 Bis-(N-phenylquinaldamide) ruthenium dichloride, $C_{32}H_{23}O_2N_4RuCl_2$, (3.1)	- 191 -
6.4.3 Bis-(N-2-Methoxyphenylquinaldamide) ruthenium dichloride, $C_{34}H_{27}O_4N_4RuCl_2$, (3.2)	- 192 -
6.4.4 Bis-(N-2,4-diMethoxyphenylquinaldamide) ruthenium dichloride, $C_{36}H_{31}O_6N_4RuCl_2$, (3.3)	- 192 -
6.4.5 Bis-(N-2,5-diMethoxyphenylquinaldamide) ruthenium dichloride, $C_{36}H_{31}O_6N_4RuCl_2$, (3.4)	- 192 -
6.4.6 Bis-(N-2-Methylphenylquinaldamide) ruthenium dichloride, $C_{34}H_{27}O_2N_4RuCl_2$, (3.5)	- 193 -
6.4.7 Bis-(N-3-Methylphenylquinaldamide) ruthenium dichloride, $C_{34}H_{27}O_2N_4RuCl_2$, (3.6)	- 193 -
6.4.8 Bis-(N-4-Methylphenylquinaldamide) ruthenium dichloride, $C_{34}H_{27}O_2N_4RuCl_2$, (3.7)	- 194 -
6.4.9 Bis-(N-2,4,6-triMethylphenylquinaldamide) ruthenium dichloride, $C_{38}H_{35}O_2N_4RuCl_2$, (3.8)	- 194 -
6.4.10 Bis-(N-2-Ethylphenylquinaldamide) ruthenium dichloride, $C_{36}H_{31}O_2N_4RuCl_2$, (3.9)	- 194 -
6.4.11 Bis-(N-3-Ethylphenylquinaldamide) ruthenium dichloride, $C_{36}H_{31}O_2N_4RuCl_2$, (3.10)	- 195 -

6.4.12 Bis-(N-4-Ethylphenylquinaldamide) ruthenium dichloride, C ₃₆ H ₃₁ O ₂ N ₄ RuCl ₂ , (3.11)	- 195 -
6.4.13 Bis-(N-2- ⁱ Propylphenylquinaldamide) ruthenium dichloride, C ₃₈ H ₃₅ O ₂ N ₄ RuCl ₂ , (3.12)	- 196 -
6.4.14 Bis-(N-3- ⁱ Propylphenylquinaldamide) ruthenium dichloride, C ₃₈ H ₃₅ O ₂ N ₄ RuCl ₂ , (3.13)	- 196 -
6.4.15 Bis(N-4- ⁱ Propylphenylquinaldamide) ruthenium dichloride, C ₃₈ H ₃₅ O ₂ N ₄ RuCl ₂ , (3.14)	- 196 -
6.4.16 Bis-(N-2,6-di ⁱ Propylphenylquinaldamide) ruthenium dichloride, C ₄₄ H ₄₇ O ₂ N ₄ RuCl ₂ , (3.15)	- 197 -
6.4.17 Bis-(N-2-Methyl-6- ⁱ Propylphenylquinaldamide) ruthenium dichloride, C ₄₀ H ₃₉ O ₂ N ₄ RuCl ₂ , (3.16)	- 197 -
6.4.18 Bis-(N-2- ^t Butylphenylquinaldamide) ruthenium dichloride, C ₄₀ H ₃₉ O ₂ N ₄ RuCl ₂ , (3.17)	- 198 -
6.4.19 Bis-(N-4- ^t Butylphenylquinaldamide) ruthenium dichloride, C ₄₀ H ₃₉ O ₂ N ₄ RuCl ₂ , (3.18)	- 198 -
6.4.20 Bis-(N-2-triFluoromethylphenylquinaldamide) ruthenium dichloride, C ₃₄ H ₂₁ O ₂ N ₄ F ₆ RuCl ₂ , (3.19)	- 198 -
6.4.21 Bis-(N-3-triFluoromethylphenylquinaldamide) ruthenium dichloride, C ₃₄ H ₂₁ O ₂ N ₄ F ₆ RuCl ₂ , (3.20)	- 199 -
6.4.22 Bis-(N-4-triFluorophenylquinaldamide) ruthenium dichloride, C ₃₄ H ₂₁ O ₂ N ₄ F ₆ RuCl ₂ , (3.21)	- 199 -
6.4.23 Bis-(N-3,5-ditriFluoromethylphenylquinaldamide) ruthenium dichloride, C ₃₆ H ₁₉ O ₂ N ₄ F ₁₂ RuCl ₂ , (3.22)	- 200 -
6.4.24 Bis-(N-2-Fluorophenylquinaldamide) ruthenium dichloride, C ₃₂ H ₂₁ O ₂ N ₄ F ₂ RuCl ₂ , (3.23)	- 200 -
6.4.25 Bis-(N-3-Fluorophenylquinaldamide) ruthenium dichloride, C ₃₂ H ₂₁ O ₂ N ₄ F ₂ RuCl ₂ , (3.24)	- 200 -
6.4.26 Bis-(N-4-Fluorophenylquinaldamide) ruthenium dichloride, C ₃₂ H ₂₁ O ₂ N ₄ F ₂ RuCl ₂ , (3.25)	- 201 -

6.4.27 Bis-(N-2,4-diFluorophenylquinaldamide) ruthenium dichloride, C ₃₂ H ₁₉ O ₂ N ₄ F ₄ RuCl ₂ , (3.26)	- 201 -
6.4.28 Bis-(N-2,5-diFluorophenylquinaldamide) ruthenium dichloride, C ₃₂ H ₁₉ O ₂ N ₄ F ₄ RuCl ₂ , (3.27)	- 201 -
6.4.29 Bis-(N-2-Chlorophenylquinaldamide) ruthenium dichloride, C ₃₂ H ₂₁ O ₂ N ₄ RuCl ₄ , (3.28)	- 202 -
6.4.30 Bis-(N-3-Chlorophenylquinaldamide) ruthenium dichloride, C ₃₂ H ₂₁ O ₂ N ₄ RuCl ₄ , (3.29)	- 202 -
6.4.31 Bis-(N-4-Chlorophenylquinaldamide) ruthenium dichloride, C ₃₂ H ₂₁ O ₂ N ₄ RuCl ₄ , (3.30)	- 203 -
6.4.32 Bis-(N-2,4-diChlorophenylquinaldamide) ruthenium dichloride, C ₃₂ H ₁₉ O ₂ N ₄ RuCl ₆ , (3.31)	- 203 -
6.4.33 Bis-(N-2,5-diChlorophenylquinaldamide) ruthenium dichloride, C ₃₂ H ₁₉ O ₂ N ₄ RuCl ₆ , (3.32)	- 203 -
6.4.34 Bis-(N-2-Bromophenylquinaldamide) ruthenium dichloride, C ₃₂ H ₂₁ O ₂ N ₄ Br ₂ RuCl ₂ , (3.33)	- 204 -
6.4.35 Bis-(N-3-Bromophenylquinaldamide) ruthenium dichloride, C ₃₂ H ₂₁ O ₂ N ₄ Br ₂ RuCl ₂ , (3.34)	- 204 -
6.4.36 Bis-(N-4-Bromophenylquinaldamide) ruthenium dichloride, C ₃₂ H ₂₁ O ₂ N ₄ Br ₂ RuCl ₂ , (3.35)	- 205 -
6.4.37 Bis-(N-2,4-diBromophenylquinaldamide) ruthenium dichloride, C ₃₂ H ₁₉ O ₂ N ₄ Br ₄ RuCl ₂ , (3.36)	- 205 -
6.4.38 Bis-(N-2,5-diBromophenylquinaldamide) ruthenium dichloride, C ₃₂ H ₁₉ O ₂ N ₄ Br ₄ RuCl ₂ , (3.37)	- 205 -
6.4.39 Bis-(N-2-Iodophenylquinaldamide) ruthenium dichloride, C ₃₂ H ₂₁ O ₂ N ₄ I ₂ RuCl ₂ , (3.38)	- 206 -
6.4.40 Bis-(N-3-Iodophenylquinaldamide) ruthenium dichloride, C ₃₂ H ₂₁ O ₂ N ₄ I ₂ RuCl ₂ , (3.39)	- 206 -
6.4.41 Bis-(N-4-Iodophenylquinaldamide) ruthenium dichloride, C ₃₂ H ₂₁ O ₂ N ₄ I ₂ RuCl ₂ , (3.40)	- 207 -
6.5 Cell Culture Work	- 207 -

6.5.1 General Experimental Procedures	- 207 -
6.5.2 Thawing Cells and from Cryo-Preservation	- 208 -
6.5.3 Sub culturing by trypsination of Monolayer Cultures	- 208 -
6.5.4 Cell Counting	- 208 -
6.5.5 Cryo-preservation (cell stock)	- 208 -
6.5.6 MTT stock solution	- 209 -
6.5.7 Validation of pipetting technique	- 209 -
6.5.8 Chemo-sensitivity MTT assays (Normoxic Conditions)	- 209 -
6.5.9 Data Analysis	- 210 -
6.5.10 Chemo-sensitivity MTT assays (Hypoxic Conditions)	- 210 -
6.5.11 Viability assay and drug induced Cell Cycle Arrest using the NucleoCounter (NC-3000) cytometer	- 210 -
6.5.12 Antimicrobial Studies	- 212 -
6.5.13 Antibacterial Evaluation	- 212 -
6.5.14 Antibacterial Hit Confirmation	- 212 -
6.5.15 Antifungal Evaluation	- 213 -
6.5.16 Antifungal Hit Confirmation	- 214 -
6.5.17 Cytotoxicity Assay (CO-ADD protocol)	- 215 -
6.5.18 Haemolysis Assay	- 215 -
6.6 Mechanistic studies	- 216 -
6.6.1 Hydrolysis	- 216 -
6.6.2 Hydrophobicity	- 217 -
6.7 References	- 218 -
Chapter 7 Conclusions and Future Work	
7.1 Conclusions	- 220 -
7.2 Future Work	- 223 -

List of Abbreviations

°	degrees
δ	chemical shift
η	hapticity
λ	wavelength
μg	microgram
μL	microliter
μM	micromolar
μm	micrometre
Å	Angstrom
A	adenine
ARPE-19	human retinal pigment epithelial cell line
ATP	adenosine triphosphate
[C]	concentration
°C	degrees Celsius
CO-ADD	Community for Open Antimicrobial Drug Discovery
<i>d</i>	deuterated
d	doublet
Da	Dalton
DNA	deoxyridonucleic acid
DMEM	Dulbecco's modified eagle medium
ESI	electrospray
<i>et al.</i>	and others
FBS	foetal bovine serum
FDA	Food and Drug Administration
g	gram

G	guanine
h	hours
HC ₁₀	concentration for 10 % haemolysis
HCT116 p53(+/+)	human colon cancer cell line
HEK293	human embryonic kidney cell line
HIF-1	hypoxia inducible factor-1
IC ₅₀	concentration for 50 % growth inhibition
IR	infrared
<i>in vacuo</i>	under vacuum
<i>in vitro</i>	in glass
<i>in vivo</i>	in a living organism
<i>J</i>	coupling constant
K	degrees Kelvin
Log <i>P</i>	partition coefficient
m	multiplet
MHz	mega Hertz
MIA PaCa_2	human pancreatic adenocarcinoma cell line
MIC	minimum inhibitory concentration
min	minute
mL	millilitre
mM	millimolar
mm	millimetre
mmol	millimole
HRMMS	high resolution mass spectrometry
MTT	3-(4,5-dimethylthiazol-2-yl)-2,5-diphenyltetrazolium bromide
NAD(H)	nicotinamide adenine dinucleotide
NADP(H)	nicotinamide adenine dinucleotide phosphate

NHS	National Health Service
nm	nanometre
NMR	nuclear magnetic resonance
PBS	phosphate buffered saline
PDT	photodynamic therapy
pH	potential of hydrogen
ppm	parts per million
PTA	1,3,5-triaza-7-phosphaadamantane
ROS	reactive oxygen species
s	second
s	singlet
SAR	structure activity relationship
SD	standard deviation
SFI	superficial fungal infection
t	triplet
tpa	<i>tris</i> (2-methylpyridyl)amine
UK	United Kingdom
UV/vis	ultraviolet-visible
<i>via</i>	by way of

Glossary

Angiogenesis	the formation of new blood vessels
Apoptosis	the process of programmed cell death
Biofilm	any group of microorganisms in which cells adhere to each other and to a solid surface
Carcinogenesis	the initiation of cancer formation
Carcinoma	a cancer arising in the epithelial tissue of the skin or of the lining of the internal organs
Chromosome	a thread-like structure of nucleic acids and protein found in the nucleus, carrying genetic information in the form of genes
Cytosol	the aqueous component of the cytoplasm of a cell
Eukaryote	an organism with a complex cell or cells, in which the genetic material is organised into a clearly defined membrane-bound nucleus
Gene	sequence of nucleotides that forms part of a chromosome
Genome	the genetic material of an organism
Hypoxia	deficiency in the amount of oxygen reaching the tissues
Intercalation	insertion of a molecule into DNA between the bases
Kinase	an enzyme that catalyses the transfer of phosphate groups from high-energy, phosphate-donating molecules to specific substrates
Lymphoma	a cancer of the lymphatic system
Metastasis	the spread of a cancer or other disease from one organ or part of the body to another
Mitochondria	an organelle in which the biochemical processes of respiration and energy production occur

Mitosis	a part of the cell cycle when replicated chromosomes are separated into two new nuclei
Mutation	a change that occurs in the DNA sequence
Nephrotoxicity	toxicity to the kidneys
Neurotoxicity	toxicity to the nervous system
Normoxia	normal levels of oxygen reaching the tissues
Nucleosome	structural unit of DNA coiled around a core of histones
Oncogene	a gene that has the potential to cause cancer
Replication	the biological process of producing two identical replicas of DNA from one original DNA molecule
Telomerase	a protein which adds a repeat sequence to the end of telomeres
Telomere	a region of repetitive nucleotide sequences at each end of a chromosome
Transcription	the first step of gene expression, in which a particular segment of DNA is copied into RNA
Transcription factors	proteins that control the rate of transcription
Translation	synthesis of proteins by decoding the RNA

List of Figures

- Figure 1-1:** Scheme of the Central Dogma of Biology: bold lines represent permitted transitions; dashed lines possible ones and the absence of lines means prohibited process. - 2 -
- Figure 1-2:** Left: structure of DNA showing the minor and the major grooves. Top Right: colour code of the elements that form DNA. Bottom Right: structure of the nitrogenous bases that constitute DNA. - 3 -
- Figure 1-3:** Representation of gene expression. Image adapted from the National Human Genome Research Institute by Allyson Cunningham. - 5 -
- Figure 1-4:** Chemical Structure of Ethidium Bromide - 5 -
- Figure 1-5:** Chemical structure of $[\text{Zn}(\text{DIP})_2(\text{DMP})]^{2+}$ - 6 -
- Figure 1-6:** Chemical structure of the DNA groove intercalator naphthalene derivative. - 7 -
- Figure 1-7:** Top, structures of guanine (left) and adenine (right). Bottom, structure Chlormethine (left) and Busulfan (right). - 7 -
- Figure 1-8:** Left, two $\Delta\text{-}[\text{Ru}(\text{Bpy})_2(\text{dppz})]^{2+}$ complexes (red) intercalating two adenine-adenine mismatches (blue). Right, structure of a ruthenium complex which inserts into two mismatch site. - 8 -
- Figure 1-9:** Structure of cisplatin. - 9 -
- Figure 1-10:** Hydrolysis of cisplatin. - 10 -
- Figure 1-11:** DNA-cisplatin crosslinking adducts. - 10 -
- Figure 1-12:** Molecular structure of 1) Carboplatin, 2) Nedaplatin, 3) Oxaliplatin 4) Lobaplatin, 5) ZN0473 and 6) Satraplatin. - 12 -
- Figure 1-13:** Adaption of 'activation by reduction' hypothesis. - 13 -
- Figure 1-14:** Chemical Structures of NAMI (left) and NAMI-A (right). - 14 -
- Figure 1-15:** Different hydrolysis pathways of NAMI-A. - 15 -
- Figure 1-16:** Top, molecular structures of KP418; bottom, KP1019. - 16 -
- Figure 1-17:** General structure of a ruthenium organometallic η^6 -arene complex.⁸⁷ - 16 -
- Figure 1-18:** (N,O) binding mode and (N,N) binding mode.^{92,93} - 18 -
- Figure 1-19:** Recently reported active trans-platinum anti-cancer (TPA) complexes.¹⁰⁸ - 19 -
- Figure 1-20:** cis- $[\text{Ru}(\text{II})(\text{DMSO})_4(\text{Cl})_2]$ and trans- $[\text{Ru}(\text{II})(\text{DMSO})_4(\text{Cl})_2]^{111}$ - 20 -
- Figure 1-21:** Tetrazolium salts used for cell survival. Left, MTT assay; Right, XTT assay. - 21 -

Figure 1-22: Structure of Sulforhodamine B.	- 22 -
Figure 1-23: General structure for the di-halide complexes explaining the different fragments.	- 23 -
Figure 2-1: Backbones of 2-picolinamide (left) and 2-quinaldamide (right).	- 33 -
Figure 2-2: Different coordination modes for the quinaldamide ligands, (top left) [N,N] anionic, (top right) [N,O] anionic and (bottom) [N,O] neutral.	- 34 -
Figure 2-3: Left, chemical structure of the quinaldamide-core ligands; Right, ligands reported and highlighted in blue are in the CCDC data base.	- 34 -
Figure 2-4: Novel functionalised quinaldamide ligands.	- 35 -
Figure 2-5: Summary of ligands with their respective numbering. Blue highlighted ligands are novel. Green highlighted are found in literature with no characterisation data. Black highlighted ligands are already known but used in this research project.	- 37 -
Figure 2-6: IR spectrum of the ligand 2.3.	- 38 -
Figure 2-7: Labelled diagram of ligand 2.3.	- 39 -
Figure 2-8: ^1H NMR spectrum of the ligand 2.3 (CDCl_3 , 300 MHz, 300 K).	- 39 -
Figure 2-9: $^{13}\text{C}\{^1\text{H}\}$ NMR spectrum of the ligand 2.3 (CDCl_3 , 75 MHz, 300 K).	- 40 -
Figure 2-10: Molecular structure of ligand 2.3 showing intramolecular hydrogen bonds. Displacement ellipsoids are at the 50% probability level.	- 41 -
Figure 2-11: Packing diagram of ligand 2.3 in the a axis showing π - π stacking and intermolecular hydrogen bonds between the 4-methoxy oxygen and the 4'-methoxy hydrogens of the molecule below.	- 42 -
Figure 2-12: Intermolecular hydrogen bonds (left) in the b axis and (right) in the c axis arranged in a herringbone motif.	- 42 -
Figure 2-13: Molecular structure of ligand 2.30 showing intramolecular hydrogen bonds. Displacement ellipsoids are at the 50% probability level	- 43 -
Figure 2-14: Packing diagram of ligand 2.30 (on the left) showing hydrogen bonds between the carbonyl group and the perpendicular proton on the opposite quinaldamide core (axis a) and the π - π stacking on the right (axis b).	- 44 -
Figure 2-15: Herringbone motif or zig-zag interaction of the ligand 2.30, held by π - π interactions.	- 44 -
Figure 2-16: Molecular structure of ligand 2.37 showing intramolecular hydrogen bonds. Displacement ellipsoids are at the 50% probability level.	- 45 -
Figure 2-17: Packing diagram of ligand 2.37 showing π - π stacking and intermolecular hydrogen bonds.	- 46 -

Figure 2-18: Packing of the ligand in a square motif.	- 47 -
Figure 3-1: Possible isomers for ruthenium complexes type RuX ₂ L ₂ bearing homoleptic bidentate ligands. Optical isomers are also shown.	- 50 -
Figure 3-2: Left, ligand used by Krause; Right, ligand developed by Reedijk.	- 51 -
Figure 3-3: Possible isomers of dichloride bisquinaldamide ruthenium complexes.	- 52 -
Figure 3-4: Trans-dichloride bisquinaldamide ruthenium (III) backbone where R is a functional group either electron donating or withdrawing.	- 53 -
Figure 3-5: Chemical structures of the compounds functionalised in different position 2 (left), position 3 (middle) and position 4 and disubstituted (right).	- 54 -
Figure 3-6: Comparison of the IR spectra of the ligand 2.1 (purple line) and its ruthenium complex 3.1 in red.	- 56 -
Figure 3-7: HRMS spectra of the complex 3.1 (left) experimentally determined and (right) simulated pattern.	- 56 -
Figure 3-8: Chemical structure of compound 3.1.	- 57 -
Figure 3-9: Solvent dependent crystal structures for complex 3.1.	- 58 -
Figure 3-10: Crystal packing interactions of the complex 3.1 (similar packing for both complexes).	- 60 -
Figure 3-11: Extended crystal structure for complex 3.1.	- 60 -
Figure 3-12: XRPD data overlap of complex 3.1 showing the experimental (black) and simulated (red) diffractograms recorded at scan rate of 40 sec/scan.	- 61 -
Figure 3-13: Chemical structure for complex 3.18 (left); labelled crystal structure (right).	- 62 -
Figure 3-14: π - π interactions for complex 3.18.	- 64 -
Figure 3-15: Crystal packing showed in the z-axis.	- 65 -
Figure 3-16: Chemical structure of complex 3.23 (left); labelled crystal structure (right).	- 66 -
Figure 3-17: Extended crystal structure of compound 3.23, showing the intermolecular π - π interactions.	- 67 -
Figure 3-18: Expansion of the crystal structure for complex 3.23.	- 68 -
Figure 3-19: Chemical structure of complex 3.29 (left); labelled crystal structure (right).	- 69 -
Figure 3-20: Extended crystal structure of compound 3.29, showing the intermolecular π - π interactions.	- 70 -
Figure 3-21: Expansion of the crystal packing of the complex (3.29).	- 71 -
Figure 3-22: XRPD data overlap of complex 3.29 showing the experimental (black) and simulated (red) diffractograms recorded at scan rate of 40 sec/scan.	- 72 -

Figure 3-23: Chemical structure of compound 3.32 (left); labelled crystal structure (right).	- 73 -
Figure 3-24: π - π interactions of the complex 3.32.	- 74 -
Figure 3-25: Crystal packing of compound 3.32.	- 76 -
Figure 3-26: Chemical structure of complex 3.38 (left); labelled crystal structure (right).	- 77 -
Figure 3-27: π - π stacking interactions of compound 3.38.	- 78 -
Figure 3-28: Z-axis view of the crystal packing expansion of complex 3.38.	- 80 -
Figure 3-29: Chemical structure of the charged side product (left) and the labelled crystal structure of the cis-dichloride bis-(2,5-difluoroquinaldamide) ruthenate (III) triethylammonium salt.	- 81 -
Figure 3-30: Expanded Crystal Structure of the side product cis-dichloride bis-(2,5-difluoroquinaldamide) Ru(III) charged complex.	- 82 -
Figure 3-31: (Left) chemical structure of side product of the base free reaction with 4-bromoquinaldamide ligand; (Right) crystal structure of the compound isolated.	- 83 -
Figure 3-32: (Top) experimental HRMS spectrum obtained of the complex from the mother liqueurs of the reaction with the unsubstituted ligand 2.1; (Bottom) simulated pattern of the compound.	- 84 -
Figure 3-33: Chemical structure of bisquinaldamide neutral complex and decomposition product.	- 85 -
Figure 3-34: Labelled crystal structure of the proposed decomposition product.	- 86 -
Figure 4-1: Mechanism of reduction of the water soluble yellow MTT salt to the insoluble violet formazan neutral molecule by NAD(P)H.	- 91 -
Figure 4-2: General structure of the <i>trans</i> -dichloride ruthenium (III) bisquinaldamide complexes. Grey dashed lines and black highlighted parts were drawn for 3D clarity.	- 93 -
Figure 4-3: Bar-chart of all the IC ₅₀ \pm S. E. values against HCT 116 p53 (+/+), HCT 116 p53 (-/-), MIA PaCa-2 and ARPE-19.	- 95 -
Figure 4-4: Comparison of the activity of the complexes functionalised in the position 2.	- 99 -
Figure 4-5: Comparison of the activity of the complexes functionalised in the position 3.	- 99 -
Figure 4-6: Comparison of the activity of the complexes functionalised in the position 4.	- 100 -
Figure 4-7: Comparison of the activity of the complexes functionalised in the position 2 and 4.	- 100 -
Figure 4-8: Comparison of the activity of the complexes functionalised in the position 2 and 5.	- 101 -

- Figure 4-9:** Comparison of the activity of the complexes functionalised in the position 2 and 6. - 101 -
- Figure 4-10:** Selectivity ratio bar-chart of all the complexes. - 104 -
- Figure 4-11:** Bar-chart summary of the $IC_{50} \pm S.E.$ values of the lead compounds analysing the colorectal cell lines HCT 116 p53 (+/+), HCT 116 p53 (-/-) and MIA PaCa_2. - 108 -
- Figure 4-12:** Bar-chart summary of the selectivity factor of the lead compounds analysing the colorectal cell lines HCT 116 p53 (+/+), HCT 116 p53 (-/-) and MIA PaCa_2. - 108 -
- Figure 4-13:** Bar-chart summary of the IC_{50} values of the compounds 3.13, 3.18, 3.23, 3.29, 3.32, cisplatin, carboplatin and oxaliplatin tested against the Kras oncogene family, and the non-cancerous cell line ARPE-19. - 109 -
- Figure 4-14:** Bar-chart summary of the selectivity of the Lead Compounds and platinum compounds against HCT 116 with mutated Kras oncogene family. - 110 -
- Figure 4-15:** Bar-chart of the ruthenium complexes preferential activity for the tumour suppressor gene p53. - 113 -
- Figure 4-16:** Bar-chart of the ruthenium Lead Compounds preferential activity for the oncogene Kras. - 114 -
- Figure 4-17:** Bar chart of IC_{50} values of compounds 3.13, 3.18, 3.23, 3.29, 3.32, cisplatin, carboplatin and oxaliplatin. - 116 -
- Figure 4-18:** Summary of the selectivity factors of 3.13, 3.18, 3.23, 3.29, 3.32, cisplatin, carboplatin and oxaliplatin. - 116 -
- Figure 4-19:** Mechanism of HIF-1 α regulation within the cell - 118 -
- Figure 4-20:** Mechanism proposed for pro-drug activation by hypoxia. - 119 -
- Figure 4-21:** General structure of complexes: 3.13 (R= 3-ⁱPr), 3.18 (R = 4-ⁱBu), 3.23 (R = 2-F), 3.29 (R = 3-Cl) and 3.23 (R = 2,5-diCl) - 119 -
- Figure 4-22:** Bar-chart of compounds 3.13 (R= 3-ⁱPr), 3.18 (R = 4-ⁱBu), 3.23 (R = 2-F), 3.29 (R = 3-Cl) and 3.23 (R = 2,5-diCl) tested against HCT 116 p53(+/+), HCT 116 p53 (-/-) and MIA PaCa_2. Normoxia results highlighted in blue, hypoxia results in red. - 120 -
- Figure 4-23:** Hypoxia cytotoxicity ratio (HCR) bar-chart of compounds 3.13 (R= 3-ⁱPr), 3.18 (R = 4-ⁱBu), 3.23 (R = 2-F), 3.29 (R = 3-Cl) and 3.23 (R = 2,5-diCl). - 123 -
- Figure 4-24:** Bar-chart of the hypoxia enhancement ratio (HER) of the Lead compounds tested. - 123 -
- Figure 4-25:** Bar-chart comparison of the hypoxia enhancement ratio and the selectivity under normoxic conditions for 3.13 (R= 3-ⁱPr), 3.18 (R = 4-ⁱBu), 3.23 (R = 2-F), 3.29 (R = 3-Cl) and 3.23 (R = 2,5-diCl) against the cell lines tested. - 124 -

- Figure 4-26:** Bar-chart of compounds 3.23 (R = 2-F in blue) and 3.32 (R = 2,5-diCl in red) for the different time exposure cytotoxic assays against HCT 116 p53(+/+), HCT 116 p53 (-/-), MIA PaCa_2 and ARPE-19. - 127 -
- Figure 4-27:** Selectivity ratios of (left) complex 3.23 and (right) complex 3.32 at different time points. - 129 -
- Figure 4-28:** The eukaryotic cell cycle. - 131 -
- Figure 4-29:** Representative optical microscopy images (x10) of ARPE-19 cells after 24h, 48h and 72h in: (top) control experiment, (medium) treatment with complex 3.23 (2-F) and (bottom) treatment with complex 3.32 (2,5-diCl). - 135 -
- Figure 4-30:** Optical image (x10) of ARPE-19 treated with the complex 3.32 (2,5-diCl) after 48h. Several needle-like crystals can be seen when using polarised light. - 136 -
- Figure 4-31:** Bar chart representing the proportions of the cell cycle for the cell line ARPE-19 after 24h, 48h and 72h, including the drug exposure experiments. - 137 -
- Figure 4-32:** Representative optical microscopy images (x10) of MIA PaCa_2 cells after 24h, 48h and 72h in: (top) control experiment, (medium) treatment with complex 3.23 (2-F) and (bottom) treatment with complex 3.32 (2,5-diCl). - 141 -
- Figure 4-33:** Optical image (x10) of MIA PaCa_2 treated with the complex 3.32 (2,5-diCl) after 48h. Several needle-like crystals can be seen when using polarised light, displaying three different colours: blue, red and green. - 142 -
- Figure 4-34:** Bar chart representing the proportions of the cell cycle for the cell line MIA PaCa_2 after 24h, 48h and 72h, including the drug exposure experiments. - 145 -
- Figure 4-35:** Chemical structures of the ruthenium (III) polypyridyl complexes (left) dichloride complex and (right) its Guanide (G) derivative. - 148 -
- Figure 4-36:** Bar-chart summary of the growth inhibition (%) of the ruthenium complexes against the different bacterial strains tested by the Community for Antimicrobial Drug Discovery. - 151 -
- Figure 5-1:** Recorded spectra for time-evolution hydrolysis studies and functional groups for the selected *trans*-dichloride Ru complexes. - 166 -
- Figure 5-2:** Log P values of the *trans*-dichloride bis-quinaldamide ruthenium complexes and cisplatin from the average of six independent experiments. - 171 -
- Figure 5-3:** Representation of IC₅₀ values and Log P of the complexes analysed. - 173 -

List of Schemes

- Scheme 2-1:** General protocol to synthesise quinaldamide ligands containing electron withdrawing groups (EWGs) - 36 -
- Scheme 2-2:** General synthetic pathway to obtain quinaldamide ligands containing electron donating groups (EDGs) - 36 -
- Scheme 3-1:** Optimised synthetic pathway to obtain the ruthenium complexes. - 54 -
- Scheme 3-2:** Reaction scheme followed to synthesis the monoquinaldamide ruthenium (III) trischloride neutral complexes. - 84 -
- Scheme 5-1:** Proposed hydrolysis mechanism for the trans-dichloride bis-quinaldamide ruthenium complexes - 165 -

List of Tables

Table 2-1: ^1H and $^{13}\text{C}\{^1\text{H}\}$ NMR chemical shift assignments for the ligand 2.3	- 40 -
Table 2-2: Selected angles for ligand 2.3 with esds shown in parenthesis	- 41 -
Table 2-3: Selected bond lengths for ligand 2.3 with esds shown in parenthesis	- 42 -
Table 2-4: Selected angles for ligand 2.30 with esds shown in parenthesis	- 43 -
Table 2-5: Selected bond lengths for ligand 2.30 with esds shown in parenthesis	- 44 -
Table 2-6: Selected angles for ligand 2.37 with esds shown in parenthesis	- 46 -
Table 2-7: Selected bond lengths for ligand 2.3 with esds shown in parenthesis	- 46 -
Table 3-1: Numbering of the complexes and functionality given by the R group	- 53 -
Table 3-2: Selected bond lengths for complex 3.1 with labelled atoms corresponding to the complex on the left of Figure 3-9	- 59 -
Table 3-3: Selected bond angles for complex 3.1 with labelled atoms corresponding to the complex on the left of Figure 3-9	- 59 -
Table 3-4: Selected bond lengths for complex 3.18 with labelled atoms corresponding to the complex in Figure 3-13	- 63 -
Table 3-5: Selected bond angles for complex 3.18 with labelled atoms corresponding to the complex on Figure 3 13	- 64 -
Table 3-6: Selected bond lengths with esdv for complex 3.23 and atom labels found in Figure 3-16	- 67 -
Table 3_7: Selected bond angles with esdv for complex 3.23 and atom labels found in Figure 3-16	- 68 -
Table 3-8: Selected bond lengths for complex 3.29 with labelled atoms corresponding to the complex in Figure 3-19	- 71 -
Table 3-9: Selected bond angles for complex 3.29 with labelled atoms corresponding to the complex in Figure 3-19	- 72 -
Table 3-10: Selected bond lengths and sdvs for complex 3.32 labelled as shown in Figure 3-23	- 75 -
Table 3-11: Selected bond angles and sdvs for complex 3.32 and atom labels found in Figure 3-23	- 75 -
Table 3-12: Selected bond lengths for complex 3.38 with labelled atoms corresponding to the complex in Figure 3-26	- 79 -
Table 3-13: Selected bond angles for complex 3.38 with labelled atoms corresponding to the complex in Figure 3-26	- 79 -
Table 3-14: Selected bond distances with esdv of the charged complex described in Figure 3-29	- 81 -
Table 3-15: Selected bond angles with esdv of the charged complex described in Figure 3-29	- 82 -

Table 3-16: Selected bond distances of the labelled complex in Figure 3-34	- 86 -
Table 3-17: Selected bond angles of the labelled complex in Figure 3-34	- 87 -
Table 4-1: Summary of the complex codes and R groups	- 93 -
Table 4-2: IC ₅₀ values ± S.E. (μM) of the complexes 3.1 – 3.24 expressed as the mean IC ₅₀ ± S.E. for three independent experiments	- 96 -
Table 4-3: IC ₅₀ ± S.E. values (μM) of the complexes 3.25 – 3.40 expressed as the mean IC ₅₀ ± S.E. for three independent experiments	- 97 -
Table 4-4: IC ₅₀ values (μM) after of the current clinical chemotherapeutic drugs (cisplatin, carboplatin and oxaliplatin) expressed as the mean IC ₅₀ ± S.E. for three independent experiments after 72 hours exposure	- 98 -
Table 4-5: Selectivity factor (s. f) values for the compounds 3.1 – 3.24	- 105 -
Table 4-6: Selectivity factor (s. f) values for the compounds 3.25 – 3.40	- 106 -
Table 4-7: Selectivity factor (s. f.) values of the current chemotherapeutic drugs (cisplatin, carboplatin and oxaliplatin) after 72 hours exposure	- 107 -
Table 4-8: IC ₅₀ ± S.E. values (μM) of compounds 3.13, 3.18, 3.23, 3.29, 3.32, cisplatin, carboplatin and oxaliplatin against the Kras oncogene family	- 110 -
Table 4-9: Selectivity factor (s. f.) values of 3.13, 3.18, 3.23, 3.29, 3.32, cisplatin, carboplatin and oxaliplatin against the Kras colorectal cell lines	- 111 -
Table 4-10: Preferential activity values towards the colonic cancer cell line HCT 116 p53 (-/-)	- 112 -
Table 4-11: Preferential activity values towards the colonic cancer cell line HCT 116 Kras Mutant. In green highlighted shows the most selective and blue highlighted means the selectivity factor is above 1	- 115 -
Table 4-12: Summary of the IC ₅₀ under hypoxic conditions of complexes 3.13, 3.18, 3.23, 3.29 and 3.32. (Blue highlighted show compounds anticancer activity under these conditions)	- 122 -
Table 4-13: IC ₅₀ values (μM) of compounds 3.23 (R = 2-F) and 3.32 (R = 2,5-diCl) for the different time exposure cytotoxic assays against HCT 116 p53(+/+), HCT 116 p53 (-/-), MIA PaCa_2 and ARPE-19.	- 128 -
Table 4-14: Selectivity values of compounds 3.23 (R = 2-F) and 3.32 (R = 2,5-diCl) for the different time exposure cytotoxic assays against HCT 116 p53(+/+), HCT 116 p53 (-/-) and MIA PaCa_2.	- 130 -
Table 4-15: ARPE-19 cell viability summary for control, complexes 3.23 and 3.32 after 24h, 48h and 72h (* = Not determined)	- 134 -
Table 4-16: ARPE-19 cell cycle analysis after 24h, 48h and 72h, showing the control, drug treatment with complex 3.23 (2-F) and complex 3.32 (2,5-diCl) at a concentration of 18 μM	- 139 -
Table 4-17: MIA PaCa_2 cell viability summary for control, complexes 3.23 and 3.32 after 24h, 48h and 72h (* = Not determined)	- 143 -

Table 4-18: MIA PaCa_2 cell cycle analysis after 24h, 48h and 72h, showing the control, drug treatment with complex 3.23 (2-F) and complex 3.32 (2,5-diCl) at a concentration of 18 μ M	- 146 -
Table 4-19: Growth inhibition of trans-dichloride ruthenium bisquinaldamide 3.1 – 3.24 complexes against bacterial strains expressed in %	- 152 -
Table 4-20: Growth inhibition of trans-dichloride ruthenium bisquinaldamide 3.25 – 3.40 complexes against bacterial strains expressed in %	- 153 -
Table 4-21: Antibacterial toxicity (MIC), cytotoxicity (CC ₅₀) and haemolysis (HC ₁₀) of 3.12, 3.28, 3.30, 3.33 – 3.35 and 3.38, all data expressed in μ g/ml (μ M)	- 155 -
Table 4-22: Growth inhibition of trans-dichloride ruthenium bisquinaldamide 3.1 – 3.40 complexes against fungal strains expressed in %	- 158 -
Table 5-1: Absorption wavelength bands (λ max) for the Ru complexes	- 167 -
Table 5-2: IC ₅₀ values against the cell lines tested and percentage of hydrolysed ruthenium complexes tested	- 169 -

Chapter 1 Introduction and objectives

1.1 Introduction

1.1.1 Structure and role of DNA

The nature of living organisms is determined by their genes, which are specific sequences of nucleic acids required for protein synthesis.¹ Genes are embedded in DNA, which is a biopolymer whose discovery involved several scientists and stages. The first X-ray crystallography images of DNA obtained by Rosalind Franklin² together with the seminal idea of DNA coined by Maurice Wilkins allowed James Watson and Francis Crick to understand and to solve the ‘mysterious’ molecule of life.³ In 1958, Crick postulated that the transference of genetic information between two consecutive generations is essential for life.⁴ This later became known as the “Central Dogma of Biology” (**Figure 1-1**).⁵

After considering all the plausible biological mechanisms, Crick concluded that genetic information is transcribed in a unidirectional manner from the DNA to proteins through RNA, which cannot be modified nor affect genes. This process encompasses three transitions: biologically permitted, possible for specific situations and prohibited. However, the unidirectionality of this process remains one of the most controversial topics within biology.⁵

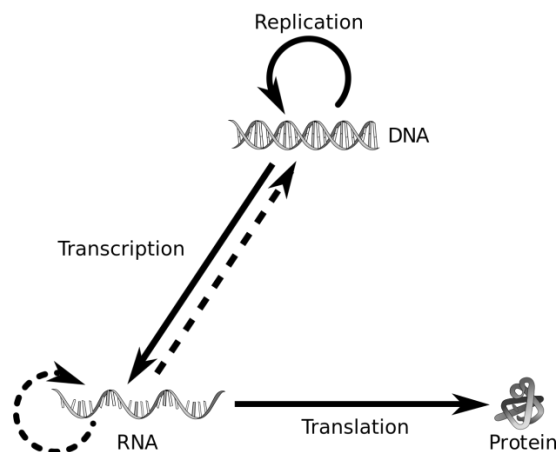


Figure 1-1: Scheme of the *Central Dogma of Biology*: bold lines represent permitted transitions; dashed lines possible ones and the absence of lines means prohibited process.⁶

1.1.2 Structure of DNA and its participation in cellular recognition

DNA is a biopolymer derived from nucleotides which are characterised by having a highly negatively charged phosphate backbone. Structurally, it is found as a regular double helix whose strands are linked together through hydrogen bonds and hydrophobic interactions between the nitrogenous bases as shown in **Figure 1-2** (Adenine (A), Guanine (G), Cytosine (C), and Thymine (T)).

Depending on the conditions of the medium, this helix adopts different conformations: the A-Form, the B-Form and the Z-Form. However, the B-DNA form is the most common and recognisable by most transcription factors.⁷ It has a diameter of around 20 Å with 10 bases per loop; the distance within two bases is 3.4 Å and the rotation per residue is 36°. Despite its regularity, it can show deviations depending on the torsion angles of the nucleotide sequence.^{8,9} Thus, two different grooves are found: the major is wide and relatively shallow, whereas the minor is narrow and deep, as shown in **Figure 1-2**. The width is given by the nitrogenous bases sequence and, generally, the areas rich in A/T are narrower than G/C. Groove hydration studies show association to the major groove is a process principally driven by enthalpy and unfavourable to the minor which is compensated by entropic contribution.¹⁰ These factors justify that proteins recognise DNA preferably through the major groove.

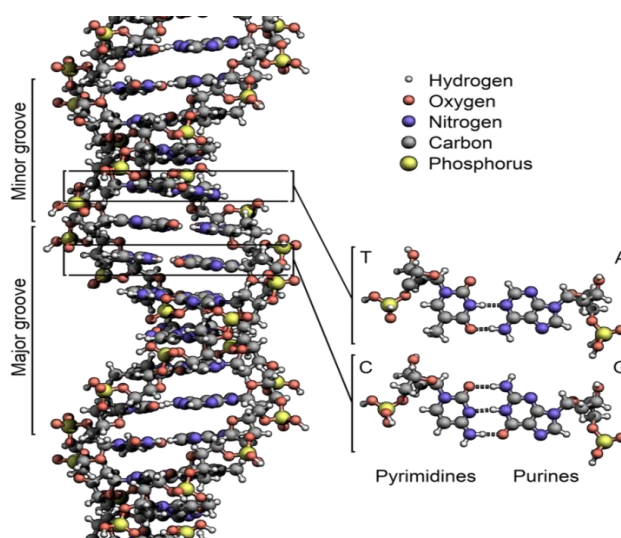


Figure 1-2: *Left:* structure of DNA showing the minor and the major grooves. *Top Right:* colour code of the elements that form DNA. *Bottom Right:* structure of the nitrogenous bases that constitute DNA.

The cellular genome is organised in chromosomes, formed by one single molecule of linear DNA. Unlike prokaryotic cells, which lack a nuclear membrane, eukaryotic chromosomes are not found free inside the cytoplasm but contained inside the cellular nucleus, which, at the same time, is separated from the cytoplasm by the nuclear membrane. Chromosomes are formed by tangled fibres of a protein-DNA complex called chromatin whose minimal structural unit is the nucleosome constituted by a DNA sequence linked to an eight-protein complex named histone. The role of chromatin is primordial in the regulation of the gene expression, facilitating or impeding access to the transcriptional machinery of the DNA strands, and, consequently triggering or inhibiting the transcription process.^{11,12}

1.1.3 Gene Expression

Gene expression is the process that the cell uses to generate a protein by decoding the information kept in the nucleotide sequence of a gene. This includes the transcription process, whereby a specific nucleotide sequence is copied to give the RNA molecule, and the translation process which uses the RNA as template to synthesise proteins (**Figure 1-3**).

In some cases, the final product of the gene expression is the RNA itself, although the vast majority is used to determine the synthesis of a specific protein. The RNA copied is known as messenger RNA (mRNA), which, in eukaryotic cells, is held to a transformation process in the nucleus to give the mature mRNA that will be transported to the cytosol for translation. This process is constituted by three steps: initiation, elongation and termination.

Gene expression is a perfectly regulated process, following a specific pattern in each cell that determines its function and morphology. This control can occur in any of the steps, but mostly the regulation of the gene expression is produced in the transcription process.¹³

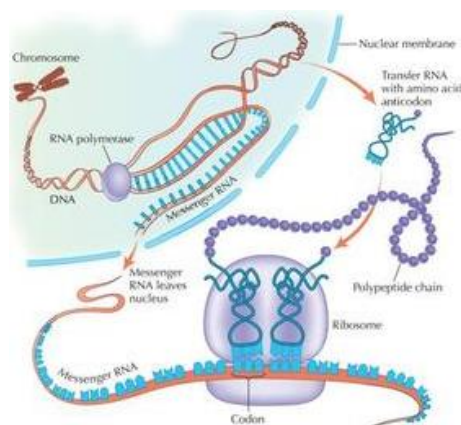


Figure 1-3: Representation of gene expression. Image adapted from the *National Human Genome Research Institute* by Allyson Cunningham.¹⁴

1.2 Interactions of small molecules with DNA

One of the most active fields in biological chemistry and medicinal chemistry is the development of therapeutic molecules, especially when acting at the DNA level.¹⁵ These compounds, also called linking agents (binders), can be organic molecules as well as organometallic/coordination compounds that interact with DNA in five ways:

a) Intercalation

An intercalator is any molecule that can be placed between the base pairs of a nucleic acid in either groove being driven by π -stacking, charge transfer interactions, hydrogen bonds or electrostatic interactions. Intercalation leads to the deformation of the DNA helix and is generally non-selective. A classic example is ethidium bromide (**Figure 1-4**), widely used as a fluorescent probe for DNA determining affinity constants by FID (Fluorescent Intercalator Displacement).^{16,17}

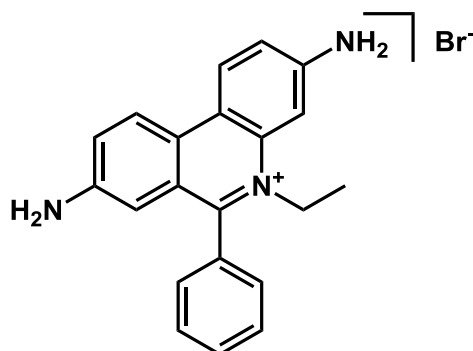


Figure 1-4: Chemical structure of ethidium bromide.

b) External electrostatic interaction

DNA is negatively charged, thus metallic cations and polycationic organic molecules can stabilise it by neutralising the repulsive forces between phosphates. The complex $[\text{Zn}(\text{DIP})_2(\text{DMP})](\text{NO}_3)_2 \cdot 2\text{H}_2\text{O}$ (**Figure 1-5**) was reported to have this behaviour. It is favoured due to the release of counterions to the medium (entropically favourable), while also being enthalpy favoured through interaction between DNA and stabilising molecules.¹⁸

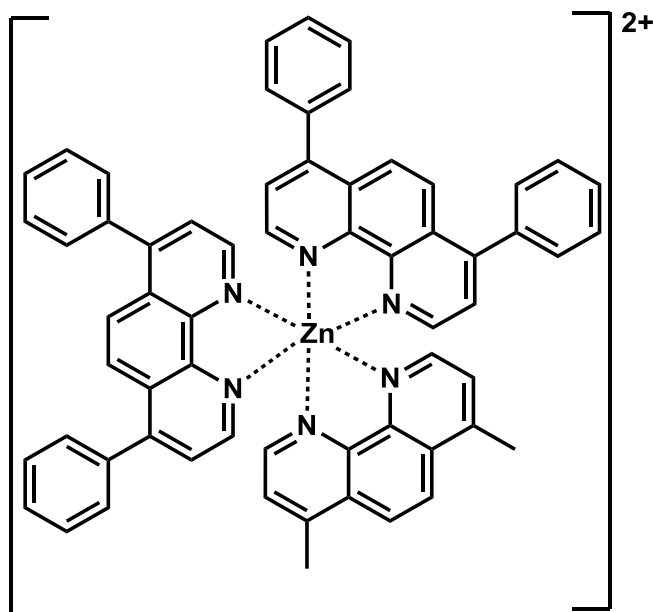


Figure 1-5: Chemical structure of $[\text{Zn}(\text{DIP})_2(\text{DMP})]^{2+}$

c) Insertion into DNA grooves

It has been observed there are some small oligonucleotides (~10-20 base pairs) capable of forming a triple helix interacting through the major groove. These interactions are established due to the formation of Hoogsteen-like bonds between base pairs,¹⁹ which differ from Watson-Crick base pairs in the geometry of the bonds and are rarely observed. These agents have been used to regulate gene expression because they can alter the functionality of transcription factors that use this groove to activate or silence genes.²⁰ Unlike what happens with transcription factors, molecules of relatively small size have a predisposition to joining to a selective minor groove sequence. The first natural products showing this behaviour were dicationic compounds.^{21,22} The interaction in the minor groove is determined by hydrogen bond formation, van der Waals bonds, electrostatic

and hydrophobic interactions. The core structure of a well-known family is shown in **Figure 1-6**.

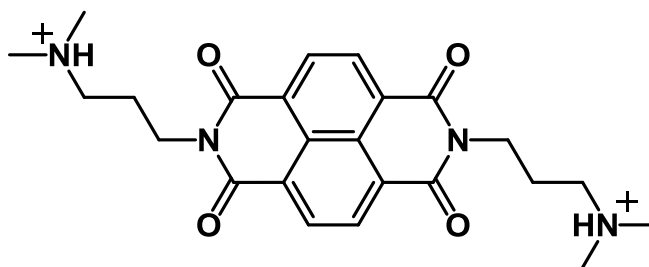


Figure 1-6: Chemical structure of the DNA groove intercalator naphthalene derivative

d) Covalent Interaction

Molecules that interact in this way are called alkylating agents. The most favourable DNA positions to be modified are the N⁷ and the C²-NH₂ of guanine and N³ and N⁷ of adenine. Chlormethine and busulfan (**Figure 1-7**) are examples of alkylating agents.

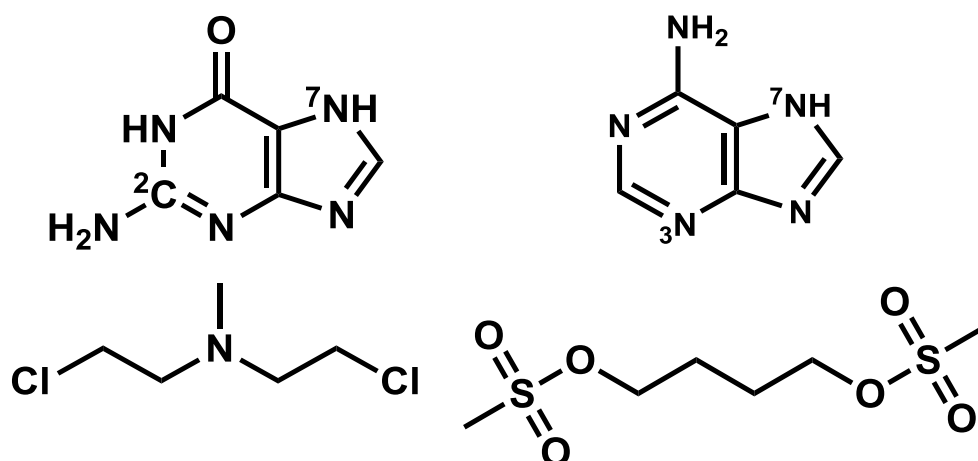


Figure 1-7: Top, structures of guanine (*left*) and adenine (*right*).

Bottom, structure chlormethine (*left*) and busulfan (*right*).

e) Non-classical Insertion

DNA may contain specific areas with non-complementary base pairs. These disturbances can be recognized by metal complexes with ligands incapable of intercalation but inserting between the non-complementary pair. An example of this binding agent is Δ -[Ru(Bpy)₂(dppz)]²⁺.^{23,24}

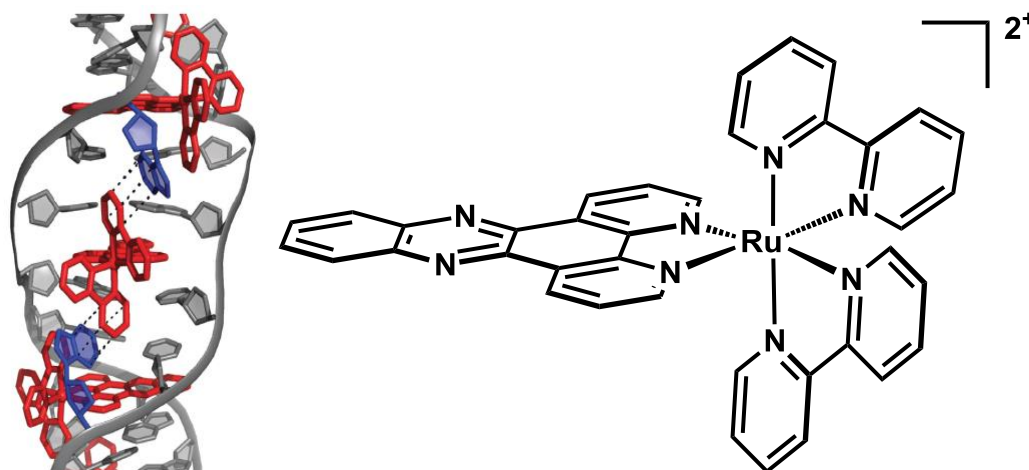


Figure 1-8: Left, two Δ -[Ru(Bpy)₂(dppz)]²⁺ complexes (red) intercalating two adenine-adenine mismatches (blue). Right, structure of a ruthenium complex which inserts into two mismatch site.²⁴

1.3 Cancer

Gene expression is controlled by different biomolecules and, like a machine, does not always work perfectly. When a mistake in the translation process is made, cells try to fix it. Often, the repair does not occur causing a mutation, which is a permanent alteration of the nucleotide sequence in the genome. It can have different effects in the phenotype, but the worst scenario is when this alteration cannot be controlled, and cells start dividing uncontrollably.

Cancer is the term for this kind of mutation and is well-known for being the world's leading fatal disease. The cells divide through a process called mitosis which is controlled by oncogenes and tumour suppressor genes. The fast and uncontrolled growing of cells, the survival of the old and damaged ones and the lower bio-specificity of cancerous cells are some molecular symptoms of suffering this illness.²⁵ Normal or healthy cells regularly undergo apoptosis or programmed cell death whereas cancerous cells do not, causing a lump or tumour which is an abnormal mass of tissue caused by the unrestricted over-expression of mutations. Additionally, there are two kinds of tumours, benign, which are harmless, not cancerous and easily treated if detected early, and malignant, which are harmful and life threatening. The main difference relies on its invasion to other tissues, benign being small and with a spherical shape, meanwhile the malignant tumour does not have a regular shape and spreads very quickly.

In general, cancer affects any organ and can be spread throughout the body (metastasis). Cancer therapy is used to fight this illness, and involves many different techniques including surgery, chemo- and radiotherapy, immunotherapy and hormonal therapy.²⁶

1.4 First Generation of Platinum Based Anti-Cancer Compounds: *Cisplatin*

Platinum-based anti-cancer complexes are the most successful drugs to date for the treatment of various cancers, either as first-line treatments or as supporters in combinatorial treatment. Among all the platinum-based drugs, cisplatin or *cis*-diamminedichloroplatinum(II) is the most famous. Its anti-cancer activity was serendipitously discovered in 1965 by Rosenberg when it was found to inhibit bacterial cell division from the effect of an electromagnetic field using an aqueous solution of NH_4Cl and platinum electrodes.²⁷ After demonstrating its effect on a mouse model, *cisplatin* was the first metal-based drug entering to clinical trials in 1971 and was approved in 1978 as an anti-cancer agent by the Food and Drug Administration.

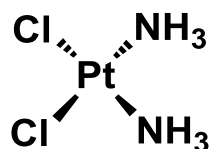


Figure 1-9: Structure of *cisplatin*

Cisplatin is a neutral complex showing a square planar geometry. The *cis*-chloro conformer is responsible for its anti-cancer activity as the *trans*-chloro derivative is highly unstable. Blood plasma has a high chloride concentration (~100 mM) prohibiting the hydrolysis of cisplatin, whereas the very low chloride concentration inside the cells (~3 mM) facilitates hydrolysis, making cisplatin an active electrophile reacting with nucleophilic sites. The N⁷ atoms of the imidazole rings of guanine and adenine bases from DNA are found to be the most preferred cytotoxic targets.²⁸

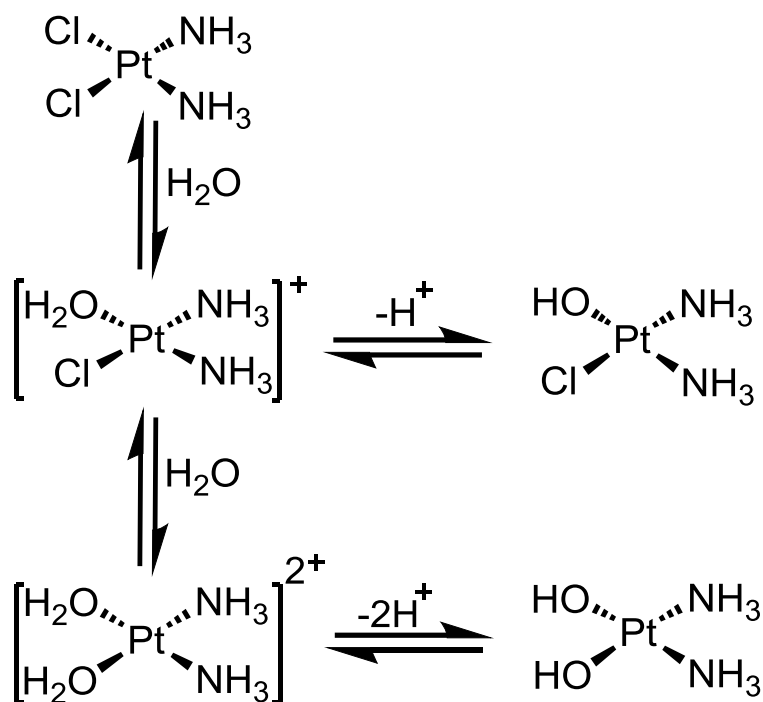


Figure 1-10: Hydrolysis of *cisplatin*

X-ray diffraction shows that aquated cisplatin species can crosslink to DNA in different trends being the following the main three types.²⁹ DNA monoadducts are formed when one molecule of water is lost from the aquated cisplatin. Intrastrand crosslinks take place when two chloride ligands of the aquated cisplatin are replaced by purine nitrogen atoms on adjacent bases of the same DNA strand.³⁰⁻³³ Additionally, DNA crosslinks include the interstrand crosslinks (**Figure 1-11**). All cisplatin crosslinks to DNA lead to the disruption of its helical structure that cannot be identified by repair enzymes, hence triggering a series of events leading to the inhibition of DNA replication^{34,35} which is responsible for the anti-cancer activity of cisplatin.

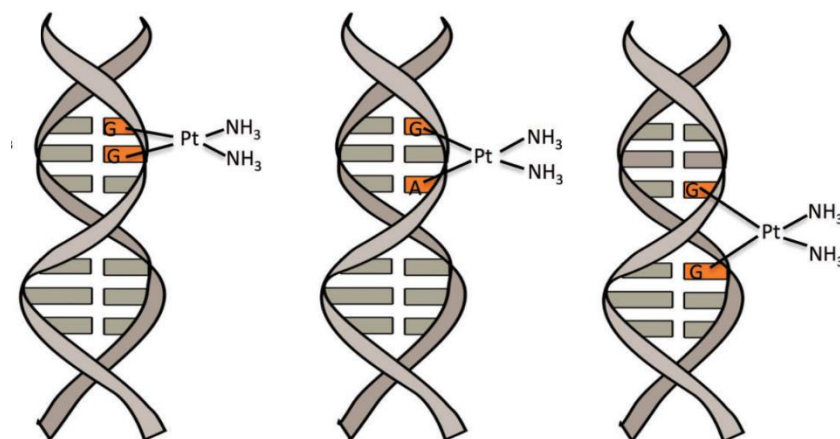


Figure 1-11: DNA-cisplatin crosslinking adducts.³⁶

Since only a small fraction of intracellular cisplatin is bound to DNA,^{37,38} there is a high interest in knowing the mechanism of action of cisplatin in killing cancer cells. Despite the success of cisplatin towards the death of cancer cells, this therapeutic agent is associated with toxicities such as nephrotoxicity and ototoxicity. It has also been shown that some cancer cell lines are able to develop resistance towards cisplatin through changes in the cell environment.³⁹⁻⁴² These include drug transport that leads to a decrease of intracellular cisplatin accumulation, an increase in drug detoxification systems, an increase in DNA repair system, changes in tolerance mechanisms from damage of DNA and changes in cell death pathways leading to apoptosis.

1.5 Second Generation Platinum Anti-Cancer Compounds

Due to the side effects discussed above, a second generation of platinum-based complexes was introduced. Carboplatin, (**Figure 1-12, 1**) [*cis*-diammine-1,1-cyclobutane dicarboxylate platinum(II)] introduced into the clinic in 1989,^{43,44} has a bidentate dicarboxylate ligand replacing the chlorides of cisplatin, being more lipophilic than the latter. It hydrolyses forming adducts with DNA,⁴⁵ but the main difference relies on the variation in aquation rates releasing the active Pt(II) complex that contributes to cancer cell death.⁴⁶

Nedaplatin (**Figure 1-12, 2**) was found to have the highest anti-cancer activity of this second generation possessing lower nephrotoxicity in comparison to cisplatin.⁴⁷ Oxaliplatin (**Figure 1-12, 3**) was found to be effective in cisplatin-resistant cells for a range of different cancers.^{48,49} It is the third successful derivative of platinum drugs and entered the clinic in 1994.^{50,51} Formed by an oxalate ligand which undergoes hydrolysis and diaminocyclohexane, it differs to cisplatin and carboplatin in the effect rather than the mechanism of action showing lower nephrotoxicity and ototoxicity.

Lobaplatin (**Figure 1-12, 4**) is currently in phase II clinical trials for cisplatin-resistant ovarian cancer, head, neck and small-cell lung cancers, showing cell cycle arrest in the S phase of DNA (growing phase).⁵²⁻⁵⁴ ZN0473 (**Figure 1-12, 5**) is sterically hindered and hydrolyses around four times slower than cisplatin, which contributes to its high activity against cisplatin-resistant cell lines.⁵⁵ Satraplatin (JM216) (**Figure 1-12, 6**) is the first orally administrated

platinum complex,⁵⁶ differing from its counterparts by being a platinum(IV) complex designed to accommodate two axial acetate groups, increasing lipophilicity,⁵⁷ with comparable efficiency to many well established platinum drugs. It is active against cisplatin resistant cell lines *in vitro* and shows low toxicity levels.⁵⁸ Satraplatin could possibly be a highly successful drug if it passes through its current phase III trials in combination therapy by the FDA.⁵⁹

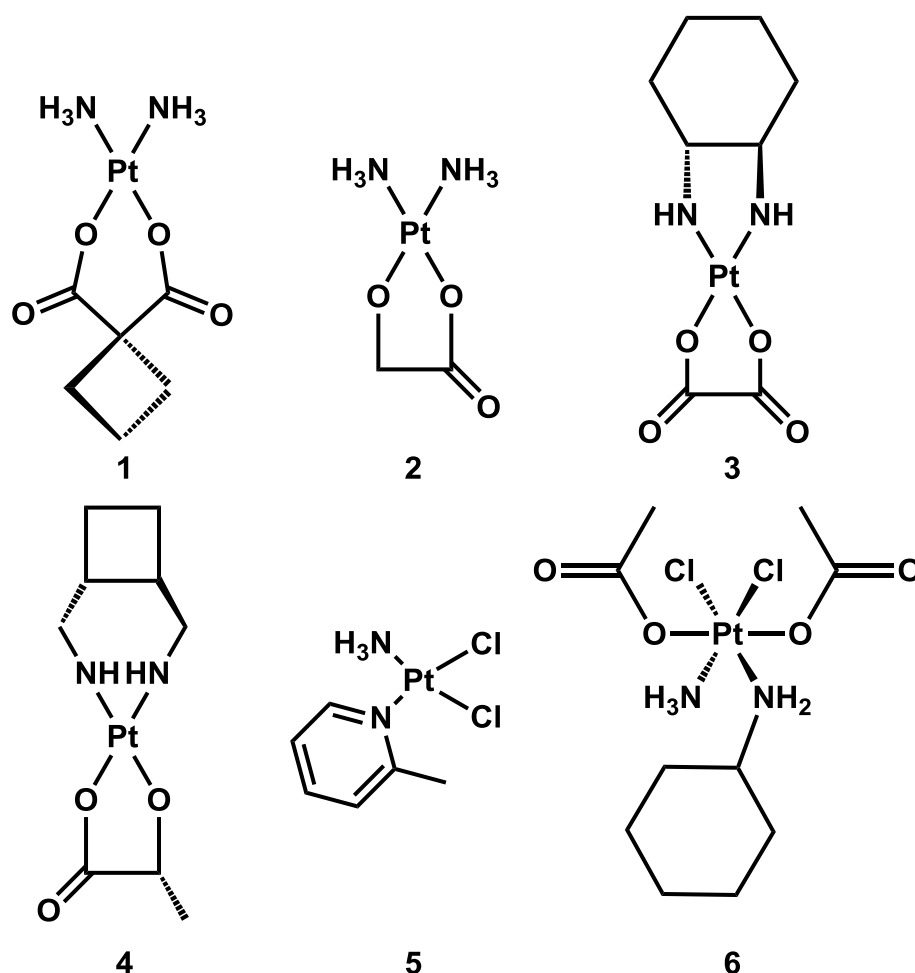


Figure 1-12: Molecular structure of 1) Carboplatin, 2) Nedaplatin, 3) Oxaliplatin
4) Lobaplatin, 5) ZN0473 and 6) Satraplatin

1.6 Introduction of Ruthenium into Medicine

Currently, further research is ongoing into new metal-based drugs in order to eradicate the problem of resistance to platinum-based drugs and to reduce its toxic effects. To this aim, ruthenium-based complexes were proposed as good candidates.⁶⁰⁻⁶² The rationale behind this choice is because of the intrinsic properties of Ru. Firstly, under aqueous conditions, it undergoes ligand exchange

relatively slowly compared to platinum complexes.⁶³ It is widely thought that this is a key process in the effectiveness of metal-based drugs, hence most complexes alter structurally before interaction with biological targets.^{64,65} Secondly, under physiological conditions, ruthenium can be found in different oxidation states (II, III, IV). The “activation by reduction” hypothesis⁶⁶ states that ruthenium(III) behaves as a prodrug, which can be reduced to the more active and more selective ruthenium(II) drug in the hypoxic environment (**Figure 1-13**).^{65,67} This is because cancer cells have a greater rate of metabolism than normal cells using anaerobic respiration producing a considerable amount of lactic acid, hence lowering the pH and creating a reducing environment due to the oxygen deficiency.⁶⁸ Finally, ruthenium has iron-mimicking capability in binding *in vivo* to different biomolecules. For example, it can be transported into tumour cells *via* transferrin receptors allowing greater selectivity.⁶⁵ Metal complexes of Ru(II) and (III) have been previously investigated as potential anticancer agents, immunosuppressant,⁶⁹ anti-microbial⁷⁰ and anti-malarial agents.⁷¹

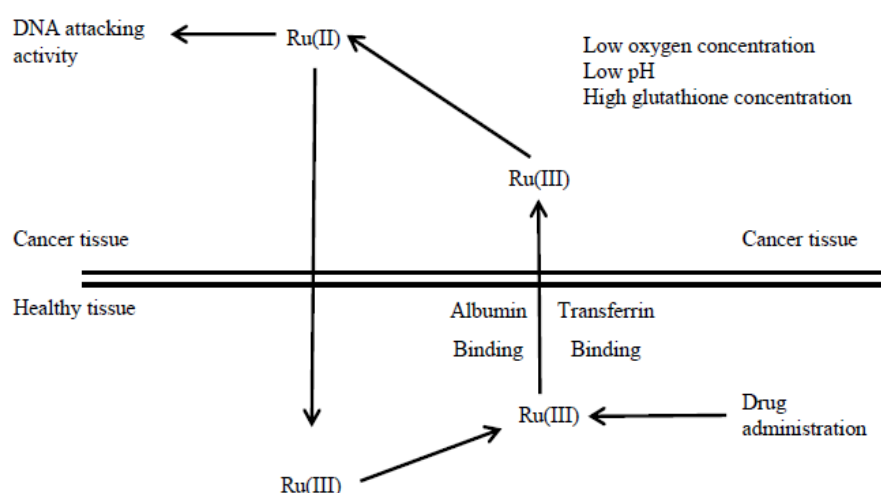


Figure 1-13: Adaption of ‘activation by reduction’ hypothesis

Historically, the interest in ruthenium compounds as anti-cancer agents began in the 1970s when ruthenium red was probed and found to exhibit anti-tumor properties.⁷² This compound (ammoniated ruthenium oxychloride, $\{[(\text{NH}_3)_5\text{Ru}-\text{O}-\text{Ru}(\text{NH}_3)_4-\text{O}-\text{Ru}(\text{NH}_3)_5]\text{Cl}_6 \cdot 4\text{H}_2\text{O}\}$) is widely used to stain polysaccharides, but also exhibits a variety of biological effects inhibiting Ca^{2+} signalling and interfering with the movement of other cations.^{72,73} This triggered a systematic investigation into ruthenium complexes.^{74,75}

1.6.1 NAMI and NAMI-A

Sodium *trans*-[Ru(III)Cl₄(Im)(DMSO-S)] (NAMI, 'New Anti-tumor Metastasis Inhibitor') was first synthesised and found to be active against solid metastasising tumours in mice.⁷⁶ At a later stage in pre-clinical experiments, its sodium counterion was replaced by imidazolium (NAMI-A), to avoid co-precipitation of DMSO with Na⁺.⁷⁷ The imidazolium salt was discovered by Sava *et al.* It is more stable towards air oxidation and was the first Ru drug to successfully finish Phase 1 clinical trials, being the most successful ruthenium anti-cancer drug to date (**Figure 1-14**).⁷⁸ It was found to be inactive against primary cancer cell lines, however it has the same anti-metastatic properties as NAMI.

NAMI-A is synthetically easier to reproduce. Biologically, both complexes have shown activity, reducing lung metastasis in mice, and their anti-metastatic activity has been shown to have no relation to their cytotoxicity against cancerous cells.⁷⁸ Contrary to cisplatin and other ruthenium complexes, they have a different mode of action which involves extracellular activity, being something unique related to both agents.^{78,79,80}

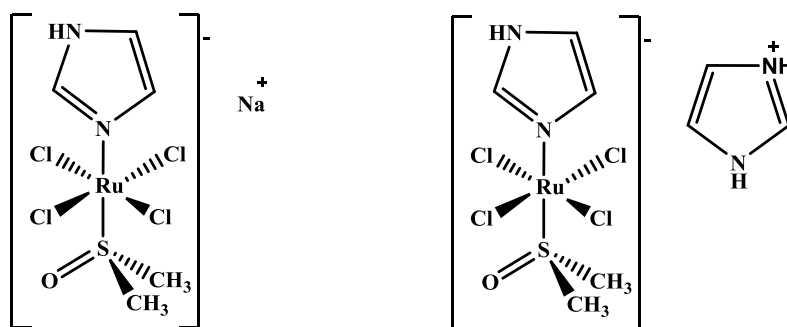


Figure 1-14: Chemical Structures of NAMI (left) and NAMI-A (right)

In NAMI-A, the π -acceptor DMSO ligand stabilises Ru(III) influencing its behaviour in aqueous solution, showing two well-separated hydrolysis steps. After administration, gives a reactive aqua complex in slightly acidic environment by suppressing the hydrolysis of Cl⁻ and slowly dissociating DMSO.⁸¹ At physiological pH, the thiol groups of glutathione reduce NAMI-A to Ru(II) species (NAMI-AR) with further chloride hydrolysis. It was proposed that its anti-metastatic activity is strictly related to the presence of the DMSO ligand.⁸²

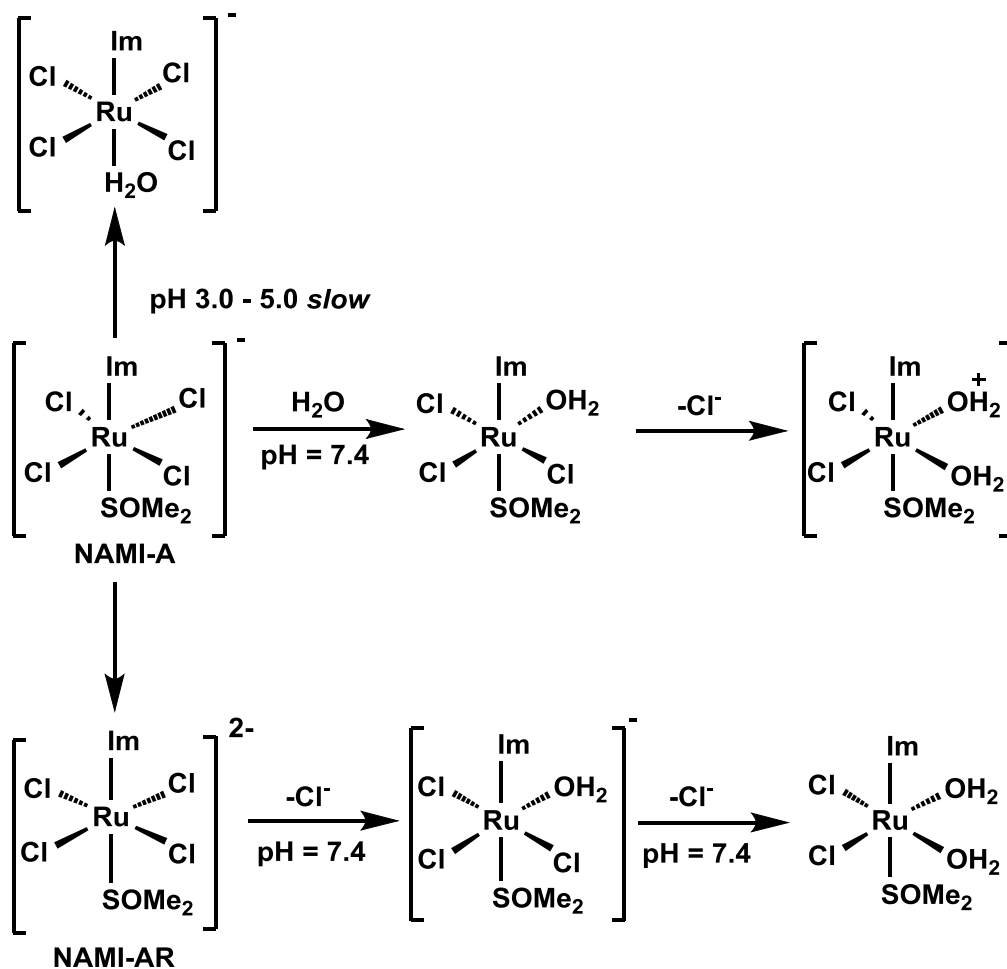


Figure 1-15: Different hydrolysis pathways of NAMI-A

1.6.2 KP418, KP1019 and NKP1019

Imidazolium [trans-tetrachlorobis(imidazole)-ruthenate(III)] (KP418 or ICR) has been shown to be much less toxic than its indazole analogue, however it still shows high activity against colorectal carcinoma models in mice.⁸³ Indazolium [trans-tetrachlorobis(indazole)-ruthenate(III)] (KP1019) (**Figure 1-16**) was discovered by Keppler *et al.* and has shown great activity *in vitro* against a range of cell lines. KP1019 is active against colon carcinomas and primary human tumours. Inhibiting approximately one third of tumours, the only side-effect of KP1019 is production of red blood cells.⁸⁴

Although KP1019 has poor water solubility, the substitution of the indazolium for sodium (NKP1019) increases its water solubility, improving its potential for clinical use.⁸⁵ The active species are hydrolysis products, where KP418 shows an aquation rate similar to cisplatin. However, KP1019 hydrolyses more slowly and

via a different pathway, being dependent upon both temperature and pH. It is thought that ruthenium complexes target the N⁷ position of both guanine and adenine. KP1019 shows less interstrand cross-linking than cisplatin.⁸⁴

After *in vivo* studies of KP1019 and the analysis of all the data obtained, the 'Trojan Horse' hypotheses was introduced. It describes the selective cellular delivery of KP1019 into the tumour using transferrin receptors forming endosomes whose pH is lower than the plasma's triggering the release of the complex.⁸⁶

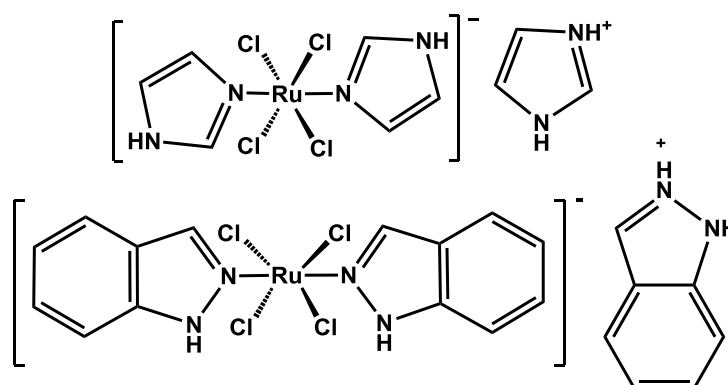


Figure 1-16: *Top*, molecular structures of KP418; *bottom*, KP1019.

1.6.3 'Piano-Stool' Complexes

Organometallic complexes contain at least one covalent metal-carbon bond, and their potential as anti-cancer agents were once restricted to ruthenocene. However, Sheldrick *et al.* were pioneers in the use of organometallic η^6 -arene ruthenium complexes as anti-cancer agents. The most promising complexes as anti-cancer drugs to date take the form $[(\eta^6\text{-arene})\text{Ru}(\text{II})(\text{ethylenediamine})\text{X}]^+$ (X = halide) as shown in **Figure 1-17**.⁸⁷ Sheldrick also reported that different functionalised-arene rings have activity both *in vitro* and *in vivo* against a range of cancer cell lines, including cisplatin-resistant cell lines.

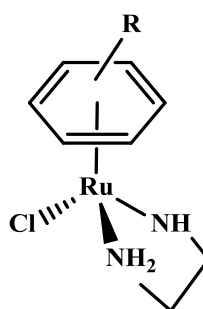


Figure 1-17: General structure of a ruthenium organometallic η^6 -arene complex⁸⁷

Sadler *et al.* have also studied these types of complexes reporting that the 2-phenoxy derivatives showed the highest cytotoxicity amongst the polar substituents, but further results showed the non-polar substituents had higher activity than polar groups.⁸⁸ They also showed that, on average, polycyclic arenes had higher activity than monocyclic arenes. There is a general thought that on increasing the number of arenes, the hydrophobicity will increase, allowing better passive transport towards the cell.^{89,90}

McGowan *et al.* have carried out an extensive work on arene-ruthenium complexes in order to increase the activity against cancerous cells, including cisplatin-resistant cell lines. These include a range of picolinamide and quinaldamide complexes that have been synthesised from the *p*-cymene ruthenium (II) chloride dimer.⁹¹ These (*N,N*) chelating ligands are highly interesting due to previous results discussed within the work of Sheldrick⁸⁷ and they have the advantage of also being (*N,O*) chelating ligands, which gives them the potential to target different organelles within cancerous cells. *N,N*-coordination to the metal centre stabilises metal ions in their high oxidation states because of the strong σ -donor effect,⁹² whereas *N,O*-coordination, relatively favours lower oxidation states.⁹³ NMR studies have shown that the equilibrium in the coordination throughout the (*N,O*) and (*N,N*) can be altered by changing temperature and pH,⁹⁴ hence the biological properties may differ between species. The IC_{50} values of the ruthenium complexes with 3-nitro, 4-nitro and 4-fluoro picolinamide ligands have shown great activity against a range of tumour cells in the same order of magnitude as cisplatin and carboplatin, with the advantage of being active against cisplatin resistant cell lines. The binding mode of these complexes is essential to its cytotoxic behaviour. Studies showed that the (*N,N*) chelating complexes have quick hydrolysis and bind to guanine preferentially, whereas switching to (*N,O*) slows the hydrolysis rate thus switching off the activity.⁹⁴⁻⁹⁶

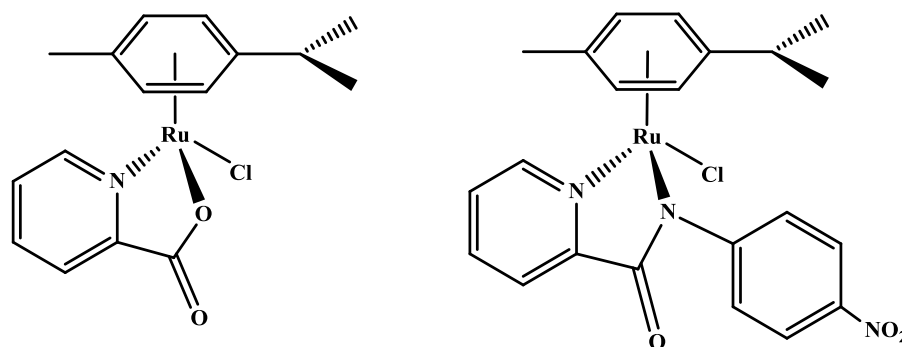


Figure 1-18: (N,O) binding mode *and* (N,N) binding mode. ^{92,93}

Work has since focused on rhodium and iridium pentamethylcyclopentadienyl (Cp*) complexes introducing either a picolinamide (N,N), a ketoiminate (N,O) or a naphthoquinone (O,O) ligand. The difference in binding mode showed that compounds bound (N,N) displayed better IC₅₀ values against HT-29 and MCF-7.⁹⁷

1.7 Trans-dihalide Metal Complexes as Novel Anti-cancer Agents

Iodide has been used as a labile ligand in the design of metal anti-cancer drugs for many years.⁹⁸ After several studies on cisplatin, it was clearly demonstrated that complexes containing chlorides as labile ligands are the most reactive but, also less selective.^{99,100} This fact opened a new interest observing the influence of monodentate halogenated ligands as leaving groups in biological assays on cisplatin. Sadler *et al.* have reported metal (Ru or Os) *p*-cymene complexes with a chloride or iodide as the labile ligand, and either azopyridine or iminopyridine as the chelating ligand. When substituting the chloride for iodide, the biological activities vary drastically, with astounding advantages when containing the iodide ligand bonded to the metal centre.^{101,102}

The structure-activity rules for metal anti-cancer drugs were established by Rosenberg,¹⁰³ and Cleare & Hoeschele.¹⁰⁴ Their studies were based on variations on the structure of cisplatin, changing geometries, ligands and charge, which displayed interesting *in vivo* anti-cancer properties. The *trans*-platinum complex was found to be inactive, meaning that the *cis* isomer is relevant for anti-cancer activity.^{105,106} This feature could be easily explained due to two main factors: *trans* complexes are highly reactive due to kinetic instability, leading to an increase in toxicity, and the *cis* geometry can help to chelate biological targets within the

cells, which is unfeasible for *trans*. Studies showed that when changing the chloride ligand to iodide, their biological activities still show that *cis* dichloride ligands are more potent, as a very high dose was required for the platinum diiodide complex to create a maximum effect for its anti-cancer activity.

Lately, several *trans*-platinum complexes have been shown to have more anti-cancer activity when compared to their *cis* analogues, going against the structure-activity rules for metal anti-cancer complexes.^{107,108} The cytotoxicity of *trans*-platinum complexes increases significantly both *in vitro* and *in vivo* when substituting the inert ligands from simple amines to more bulky ligands. Mechanistic studies suggest that these bulky ligands can impede the substitution of the *trans* dichloride ligands, which increases the kinetic instability of the *trans*-platinum complexes, hence leading to lower toxicity. *Trans*-platinum anti-cancer complexes were proposed by Farrell *et al.*, in which *trans* dichloride platinum complexes that contain at least one aromatic N-donor ligand have shown a 100-fold higher cytotoxicity than transplatin and comparable with cisplatin,¹⁰⁹ against different leukemia cells and human ovarian cells.

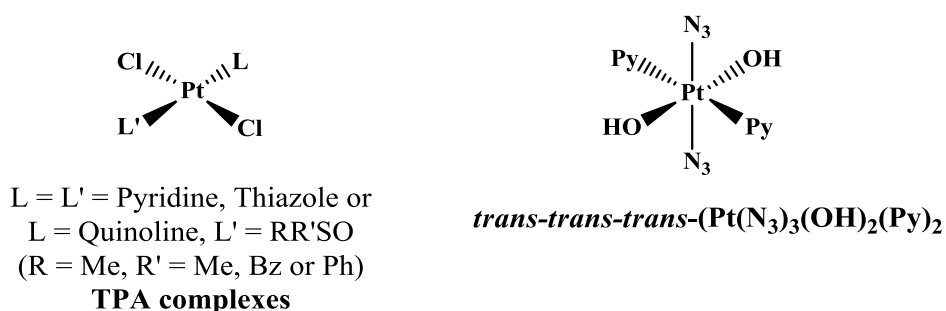


Figure 1-19: Recently reported active *trans*-platinum anti-cancer (TPA) complexes¹⁰⁸

On the other hand, there are very few known ruthenium based anti-cancer complexes containing iodide monodentate ligands or *trans* labile ligands. Additionally, two iodide ligands are also rare, encouraging the exploration of structure-activity relationships on *trans*-dihalide metal-based anti-cancer complexes. McGowan *et al.* have shown that *trans*-diiodide bis-picolinamide metal complexes represent a family of new anti-cancer drugs that exhibit interesting and promising results. This new family interacts with different biomolecules in a different mode of action which is still unknown.¹¹⁰

To strengthen the success of *trans* ruthenium complex, it is important to introduce the family of the dimethyl sulfoxide complexes. Briefly, the results obtained from antitumor activity are very striking, showing that the *trans*-[Ru(II)(DMSO)₄(Cl)₂] has greater activity than its *cis* analogue.¹¹¹

In the *cis* isomer three DMSO molecules are bound through sulfur in a *fac* configuration and the fourth is oxygen bonded, whereas the *trans* isomer have all the DMSO ligands S-bound. When dissolved in water, the *cis* isomer loses the O-bonded DMSO ligand, however, the *trans* compound loses two S-bonded DMSO ligands giving *cis*-diaqua species. Then, both hydrolysed isomers undergo slow reversible chloride dissociation forming cationic compounds. After this step, the *trans* species contain three reactive groups, whereas the *cis* one only has two. The three remaining DMSO ligands in the *cis* compound represent a considerable steric hindrance making the *cis* aqua species inert compared to the *trans* isomer. This difference correlates with a higher activity of the *trans* isomer as an antitumor agent. This was proved using circular dichroism (CD) to study the interaction between the ruthenium species and DNA.

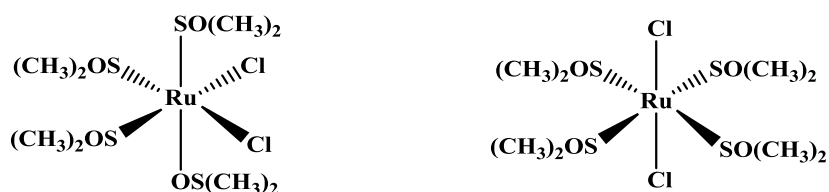


Figure 1-20: *cis*-[Ru(II)(DMSO)₄(Cl)₂] and *trans*-[Ru(II) (DMSO)₄(Cl)₂]¹¹¹

1.8 Biological Assays

The first stage of the preclinical phase for anti-cancer drug discovery and development is *in vitro* cytotoxicity screening.¹¹² These assays are widely used to measure the effectiveness of drugs towards a range of human cancer cell lines and to identify potential drugs for further analysis. After that, drug candidates can be classified as inactive, moderately active or highly active based on their IC₅₀ values. By definition, IC₅₀ is the concentration of the drug that is required to inhibit 50% of cell proliferation.

The first cytotoxicity screening assay was the MTT assay developed by Mosmann (1983).¹¹³ It measures the mammalian cell survival and proliferation by means of a yellow dye [3-(4,5-dimethylthiazol-2-yl)-2,5-diphenyl tetrazolium bromide]

(MTT) which is reduced *in situ* by living cells to a purple formazan.¹¹³ This process takes place principally in the mitochondria.¹¹⁴ However, the results of this assay might vary depending on the age and the type of the cell medium. This fact was linked to the amount of D-glucose present inside the cells, being inversely proportional to the reduction of MTT.

In 1988, Paul *et al.* developed the XTT assay, which replaces the MTT reagent for sodium 3'-[1-[(phenylamino)-carbonyl]-3,4-tetrazolium]-bis(4-methoxy-6-nitro) benzene sulfonic acid hydrate (XTT).¹¹⁵ This undergoes bio-reduction to give a -2 charge formazan being, therefore, more water soluble. Additionally and unlike MTT, it is soluble in the cell medium giving faster and more efficient results. Although, this assay also has problems with either the absence or inhibition reduction when missing the electron-coupling reagent.¹¹⁶ It is also thought that because of the presence of a disulfonate group, this XTT may have difficulties penetrating the cell membrane, which was previously reported.¹¹⁷

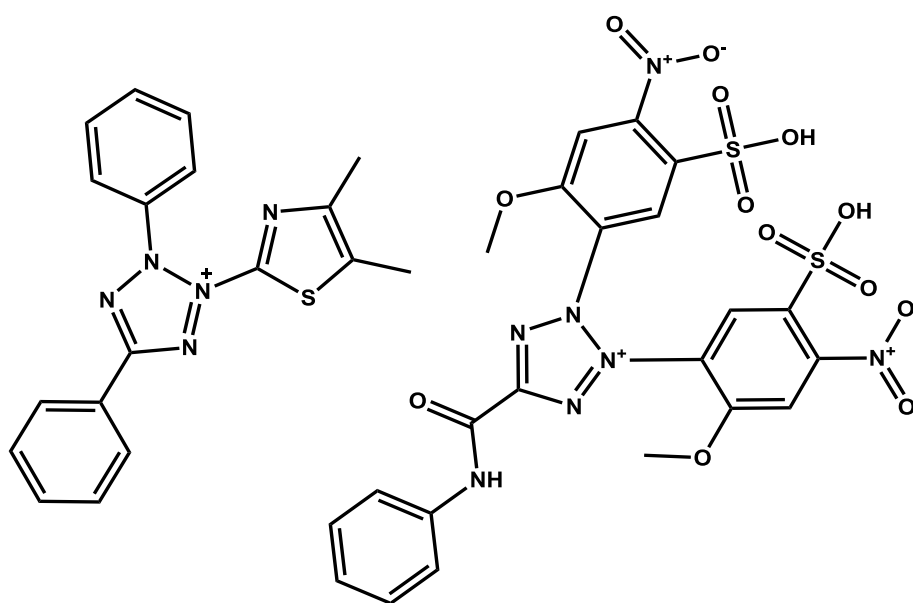


Figure 1-21: Tetrazolium salts used for cell survival. *Left*, MTT assay; *Right*, XTT assay.

In order to solve the problems associated with both assays, a new non-formazan assay based was developed by Skehan *et al.* in 1990. This was named the SRB assay.¹¹⁸ Chemically, it is an aminoxanthene dye known as Sulforhodamine B (SRB) which, under mild conditions, binds to an amino acid residue through two sulfonic groups.¹¹⁹ Compared to the MTT and XTT assays, it has a shorter incubation period and more consistent results over a larger range of cell lines.

However, the outcome *versus* elaboration balance is very similar, thus the MTT assay remains widely used.¹²⁰

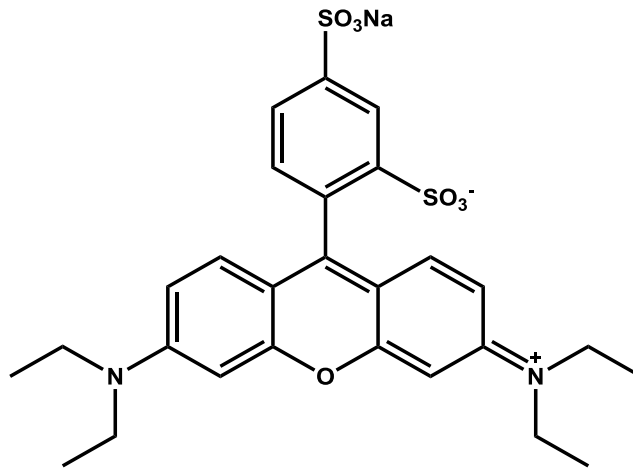


Figure 1-22: Structure of Sulforhodamine B

1.9 Objectives

Previously in the McGowan group, attention was paid to how isomers affect the anticancer activity. Pure ruthenium (III) *trans*-dichloride bis-picolinamide complexes were impossible to isolate, hence acknowledging what structural isomer gave the anticancer activity was difficult. By increasing the size of the organic ligands, it is expecting the formation of just one single structural isomer.

The objectives of this research project are the following:

- I) Design, synthesis and characterisation of quinaldamide ligands obtained through a condensation reaction.
- II) Synthesis of functionalised bis-quinaldamide¹²¹ *trans*-dichloride ruthenium complexes changing the electronics and the sterics of the quinaldamide ligands to establish structure activity relationship (SARs) and assess their potential biological activity.
- III) Determine the biological activity of the complexes describe in point II under the supervision of the collaborator Professor Roger M. Phillips at the University of Huddersfield.

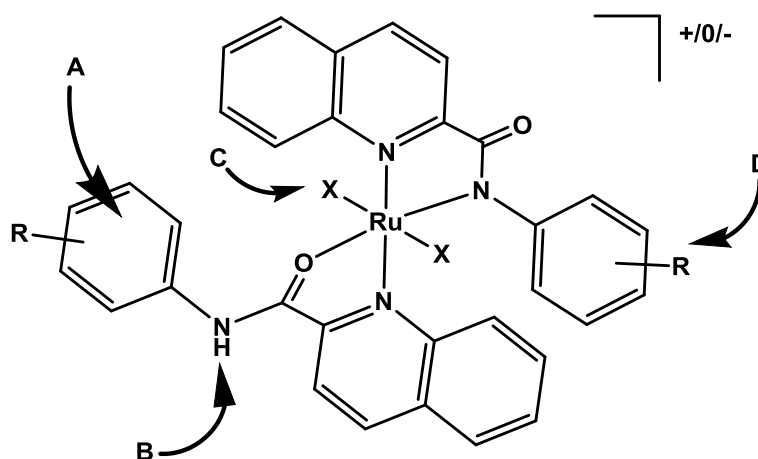


Figure 1-23: General structure for the di-halide complexes explaining the different fragments

The metal complexes describe in objectives, part II and part III contain several fragments (**Figure 1-23**), which have been proven to be important for anti-cancer activity. For the neutral complexes, these features are:

- A)** planar aromatic groups which may cause an intercalation process with the DNA nucleobases,
- B)** the acidic proton which may interact with acceptor sites on the DNA chain as a hydrogen binding donor,
- C)** the halide labile ligand which will allow to control hydrolysis and,
- D)** the functional groups which will either increase or decrease the hydrophilicity of the complexes.

All novel ligands and complexes synthesised will be characterised by means of IR spectroscopy, NMR spectroscopy for the ligands, ESI-MS (Electrospray Ionization Mass Spectrometry), EA (Elemental Analysis) and X-ray diffraction when appropriate.

The complexes will be assessed for their anti-cancer potential activity by determining their cytotoxicities using the MTT assay and gaining structure activity relationships by carrying hydrophobicity studies, hydrolysis and further biological assays. Complementary biological studies like antibacterial and antifungal properties will be determined.

References

- ¹Lodish, H.; Berk, A.; Zipursky, L. S.; Matsudaira, P.; Baltimore, D.; Darnell, J. *Molecular Cell Biology*, ISBN 0-7167-3136-3, W. H. Freeman, New York, **2000**, Cap. 9.
- ²Franklin, R.; Gosling, R.G.; *Nature*, **1953**, 172, 156-157.
- ³Watson, J. D.; Crick, F. H. C.; *Nature*, **1953**, 171, 737-738.
- ⁴Crick, F. H. C.; *Symp. Soc. Exp. Biol.* **1958**, 12, 138-163.
- ⁵Crick, F. H. C. *Nature*, **1970**, 227, 561-563.
- ⁶Barillot, E.; Calzone, L.; Hupé, P.; Vert, J-P.; Zinovyev, A.; *Computational Systems Biology of Cancer*, ISBN 9781439831441, CRC Press, **2012**.
- ⁷Blackburn, G. M.; Gait, M.J.; Loakes, D.; Williams, D. M.; *Nucleic Acids in Chemistry and Biology*, ISBN-10: 0-85404-654-2, RSC Publishing, Cambridge, **2006**; cap. 2.
- ⁸Otwinowski, Z.; Schevitz, R. W.; Zhang, R-G.; Lawson, C.L.; Joachimiak, A.; Marmorstein, R. Q.; Luisi, B. F.; Sigler, P. B. *Nature*, **1988**, 335, 321-329.
- ⁹Dickerson, R. E.; Drew, H. R. *J. Mol. Biol.* **1981**, 149, 761-786.
- ¹⁰Privalov, P. L.; Dragan, A. I.; Crane-Robinson, C.; Breslauer, K. J.; Remeta, D. P.; Minetti, C. A. S. A. *J. Mol. Biol.*, **2007**, 365, 1-9.
- ¹¹Li, Y. J.; Fu, X. H.; Liu, D. P.; Liang, C. *Int. J. Biochem. Cell. Biol.* **2004**, 36, 1411-1423.
- ¹²Khorasanizadeh, S. *Cell*, **2004**, 116, 259-272.
- ¹³Alberts, B.; Johnson, A.; Lewis, J.; Raff, M.; Roberts, K.; Walter, P. *How cells read the genome: from DNA to protein. Molecular Biology of the Cell, 4 ed.*; Garland Science: New York, **2001**; pp 299-466.
- ¹⁴www.genome.gov (accessed 31/03/2019)
- ¹⁵Cai, X.; Gray Jr, P. J.; Von Hoff, D. *Cancer Treat. Rev.* **2009**, 35, 437-450.
- ¹⁶Berthet, N.; Michon, J.; Lhomme, J.; Teulade-Fichou, M. P.; Vigneron, J-P.; Lehn, J-M. *Chem. Eur. J.* **1999**, 5, 3625-3630.
- ¹⁷Davies, J.; Dodson, E. J.; Moore, M. H. *Biochemistry-US*, **1995**, 34, 415-425.
- ¹⁸Shahabadi, N.; Mohammadi, S.; *Bioinorg. Chem. Appl.* **2012**, 2012, ID: 571913.
- ¹⁹Praseuth, D.; Guieysse, A. L.; Hélène, C. *Biochem. Biophys. Acta* **1999**, 1489, 181-206.

- ²⁰Da Ros, T.; Spalluto, G.; Prato, M.; Saison-Behmoaras, T; Boutorine, A.; Cacciari, B. *Curr. Med. Chem.*, **2005**, 12, 71-88.
- ²¹Wemmer, D. E.; *Proc. Annu. Rev. Biophys. Biomol. Struct.* **2000**, 29, 439-461.
- ²²Nelson, S.M.; Ferguson, L. R.; Denny, W. A.; *Mutat. Res.* **2007**, 623, 24-40.
- ²³Komor, A.C.; Barton, K.; *Chem. Commun.*, **2013**, 49, 3617-3630.
- ²⁴Song, H.; Kaiser, J. T.; Barton, J. K. *Nat. Chem.*, **2012**, 4, 615-620.
- ²⁵Bos, J. L.; *Cancer Res.* **1989**, 49, 4682-4689.
- ²⁶Miller, A. B.; Hoogstraten, B.; Staquet, M.; Winkler, A.; *Cancer*, **1981**, 47, 207-214.
- ²⁷Rosenberg, B.; Vancamp, L.; Krigas, T.; *Nature*, **1965**, 205, 698-699.
- ²⁸Zorbas, H.; Keppler, B. K.; *Chembiochem*, **2005**, 6, 1157-1166.
- ²⁹Fichtinger-Schepman, A. M. J.; Van der Veer, J. L.; Den Hartog, J. H. J.; Lohman, P. H. M.; Reedijk, J.; *Biochem.*, **1985**, 24, 707-713.
- ³⁰Szymkowski, D. E.; Yarema, K.; Essigmann, J. M.; Lippard, S. J.; Wood, R. D.; *Biochem.*, **1992**, 89, 10772-10776.
- ³¹Burstyn, J. N.; Heiger-Bernays, W. J.; Cohen, S. M.; Lippard, S. J.; *Nucleic Acids Res.*, **2000**, 28, 4237-4243.
- ³²Stehlikova, K.; Kosthunova, H.; Kasparkova, J.; Brabec, V.; *Nucleic Acids Res.*, **2002**, 30, 2894-2898.
- ³³Ferlay, S. H.; Bray, F.; Forman, D.; Mathers, C. D.; Parkin, D.; Lyon, France: *International Agency for Research on Cancer*, **2010**.
- ³⁴Ciccarelli, R. B.; Solomon, M. J.; Varshavsky, A.; Lippard, S. J.; *Biochem.*, **1985**, 24, 7533-7540.
- ³⁵Barry, M. A.; Behnke, C. A.; Eastman, A.; *Biochem. Pharmacol.*, **1990**, 40, 2353-2362.
- ³⁶Ribeiro Reily Rocha, C.; Molina Silva, M.; Quinet, A.; Cabral-Neto, J. B.; Martins Menck, C. F.; *Clinics*, **2018**, 73 (suppl 1), e478s.
- ³⁷Jamieson, E. R.; Lippard, S. J.; *Chem. Rev.*, **1999**, 99, 2467-2498.
- ³⁸Yu, F.; Megyesi, J.; Price, P. M.; *Am. J. Physiol.*, **2008**, 295, F44-52.
- ³⁹Rabik, C. A.; Dolan, M. E.; *Cancer Treat. Rev.*, **2007**, 33, 9-23.
- ⁴⁰Perez, R. P.; *Eur. J. Cancer*, **1998**, 34, 1535-1542.
- ⁴¹Eastman, A.; *Cancer Treat. Rev.*, **1991**, 57, 233-249.
- ⁴²Köberle, B.; Tomicic, M. T.; Usanova, S.; Kaina, B.; *Biochim. Biophys. Acta*, **2010**, 1806, 172-182.

- ⁴³Shea, T. C.; Flaherty, M.; Elias, A.; Eder, J. P.; Antman, K.; Begg, C.; Schnipper, L.; Frei, E.; Frei, W. D.; *J. Clin. Oncol.*, **1989**, 7, 651-661.
- ⁴⁴Calvert, A. H.; Newell, D. R.; Gumbrell, L. A.; O'Reilly, S.; Burnell, M.; Boxall, F. E.; Siddik, Z. H.; Judson, I. R.; Gore, M. E.; Wiltshaw, E.; *J. Clin. Oncol.*, **1989**, 7, 1748-1756.
- ⁴⁵Natarajan, G.; Malathi, R.; Holler, E.; *Biochem. Pharm.*, **1999**, 58, 1625-1629.
- ⁴⁶Berners-Price, S. J.; Ronconi, L.; Sadler, P. J.; *Prog. Nucl. Mag. Res. Sp.*, **2006**, 49, 65-98.
- ⁴⁷Uchida, N.; Takeda, Y.; Sadler, P. J.; *Inorg. Chem. (Wash., D. C.)*, **1993**, 32, 1333-1340.
- ⁴⁸Stordal, B.; Pavlakis, N.; Davey, R.; *Cancer Treat. Rev.*, **2007**, 33, 347-357.
- ⁴⁹Faivre, S.; Chan, D.; Salinas, R.; Woynarowska, B.; Woynarowski, J. M.; *Biochem. Pharm.*, **2003**, 66, 225-237.
- ⁵⁰Misset, J. L.; *Br. J. Cancer*, **1998**, 77 Suppl 4, 4-7.
- ⁵¹Bleiberg, H.; *Br. J. Cancer*, **1998**, 77 Suppl 4, 1-3.
- ⁵²Degardin, M.; Armand, J. P.; Chevallier, B.; Cappelaere, P.; Lentz, M.-A.; David, M.; Roche, H.; *Invest. New Drugs*, **1995**, 13, 253-255.
- ⁵³Gietema, J. A.; Veldhuis, G. J.; Guchelaar, H. J.; Willemse, P. H.; Uges, D. R.; Cats, A.; Boonstra, H.; van der Graaf, W. T.; Sleijfer, D. T.; de Vries, E. G. *Br. J. Cancer*, **1995**, 71, 1302-1307.
- ⁵⁴Welink, J.; Boven, E.; J. Vermorken, B.; Gall H. E.; Van der Vijgh, W. J. F.; *Clin. Cancer Res.*, **1999**, 5, 2349-2358.
- ⁵⁵Chen, Y.; Guo, Z.; Parsons, S.; Sadler, P. J.; *Chem.- A Eur. J.*, **1998**, 4, 672-676.
- ⁵⁶Raynaud, F. I.; Mistry, P.; Donaghue, A.; Poon, G. K.; Kelland, L. R.; Barnard, C. F. J.; Murrer, B. A.; Harrap, K. R.; *Cancer Chemoth. Pharm.*, **1996**, 38, 155-162.
- ⁵⁷Kelland, L. R.; *Expert opinion on investigational drugs*, **2000**, 9, 1373-1382.
- ⁵⁸Choy, H.; Park, C.; Yao, M.; *Clinical Cancer Research*, **2008**, 14, 1633-1638.
- ⁵⁹Ceresa, C.; Bravin, A.; Cavaletti, G.; Pellei, M.; Santini, C.; *Curr. Med. Chem.*, **2014**, 21, 2237-2265.
- ⁶⁰Alessio, E.; Mestroni, G.; Bergamo, A.; Sava, G.; *Curr. Top. Med. Chem.*, **2004**, 4, 1525-1535.

- ⁶¹ Alessio, E.; Mestroni, G.; Bergamo, A.; Sava, G.; Ruthenium anticancer drugs. In: *Metal Ions Biological Systems (42) Metal Complexes in Tumor Diagnosis and as Anticancer agents*. CRC Press, **2004**, 323-351.
- ⁶² Anghileri, L. J.; Krebsforsch, Z.; *Klin. Onkol. Cancer Res. Clin. Oncol.*, **1975**, 83, 213-217.
- ⁶³ Suss-Fink, G.; *Dalton Trans.*, **2010**, 39, 1673-1688.
- ⁶⁴ Reedijk, J.; *Platinum Met. Rev.*, **2008**, 52, 2-11.
- ⁶⁵ Allardyce, C. S.; Dyson, P. J.; *Platinum Met. Rev.*, **2001**, 45, 62-69.
- ⁶⁶ Clarke, M. J.; Zhu, F.; Frasca, D. R.; *Chem. Rev.*, **1999**, 99, 2511-2533.
- ⁶⁷ Clarke, M. J.; *Coord. Chem. Rev.*, **2003**, 236, 209-233.
- ⁶⁸ Fernandez, R.; Melchart, M.; Habtemariam, A.; Parsons, S.; Sadler, P. J.; *Chem. Eur. J.*, **2004**, 10, 5173-5179.
- ⁶⁹ Clarke, M. J.; Bailey, V.; Doan, P.; Hiller, C.; LaChance-Galang, K. J.; Daghljan, H.; Mandal, S.; Bastos, C. M.; Lang, D.; *Inorg. Chem.*, **1996**, 35, 4896-4903.
- ⁷⁰ Allardyce, C. S.; Dyson, P. J.; Ellis, D. J.; Salter, P. A.; Scopelliti, R.; *J. Organomet. Chem.*, **2003**, 668, 35-42.
- ⁷¹ Sanchez-Delgado, R. A.; Navarro, M.; Perez, H.; Urbina, J. A.; *J. Med. Chem.*, **1996**, 39, 1095-1099.
- ⁷² Anghileri, L.J.; Krebsforsch, Z.; *Klin. Onkol. Cancer Res. Clin. Oncol.*, **1975**, 83, 213-217.
- ⁷³ Chu, A.J.; Wang, Z.G.; Nwobi, O.I.; Beydoun, S.; *Br. J. Pharmacol.*, **2001**, 133, 659-664.
- ⁷⁴ Kepler, B.K.; (ed.). *Metal Complexes in Cancer Chemotherapy*. VCH Weinheim, NY, USA (**1993**)
- ⁷⁵ Clarke M.J.; Zhu, F.C.; Frasca, D. R.; *Chem. Rev.*, **1999**, 99, 2511-2533.
- ⁷⁶ Sava, G.; Capozzi, I.; Clerici, K.; Gagliardi, G.; Alessio, E.; Mestroni, G.; *Clin. Exp. Metastasis*, **1998**, 16, 371-379.
- ⁷⁷ Bergamo, A.; Gagliardi, R.; Scarcia, V.; Furlani, A.; Alessio, E.; Mestroni, G.; Sava, G. *J. Pharm. Expt. Ther.*, **1999**, 289, 559-564.
- ⁷⁸ Sava, G.; Capozzi, I.; Clerici, K.; Gagliardi, G.; Alessio, E.; Mestroni, G.; *Clin. Exp. Met.*, **1998**, 16, 371-379.
- ⁷⁹ Sava, G.; Pacor, S.; Bergamo, A.; Cocchietto, M.; Mestroni, G.; Alessio, E.; *Chem. Biol. Interact.*, **1995**, 95, 109-126.

- ⁸⁰ Smith, C. A.; Sutherland-Smith, A. J.; Keppler, B. K.; Kratz, F.; Baker, E. N.; *J. Biol. Inorg. Chem.*, **1996**, 1, 424-431.
- ⁸¹ Bratsos, I.; Jedner, S.; Gianferrara, T.; Alessio, E.; *Chimia*, **2007**, 61, 692-697.
- ⁸² Webb, M. I.; Walsby, C. J.; *Dalton Trans.*, **2011**, 40, 1322-1331.
- ⁸³ Keppler, B. K.; Rupp, W.; Juhl, U. M.; Endres, H.; Niebl, R.; Balzer, W.; *Inorg. Chem.*, **1987**, 26, 4366-4370.
- ⁸⁴ Hartinger, C. G.; Zorbas-Seifried, S.; Jakupec, M. A.; Kynast, B.; Zorbas, H.; Keppler, B. K.; *J. Inorg. Biochem.*, **2006**, 100, 891-904.
- ⁸⁵ Peti, W.; Pieper, T.; Sommer, M.; Keppler, B. K.; Giester, G.; *Eur. J. Inorg. Chem.*, **1999**, 1551-1555.
- ⁸⁶ Trondl, R.; Heffeter, P.; Kowol, C. R.; Jakupec, W. B.; Keppler, B. K.; *Chem. Sci.* **2014**, 5, 2925-2932.
- ⁸⁷ Sheldrick, W. S.; Heeb, S.; *Inorg. Chim. Acta*, **1990**, 168, 93-100.
- ⁸⁸ Habtemariam, A.; Melchart, M.; Fernandez, R.; Parsons, S.; Oswald, I. D. H.; Parkin, A.; Fabbiani, F. P. A.; Davidson, J. E.; Dawson, A.; Aird, R. E.; Jodrell, D. I.; Sadler, P. J.; *J. Med. Chem.*, **2006**, 49, 6858-6868.
- ⁸⁹ Morris, R. E.; Aird, R. E.; Murdoch, P. D. S.; Chen, H.; Cummings, J.; Hughes, N. D.; Parsons, S.; Parkin, A.; Boyd, G.; Jodrell, D. I.; Sadler, P. J.; *J. Med. Chem.*, **2001**, 44, 3616-3621.
- ⁹⁰ Aird, R. E.; Cummings, J.; Ritchie, A. A.; Muir, M.; Morris, R. E.; Chen, H.; Sadler, P. J.; Jodrell, D. I. *Br. J. Cancer*, **2002**, 86, 1652-1657.
- ⁹¹ Almodares, Z.; *Ph.D Thesis*, University of Leeds, 2010.
- ⁹² Canty, A. J.; Lee, C. V.; *Inorg. Chim. Acta*, **1981**, 54, L205-L206.
- ⁹³ Collins, T. J.; *Acc. Chem. Res.*, **1994**, 27, 279-285.
- ⁹⁴ van Rijt, S. H.; Hebden, A. J.; Amaresekera, T.; Deeth, R. J.; Clarkson, G. J.; Parsons, P.; McGowan, P. C.; Sadler, P. J.; *J. Med. Chem.*, **2009**, 52, 7753-7764.
- ⁹⁵ Camm, K. D.; El-Sokkary, A.; Gott, A. L.; Stockley, P. G.; Belyaeva T.; McGowan, P. C.; *Dalton Trans.*, **2009**, 10914-10925.
- ⁹⁶ Rafferty, K.; *Ph.D Thesis*, University of Leeds, 2008.
- ⁹⁷ Lucas, S. J.; Lord, R. M.; Wilson, R. L.; Phillips, R. M.; Sridharana, V.; McGowan, P. C.; *Dalton Trans.*, **2012**, 41, 13800-13802.
- ⁹⁸ Cleare, M. J.; Hoeschele, J. D.; *Bioinorg. Chem.*, **1973**, 2, 187-210.
- ⁹⁹ Banerjea, D.; Basolo, F.; Pearson, R. G.; *J. Am. Chem. Soc.*, **1957**, 79, 4055-4062.

- ¹⁰⁰ Reishus, J. W.; Martin, D. S.; *J. Am. Chem. Soc.*, **1961**, 83, 2457-2462.
- ¹⁰¹ Romero-Canelon, I.; Salassa, L.; Sadler, P. J.; *J. Med. Chem.*, **2013**, 56, 1291-1300.
- ¹⁰² Sanford, M. S.; Love, J. A.; Grubbs, R. H.; *J. Am. Chem. Soc.*, **2001**, 123, 6543-6554.
- ¹⁰³ Rosenberg, B.; Van Camp, L.; Grimley, E. B.; Thomson, A. J.; *J. Biol. Chem.*, **1967**, 242, 1347-1352.
- ¹⁰⁴ Cleare, M. J.; Hoeschele, J. D.; *Bioinorg. Chem.*, **1973**, 2, 187-210.
- ¹⁰⁵ Cleare, M. J.; Hoeschele, J. D.; *Plat. Metals Rev.*, **1973**, 17, 2-13.
- ¹⁰⁶ Natile, G.; Coluccia, M.; *Coor. Chem. Rev.*, **2001**, 218-217, 383-410.
- ¹⁰⁷ Coluccia, M.; Natile, G.; *Anti-Cancer Agents Med. Chem.*, **2007**, 7, 111-123.
- ¹⁰⁸ Farrell, N.; Kelland, L. R.; Roberts, J. D.; Van Beusichem, M.; *Cancer Res.*, **1992**, 52, 5065-5072.
- ¹⁰⁹ Farrer, N. J.; Woods, J. A.; Salassa, L.; Zhao, Y.; Robinson, K. S.; Clarkson, G.; Mackay, F. S.; Sadler, P. J.; *Angew. Chem. Intl. Ed.*, **2010**, 49, 8905-8908.
- ¹¹⁰ Basri, A. M. B. H.; *Ph.D. Thesis*; **2014**.
- ¹¹¹ Brabec V.; Nováková O.; *Drug Resist Updat*, **2006**, 9, 111-122.
- ¹¹² Hughes, J. P.; Rees, S.; Kalindjian, S. B.; Philpott, K. L.; *Br. J. Pharm.*, **2011**, 162, 1239-1249.
- ¹¹³ Mosmann, T.; *J. Immunol. Methods*, **1983**, 65, 55.
- ¹¹⁴ Vistica, D. T.; Skehan, P.; Scudiero, D.; Monks, A.; Pittman, A.; Boyd, M. R.; *Cancer Res.*, **1991**, 51, 2515.
- ¹¹⁵ Paull, K. D.; Shoemaker, R. H.; Boyd, M. R.; Parsons, J. L.; Risbood, P. A.; Barbera, W. A.; Sharma, M. N.; Baker, D. C.; Hand, E.; Scudiero, D. A.; Monks, A.; Alley, M. C.; *J. Heterocycl. Chem.*, **1988**, 25, 911.
- ¹¹⁶ Scudiero, D. A.; Shoemaker, R. H.; Paull, K. D.; Monks, A.; Tierney, S.; Nofziger, T. H.; Currens, M. J.; Seniff, D.; Boyd, M. R.; *Cancer Res.*, **1988**, 48, 4827.
- ¹¹⁷ Knauf, P. A.; Rothstein, A.; *J. Gen. Physiol.*, **1971**, 58, 190-211.
- ¹¹⁸ Skehan, P.; Storeng, R.; Scudiero, D.; Monks, A.; McMahon, J.; Vistica, D.; Warren, J. T.; Bokesch, H.; Kenney, S.; Boyd, M. R.; *J. Natl Cancer Inst.*, **1990**, 82, 1107.
- ¹¹⁹ Lillie, R. D.; *Conn's Biological Stains*, Willians and Wilkins, **1977**.

¹²⁰ Keepers, Y. P.; Pizao, E. P.; van Ark-Otte, J.; Pinedo, H. M.; Peters, G. J.;
Eur. J. Cancer, **1997**, 27, 897-900.

¹²¹ Basri, A. M. B. H.; *Ph.D. Thesis*; **2014**, 45-77.

Chapter 2 Synthesis of functionalised quinaldamide ligands

2.1 Background

The development of chemistry in synthesising peptide-based ligands has great relevance due to their roles played in biological activity, where the amide bond [-C=O-NH-] is the fundamental linker when forming proteins.¹ Comparing them to the Schiff bases [R₂C=NR'], they show better stability towards hydrolysis reactions,² being an important fact for biological systems that allows both protein construction and maintenance. The synthetic pathways towards quinaldamide derivatives involve the reaction between amines with either 2-quinaldic carboxylic acid,³ or the acyl chloride derivative.⁴ Bhattacharya *et al.* have developed a preparation for high yielding picolinamide ligands adapted from Barnes *et al.*, by a condensation reaction of 2-picolinic acid and the respective aniline in presence of a base.^{5,6} The structural similarity between the 2-picolinic acid and the 2-quinaldic acid (**Figure 2-1**) allows the reproduction under modified conditions of the synthesis of the quinaldamide ligands. 2-quinoline carboxylic acid differs from 2-picoline carboxylic acid because the former contains a benzene group fused to the *N*-containing ring. This group was specifically chosen as similar structures have been proved to show a great anticancer activity on their own, but not when coordinated to a metal. Moreover, these building blocks are present in some of the current pharmaceutical drugs, but their bulkiness and rigidity make them challenging to work with.⁷

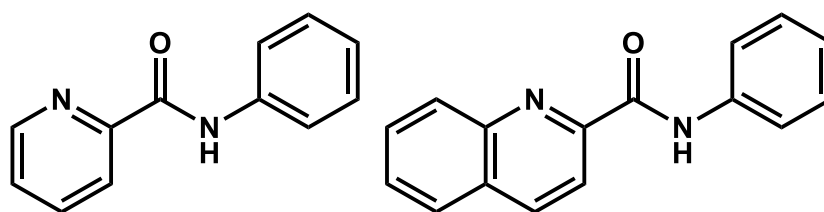


Figure 2-1: Backbones of 2-picolinamide (*left*) and 2-quinaldamide (*right*)

Both ligands have the ability to chelate to metal centres in three ways: as monoanionic *N,N*-donors, monoanionic *N,O*-donors and neutral *N,O*-donors, as shown in **Figure 2-2**.

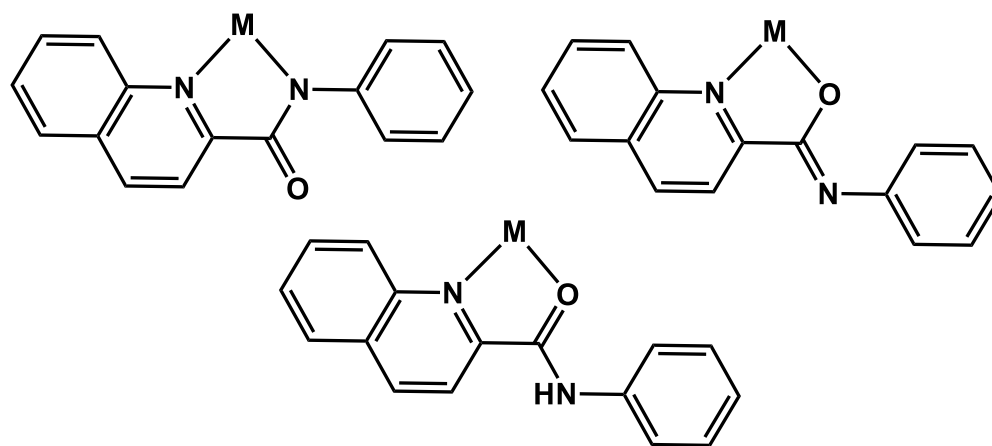


Figure 2-2: Different coordination modes for the quinaldamide ligands, (*top left*) $[N,N]$ anionic, (*top right*) $[N,O]$ anionic and (*bottom*) $[N,O]$ neutral

Coordination chemistry has a wide range of applications, specifically in biology, medicine and pharmacology. It was shown that the strong monoanionic σ -donor bonds coordinate to the metal centres stabilising the high oxidation state,⁸ whereas the neutral dative/coordinative bonds favour the lower oxidation states.⁹ These differences in the potential modes of coordination contained within the ligands can tune the cytotoxic activities of the synthesised complexes in this thesis.

2.2 Synthesis of quinaldamide ligands

The quinaldamide-core ligand is shown in **Figure 2-3**. All ligands were synthesised and used in this project some were previously found in the literature;^{10,11} however, only the functional groups highlighted in blue have crystal structures reported in the CCDC data base. Some of the novel ligands synthesised in this project with full characterisation are shown in **Figure 2-4**.

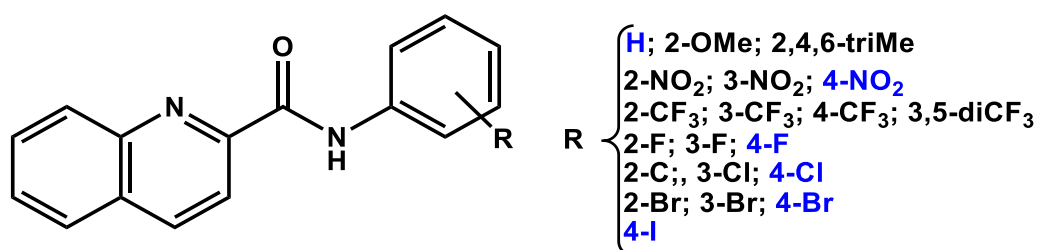


Figure 2-3: *Left*, chemical structure of the quinaldamide-core ligands; *Right*, ligands reported and highlighted in blue are in the CCDC data base

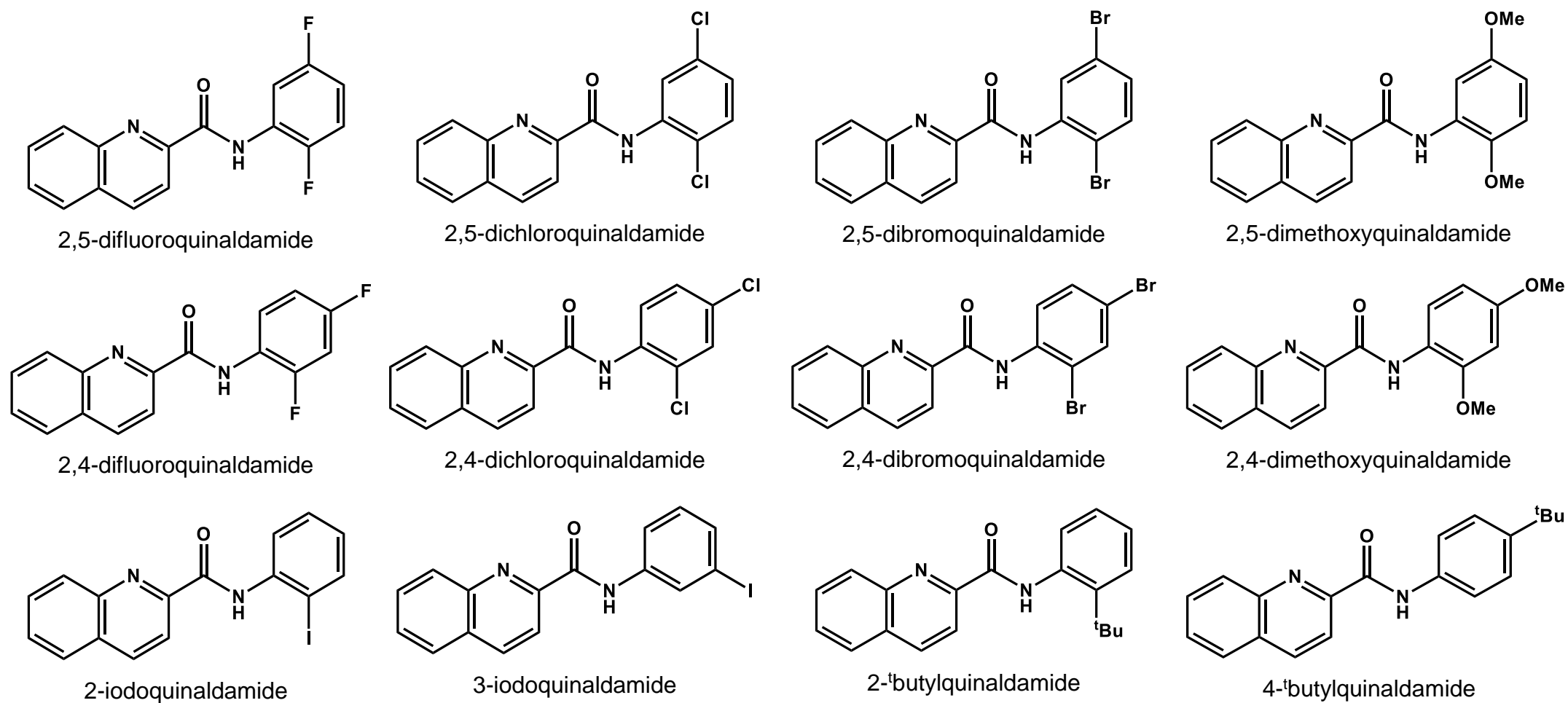
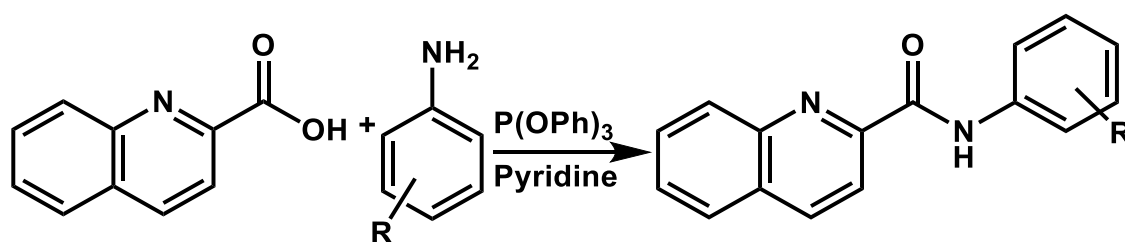


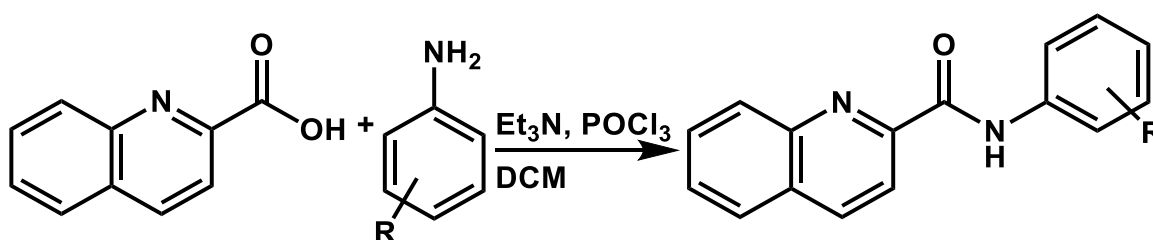
Figure 2-4: Novel functionalised quinaldamide ligands

The ligands containing electron withdrawing groups (EWGs) were synthesised according to the **Scheme 2.1** by a condensation reaction. (See **Chapter 6** for reaction conditions)



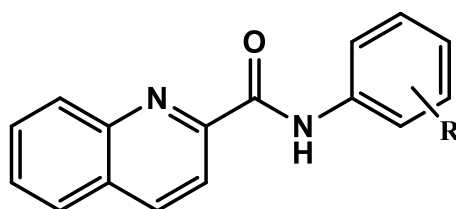
Scheme 2.1: General protocol to synthesise quinaldamide ligands containing electron withdrawing groups (EWGs)

The ligands containing electron donating groups (EDGs) were synthesised according to the **Scheme 2.2** developed by Qi,¹² as following **Scheme 2.1** gave an insoluble residue proved difficult to characterise. (See **Chapter 6** for reaction conditions).



Scheme 2.2: General synthetic pathway to obtain quinaldamide ligands containing electron donating groups (EDGs)

In **Figure 2.5**, the general structure, the different R groups with the numbering used through this thesis can be found.



R=	H	(2.1)	2- ⁱ Pr	(2.12)	4-CF ₃	(2.21)	2,4-diCl	(2.31)
	2-OMe	(2.2)	3- ⁱ Pr	(2.13)	3,5-diCF ₃	(2.22)	2,5-diCl	(2.32)
	2,4-diOMe	(2.3)	4- ⁱ Pr	(2.14)	2-F	(2.23)	2-Br	(2.33)
	2,5-diOMe	(2.4)	2,6-Di ⁱ Pr	(2.15)	3-F	(2.24)	3-Br	(2.34)
	2-Me	(2.5)	2-Me-6- ⁱ Pr	(2.16)	4-F	(2.25)	4-Br	(2.35)
	3-Me	(2.6)	2- ^t Bu	(2.17)	2,4-diF	(2.26)	2,4-diBr	(2.36)
	4-Me	(2.7)	4- ^t Bu	(2.18)	2,5-diF	(2.27)	2,5-diBr	(2.37)
	2,4,6-triMe	(2.8)	2-Cl	(2.19)	2-Cl	(2.28)	3-I	(2.39)
	2-Et	(2.9)	2-CF ₃	(2.20)	3-Cl	(2.29)	4-I	(2.40)
	3-Et	(2.10)	3-CF ₃	(2.30)	4-Cl	(2.30)		
	4-Et	(2.11)						

Figure 2-5: Summary of ligands with their respective numbering. Blue highlighted ligands are novel. Green highlighted are found in literature with no characterisation data. Black highlighted ligands are already known but used in this research project.

2.3 Characterisation of functionalised quinaldamide ligands

N-functionalised quinaldamide or 2-quinolinecarboxamide ligands were prepared *via* **Scheme 2.1** to obtain ligands electron-withdrawing ligands, and *via* **Scheme 2.2** to obtain electron-donating ligands as pure products in yields ranging between 32 and 86%. They were characterised by means of IR, ¹H NMR, ¹³C{¹H} NMR, ¹⁹F{¹H} NMR when appropriate, COSY, NOESY, HMQC, DEPT, elemental analysis, high resolution mass spectrometry and single crystal x-ray diffraction when crystals were suitable. Due to the similar chemical structure of all the quinaldamide ligands, their respective IR and NMR spectra show similar trends. Thus, only the spectra recorded for **2.3** are discussed in this section as well as its crystal structure. Crystal structures of ligands **2.30** and **2.37** are also discussed in this chapter. The full data collected for the remaining ligands can be found in the experimental chapter and appendix.

2.3.1 IR spectrum for ligand 2.3

The IR spectrum for the ligand **2.3** is as shown in **Figure 2-6**. It can be seen several bands of different intensities between 1600-800 cm^{-1} . The ligand is constituted by two main functional groups: the moderate NH monosubstituted stretching band is observed at 3365 cm^{-1} and the intense C=O stretching band at 1681 cm^{-1} . The peaks coincide with the reported values of amide bonds, where the C=O band falls between 1640-1690 cm^{-1} , the NH stretching falls between 3100-3500 cm^{-1} and the NH bending falls between 1550-1640 cm^{-1} . The ranges for C-H aromatic and C=C are in the right regions for reported aromatic rings however with little relevance.

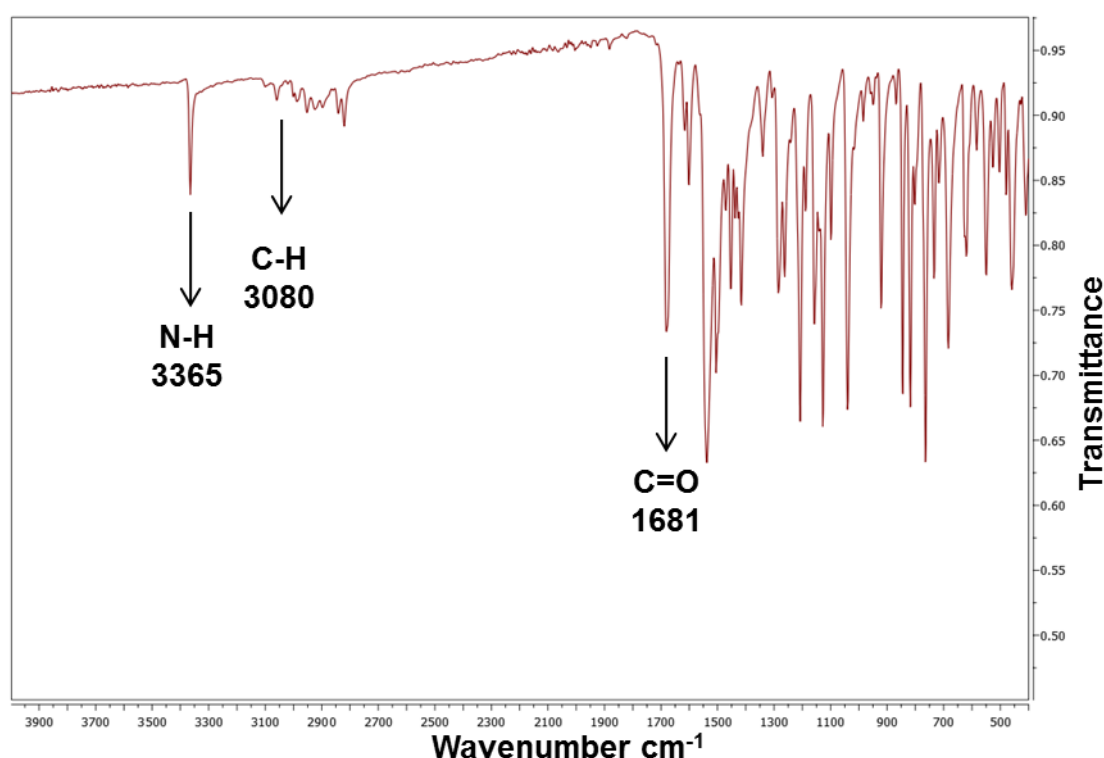


Figure 2-6: IR spectrum of the ligand **2.3**

2.3.2 NMR spectra for ligand 2.3

A labelled diagram of ligand **2.3** is shown in **Figure 2-7**. The ^1H and $^{13}\text{C}\{^1\text{H}\}$ spectra are shown in **Figure 2-8** and **Figure 2-9**, respectively. In **Table 2.1**, the chemical shift assignments are collected. In order to assign all of the aromatic protons and the carbon atoms contained within the molecular structure, NOESY, HMQC, HMBC and DEPT were carried out. A broad NH singlet is seen at 10.54 ppm, different peaks with a variety of multiplicities are found between 8.50-7.50 ppm that correspond to the aromatic protons of the quinaldamide core and specified in **Table 2.1**. Two intense peaks assigned to the protons of the

methoxy groups are found at 3.92 and 3.78 ppm. The $^{13}\text{C}\{^1\text{H}\}$ NMR spectrum shows a C=O peak at 161.8 ppm and the C-OMe peaks can be seen at 55.9 and 55.5 ppm.

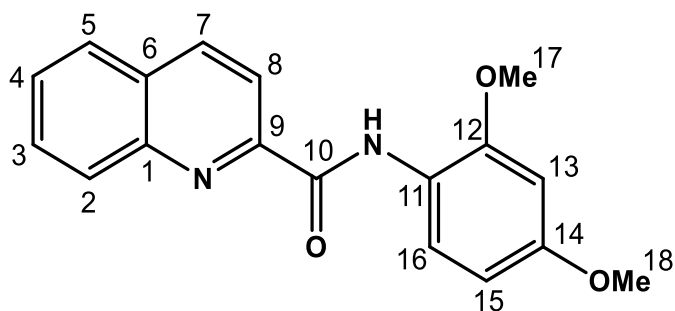


Figure 2-7: Labelled diagram of ligand 2.3

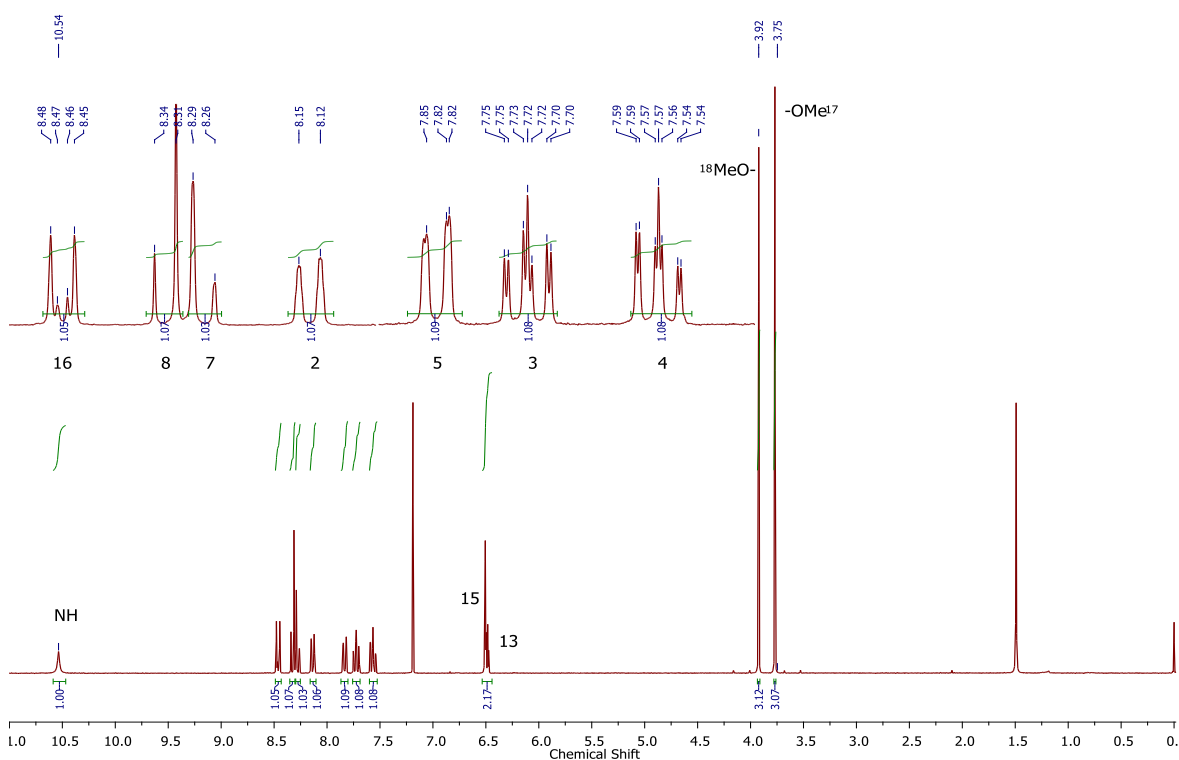


Figure 2-8: ^1H NMR spectrum of the ligand 2.3 (CDCl_3 , 300 MHz, 300 K)

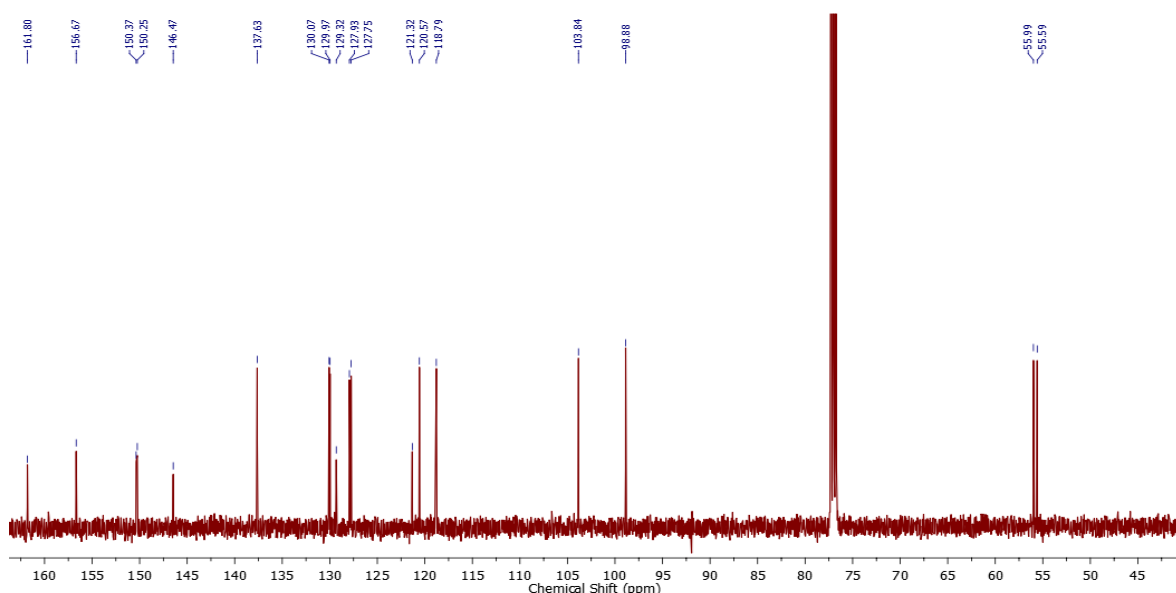


Figure 2-9: $^{13}\text{C}\{^1\text{H}\}$ NMR spectrum of the ligand **2.3** (CDCl_3 , 75 MHz, 300 K)

Table 2.1: ^1H and $^{13}\text{C}\{^1\text{H}\}$ NMR chemical shift assignments for the ligand **2.3**

Chemical Shift	Multiplicity	Assignment	Chemical Shift	Assignment
10.54	bs	NH	161.80	C^{10}
8.46	dd	H^{16}	156.67	C^1
8.33	d	H^8	150.37	C^6
8.28	d	H^7	150.25	C^{14}
8.14	d	H^2	146.47	C^{12}
7.84	dd	H^5	137.63	C^7
7.72	ddd	H^3	130.07	C^2
7.57	ddd	H^4	129.97	C^3
6.51	d	H^{15}	129.32	C^9
6.49	d	H^{13}	127.93	C^4
3.92	s	OMe^{18}	127.75	C^5
3.75	s	OMe^{17}	121.32	C^{11}
			120.57	C^{16}
			118.79	C^8
			103.84	C^{15}
			98.88	C^{13}
			55.99	C^{18}
			55.59	C^{17}

2.3.3 X-Ray structure for ligand 2.3

Colourless prisms suitable for X-ray diffraction were obtained from a concentrated chloroform solution. Ligand **2.3** crystallised in a monoclinic cell and structural solution was performed in the space group $I2$ containing one molecule in the asymmetric unit. The molecular structure is shown in **Figure 2-10** and selected bond lengths and angles are given in **Table 2.2**. Ligand **2.3** adopts a *quasi*-planar configuration, in which the dihedral angle between the quinaldic ring and the aniline ring N(1)-C(9)-C(10)-N(2) is $1.422(3)^\circ$. Intramolecular hydrogen bonding exists between N(2)...N(1) with a bond distance of $2.676(2)$ Å, and between C(16)-H...O(1) with a bond distance of 2.493 Å. Ligand **2.3** arranges itself in parallel planes along the *a* axis as shown in **Figure 2-11** proving that there is π - π stacking with a centroid-centroid distance of 3.911 Å for the quinaldic ring and a centroid-centroid distance of 3.638 Å for the aniline rings, when viewed along the *c* axis (**Figure 2-12**) the ligand adopts a herringbone motif where the planes are held together by intermolecular hydrogen bonding between the methoxy hydrogens and the oxygens of the next molecules.

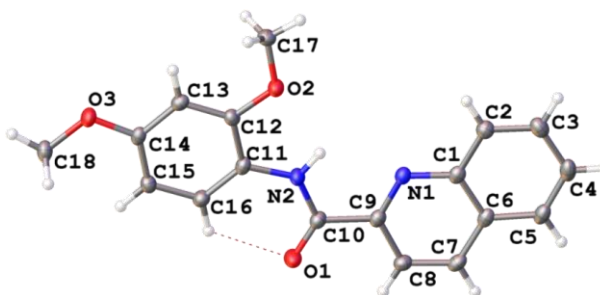


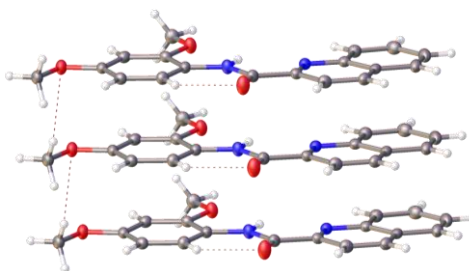
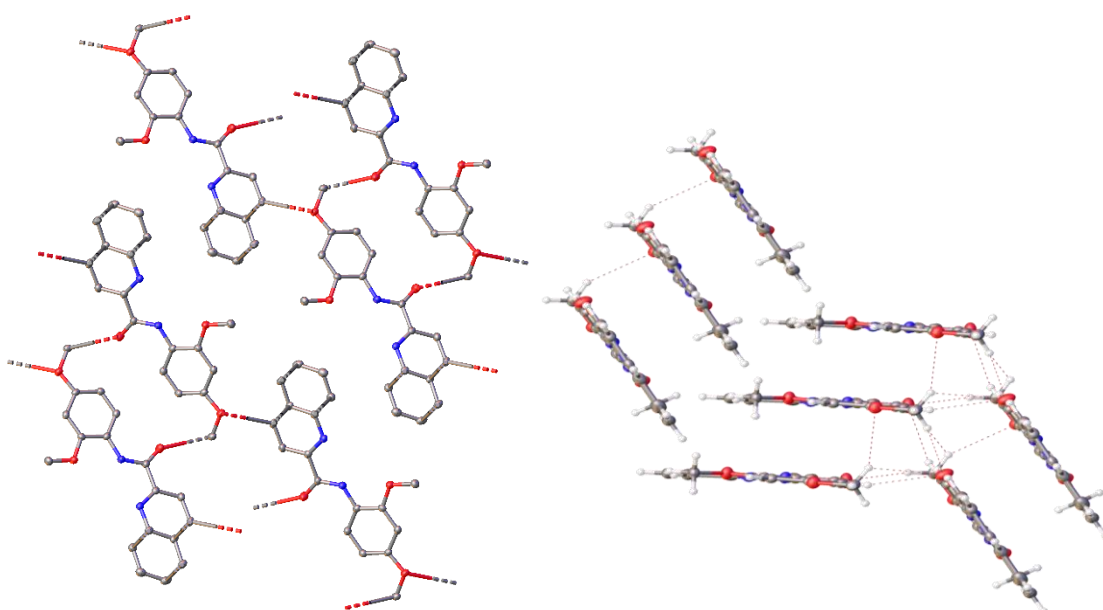
Figure 2-10: Molecular structure of ligand **2.3** showing intramolecular hydrogen bonds. Displacement ellipsoids are at the 50% probability level

Table 2.2: Selected angles for ligand **2.3** with esds shown in parenthesis

Bond	Angle (°)
N(1)-C(9)-C(10)	117.95(18)
C(9)-C(10)-O(1)	120.44(19)
O(1)-C(10)-N(2)	125.4(2)
C(10)-N(2)-C(11)	127.8(2)
N(2)-C(11)-C(16)	116.35(19)

Table 2.3: Selected bond lengths for ligand **2.3** with esds shown in parenthesis

Bond	Distance (Å)
C(1)-N(1)	1.370(3)
N(1)-C(9)	1.316(3)
C(9)-C(10)	1.510(3)
C(10)-O(1)	1.226(3)
C(10)-N(2)	1.344(3)
N(2)-C(11)	1.413(3)
C(11)-C(12)	1.384(3)
C(12)-O(2)	1.337(3)
O(2)-C(17)	1.417(3)

**Figure 2-11:** Packing diagram of ligand **2.3** in the a axis showing π - π stacking and intermolecular hydrogen bonds between the 4-methoxy oxygen and the 4'-methoxy hydrogens of the molecule below.**Figure 2-12:** Intermolecular hydrogen bonds (*left*) in the b axis and (*right*) in the c axis arranged in a herringbone motif.

2.3.4 X-Ray structure for ligand 2.30

Colourless needles suitable for x-ray diffraction were obtained from slow evaporation of a solution in methanol. Ligand **2.30** crystallised in an orthorhombic cell and solved in the space group $P2_12_12_1$ containing one molecule in the asymmetric unit. The molecular structure is shown in **Figure 2-13** and selected bond lengths and angles are given in **Table 2.4**. Ligand **2.30** adopts a *quasi*-planar configuration, in which the torsion angle between the quinaldic ring and the aniline ring N(1)-C(9)-C(10)-N(2) is $1.792(8)^\circ$. Intramolecular hydrogen bonding exists between N(2)...N(1) with a bond distance of $2.612(2)$ Å, and between C(16)-H...O(1) with a bond distance of 2.274 Å. Ligand **2.30** arranges itself in parallel planes along the b axis as shown in **Figure 2-13** showing π - π stacking interactions with a centroid-centroid distance of 3.783 Å for the quinaldic ring and a centroid-centroid distance of 3.753 Å for the aniline ring, when viewed along the c axis (**Figure 2-12**) the ligand adopts a herringbone motif where the planes are held together by the π - π stacking described above and hydrogen bonds of 2.420 Å between the oxygen of the carbonyl group and the hydrogens in the C5 positions.

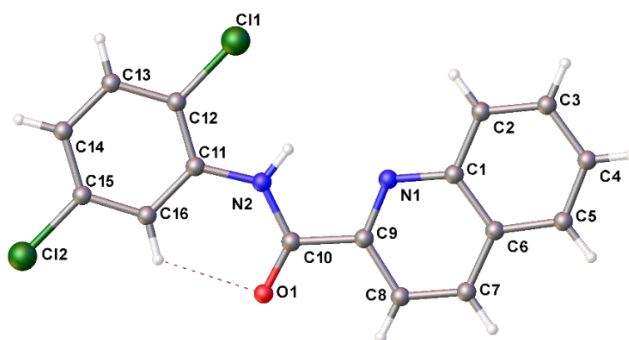


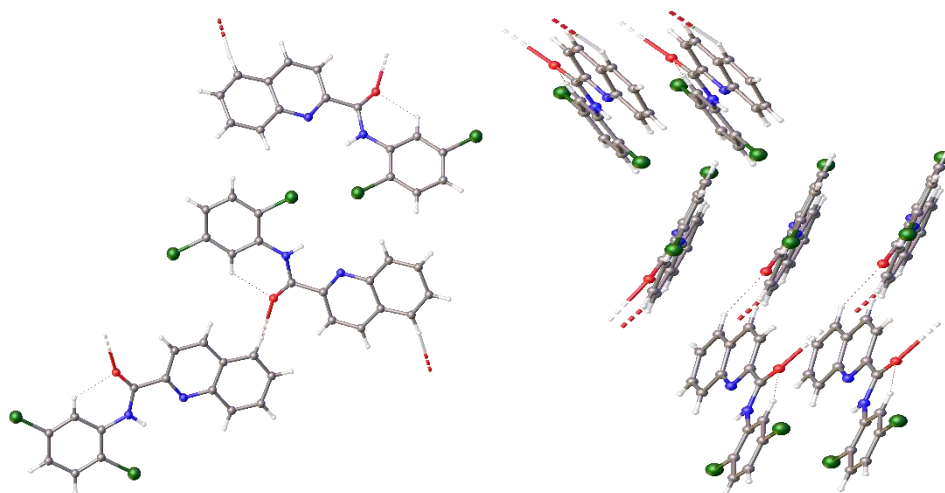
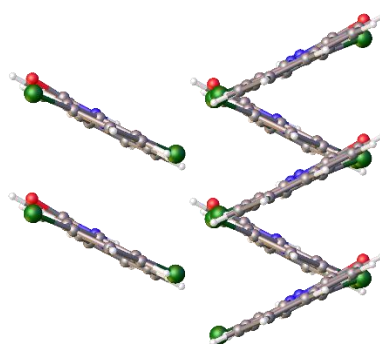
Figure 2-13: Molecular structure of ligand **2.30** showing intramolecular hydrogen bonds. Displacement ellipsoids are at the 50% probability level

Table 2.4: Selected angles for ligand **2.30** with esds shown in parenthesis

Bond	Angle (°)
N(1)-C(9)-C(10)	115.70(8)
C(9)-C(10)-O(1)	121.52(2)
O(1)-C(10)-N(2)	125.61(8)
C(10)-N(2)-C(11)	129.20(7)
N(2)-C(11)-C(16)	121.60(4)

Table 2.5: Selected bond lengths for ligand **2.30** with esds shown in parenthesis

Bond	Distance (Å)
C(1)-N(1)	1.370(3)
N(1)-C(9)	1.321(5)
C(9)-C(10)	1.511(7)
C(10)-O(1)	1.230(5)
C(10)-N(2)	1.356(6)
N(2)-C(11)	1.402 (6)
C(11)-C(12)	1.373(6)
C(12)-Cl(1)	1.748(5)

**Figure 2-14:** Packing diagram of ligand **2.30** (on the left) showing hydrogen bonds between the carbonyl group and the perpendicular proton on the opposite quinaldamide core (axis a) and the π - π stacking on the right (axis b).**Figure 2-15:** Herringbone motif or zig-zag interaction of the ligand **2.30**, held by π - π interactions.

2.3.5 X-Ray structure for ligand 2.37

A colourless block suitable for X-ray diffraction was obtained from a concentrated chloroform solution. Ligand **2.37** crystallised in a monoclinic cell solved in the space group $P2_{1/c}$ containing one molecule in the asymmetric unit. The molecular structure is shown in **Figure 2-16** and selected angles and bond lengths are given in **Table 2.6** and **Table 2.7**. Ligand **2.37** adopts a *quasi*-planar configuration, in which the dihedral angle between the quinaldic ring and the aniline ring N(1)-C(9)-C(10)-N(2) is $3.971(2)^\circ$. This distortion is attributed to the bulkiness of the R group in the aniline ring, it is observed that the bulkier the group the bigger the torsion angle. Intramolecular hydrogen bonding exists between N(2)...N(1) with a bond distance of $2.660(4)$ Å, and between C(12)-H...O(1) with a bond distance of 2.279 Å. Ligand **2.37** arranges itself in perpendicular and parallel planes alternating the position of the ligand as shown in **Figure 2-17** held together by π - π stacking interactions with a centroid-centroid distance of 3.981 Å between two aniline rings and a centroid shift of 1.890 Å, a centroid-centroid distance of 3.751 Å with a centroid shift of 1.589 Å between the quinaldic cores and a distance of 3.771 Å with a shift of 1.867 Å between the quinaldic core and the aniline ring, when viewed along the c axis (**Figure 2-17**). The ligand adopts a square-pattern motif as shown in **Figure 2-18**.

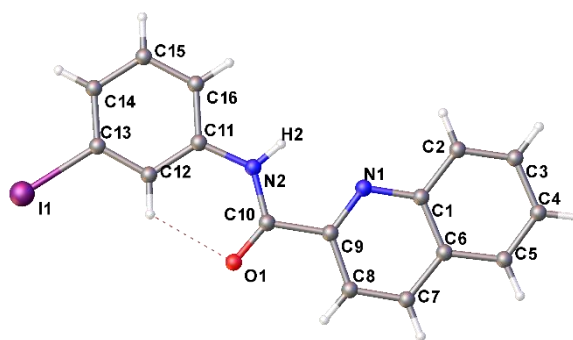


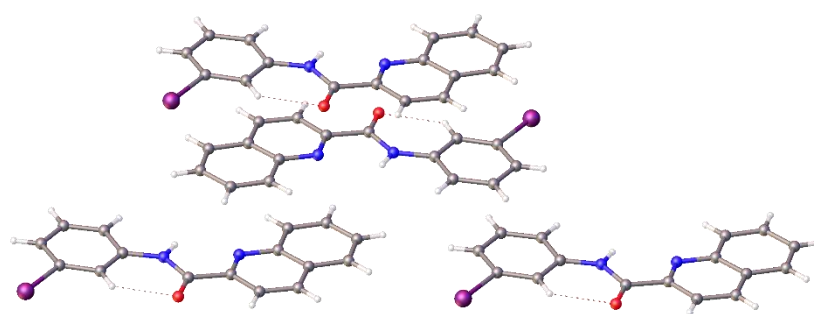
Figure 2-16: Molecular structure of ligand **2.37** showing intramolecular hydrogen bonds. Displacement ellipsoids are at the 50% probability level

Table 2.6: Selected angles for ligand **2.37** with esds shown in parenthesis

Bond	Angle (°)
N(1)-C(9)-C(10)	117.47 (6)
C(9)-C(10)-O(1)	121.18(2)
O(1)-C(10)-N(2)	125.35(5)
C(10)-N(2)-C(11)	128.77(7)
N(2)-C(11)-C(16)	117.32(4)

Table 2.7: Selected bond lengths for ligand **2.3** with esds shown in parenthesis

Bond	Distance (Å)
C(1)-N(1)	1.372(3)
N(1)-C(9)	1.321(3)
C(9)-C(10)	1.510(4)
C(10)-O(1)	1.222(3)
C(10)-N(2)	1.353(3)
N(2)-C(11)	1.407(3)
C(11)-C(12)	1.401(4)
C(13)-I(1)	2.107(3)

**Figure 2-17:** Packing diagram of ligand **2.37** showing π - π stacking and intermolecular hydrogen bonds.

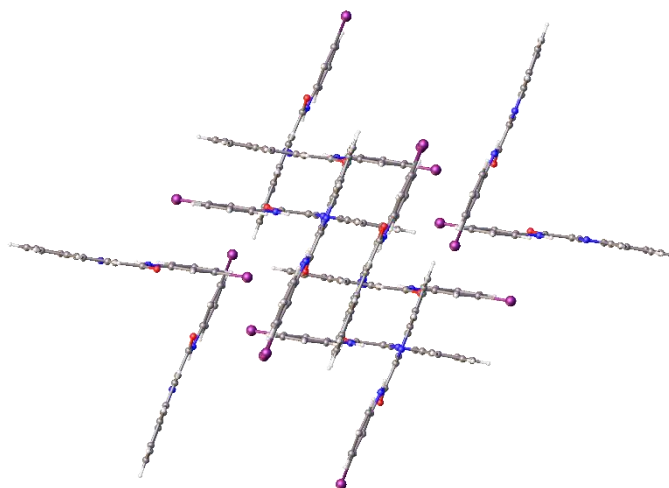


Figure 2-18: Packing of the ligand in a square motif

Crystal data for ligands **2.4**, **2.15**, **2.16**, **2.24**, **2.25**, **2.29** and **2.37** are given in the appendix.

2.4 Conclusion

Biological systems are strongly influenced by proteins, thus the peptide chemistry of amide ligands is a research field vastly investigated due to their well-known stability and cell uptake. Twelve novel functionalised quinaldamide ligands have been synthesised and fully characterised by IR, H.R.M.S, NMR (1D and 2D) techniques and by elemental analysis and by X-ray crystallography. The crystal structures obtained so far have probed the planarity of the ligands with a twist between the two fragments, the quinaldic ring and the aniline ring. Only three compounds showing different crystals structures were described due to their packing similarities independently in the functional groups were electron donating groups or electron withdrawing groups.

2.5 References

- ¹ Alberts, B.; Johnson, A.; Lewis, J.; Raff, M.; Roberts K.; Walter, P.; *Molecular Biology of the Cell*, Garland Science, New York, **2007**.
- ² Testa, B; Mayer, J. M.; *Hydrolysis in Drug and Prodrug Metabolism, Chemistry, Biochemistry, and Enzymology*, John Wiley & Sons, Switzerland, **2003**. ISBN: 3-906390-25-X.
- ³ Swain, A. P.; Naegele, S. K.; *J. Am. Chem. Soc.*, **1957**, 79, 5250-5253.
- ⁴ Huang, T.-T.; Huang, Y.-C.; Qing, X.-Y.; Xia, Y.; Luo, X.; Ye, T.-H.; Yu, L.-T.; *Molecules*, **2012**, 17, 6317-6330.
- ⁵ Dutta, S.; Pal, S.; Bhattacharya, P. K.; *Polyhedron*, **1999**, 18, 2157-2162.
- ⁶ Barnes, D. J. ; Chapman, R. L.; Vagg, R. S.; Watton, E. C.; *J. Chem. Eng. Data*, **1978**, 23, 349-350.
- ⁷ Köprülü, K. T.; Ökten, S.; Tekin, Ş.; Osman, Ç.; *J. Biochem. Mol. Toxicol.* **2018**, 15:e22260.
- ⁸ Canty, A. J.; Lee, C. V.; *Inorg. Chim. Acta*, **1981**, 54, L205-L206.
- ⁹ Collins, T. J.; *Acc, Chem, Res.* **1994**, 27, 279-285.
- ¹⁰ Rafferty, K.; *Ph. D Thesis*, University of Leeds, **2008**.
- ¹¹ Jo, H.; Choi, M.; Kumar, A. S.; Jung, Y.; Kim, S.; Yun, J.; Kang, J-S.; Kim, Y.; Han, S-b.; Jung, J-K.; Cho, J.; Lee, K.; Kwak, J-H.; Lee, H.; *Med. Chem. Lett.* **2016**, 7, 385-390.
- ¹² Huang, L.; Li, Q.; Wang, C.; Qi, C.; *J. Org, Chem.*, **2013**, 78, 3030-3038.

**Chapter 3 Ruthenium (III) dichloride bis-quinaldamide
complexes**

3.1 Background

Farrell, reported that *trans*-dichloride platinum anti-cancer complexes containing at least one aromatic *N*-donor ligand have shown greater cytotoxicity than transplatin and comparable with cisplatin¹ against different leukemia cells and human ovarian cells. Metal complexes of the type MX_2L_2 (X = halide, and L = bidentate ligand) were explored by Krause *et al.* and seen previously to undergo isomerisation, giving rise to six different structural geometries (**Figure 3-1**).² Reedijk *et al.*, following the work from Krause with (2-(phenylazo)pyridine (azpy) (left structure in **Figure 3-2**), have reported the anticancer activities of $\text{Ru}(\text{azpy})_2\text{Cl}_2$ complexes attributing to the different structural isomers. The low cytotoxicity against cancer cells was predominately seen for the *trans* dichloride geometries.³ However, after developing a new ligand, H-pyrimol (4-methyl-2-*N*-(2-pyridylmethylene) aminophenol) (right structure in **Figure 3-2**), which upon complexation yielded a series of *trans*-dichloride Ru(II) compounds, Reedijk *et al.* showed that their *trans* complexes were more potent than cisplatin to different cell lines.⁴

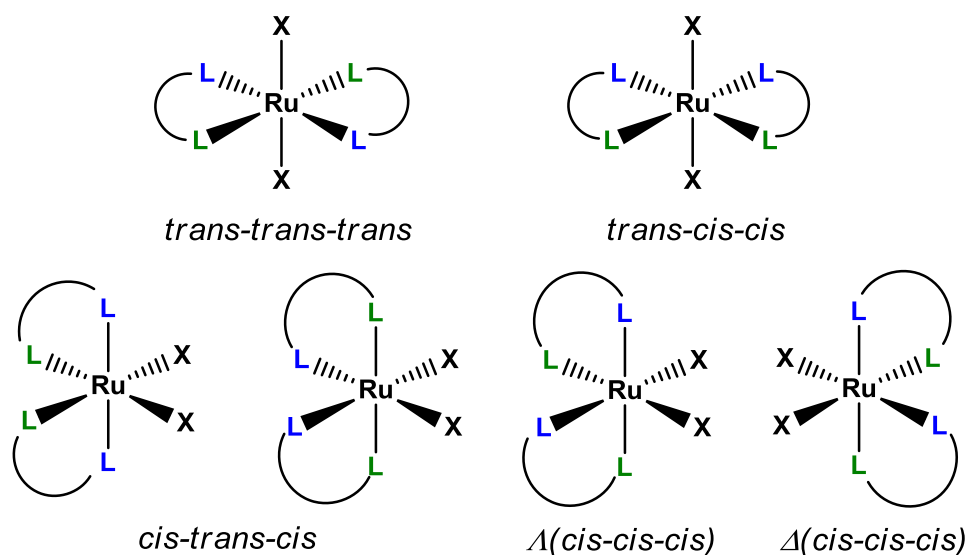


Figure 3-1: Possible isomers for ruthenium complexes type RuX_2L_2 bearing homoleptic bidentate ligands. Optical isomers are also shown.

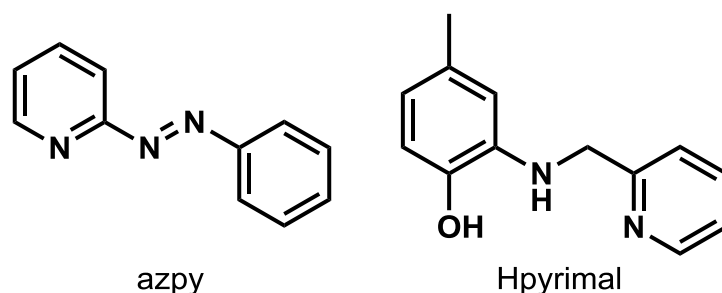


Figure 3-2: *Left*, ligand used by Krause; *Right*, ligand developed by Reedijk.

More recently, Glazer et al. has compared the anticancer activities of polypyridyl based complexes, *cis*-Ru(bpy)₂Cl₂ with *trans*-Ru(qpy)Cl₂, showing the *trans* isomer to be 7-10 times more active than the *cis* being and similar to the potency of cisplatin.⁵ The wide range of effects caused by the different geometries of the complexes in biological fields, triggered research into the formation of different isomers focusing on the synthesis and development of transition metal based candidates using well known scaffolds like: metal-arenes,⁶ metal-Cp*,⁷ and ferrocene derivatives.⁸

Ruthenium complexes of the type Ru(X)₂(L)₂ where X is chloride or halide and L is a bidentate ligand (picolinamide) have been introduced in the McGowan group showing the *trans*-arrangement of the halides has more potency against a variety of cancerous cell lines reaching the nanomolar range. The anticancer activity was also increased by replacing the chlorides for iodides.⁹

This chapter discusses the selective synthesis, isolation and characterisation of a novel family of neutral *trans*-dichloride ruthenium bisquinaldamide complexes. The aim is to add and to expand a new family of compounds based in amide linkages and evaluate the biological properties of the complexes.

3.2 Rationale behind Ru(Cl)₂(L)₂ type complexes

The molecular design of Ru(Cl)₂(L)₂ type complexes involves planar aromatic groups and an amide linkage which may interact with the DNA acceptor sites. These features will determine the rate of hydrolysis, hydrophobicity and anti-cancer properties. The general synthesis proceeds *via* direct addition of two equivalents of ligand (L) fully dissolved before addition to the ruthenium precursor in hot ethanol. This chapter will compare what the effects are upon addition of a

base and if the is base free. The coordination of the quinaldamide is tightly related to the substituent groups in the aniline. Theoretically, up to five structural isomers are possible in solution state, however, only the *trans*-dichloride isomer is isolated.

3.3 Synthesis of the neutral *trans*-dichloride bisquinaldamide ruthenium (III) complexes

The five possible isomers for dichloride bisquinaldamide ruthenium complexes are illustrated in **Figure 3-3**. The compounds synthesised were characterised by high resolution mass spectrometry, elemental analysis, X-ray diffraction and infrared spectroscopy confirming a *trans-trans-trans* arrangement.

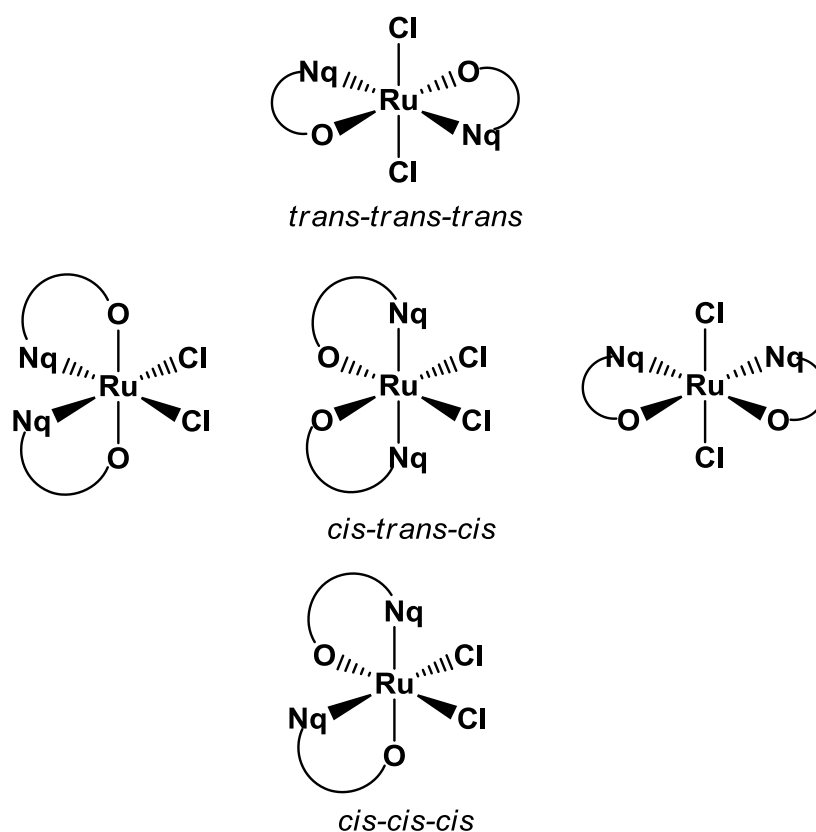


Figure 3-3: Possible isomers of dichloride bisquinaldamide ruthenium complexes. The complexes (general structure found in **Figure 3-4** and the numbering of the synthesised complexes in **Table 3-1**) were obtained following both a procedure developed in the McGowan group⁹ and an adaptation of it - the base free reaction.

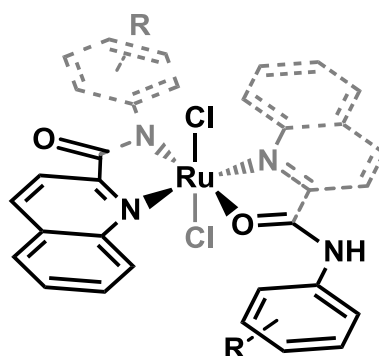
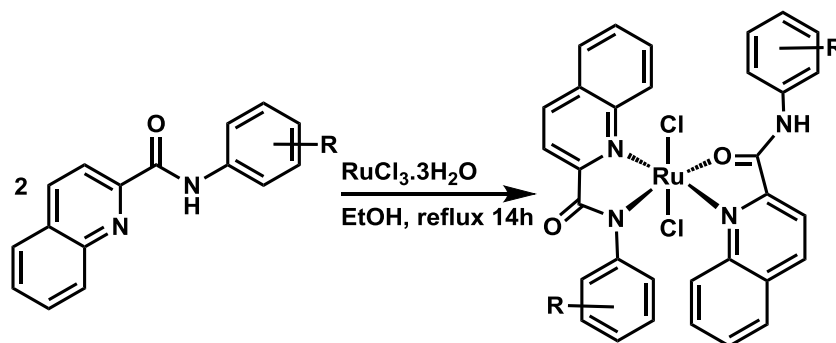


Figure 3-4: *Trans*-dichloride bisquinaldamide ruthenium (III) backbone where R is a functional group either electron donating or withdrawing.

Table 3-1: Numbering of the synthesised complexes and functionality given by the R group

Complex	R	Complex	R
3.1	H	3.25	4-F
3.5	2-Me	3.26	2,4-diF
3.6	3-Me	3.27	2,5-diF
3.7	4-Me	3.28	2-Cl
3.9	2-Et	3.29	3-Cl
3.10	3-Et	3.30	4-Cl
3.11	4-Et	3.31	2,4-diCl
3.12	2- ⁱ Pro	3.32	2,5-diCl
3.13	3- ⁱ Pro	3.33	2-Br
3.15	2,6-di ⁱ Pro	3.34	3-Br
3.16	2-Me-6- ⁱ Pro	3.35	4-Br
3.17	2- ^t Bu	3.36	2,4-diBr
3.18	4- ^t Bu	3.38	2-I
3.23	2-F	3.39	3-I
3.24	3-F	3.40	4-I



Scheme 3-1: Optimised base-free synthetic pathway to obtain the ruthenium complexes.

The optimised procedure in **Scheme 3-1** differs from the original by not adding a base. Two equivalents of a ligand dissolved in hot ethanol was added to a solution in hot ethanol of one equivalent of $\text{RuCl}_3 \cdot 3\text{H}_2\text{O}$ in 5 mL of ethanol, then the mixture was heated to 90°C with constant stirring for 14h and filtered off. Coloured solids were isolated, and the mother liqueurs were left to crystallise.

3.4 Characterisation of bis-quinaldamide *trans*-dichloride Ru (III) complexes

This section only discusses the compounds obtained *via* the base free reaction. The MChem student Daniel Kowalski isolated the complexes with substituents in position 2 and in position 3 by an MSci student Abigail Frith. The unsubstituted quinaldamide complex, those substituted in position 4, disubstituted, and the reactions carried out by adding triethyl amine as a base were carried out by the author, (**Figure 3-5**).

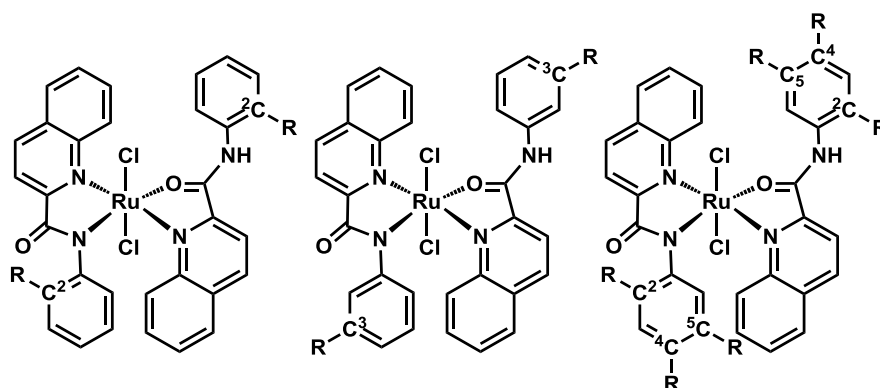


Figure 3-5: Chemical structures of the compounds functionalised in different position 2 (*left*), position 3 (*middle*) and position 4 and disubstituted (*right*).

All complexes in this thesis are novel, however, the discussion in this chapter is focused on the those displaying great anticancer activity, calling these compounds in **Chapter 5: Lead Compounds**. *Trans*-dichloride *trans*-bischelating quinaldamide ruthenium neutral complexes were prepared as shown in **Scheme 3-1** to obtain complexes in **Table 3-1** with yields ranging between 7% and 65%. The main technique used in this thesis is x-ray diffraction, thus the focus of this chapter. The lead compounds are constituted by the following R groups: H, 4-^tBu, 2-F, 3-Cl, 2,5-diCl and 2-I. The two not discussed contain R = 3-ⁱPr and 2,4-diBr (**Table 3-1**). Additionally, only the characterisation of the complex **3.1** formed by the unsubstituted ligand (R = H, ligand **2.1**) is explained in detail and throughout different sections, due to the structural similarities within this novel family allowing to outline general trends: thus the main focus is given to the successful candidates as anticancer compounds in terms of X-ray characterisation and X-ray powder diffraction. All complexes were found to be: soluble in polar aprotic solvents like dimethylformamide and dimethyl sulfoxide; scarcely soluble in acetone, chloroform, dichloromethane, acetonitrile and octanol; and insoluble in aliphatic, ethers and derivatives of benzene.

3.5 Ruthenium Complex 3.1

3.5.1 Infrared Spectroscopy of the complex 3.1

The IR spectra collected for all the complexes are very similar, with a variety of bands and different intensities in the 1700-400 cm^{-1} region. A comparison (**Figure 3-6**) between the free ligand (**2.1**) and the complex (**3.1**) can be made focusing on the main functional groups. Theoretically, it is expected a band shift towards lower wavenumbers when the complex is synthesised. The C=O stretch of the ligand is found at 1674 cm^{-1} whereas in the complex, an interval between 1519-1490 cm^{-1} is observed. The NH group of the free ligands appears at 3339 cm^{-1} and a very weak band can be seen at 3257 cm^{-1} for the complex. The peak at 3053 cm^{-1} of C-H aromatic bonds of the ligand appear in the complex around 3140 cm^{-1} .

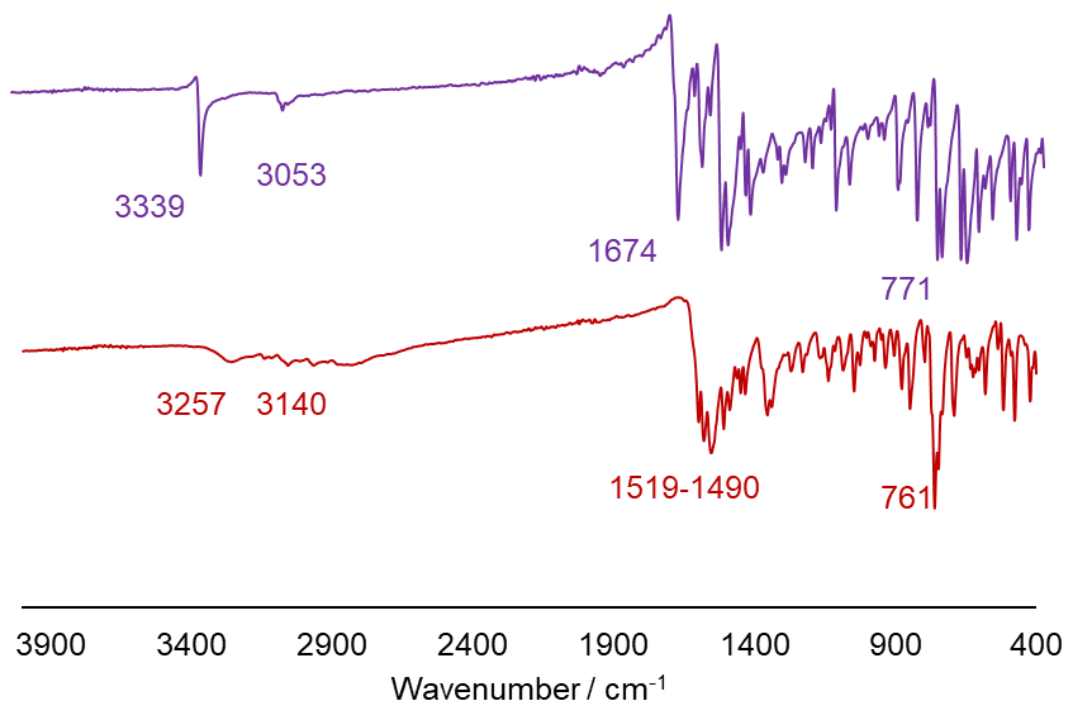


Figure 3-6: Comparison of the IR spectra of the ligand **2.1** (purple line) and its ruthenium complex **3.1** in red.

3.5.2 High Resolution Mass Spectrometry of the complex **3.1**

Ruthenium has a characteristic isotopic pattern which can be identified by HRMS.

Figure 3-7 shows the isotopic distribution of the metal complex **3.1** simulated and compared to the experimental pattern. The molecular ion $[M+H]^+$ peak is 668.0308 m/z and the simulated spectrum gives a value of 668.0317 m/z. The addition of this proton can be attributed to the nitrogen of the amide linkage of the neutral bound ligand.

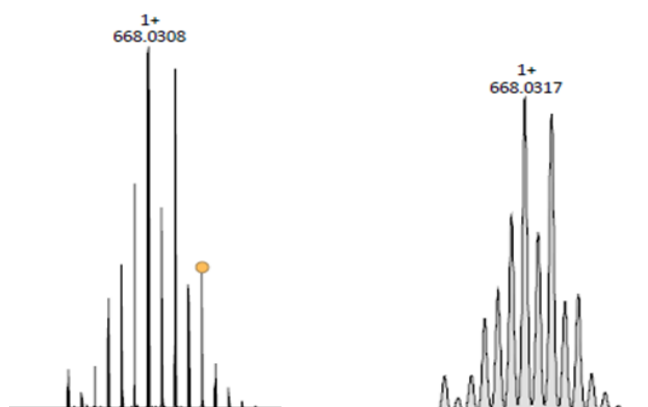


Figure 3-7: HRMS spectra of the complex **3.1** (*left*) experimentally determined and (*right*) simulated pattern.

The comparison between the results obtained and the predicted pattern proves that the complexes can be detected by High Resolution Mass Spectrometry.

3.5.3 General trends in X-ray Crystallography for the complexes and X-ray single crystal diffraction of complex 3.1

Single crystals suitable for X-ray diffraction were grown for all complexes by slow evaporation from saturated solutions in DMF or DMSO. Ligands bound in different modes as proved by the crystal structures (the chemical structure for complex R = H (**3.1**) can be found in **Figure 3-8**), one bound neutrally as an amide and the other bound anionically $[N,N]$ or $[N,O]$, being the latter found for complexes with electro-donating ligands in position 2 of the aniline ring. The complexes present a distorted octahedral geometry with bond angles in the range $169.51(10)^\circ$ - $178.59(4)^\circ$ for the chlorides *trans* to each other - interestingly, the unsubstituted ligand **2.1** gives the more distorted geometry and the 2,5-difluoroquinaldamide ligand (**2.27**) shows the labile ligands closer to 180° . The bond angles for the *trans* nitrogens of the quinaldic cores can be found between 173° - 179° . The ligands bound anionically show a chelating angle between $76.65(10)^\circ$ - $79.8(3)^\circ$ whereas the neutrally bound ligands show angles between $75.27(13)^\circ$ - $78.75(10)^\circ$.

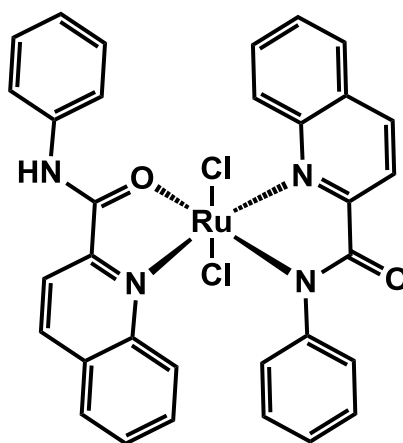


Figure 3-8: Chemical structure of compound **3.1**.

Trans-dichloride bis-(*N*-phenyl)-quinaldamide ruthenium (III) complex, **3.1**, (**Figure 3-8**) was isolated as a red powder and crystallised from DMF yielding red plates and red needles. The asymmetric unit of the first compound contains one molecule of DMF and water, it crystallised in a monoclinic cell and solved in the space group $P2_{1/n}$, whereas the second molecule crystallises with a molecule of

DMF in its asymmetric unit making this a triclinic cell and solved in the space group P-1. **Figure 3-9** shows that for both single crystal structures, only the *trans-trans-trans* isomer is isolated. The complexes are arranged in a slightly distorted octahedral geometry caused by the ligands as they bend towards one of the chlorides, proving that instead of the ideal 180° angle formed between the chlorides and the metal is $173.84(3)^\circ$ for the first structure and slightly more distorted for the second one with an angle of $171.99(2)^\circ$. However, to prove the bulk of the sample is formed only by the *trans* isomer, X-ray powder diffraction of the whole sample must be obtained. See section 3.5.4.

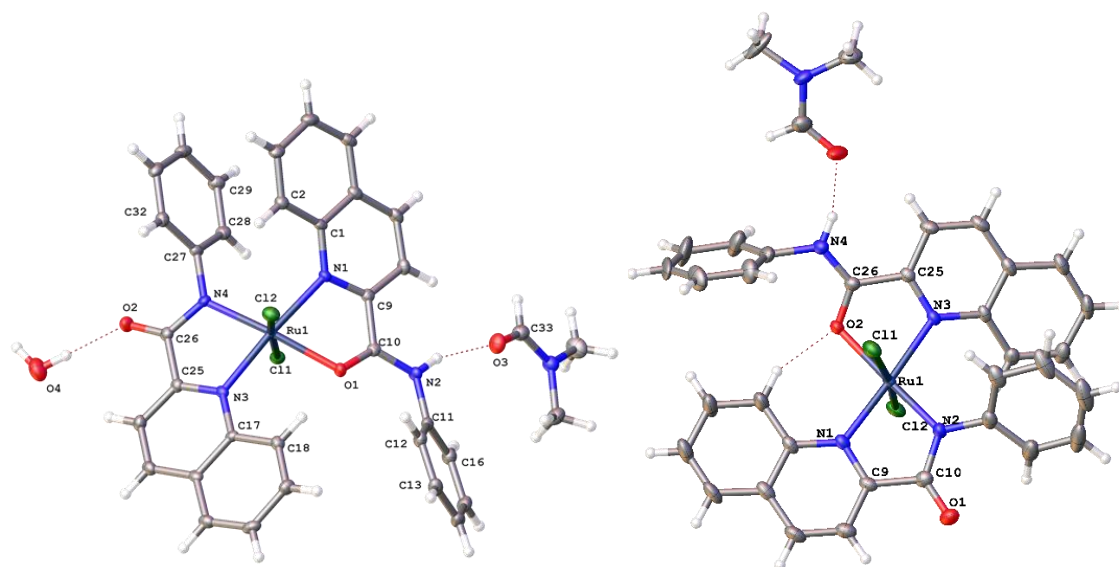


Figure 3-9: Solvent dependent crystal structures for complex 3.1.

Figure 3-10 shows that the aryl group of the ligands twists out of the plane allowing the quinolyl groups to interact with the anionically bound of another molecule and the neutrally bound with the neutral one. This rotation prevents the formation of hydrogen bond C(12)-H...O(1) but forming instead the hydrogen bond between C(18)-H...O(1) as shown on the left structure in **Figure 3-9**. Further hydrogen bonds can be seen between the ruthenium complex and both DMF (between the N(2)-H...O(3)/O_{DMF} with distance of 2.767 Å) and water (between O_{H2O}-H... O(2) with a distance of 3.021 Å).

Table 3-2 summarises the bond lengths to prove that one of the ligands is bound deprotonated and the other bound neutrally through the lone pair. The neutral ligand shows the carbonyl bond (C(10)...O(1)) distance of 1.264(4) Å, the amide nitrogen single bond C(10)...N(2) has a length of 1.324(4) Å, confirming the ligand

coordinates neutrally as a L-type. The ligand bound anionically shows similar bond lengths being the carbonyl bond length C(26)...O(2) of 1.241(4) Å and the amide nitrogen bond length C(26)...N(4) of 1.351(4) Å. Although, in this case, the proton attached to the nitrogen of the peptide bond is lost making the ligand an X-type. In **Table 3-3** all the relevant bond and dihedral angles are summarised.

Table 3-2: Selected bond lengths for complex **3.1** with labelled atoms corresponding to the complex on the left of **Figure 3-9**

Bond	Length/ Å	Bond	Length/ Å
Ru(1)-Cl(1)	2.3561(7)	N(1)-C(9)	1.343(4)
Ru(1)-Cl(2)	2.3461(7)	O(2)-C(26)	1.241(4)
Ru(1)-O(1)	2.096(2)	N(2)-C(10)	1.324(4)
Ru(1)-N(1)	2.110(2)	N(3)-C(25)	1.332(4)
Ru(1)-N(3)	2.076(2)	N(4)-C(26)	1.351(4)
Ru(1)-N(4)	2.023(2)	C(9)-C(10)	1.485(4)
O(1)-C(10)	1.264(4)	C(25)-C(26)	1.492(4)

Table 3-3: Selected bond angles for complex **3.1** with labelled atoms corresponding to the complex on the left of **Figure 3-9**

Bond	Angle/ °	Bond	Angle/ °
O(1)-Ru(1)-Cl(1)	83.25(6)	N(3)-Ru(1)-Cl(2)	89.45(7)
N(1)-Ru(1)-Cl(1)	88.43(7)	O(1)-Ru(1)-Cl(2)	99.46(7)
Cl(2)-Ru(1)-Cl(1)	173.84(3)	O(1)-Ru(1)-N(1)	75.91(8)
N(3)-Ru(1)-Cl(1)	89.43(7)	N(3)-Ru(1)-N(1)	175.59(9)
N(4)-Ru(1)-Cl(1)	86.27(7)	N(4)-Ru(1)-N(1)	104.94(9)
O(1)-Ru(1)-Cl(2)	90.98(6)	N(3)-Ru(1)-O(1)	100.00(8)
N(1)-Ru(1)-Cl(2)	92.27(7)	N(4)-Ru(1)-O(1)	169.46(9)
N(4)-Ru(1)-N(3)	78.76(9)		

In terms of π - π stacking (similar for both structures seen in **Figure 3-9**), the aromatic rings rotate to maximise the interactions and stabilise the molecule's network. The crystal packing in **Figure 3-10** shows that molecules interact with each other *via* π - π stacking of the quinaldic core of the anionically bound ligands (highlighted in blue) with a centroid-centroid distance of 3.229 Å and the angle between planes of 4.199°. Whereas the quinaldic cores for the neutrally bound ligands show a centroid-centroid distances of 3.591 Å and no distortion angle.

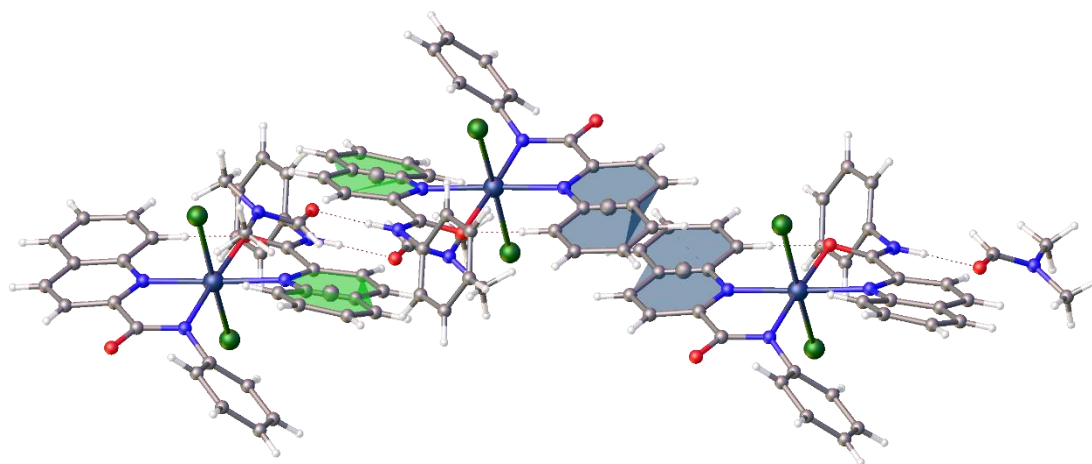


Figure 3-10: Crystal packing interactions of the complex **3.1** (similar packing for both complexes).

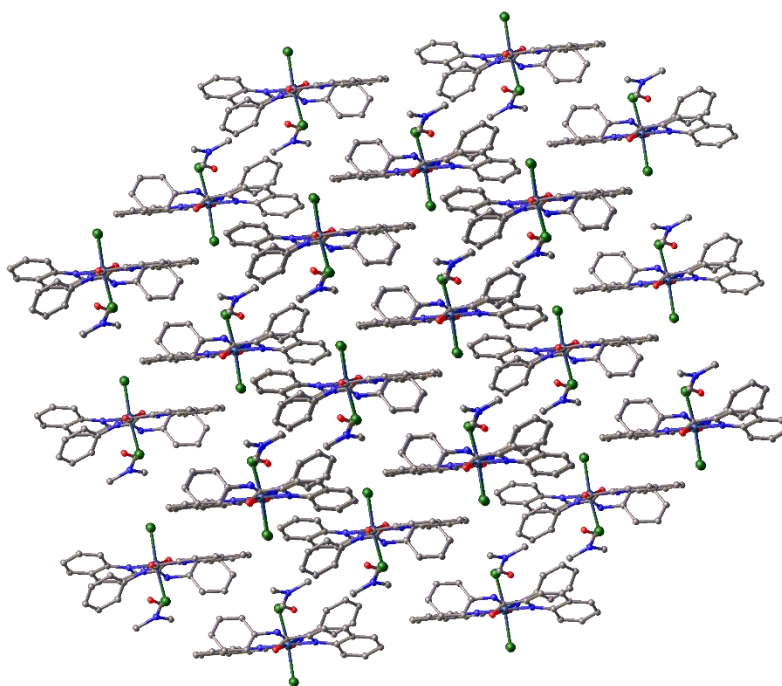


Figure 3-11: Extended crystal structure for complex **3.1**.

Figure 3-11 shows the expansion of the crystal structure from complex **3.1** displaying a zig-zag arrangement and the chlorides perpendicularly aligned.

3.5.4 X-ray powder diffraction of complex 3.1

The X-ray powder pattern diffraction for complex **3.1** was recorded to prove that only one isomer was obtained from both the bulk powder sample and the crystal structure, thus determining the purity of the sample biologically tested. **Figure 3-12** shows the comparison of the two PXRD diffractograms corroborating that both sets are constituted by only one isomer. Although there are few additional peaks, all the main peaks corresponding to the unit cell of the ruthenium complex **3.1** match very well between the simulated and the experimental data, indicating that the complex has a similar structural geometry in both samples.

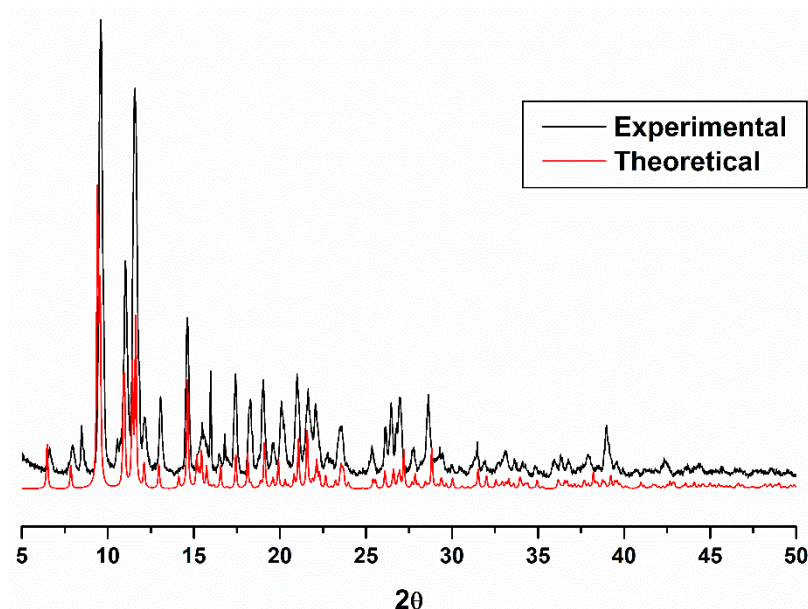


Figure 3-12: XRPD data overlap of complex **3.1** showing the experimental (*black*) and simulated (*red*) diffractograms recorded at scan rate of 40 sec/scan.

3.6 Ruthenium complex 3.18

3.6.1 X-ray single crystal diffraction of complex 3.18

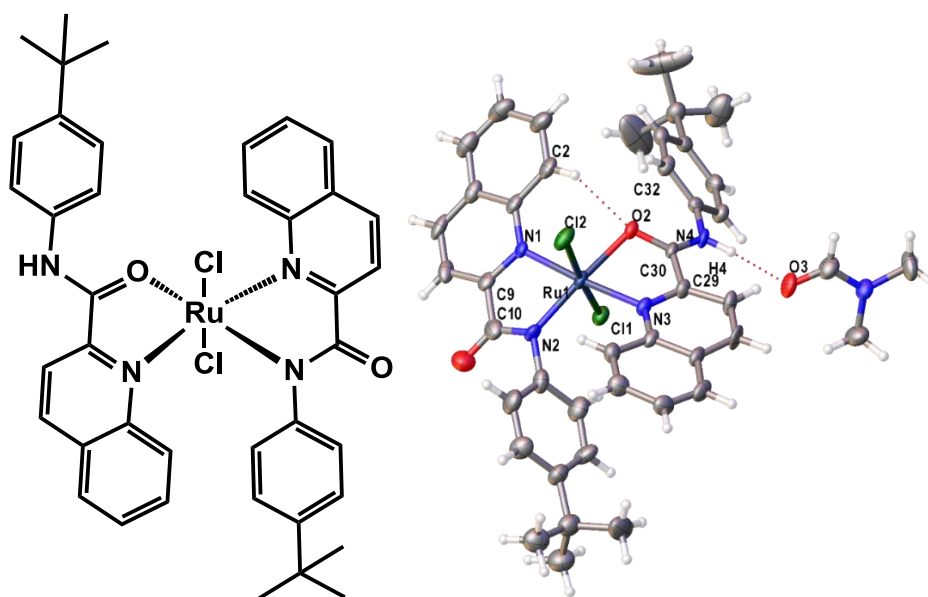


Figure 3-13: Chemical structure for complex **3.18** (*left*); labelled crystal structure (*right*).

Trans-dichloride bis-(*N*-4^tbutylphenyl)-quinaldamide ruthenium (III) complex (**3.18**) (**Figure 3-13**) was isolated as a red powder and crystallised from DMF as red prisms. The asymmetric unit contains one molecule of DMF (crystallisation solvent), crystallising in a triclinic cell and solved in the space group *P*-1. **Figure 3-13** (right) shows the single crystal being only the *trans-trans-trans* isomer isolated. The ruthenium centre shows a slightly distorted octahedral geometry caused by the ligands as they bend towards one of the chlorides displaying a Cl-Ru-Cl angle of 174.68(6)° instead of the ideal 180°. The aromatic rings twist out to maximise the stability of the compound, fact found across the series of complexes. The angle found between N(3)-Ru(1)-N(1) and O(2)-Ru(1)-N(2) is 175.55(17)° and 168.93(17)° respectively.

In terms of π - π stacking, the aromatic rings rotate to maximise the interaction and stabilise the molecule. Specifically, the aryl group of the anionically bound ligand twists towards the quinolyl group of the neutrally bound ligand. The same happens to the other ligand preventing the formation of hydrogen bond C(32)-H...(O)2 but forming instead the hydrogen bond between C(2)-H...O(2) with a distance of 2.219 Å. It can be seen another hydrogen bond between amide

proton and the oxygen from the DMF. The distance found between N(4)-H...O(3)/O_{DMF} is 1.943 Å.

Table 3-4 summarises the bond lengths corresponding to the labelled complex in **Figure 3-13** which proves one of the ligands is bound after the deprotonation of the amide and the other bound neutrally via the lone pair. The neutral ligand shows the carbonyl bond (C(30)...O(2)) of 1.268(5) Å, the amide nitrogen single bond C(30)...N(4) has a length of 1.325(6) Å acting as an L-type ligand within the normal values for free amides. The ligand bound anionically shows similar bond lengths being the carbonyl bond length C(10)...O(1) of 1.249(4) Å and the amide nitrogen bond length C(11)...N(2) of 1.341(7) Å. Although, in this case, the proton attached to the nitrogen of the peptide bond is lost making the ligand an X-type. This similarity in bond distances shows the ligands remain almost intact meaning the amide bond is weakly disturbed by the coordination of the ruthenium centre. **Table 3-4** and **Table 3-5** summarises all the relevant bond lengths, angles and dihedral angles.

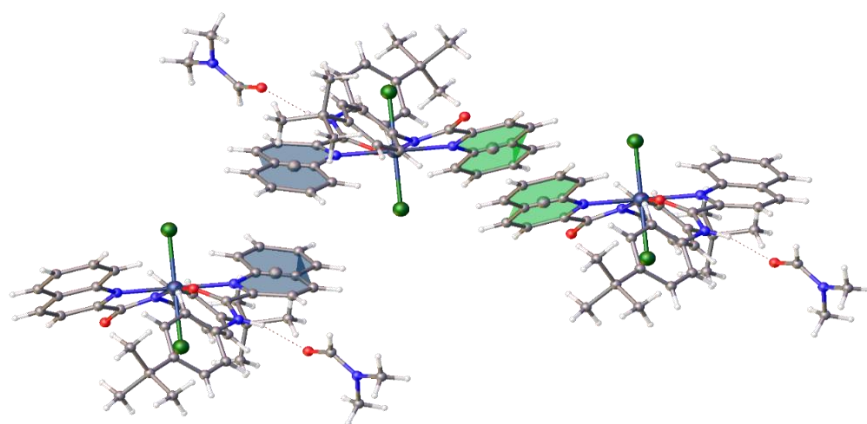
Table 3-4: Selected bond lengths for complex **3.18** with labelled atoms corresponding to the complex in **Figure 3-13**

Bond	Length/ Å	Bond	Length/ Å
Ru(1)-Cl(1)	2.3727(15)	N(1)-C(9)	1.342(6)
Ru(1)-Cl(2)	2.3399(15)	O(2)-C(30)	1.268(5)
Ru(1)-O(2)	2.094(3)	N(2)-C(10)	1.341(7)
Ru(1)-N(1)	2.086(4)	N(3)-C(29)	1.341(6)
Ru(1)-N(2)	2.018(4)	N(4)-C(30)	1.325(6)
Ru(1)-N(3)	2.112(4)	C(9)-C(10)	1.492(8)
O(1)-C(10)	1.249(6)	C(29)-C(30)	1.500(7)

Table 3-5: Selected bond angles for complex **3.18** with labelled atoms corresponding to the complex on **Figure 3-13**

Bond	Angle/ °	Bond	Angle/ °
O(2)-Ru(1)-Cl(1)	82.37(10)	N(2)-Ru(1)-Cl(2)	98.24(14)
N(1)-Ru(1)-Cl(1)	89.03(12)	N(3)-Ru(1)-Cl(2)	90.13(12)
Cl(2)-Ru(1)-Cl(1)	174.68(6)	O(2)-Ru(1)-N(3)	77.23(15)
N(2)-Ru(1)-Cl(1)	86.79(14)	N(3)-Ru(1)-N(1)	175.55(17)
N(3)-Ru(1)-Cl(1)	90.21(12)	N(2)-Ru(1)-N(3)	105.14(17)
O(2)-Ru(1)-Cl(2)	92.54(10)	N(1)-Ru(1)-O(2)	98.32(14)
N(1)-Ru(1)-Cl(2)	90.22(12)	N(2)-Ru(1)-O(2)	168.93(17)
N(2)-Ru(1)-N(1)	79.20(16)		

Figure 3-14 shows the π - π stacking of the quinaldamide cores. As previously discussed, the anionically bound interacts with the same one of another molecule and the neutrally bound with the neutral. The green planes show a centroid-centroid distance of 3.720 Å and the blue planes display a centroid-centroid distance of 4.569 Å, which is long for π - π interactions. **Figure 3-15** shows the stacking of the complex showing a concave-convex packing motif, with the chlorides pointing outwards and the organic framework showing the encapsulation of the metal centre.

**Figure 3-14:** π - π interactions for complex **3.18**.

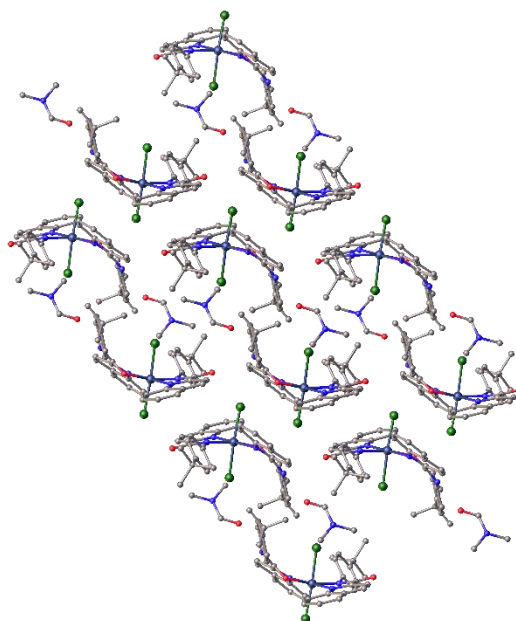


Figure 3-15: Crystal packing showed in the z-axis.

3.7 Ruthenium complex 3.23

3.7.1 X-ray single crystal diffraction for complex 3.23

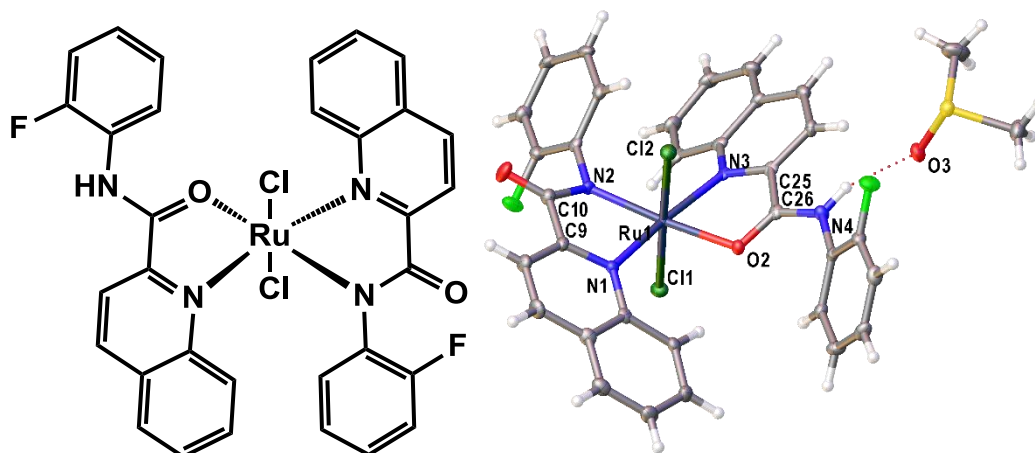


Figure 3-16: Chemical structure of complex **3.23** (*left*); labelled crystal structure (*right*).

Trans-dichloride bis-(*N*-2-fluorophenyl)-quinaldamide ruthenium (III) complex (**3.23**) (**Figure 3-16**) was isolated as a bright red powder and crystallised from DMSO as red prisms. The asymmetric unit is a cocrystal formed by one molecule of DMSO and one molecule of the complex, crystallised in a triclinic system and solved in the space group *P*-1. **Figure 3-16** shows the single crystal for the only isomer obtained: the *trans-trans-trans*. The slightly distortion of the octahedral geometry is given by the angle formed between the following *trans* arranged atoms: 178.59(4)° for Cl(1)-Ru(1)-Cl(2), 168.44(12)° for N(2)-Ru(1)-O(2) and 172.60(11)° for N(1)-Ru(1)-N(3). **Figure 3-16** also shows one ligand deprotonated (X-type ligand) and one neutral (L-type ligand) showing the following bond lengths: the carbonyl group (C(10)-O(1)) of the X-type ligand shows a distance of 1.227(5) Å and 1.255(5) Å for the L-type ligand (C(26)-O(2)). The nitrogen-carbon single bond for the anionic ligand (C(10)-N(2)) shows a distance of 1.363(5) Å and 1.336(5) Å for the neutral C(26)-N(4) bond. The relevant bond lengths and angles are collected in **Table 3-6** and **Table 3-7**.

Figure 3-17 shows the of π - π interactions that display different behaviour than the remaining complexes within the series apart from complex **3.32** (see section **3.9**). The ligands bound anionically ([N,N]⁻ coordination) highlighted in blue show the quinolyl groups interacting showing a centroid-centroid distance of 3.554 Å. Furthermore, the aryl groups (green highlighted) show a centroid-centroid

distance of 3.685 Å for the π - π stacking interaction and with a shift between centroids of 1.482 Å. The only hydrogen bond found belongs to N(4)-H...O(3)_{DMSO} showing a distance of 2.768 Å (**Figure 3-16**).

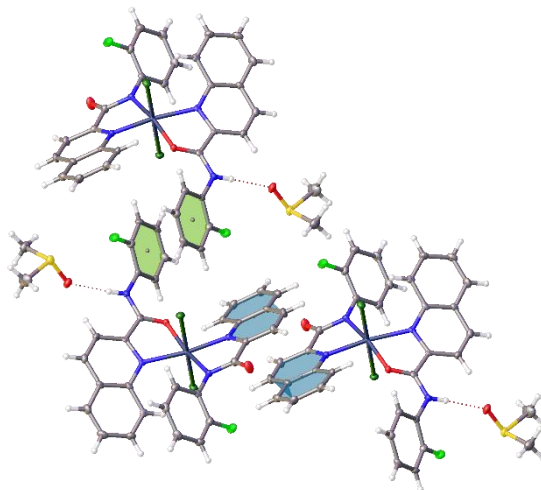


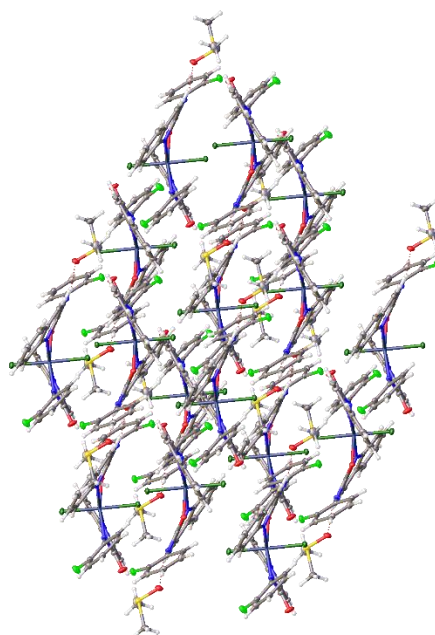
Figure 3-17: Extended crystal structure of compound **3.23**, showing the intermolecular π - π interactions.

Table 3-6: Selected bond lengths with s.u.s. for complex **3.23** and atom labels found in **Figure 3-16**

Bond	Length/ Å	Bond	Length/ Å
Ru(1)-Cl(1)	2.3371(11)	N(1)-C(9)	1.325(13)
Ru(1)-Cl(2)	2.3701(11)	N(2)-C(10)	1.363(5)
Ru(1)-O(2)	2.085(2)	N(3)-C(25)	1.348(5)
Ru(1)-N(1)	2.058(3)	N(4)-C(26)	1.336(5)
Ru(1)-N(2)	2.013(3)	C(9)-C(10)	1.495(6)
Ru(1)-N(3)	2.131(3)	C(25)-C(26)	1.490(6)
O(2)-C(26)	1.255(5)		

Table 3-7: Selected bond angles with s.u.s. for complex **3.23** and atom labels found in **Figure 3-16**

Bond	Angle/ °	Bond	Angle/ °
Cl(1)-Ru(1)-Cl(2)	178.59(4)	N(2)-Ru(1)-Cl(1)	95.49(10)
O(2)-Ru(1)-Cl(1)	95.26(9)	N(2)-Ru(1)-Cl(2)	85.75(10)
O(2)-Ru(1)-Cl(2)	83.46(8)	N(2)-Ru(1)-O(2)	168.44(12)
O(2)-Ru(1)-N(3)	76.41(11)	N(2)-Ru(1)-N(1)	78.95(13)
N(1)-Ru(1)-Cl(1)	90.51(10)	N(2)-Ru(1)-N(3)	107.26(12)
N(1)-Ru(1)-Cl(2)	89.06(10)	N(3)-Ru(1)-Cl(1)	92.83(9)
N(1)-Ru(1)-O(2)	96.72(11)	N(3)-Ru(1)-Cl(2)	87.44(9)
N(1)-Ru(1)-N(3)	172.60(11)		

**Figure 3-18:** Expansion of the crystal structure for complex **3.23**.

The crystal packing shown in **Figure 3-18** displays the oval-shape of the complexes where the ligands bend towards one of labile chlorides, encapsulating both the ruthenium metal centre and the halide.

3.8 Ruthenium complex 3.29

3.8.1 X-ray single crystal diffraction of complex 3.29

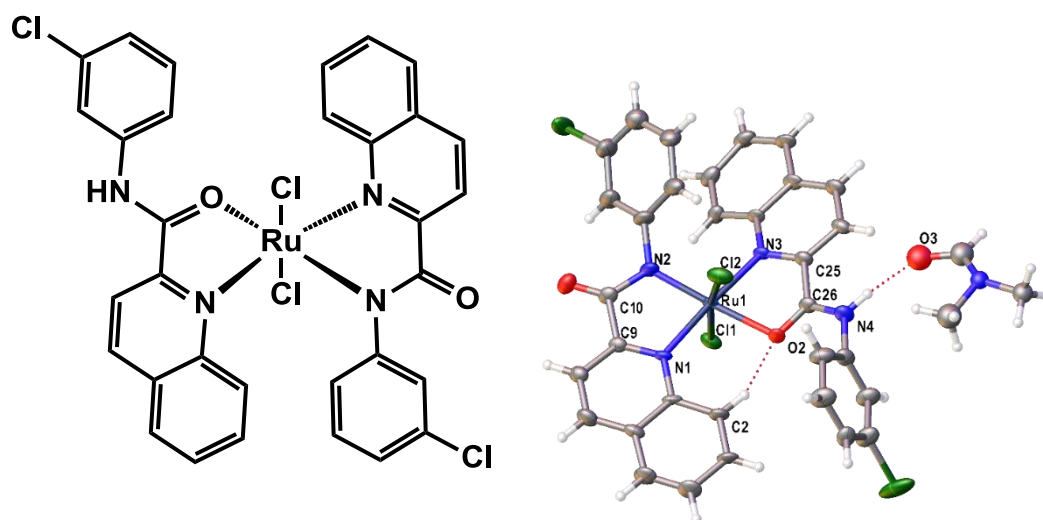


Figure 3-19: Chemical structure of complex **3.29** (left); labelled crystal structure (right).

Trans-dichloride bis-(*N*-3-chlorophenyl)-quinaldamide ruthenium (III) complex (**3.29**) (**Figure 3-19**) was isolated as a red powder and crystallised from DMF as dark red plates. The asymmetric unit contains one molecule of DMF and the complex, it crystallised in a monoclinic cell and solved in the space group *P*-1. **Figure 3-19** (right) shows the crystal structure of the *trans-trans-trans* isomer isolated. It also shows the slightly octahedral geometry distortion caused by the ligand interactions. Two opposite heteroatoms (O(1) and N(4)) point towards one of the chlorides (Cl(2)) and the other two (N(3) and N(1)) towards the other chloride (Cl(1)), what creates the chlorides to be far from 180° the angle, being the Cl-Ru-Cl angle 169.51(10)°. For *trans*-purity of the bulk see section **3.8.2**.

The π - π stacking interactions like the compounds described so far within this chapter; the aromatic rings rotate to maximise the π - π interactions and stabilise the whole molecule. The ligand bound in a neutral manner shows that the aryl group twists facing almost perpendicularly the quinolyl group of the neutrally bound ligand, preventing the formation of the intramolecular hydrogen bond C(28)-H...O(2) breaking the planarity of the ligand but forming instead the hydrogen bond between C(2)-H...O(2) with a distance of 2.965 Å. Further hydrogen bonds can be seen between the amide proton of the ruthenium complex and DMF. The N(2)-H...O(3)/O_{DMF} has a distance of 2.714 Å.

The anionically bound ligand ($[N,N]$ coordination) shows the carbonyl bond (C(10)-O(1)) has a distance of 1.219(13) Å and the amide nitrogen single bond C(10)-N(2) has a length of 1.385(14) Å. It can be confirmed the ligand coordinates neutrally as an X-type. The neutrally coordinated shows similar bond lengths being the carbonyl bond length C(26)-O(2) of 1.245(12) Å and the amide nitrogen bond length C(26)-N(4) of 1.313(13) Å making it an L-type ligand. Overall, one of the ligands is negatively charged which coordinates to the ruthenium centre without varying the oxidation state of it and one neutral which completes the octahedral geometry of the complex. Relevant bond lengths, angles and dihedral angles are summarised in **Table 3-8** and **Table 3-9**.

The extended crystal structure packing shown **Figure 3-20** shows that molecules interact with each other *via* π - π stacking of the quinaldic cores corresponding to the deprotonated ligand with a centroid-centroid distance of 3.947 Å highlighted in blue and presenting a plane shift of 3.372, whereas the green quinoline cores belonging to the neutral ligand show a centroid-centroid distance of 3.523 Å with a shift of 3.428° and a slightly torsion of 0.813° between them.

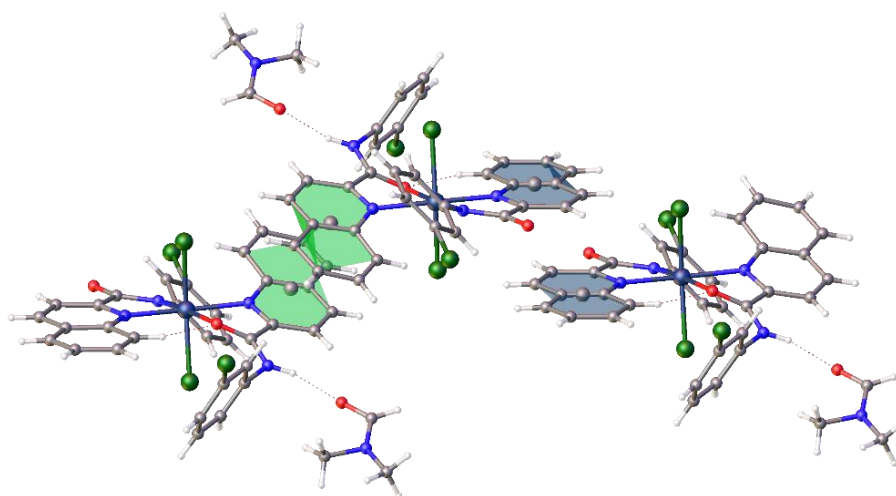


Figure 3-20: Extended crystal structure of compound **3.29**, showing the intermolecular π - π interactions.

Figure 3-21 shows the expansion of the crystal packing displaying a laminar shape where the chlorides occupy the void created by the ligands which are arranged in a quasi-planar disposition.

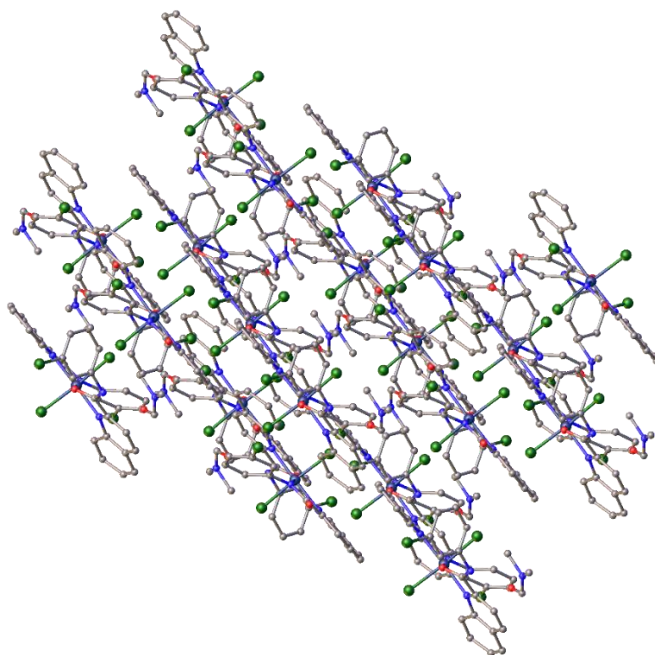


Figure 3-21: Expansion of the crystal packing of the complex (**3.29**).

Table 3-8: Selected bond lengths for complex **3.29** with labelled atoms corresponding to the complex in **Figure 3-19**

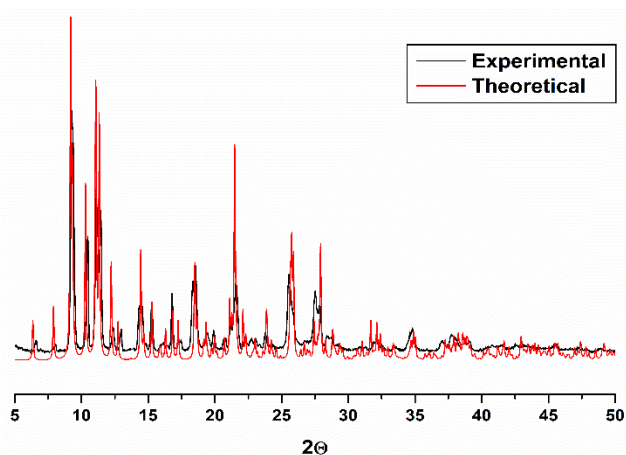
Bond	Length/ Å	Bond	Length/ Å
Ru(1)-Cl(1)	2.349(3)	N(1)-C(9)	1.325(13)
Ru(1)-Cl(2)	2.388(3)	N(2)-C(10)	1.385(14)
Ru(1)-O(2)	2.104(7)	N(3)-C(25)	1.324(13)
Ru(1)-N(1)	2.096(8)	N(4)-C(26)	1.313(13)
Ru(1)-N(2)	1.966(9)	C(9)-C(10)	1.510(13)
Ru(1)-N(3)	2.126(8)	C(25)-C(26)	1.492(13)
O(2)-C(26)	1.245(12)		

Table 3-9: Selected bond angles for complex **3.29** with labelled atoms corresponding to the complex in **Figure 3-19**

Bond	Angle/ °	Bond	Angle/ °
O(2)-Ru(1)-Cl(1)	87.6(2)	N(3)-Ru(1)-Cl(2)	91.4(2)
N(1)-Ru(1)-Cl(1)	88.4(2)	O(2)-Ru(1)-N(1)	101.3(3)
Cl(2)-Ru(1)-Cl(1)	169.51(10)	N(2)-Ru(1)-N(1)	79.8(3)
N(2)-Ru(1)-Cl(1)	97.0(3)	N(3)-Ru(1)-N(1)	176.5(3)
N(3)-Ru(1)-Cl(1)	89.9(2)	N(3)-Ru(1)-O(2)	75.6(3)
O(2)-Ru(1)-Cl(2)	82.6(2)	N(2)-Ru(1)-O(2)	175.3(4)
N(1)-Ru(1)-Cl(2)	89.8(2)	N(2)-Ru(1)-N(3)	103.5(3)
N(2)-Ru(1)-Cl(2)	92.8(3)		

3.8.2 X-ray powder diffraction

The x-ray powder pattern diffraction for complex **3.29** was recorded to prove the bulk powder sample and the crystal structure are formed by the *trans*-isomer, thus determining the purity of the sample biologically tested. **Figure 3-22** shows the comparison of the two diffractograms corroborating both sets are constituted by only one isomer. The main peaks of the diffractograms of the ruthenium complex **3.29** proved the complex has a similar structural geometry in both samples.

**Figure 3-22:** XRPD data overlap of complex **3.29** showing the experimental (*black*) and simulated (*red*) diffractograms recorded at scan rate of 40 sec/scan.

3.9 Ruthenium complex 3.32

3.9.1 X-ray single crystal diffraction of complex 3.32

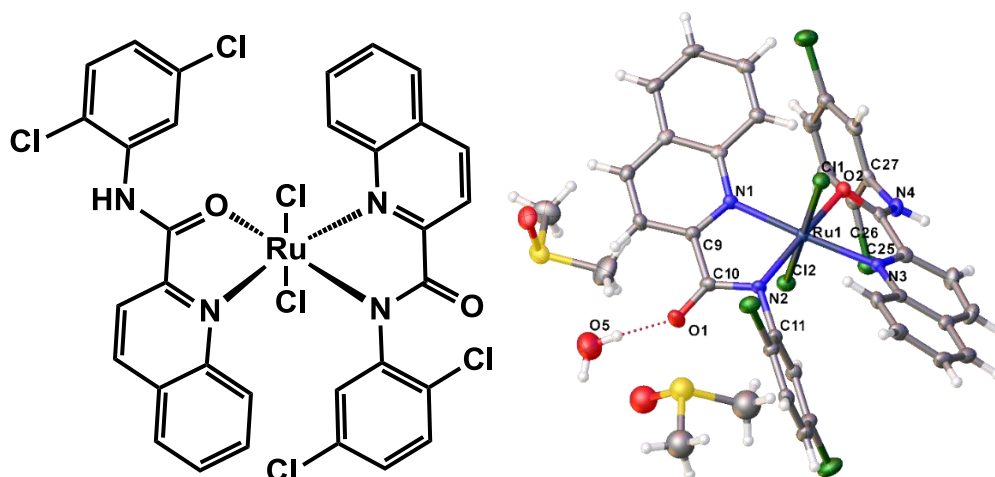


Figure 3-23: Chemical structure of compound **3.32** (left); labelled crystal structure (right).

Trans-dichloride bis-(*N*-2,5-dichlorophenyl)-quinaldamide ruthenium (III) complex (**3.32**) (**Figure 3-23**) was isolated as a dark red powder and crystallised from DMSO as red needles. The asymmetric unit contains two molecules of DMSO, one molecule of water and one molecule of the complex, crystallising in a triclinic system and solved in the space group *P*-1. **Figure 3-23** (right) shows the crystal structure of compound **3.32** and atom labels. The crystals analysed by x-ray crystallography only show the *trans-trans-trans* isomer. In this particular case, the distorted octahedral geometry can be demonstrated by the following angles: Cl(1)-Ru(1)-Cl(2) is 174.20(3)°, the N(2)-Ru(1)-O(2) is 167.34(10)° and N(1)-Ru(1)-N(3) is 176.27(11)°. It also shows the complex arranged in a slightly distorted octahedral geometry caused by the ligands as they bend towards one of the chlorides, proving that instead of 180° the angle form between the organic moiety and the metal is 173.84(3)°. The aryl fragments twist almost 90° encapsulating the ruthenium centre. This fact is easily seen in the extended crystal structure shown in **Figure 3-25**, which also shows one of the chlorides is more 'protected', due to the aryl twist making the other prone to hydrolyse. **Figure 3-23** also shows one of the ligands is bound deprotonated with a carbonyl (C(10)...O(1)) of 1.237(4) Å, the amide nitrogen single bond C(10)...N(2) has a length of 1.353(4) Å, confirming the ligand coordinates neutrally acting as an X-type. The ligand bound neutrally shows similar bond lengths being the carbonyl

bond length C(26)...O(2) of 1.265(4) Å and the amide nitrogen bond length C(26)...N(4) of 1.317(4) Å. **Table 3-10** and **Table 3-11** summarise all the relevant bond lengths, angles and dihedral angles.

Figure 3-24 shows the π - π stacking interactions. Surprisingly, this is the only compound, so far, that shows differences in terms of intermolecular interactions. The quinaldic cores of the ligands bound anionically (blue highlighted) show a π - π stacking with a centroid-centroid distance of 3.611 Å and for the first time, the aryl fragments show a π - π stacking (green highlighted) with a centroid-centroid distance of 3.923 Å. Another interesting feature is the lack of inter- and intramolecular hydrogen bonds. It was only found one hydrogen between the water of crystallisation and the oxygen of the quinaldamide bound anionically O(5)_{H₂O}-H...O(1) with a distance of 2.001 Å.

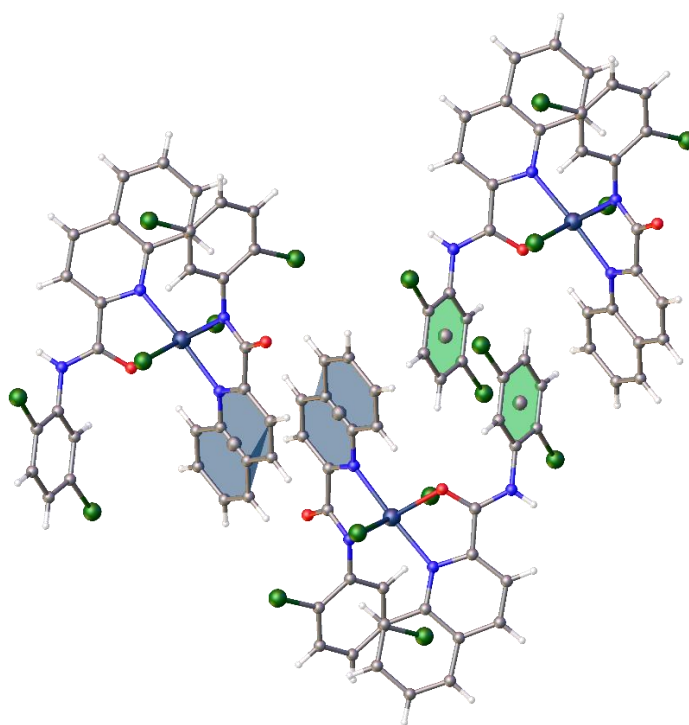


Figure 3-24: π - π interactions of the complex **3.32**.

Table 3-10: Selected bond lengths and s.u.s. for complex **3.32** labelled as shown in **Figure 3-23**

Bond	Length/ Å	Bond	Length/ Å
Ru(1)-Cl(1)	2.3326(8)	O(2)-C(26)	1.265(4)
Ru(1)-Cl(2)	2.3761(9)	N(1)-C(9)	1.321(4)
Ru(1)-O(2)	2.097(2)	N(2)-C(10)	1.353(4)
Ru(1)-N(1)	2.076(3)	N(3)-C(25)	1.335(4)
Ru(1)-N(2)	2.018(3)	N(4)-C(26)	1.317(4)
Ru(1)-N(3)	2.105(3)	C(9)-C(10)	1.494(4)
O(1)-C(10)	1.237(4)	C(25)-C(26)	1.495(5)

Table 3-11: Selected bond angles and s.u.s. for complex **3.32** and atom labels found in **Figure 3-23**

Bond	Angle/ °	Bond	Angle/ °
Cl(1)-Ru(1)-Cl(2)	174.20(3)	N(2)-Ru(1)-Cl(1)	99.04(8)
O(2)-Ru(1)-Cl(1)	93.50(7)	N(2)-Ru(1)-Cl(2)	86.34(8)
O(2)-Ru(1)-Cl(2)	81.07(7)	N(2)-Ru(1)-O(2)	167.34(10)
O(2)-Ru(1)-N(3)	76.65(10)	N(2)-Ru(1)-N(1)	78.75(10)
N(1)-Ru(1)-Cl(1)	89.90(7)	N(2)-Ru(1)-N(3)	104.90(10)
N(1)-Ru(1)-Cl(2)	89.02(8)	N(3)-Ru(1)-Cl(1)	90.28(8)
N(1)-Ru(1)-O(2)	99.62(9)	N(3)-Ru(1)-Cl(2)	90.43(8)
N(1)-Ru(1)-N(3)	176.27(11)		

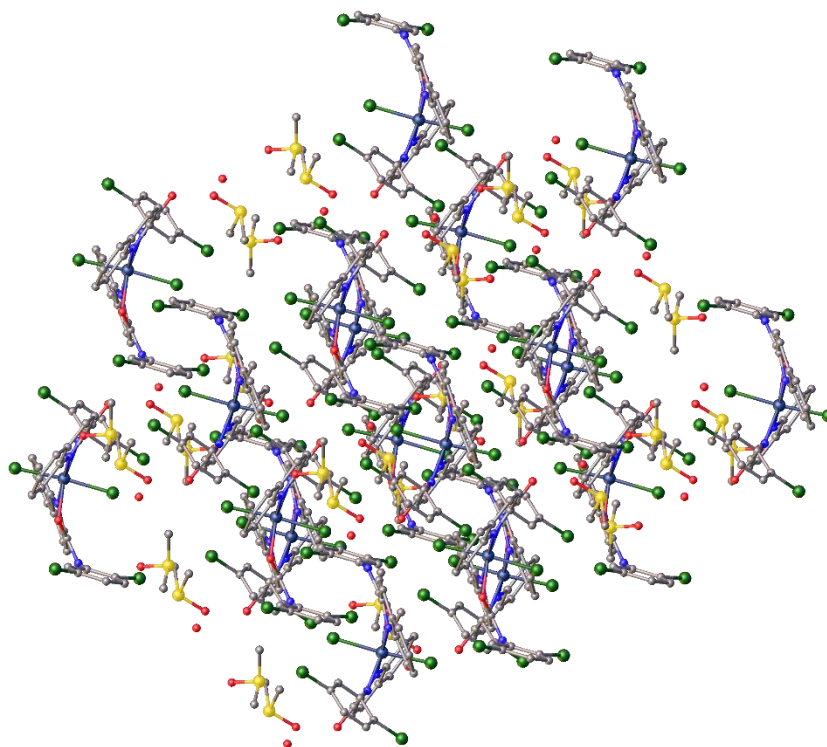


Figure 3-25: Crystal packing of compound **3.32**.

Figure 3-25 shows the extended packing of complex **3.32** displaying a shell-like motif where the ruthenium centres and one of the chlorides of each molecules are protected leaving the other chloride more exposed.

3.10 Ruthenium complex 3.38

3.10.1 X-ray single crystal diffraction of complex 3.38

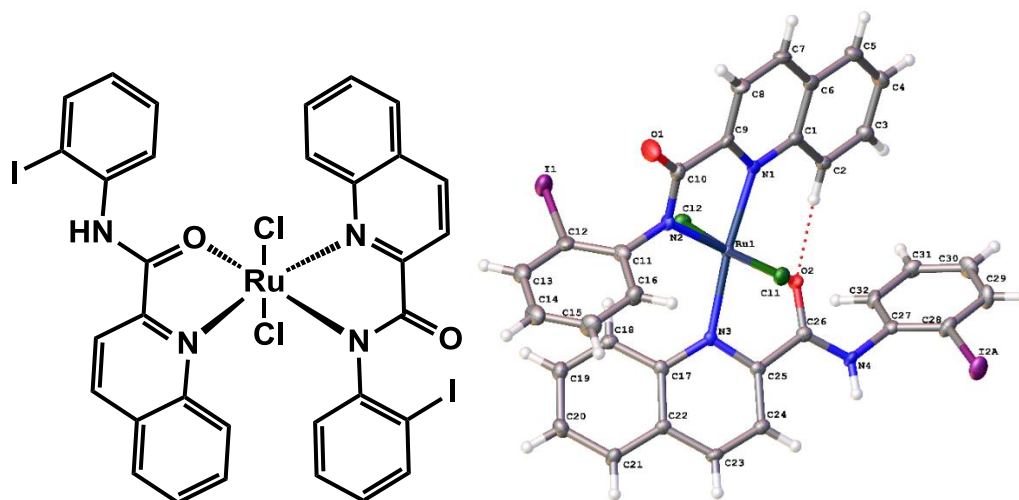


Figure 3-26: Chemical structure of complex **3.38** (*left*); labelled crystal structure (*right*).

Trans-dichloride bis-(*N*-2-iodophenyl)-quinaldamide ruthenium (III) complex (**3.38**) (**Figure 3-26**) was isolated as a red powder and crystallised from DMF which co-crystallises as red blocks. The asymmetric unit contains one molecule of DMF and the complex, solved in a monoclinic cell and solved in the space group *C2/c*. **Figure 3-26** (*right*) shows the labelled crystal structure of the *trans-trans-trans* isomer isolated, the twist of the amide links between the aromatic rings causes the slightly distorted octahedral geometry giving a concave shape to the molecule, more easily seen in the 3D expansion in **Figure 3-28**. The ligands bend towards one chloride, what makes the Cl(1)-Ru(1)-Cl(1) angle to be 174.22(4)°.

The neutral ligand shows the carbonyl bond (C(26)...O(2)) has a distance of 1.2353(5) Å and the amide nitrogen single bond C(26)...N(4) has a length of 1.331(6) Å confirming the ligand coordinates neutrally as an L-type. The ligand bound anionically shows similar bond lengths being the carbonyl bond length C(10)...O(1) of 1.225(5) Å and the amide nitrogen bond length C(10)...N(2) of 1.354(6) Å. Although, the x-ray structure confirms the absence of the amide proton making the ligand an X-type. The torsion of the ligand impedes the intramolecular hydrogen bond between C(32)...O(2) forming the intermolecular hydrogen bond C(2)...O(2) with a length of 2.919 Å holding the integrity of the

complex. A further hydrogen bond can be seen between the N(4)-H...O_{DMF} as shown in **Figure 3-26**. **Table 3-12** and **Table 3-13** show all the relevant bond lengths, angles and dihedral angles of complex **3.38** (**Figure 3-26**).

The π - π stacking (**Figure 3-27**) is similar to the compounds describe within this chapter. The ligand bound anionically (blue), shows the highlighted quinaldic cores interacting showing a centroid-centroid distance of 3.674 Å. The same happens to the neutral coordinated ligand which interacts only with another neutral bound ligand (green plane) with a centroid-centroid distance of 3.446 Å and twist angle between planes of 2.735°.

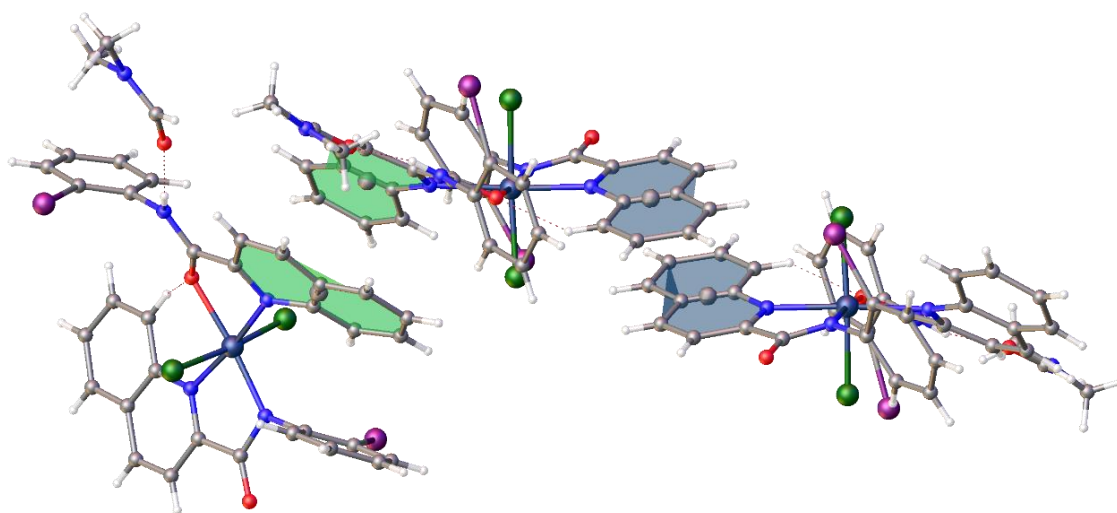


Figure 3-27: π - π stacking interactions of compound **3.38**.

Table 3-12: Selected bond lengths for complex **3.38** with labelled atoms corresponding to the complex in **Figure 3-26**

Bond	Length/ Å	Bond	Length/ Å
Ru(1)-Cl(1)	2.3585(12)	N(1)-C(9)	1.329(6)
Ru(1)-Cl(2)	2.3304(12)	O(2)-C(26)	1.2353(5)
Ru(1)-O(2)	2.091(3)	N(2)-C(10)	1.354(6)
Ru(1)-N(1)	2.086(4)	N(3)-C(25)	1.337(6)
Ru(1)-N(2)	2.011(3)	N(4)-C(26)	1.331(6)
Ru(1)-N(3)	2.123(4)	C(9)-C(10)	1.504(6)
O(1)-C(10)	1.225(5)	C(25)-C(26)	1.482(6)

Table 3-13: Selected bond angles for complex **3.38** with labelled atoms corresponding to the complex in **Figure 3-26**

Bond	Angle/ °	Bond	Angle/ °
Cl(2)-Ru(1)-Cl(1)	174.22(4)	N(3)-Ru(1)-Cl(2)	86.68(10)
N(1)-Ru(1)-Cl(1)	87.98(10)	O(2)-Ru(1)-N(1)	99.59(13)
O(2)-Ru(1)-Cl(1)	90.93(10)	N(2)-Ru(1)-N(1)	79.35(14)
N(2)-Ru(1)-Cl(1)	95.84(11)	N(3)-Ru(1)-N(1)	173.54(14)
N(3)-Ru(1)-Cl(1)	95.94(10)	N(3)-Ru(1)-N(2)	105.27(14)
O(2)-Ru(1)-Cl(2)	84.75(9)	N(2)-Ru(1)-O(2)	173.10(14)
N(1)-Ru(1)-Cl(2)	88.96(10)	N(3)-Ru(1)-O(2)	75.27(13)
N(2)-Ru(1)-Cl(2)	88.40(11)		

The crystal packing in **Figure 3-28** shows a helix-like motif where the molecules are held together through three different alternating π - π stacking interactions involving: the [N,O] quinaldic core... [N,N] aryl ring with a centroid-centroid distance of 3.654 Å; [N,O] quinaldic core...[N,O] quinaldic core of 3.976 Å and [N,N] quinaldic core...[N,N] quinaldic core of 3.679 Å.

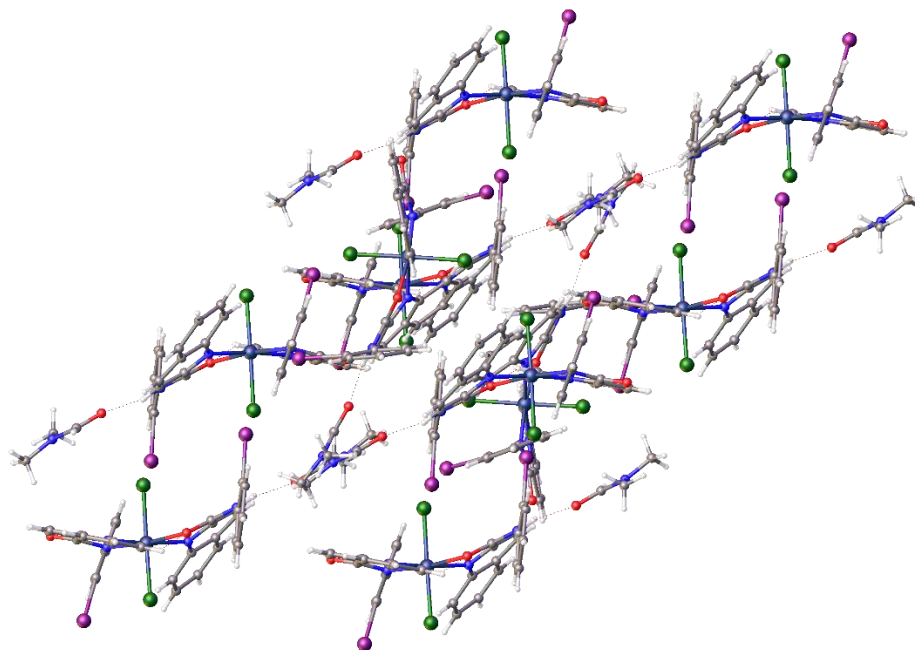


Figure 3-28: Z-axis view of the crystal packing expansion of complex **3.38**.

3.11 Side product when using basic conditions: Complex 3.25a

Previously, McGowan *et al.* reported the synthesis of picolinamide ligands and different metal salts where a base was required to deprotonate one of the amide protons to coordinate to the metal. It was assumed that, due to chemical similarity, the reactivity of the quinaldamide ligands would be similar. However, upon addition of triethylamine as a base, the reaction yielded dark coloured compounds proving impossible to crystallise and analyse. Unless for one reaction, two different sets of crystals were isolated: needles belonging to the neutral *trans*-dichloride complex and red plates belonging to a *cis*-dichloride ruthenium (III) charged complex. In **Figure 3-29**, the two quinaldamide ligands are deprotonated in a *cis* position, and the triethylammonium salt as counterion. Although, tuning the charge of the metal complexes could have great potential, the focus of this chapter is to describe the *trans*-dichloride complexes that were tested for their anticancer, antibacterial and antifungal activity (**Chapter 4**).

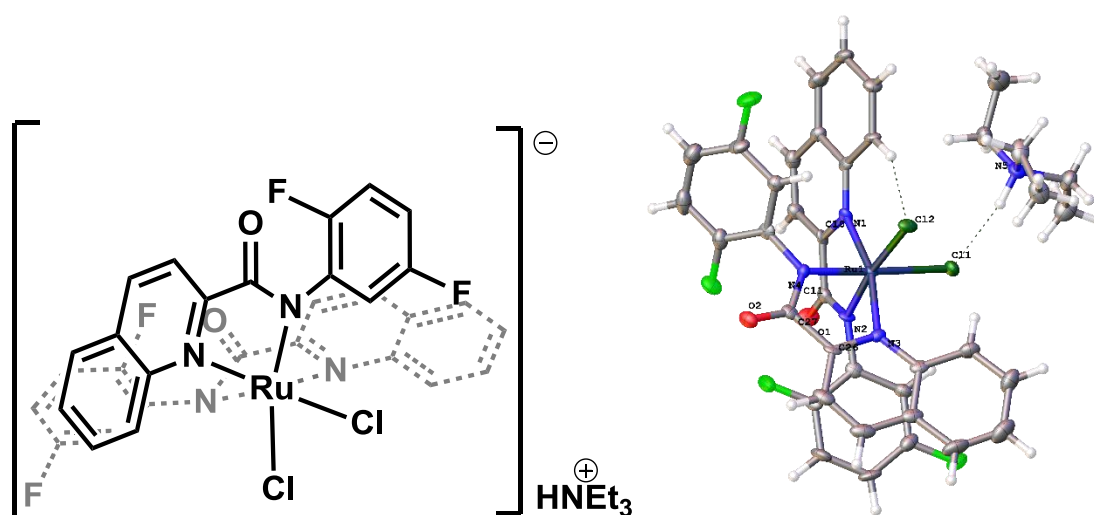


Figure 3-29: Chemical structure of the charged side product (*left*) and the labelled crystal structure of the *cis*-dichloride bis-(2,5-difluoroquinaldamide) ruthenate (III) triethylammonium salt.

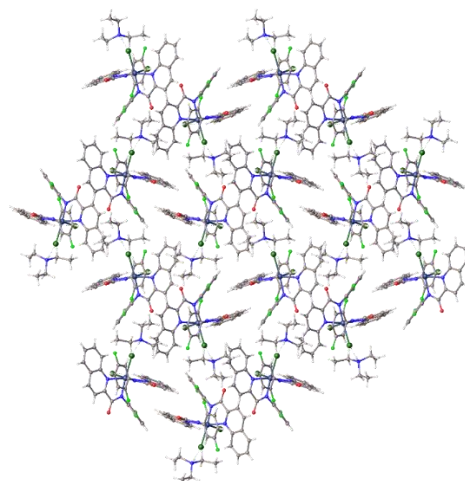
The crystalline charged complex was solved in the space group $Pn2_1a$ with selected bond distances and bond angles in **Table 3-14** and **Table 3-15**, respectively, proving that the chloride labile ligands are placed in a *cis*-arrangement, the nitrogens of the quinaldic cores are *trans* to each other and the nitrogens of the aniline fragments are *cis* to each other, displaying a final configuration of *cis-trans-cis*.

Table 3-14: Selected bond distances with s.u.s. of the charged complex described in **Figure 3-29**

Bond	Distance/ Å
Ru(1)-Cl(1)	2.4182(10)
Ru(1)-Cl(2)	2.4467(11)
Ru(1)-N(1)	2.114(3)
Ru(1)-N(2)	1.998(3)
Ru(1)-N(3)	2.086(17)
Ru(1)-N(4)	2.145(3)

Table 3-15: Selected bond angles with s.u.s. of the charged complex described in **Figure 3-29**

Bond	Angle/ °
Cl(2)-Ru(1)-Cl(1)	91.52(4)
N(2)-Ru(1)-N(1)	78.84(14)
N(4)-Ru(1)-Cl(2)	85.47(11)
N(3)-Ru(1)-N(1)	165.17(14)
N(4)-Ru(1)-Cl(1)	172.61(10)
N(2)-Ru(1)-Cl(2)	176.13(9)

**Figure 3-30:** Expanded Crystal Structure of the side product *cis*-dichloride bis-(2,5-difluoroquinaldamide) Ru(III) charged complex.

3.12 Side product of the base free reaction: complex 3.33a

The base free reaction lead to the main compound (neutral bisquinaldamide ruthenium complex), however, the slow crystallisation of the mother liqueurs yielded an unexpected product that could potentially be either the first step of the complexation or a decomposition product. The compound is the trichloride monosubstituted quinaldamide ruthenium (III) complex – the ruthenium complex containing three chloride ligands, one quinaldamide ligand and one molecule of

ethanol as shown in **Figure 3-31**. The quinaldamide ligand has a planar geometry and the ruthenium opts for an octahedral geometry. Several attempts were made in to form this class of compounds, but they were only obtained from the mother liqueurs of the reaction mixture. The compounds analysed by HRMS proved the mass for those species. Further investigations should be done into these reactions as little it is known about anticancer metallodrugs containing three labile ligands. The attempts made to synthesise these sorts of complexes involved the variation of the number of moles of the ligand, however, diluted conditions could favour the isolation of these complexes.

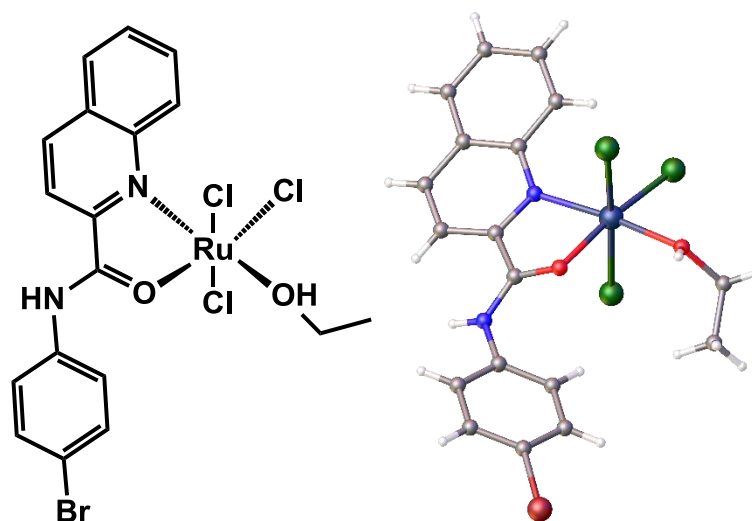


Figure 3-31: (*Left*) chemical structure of side product of the base free reaction with 4-bromoquinaldamide ligand; (*right*) crystal structure of the compound isolated.

Mother liqueurs of other reactions were left to crystallise but only a fine powder was isolated. The reaction involving the unsubstituted quinaldamide **2.1** was analysed by HRMS (**Figure 3-32**) observing the main peak at an m/z of 455.9578 corresponding to the $[M+H]^+$, calculated to be at 455.9127 u.m.a.

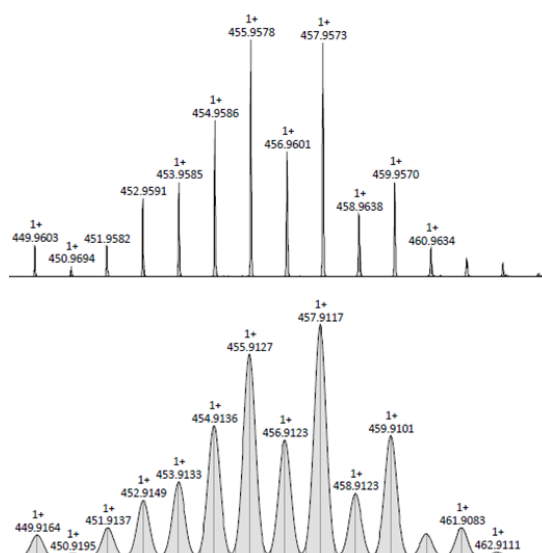
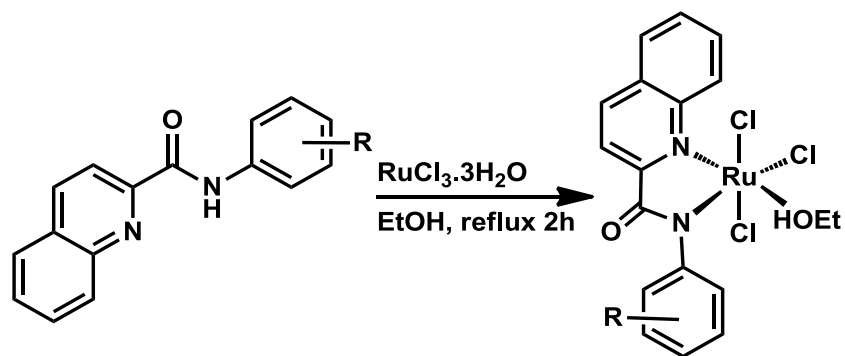


Figure 3-32: (Top) experimental HRMS spectrum obtained of the complex from the mother liquors of the reaction with the unsubstituted ligand **2.1**; (Bottom) simulated pattern of the compound.

The synthesis (**Scheme 3-2**) of the mono *N*-phenyl-2-quinolinecarboximide (ligand **2.1**) ruthenium (III) trichloride complex proved to be unsuccessful, as the solid isolated was the initial bisquinaldamide ruthenium complex.



Scheme 3-2: Reaction scheme followed to synthesis the monoquinaldamide ruthenium (III) trischloride neutral complexes.

3.13 Compound fragmentation, complex 3.15a

The reaction carried by an MChem student Daniel Kowalski that involves the complexation of 2-^tbutylquinaldamide yielded one compound (left complex in **Figure 3-33**): the expected neutral complex which is not discussed in this chapter. However, after crystallisation from DMF, the desired complex and an unexpected neutral complex were solved by X-ray crystallography. The two complexes were found in the same crystallisation batch meaning, most likely, it could be a decomposition product formed by one quinaldamide bound anionically [N,O], two chlorides and two molecules of DMF coming from the crystallisation solvent (**Figure 3-34**). The crystal structure is shown in **Figure 3-34** and solved using the triclinic space groups P -1 in which the asymmetric unit contains a single molecule of the complex and one molecule of DMF. **Table 3-16** and **Table 3-17** summarise the main bond distances and angles respectively, showing the integrity of the *trans* dichloride ligands remain intact ($176.04(2)^\circ$) and the neutrally coordinated ligand is being displaced by the DMF molecules.

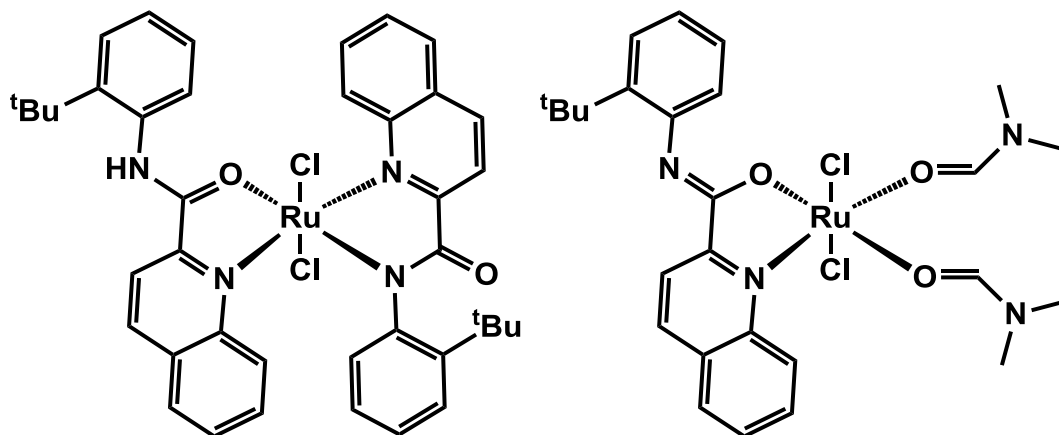


Figure 3-33: Chemical structure of bisquinaldamide neutral complex and decomposition product.

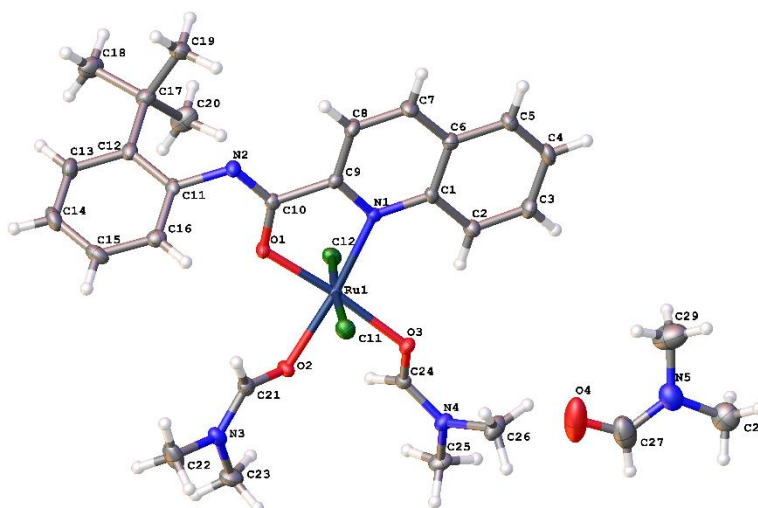


Figure 3-34: Labeled crystal structure of the proposed decomposition product.

Table 3-16: Selected bond distances of the labelled complex in **Figure 3-34**

Bond	Distance/ Å
Ru(1)-Cl(1)	2.343(6)
Ru(1)-Cl(2)	2.335(6)
Ru(1)-O(1)	1.966(18)
Ru(1)-O(2)	2.101(17)
Ru(1)-O(3)	2.086(17)
Ru(1)-N(1)	2.054(2)
N(1)-C(9)	1.343(3)
C(9)-C(10)	1.498(3)
C(10)-N(2)	1.284(3)
C(10)-O(1)	1.309(3)

Table 3-17: Selected bond angles of the labelled complex in **Figure 3-34**

Bond	Angle / °
Cl(1)-Ru(1)-Cl(2)	176.04(2)
Cl(1)-Ru(1)-O(1)	89.62(6)
Cl(1)-Ru(1)-O(2)	89.97(5)
Cl(1)-Ru(1)-O(3)	87.46(5)
Cl(1)-Ru(1)-N(1)	88.92(6)
O(1)-Ru(1)-N(1)	81.29(8)

3.14 Conclusion

A wide library of novel *trans*-dichloride bis-functionalised quinaldamide ruthenium (III) complexes have been successfully synthesised and characterised by means of IR, HRMS, elemental analysis, magnetic susceptibility and when suitable by X-ray crystallography and X-ray powder diffraction. The focus was given to the eight 'Lead Compounds' chosen due to their biological anticancer activity which is thoroughly described in chapter 4.

It was indicated by X-ray powder diffraction that only one isomer was obtained by comparing the diffractogram simulated from the crystal structures and the bulk sample. Importantly, the two main lead compounds **3.23** (R = 2-F) and **3.32** (R = 2,5-diCl) show π - π stacking between the aryl moieties, feature not seen for the other compounds analysed.

All the compounds show a *trans-trans-trans* arrangement breaking the rules of metal-based drugs. Increasing ligand size by adding fused rings plays a key role in obtaining purely one isomer out of five potential isomers, when the labile halide ligand is a chloride.

Furthermore, two unexpected compounds: a neutral trischloride monoquinaldamide ruthenium (III) complex and a charged *cis*-chloride bisquinaldamide ruthenium (III), opening two other interesting projects.

3.15 Further work

In terms of characterisation, further analysis will be studied to determine the behaviour in solution by Electron Paramagnetic Resonance spectroscopy (EPR) as it would complement a new biological approach, how paramagnetism affects anticancer studies.¹⁰ Stability studies using UV-vis at different temperatures will be done. Complementary analysis will be focused on the fluorescence of the ruthenium complexes, as the highly conjugated aromatic rings have the potential to increase this feature that could show where the compounds accumulate inside the cells.

3.16 References

- ¹ Aris, S. M.; Farrell, N. P.; *Eur. J. Inorg. Chem.*, **2009**, 10, 1293-1302.
- ² Krause, R. A.; Krause, K.; *Inorg. Chem.* **1980**, 19- 2600-2603.
- ³ Velders, A. H.; Kooijman, H.; Spek, A. L.; Haasnoot, J. G.; de Vos, D.; Reedijk, J.; *Inorg. Chem.*, **2000**, 39, 2966-2967
- ⁴ Roy, S.; Maheswari, P. U.; Golobič, A.; Kozlevčar, B.; Reedijk, J.; *Inorg. Chim. Acta*, **2012**, 393, 239-245.
- ⁵ Wachter, E.; Zamora, A.; Heidary, D. K.; Ruiz, J.; Glazer, E. C.; *Chem. Comm.* **2016**, 52, 10121-10124.
- ⁶ Kilpin, K. J.; Clavel, C. M.; Edafe, F.; Dyson, P. J.; *Organometallics*, **2012**, 31, 7031-7039.
- ⁷ Hearn, J. M.; Romero-Canelón, I.; Qamar, B.; Liu, Z.; Hands-Portman, I.; Sadler, P. J.; *ACS Chem Bio*, **2013**, 8, 1335-1343.
- ⁸ Gasser, G.; Ott, I.; Metzler-Nolte, N.; *J. Med. Chem.*, **2011**, 54, 3-25.
- ⁹ Basri, A. M.; Lord, R. M.; Allison, S. J.; Rodríguez-Bárcano, A.; Lucas, S. J.; Janeway, F. D.; Shepherd, H. J.; Pask, C. M.; Phillips, R. M.; McGowan, P. C.; *Chem. Eur. J.*, **2017**, 23, 26, 6341-6356.
- ¹⁰ Prosser, K. E.; Walsby, C. J.; *Eur. J. Inorg. Chem.*, **2017**, 1573-1585.

Chapter 4
Biological Investigations on the neutral *trans*-dichloride
bisquinaldamide Ruthenium (III) complexes

4.1 Introduction to the Drug Discovery Process

Society is constantly demanding for new drugs that are more effective, selective and potent. Academia and industry joint together in the search of the 'Holy Grail,' to cure new and old diseases, in a process that divides into two parts: drug discovery and development process. Small molecules have been identified and screened against a known biological target, identified as Lead Compounds with the desired therapeutic effects and optimised to enhance their properties. Successful candidates may be taken further into preclinical trials where biological aspects like pharmacokinetics, pharmacodynamics and toxicity are investigated. New candidates fail in clinical trials due to either being less effective than current treatments or are unsafe, or both. Hence validating Lead Compounds *in vitro* and determining their biological properties in preclinical stages are critical in order to put forward a new drug for *in vivo* analysis or clinical trials. The first stage of preclinical anticancer studies is the *in vitro* cytotoxicity screening. These assays were mentioned in **Chapter 1** and, briefly, are used worldwide to measure the effectiveness of a drugs against some human cell lines to identify Lead Compounds. The screening used and described in this chapter is the MTT assay. It falls in the category of 'Phenotypic Approach' within the Drug Discovery process which assumes there are compounds capable of targeting several pathways that yield a desirable phenotypical effect, in this case cancerous cell death. The next step is called target deconvolution where the mechanism(s) of action are determined.¹ The outcome of the MTT assay is a number called IC₅₀ value which classifies a drug as highly active, active, moderately active or inactive.²⁻⁷

4.2 Cytotoxicity: MTT assay

The robust and direct MTT assay is a colorimetric assay based on the reduction of the yellow water-soluble salt (3-(4,5-dimethylthiazol-2-yl)-2,5-diphenyl tetrazolium bromide) MTT to give the purple/dark blue water insoluble formazan crystals. This assay, initially described by Mosmann⁶ in 1983 and later optimised by Sylvester,⁸ depends on NAD(P)H reductases within the cell. Originally, it was thought that this redox reaction took place in the membranes of the mitochondria, as the mitochondrial dehydrogenase enzymes were implicated. However, recent studies have shown that cytosolic enzymes NAD(P)H-dependent are also

responsible for the MTT reduction (**Figure 4-1**).⁹ The formazan crystals are dissolved and read using a multiwell scanning spectrophotometer (TECAN reader). The amount of crystals formed are proportional to the number of living cells that are metabolically active, meaning this method could also be used to differentiate the measurement of cell proliferation and activation.¹⁰

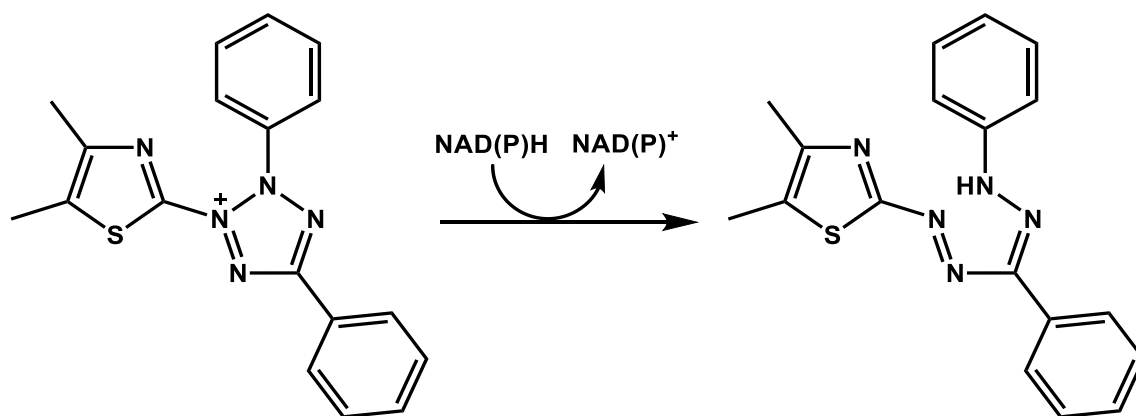


Figure 4-1: Mechanism of reduction of the water soluble yellow MTT salt to the insoluble violet formazan neutral molecule by NAD(P)H.

4.3 Normoxia cytotoxic studies of *trans*-dichloride bisquinaldamide Ruthenium complexes

4.3.1 Rationale behind the cell lines studied

In 2012 it was recorded 1.36 million new cases of colorectal cancer across the globe and 500,000 of those were diagnosed alongside Europe, being around 40,000 cases in the United Kingdom. In 2015, colorectal cancer was the 4th most common in the UK and it is expected that in 2035, 100,000 people will be affected by this deadly disease. Statistics say that only 50% of the patients will survive. Having this in mind, colorectal cancer is a desirable target in terms of development of new cures.¹¹ HCT 116 is used in this project and the cell line is from an adult male colorectal carcinoma.¹² Those used in this project have been genetically manipulated to mimic cancers in clinic. This mutation is located in the gene p53, which is a tumour suppressor. When cells behave correctly, the gene p53 would stop any sorts of anomalies to happen, however, if cells start to reproduce uncontrollably, the gene p53 will not be expressed (knockdown) hence the expression of cancer. This mutation causes the cell line HCT 116 to be divided into HCT 116 p53 (+/+) or wild type and HCT 116 p53 (-/-) or knockdown.

Any mutation on this gene would allow to understand the potential mechanism of action for this family of complexes.

Pancreatic cancer is not as recurrent in society as colorectal cancer, but there is only 1% survival. This is due to the late diagnosis and the not-known treatment. The NHS estimated that in 2012 there were 338.000 cases worldwide, being around 104.000 cases reported in Europe. In the UK, this cancer does not affect as much as in the rest of Europe, but it is estimated 9.800 new cases per year, being 37% preventable and less than 1% have survived. These numbers represent a very invasive cancer without a treatment, hence the interest on understanding the physiology of the pancreatic cancer and how to defeat it.¹³ MIA PaCa_2 is the cell line chosen for the studies and it comes from a 65 year-old Caucasian male suffering pancreatic carcinoma.¹⁴

Cytotoxic studies must be carried out against a non-cancerous cell line in order to determine if compounds are selective towards cancerous cell lines. ARPE-19 is the healthy cell line in these studies and it comes from the retinal pigmented epithelium of a 19 years-old male.¹⁵

4.3.2 Normoxia cytotoxic results and discussion

From the 40 compounds reported in this thesis (**Chapter 3**), three did not satisfy the desired purity given by elemental analysis (>95%) and seven were not tested due to either the lack of completing the series in terms of functionality (complexes **3.2**, **3.3** and **3.4**) and not enough sample to evaluate the anticancer activity. The remaining thirty compounds were screened against three cancerous cell lines: HCT116 p53 (+/+) (human colon carcinoma with tumour suppressor gene present) HCT116 p53 (-/-) (human colon carcinoma with knockdown tumour suppressor gene), MIA PaCa_2 (human pancreatic carcinoma) and a non-cancerous cell line, ARPE-19 (human retinal pigmented epithelial cell).

The general structure of the *trans*-dichloride bisquinaldamide ruthenium complexes is shown in **Figure 4-2**, R-substituents and numbering are summarised in **Table 4-1**. All the biological work of this thesis (unless otherwise stated) and chemosensitivity studies from the past two years for the McGowan group were carried by the author at the University of Huddersfield under the supervision of Professor Roger M. Phillips.

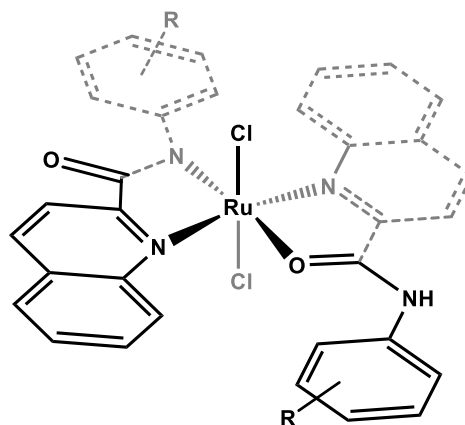


Figure 4-2: General structure of the *trans*-dichloride ruthenium (III) bisquinaldamide complexes. Grey dashed lines and black highlighted parts were drawn for 3D clarity.

Table 4-1: Summary of the complex codes and R groups

Complex	R	Complex	R
3.1	H	3.25	4-F
3.5	2-Me	3.26	2,4-diF
3.6	3-Me	3.27	2,5-diF
3.7	4-Me	3.28	2-Cl
3.9	2-Et	3.29	3-Cl
3.10	3-Et	3.30	4-Cl
3.11	4-Et	3.31	2,4-diCl
3.12	2- ⁱ Pr	3.32	2,5-diCl
3.13	3- ⁱ Pr	3.33	2-Br
3.15	2,6-di ⁱ Pr	3.34	3-Br
3.16	2-Me-6- ⁱ Pr	3.35	4-Br
3.17	2- ^t Bu	3.36	2,4-diBr
3.18	4- ^t Bu	3.38	2-I
3.23	2-F	3.39	3-I
3.24	3-F	3.40	4-I

The complexes (dissolved in DMSO at a final concentration of 100 μM , diluted further in cell media from 100 μM to 0.045 μM) were incubated with the cell lines at 37 °C in an atmosphere of 5% CO_2 for 72 hours. After incubation with MTT for three hours, the inhibition of cell survival was measured at 540 nm and by plotting the percentage cell survival (%) versus drug concentration (μM). All cytotoxic assays were performed a minimum of three times or as many times until the standard deviations or standard errors were acceptable. The accepted standard deviations/errors to publish are determined by the following calculation: standard deviation or standard error must be equal or smaller than the IC_{50} value divided by three.

The results for the cytotoxicity screening of the *trans*-dichloride bis-quinaldamide Ru(III) complexes compared against current therapeutic drugs: cisplatin, carboplatin and oxaliplatin as comparison were tested against HCT 116 p53 (+/+), HCT 116 p53 (-/-) and MIA PaCa_2 cancer cells lines and ARPE-19 are as shown in **Figure 4-3** and all the values are summarised in **Table 4-2** for complexes between **3.1 – 3.24**, **Table 4-3** for complexes **3.25 – 3.40** and **Table 4-4** for the current FDA chemotherapeutic agents (cisplatin, carboplatin and oxaliplatin). The complexes show a wide variety in anticancer potency and the values in the tables are colour coded to facilitate the visual understanding of the results; highly active complexes highlighted in green ($\text{IC}_{50} < 10 \mu\text{M}$), active complexes highlighted in blue ($10 \mu\text{M} < \text{IC}_{50} < 20 \mu\text{M}$), moderately active highlighted in orange ($20 \mu\text{M} < \text{IC}_{50} < 50 \mu\text{M}$) and non-highlighted when ($50 \mu\text{M} < \text{IC}_{50}$). Additionally, the opposite effect is desired against ARPE-19 meaning the higher the IC_{50} value the less toxicity, hence potentially less side effects.

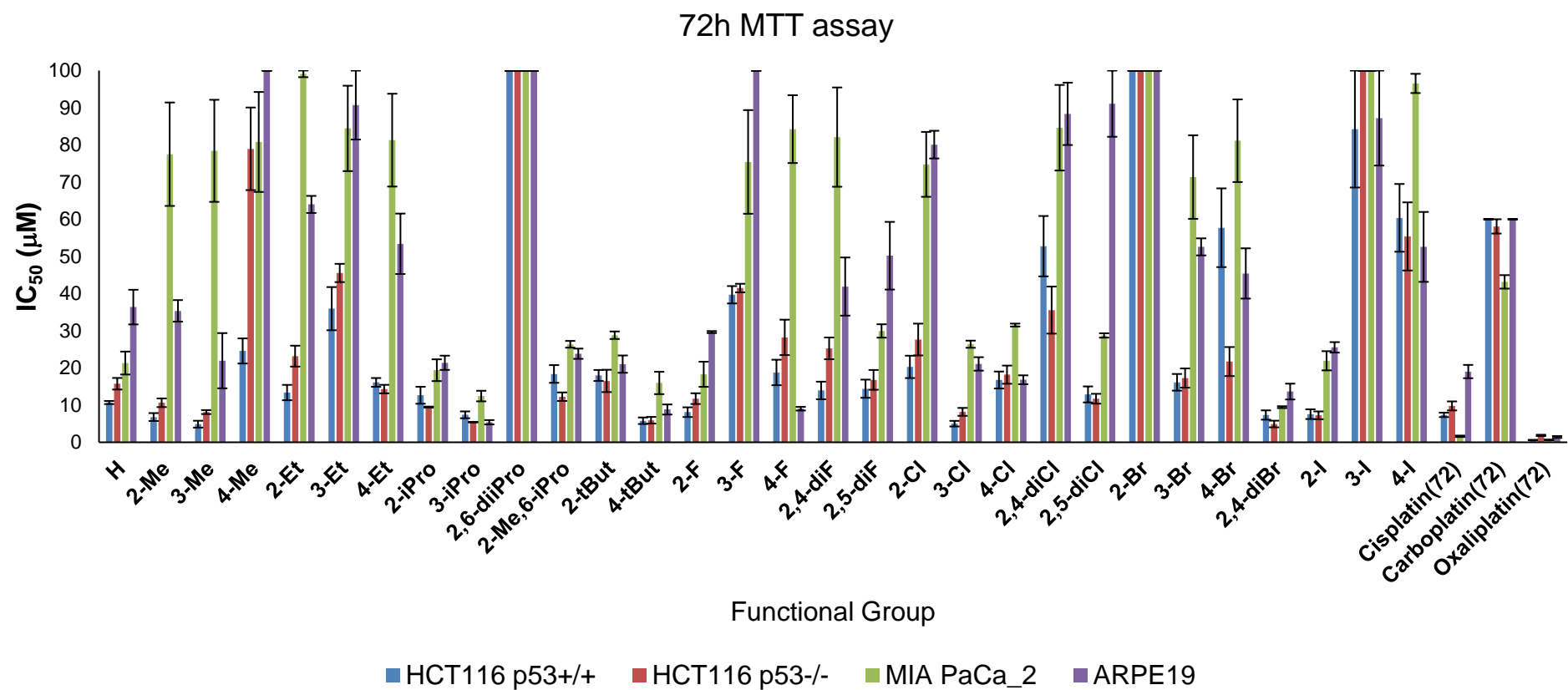


Figure 4-3: Bar-chart of all the $IC_{50} \pm S. E.$ values against HCT 116 p53 (+/+), HCT 116 p53 (-/-), MIA PaCa-2 and ARPE-19.

Table 4-2: IC₅₀ values ± S.E. (μM) of the complexes **3.1** – **3.24** expressed as the mean IC₅₀ ± S.E. for three independent experiments

Complex	R	HCT 116 p53 (+/+)	HCT 116 p53 (-/-)	MIA PaCa_2	ARPE-19
3.1	H	10.69 ± 0.42	15.75 ± 1.56	21.32 ± 3.08	36.37 ± 4.65
3.5	2-Me	6.78 ± 1.06	10.63 ± 1.16	77.5 ± 13.91	35.35 ± 2.90
3.6	3-Me	4.87 ± 0.92	8.13 ± 0.52	78.41 ± 13.73	21.95 ± 7.42
3.7	4-Me	24.57 ± 3.37	78.95 ± 11.10	80.79 ± 13.44	100
3.9	2-Et	13.37 ± 2.06	23.18 ± 2.81	99.11 ± 0.89	63.99 ± 2.29
3.10	3-Et	35.95 ± 5.80	45.55 ± 2.45	84.83 ± 11.49	90.72 ± 9.27
3.11	4-Et	16.11 ± 1.17	14.31 ± 1.14	81.28 ± 12.48	53.40 ± 8.12
3.12	2- ⁱ Pr	12.65 ± 2.82	9.46 ± 0.14	19.39 ± 2.92	21.38 ± 1.91
3.13	3- ⁱ Pr	7.39 ± 0.92	5.41 ± 0.09	12.43 ± 1.42	5.39 ± 0.54
3.15	2,6-di ⁱ Pr	100	100	100	100
3.16	2-Me-6- ⁱ Pr	18.38 ± 2.38	12.26 ± 1.15	26.36 ± 0.90	23.82 ± 1.37
3.17	2- ^t Bu	17.97 ± 1.48	16.50 ± 3.00	28.80 ± 1.01	21.03 ± 2.32
3.18	4- ^t Bu	5.79 ± 0.87	5.93 ± 0.89	15.95 ± 3.01	8.82 ± 1.35
3.23	2-F	8.10 ± 1.30	11.74 ± 1.44	18.30 ± 3.38	29.64 ± 0.26
3.24	3-F	39.69 ± 2.33	41.49 ± 1.15	75.41 ± 13.94	100

Table 4-3: IC₅₀ ± S.E. values (μM) of the complexes **3.25** – **3.40** expressed as the mean IC₅₀ ± S.E. for three independent experiments

Complex	R	HCT 116 p53 (+/+)	HCT 116 p53 (-/-)	MIA PaCa-2	ARPE-19
3.25	4-F	18.78 ± 3.43	28.22 ± 4.76	84.25 ± 9.12	9.04 ± 0.49
3.26	2,4-diF	13.94 ± 2.36	25.26 ± 2.92	82.10 ± 13.35	41.89 ± 7.82
3.27	2,5-diF	14.41 ± 2.44	16.79 ± 2.65	29.95 ± 1.79	50.19 ± 9.10
3.28	2-Cl	20.28 ± 3.00	27.64 ± 4.28	74.76 ± 8.79	80.08 ± 3.72
3.29	3-Cl	5.01 ± 0.75	8.18 ± 1.06	26.38 ± 0.95	21.08 ± 1.80
3.30	4-Cl	16.75 ± 2.28	18.19 ± 2.44	31.53 ± 0.39	16.82 ± 1.18
3.31	2,4-diCl	52.75 ± 8.12	35.56 ± 6.32	84.62 ± 11.50	88.36 ± 8.38
3.32	2,5-diCl	12.87 ± 2.15	11.71 ± 1.32	28.73 ± 0.58	91.09 ± 8.90
3.33	2-Br	100	100	100	100
3.34	3-Br	16.13 ± 2.24	17.28 ± 2.58	71.34 ± 11.23	52.57 ± 2.29
3.35	4-Br	57.72 ± 10.59	21.72 ± 3.90	81.12 ± 11.11	45.42 ± 6.76
3.36	2,4-diBr	7.33 ± 1.24	4.92 ± 0.89	9.45 ± 0.25	13.64 ± 2.12
3.38	2-I	7.56 ± 1.30	7.25 ± 1.05	21.93 ± 2.58	25.54 ± 1.41
3.39	3-I	84.27 ± 15.73	100	100	87.22 ± 12.77
3.40	4-I	60.37 ± 9.11	55.38 ± 9.16	96.53 ± 2.58	52.56 ± 9.40

Table 4-4: IC₅₀ values (μM) of the current clinical chemotherapeutic drugs (cisplatin, carboplatin and oxaliplatin) expressed as the mean IC₅₀ ± S.E. for three independent experiments after 72 hours exposure

Complex	HCT 116 (+/+)	HCT 116 (-/-)	MIA PaCa_2	ARPE-19
Cisplatin	7.37 ± 0.58	9.78 ± 1.20	1.61 ± 0.19	19.03 ± 1.78
Carboplatin	>60	58.07 ± 1.92	43.15 ± 1.81	>60
Oxaliplatin	0.61 ± 0.06	1.85 ± 0.17	0.64 ± 0.07	1.43 ± 0.25

From the IC₅₀ values obtained, few trends can be observed. The compounds **3.15** (R = 2,6-diⁱPr), **3.33** (R = 2-Br) and **3.39** (R = 3-I) do not display any anticancer activity or affect the healthy cell line. The remaining complexes target predominantly the colorectal cell lines, showing some toxicity against the pancreatic cell line, and with a variety of values for the non-cancerous cell line. Compound **3.1** (R = H) is the benchmark to compare the remaining complexes, it shows IC₅₀ values of 10.69 ± 0.42 (μM), 15.75 ± 1.56 (μM) and 21.32 ± 3.08 (μM) for HCT 116 p53 (+/+), HCT 116 p53 (-/-) and MIA PaCa-2, respectively. It also shows an IC₅₀ value of 36.37 ± 4.65 (μM) against the ARPE-19. This is an interesting result as, rarely, an unsubstituted ligand tends to have from the least to average anticancer potency. This compound will be used to find structural activity relationships when varying the electronics of the aniline ring and see if this affects more than the ruthenium benchmark complex **3.1** (R = H). Chemically speaking, in terms of position of the R groups, when increasing the bulkiness of the EDG in the position 2 of the aniline ring, the IC₅₀ values increase or show equitoxic potency (Me < Et < ⁱPr < ^tBu) whereas when decreasing the size of the EWG the anticancer activity enhances (I > Cl > F) as shown in **Figure 4-4**, this behaviour is observed for the cancerous cell lines, except for the pancreatic cell lines (green line) where 2-Me possesses little activity. In terms of coordination, the complexes bearing EDG coordinate to the Ru(III) in an [N,O] anionic manner, whereas the EWG coordinate in a [N,N] anionic manner. This reinforces that coordination is not as important but the disposition of the labile ligands.

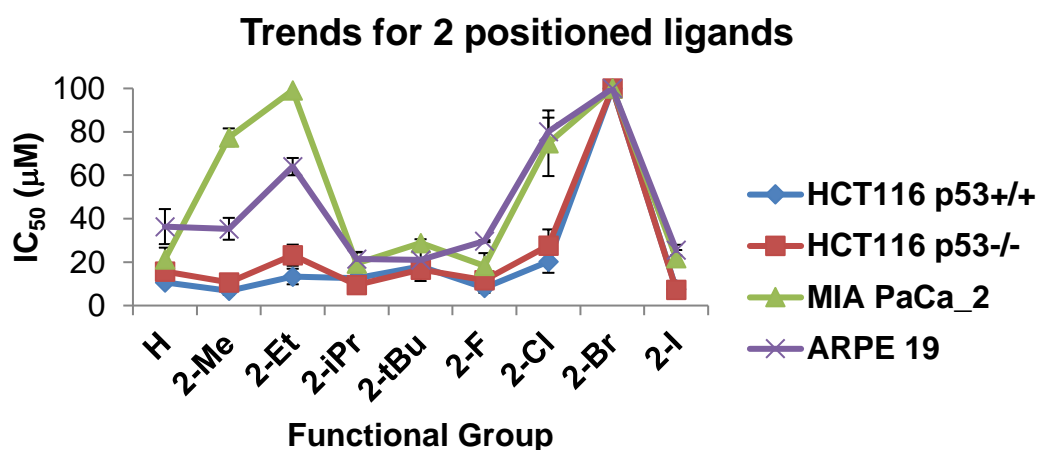


Figure 4-4: Comparison of the activity of the complexes functionalised in the position 2.

Complexes containing functional groups in the 3rd position present a different behaviour (**Figure 4-5**) than in position 2. In order of anticancer activity (IC₅₀), ⁱPr < Me ≈ Cl < Et ≈ F ≈ Br < I. It shows an alternating behaviour depending on the bulkiness of the substituents being the 3-ⁱPr substituted complex (**3.13**), the most active across the series.

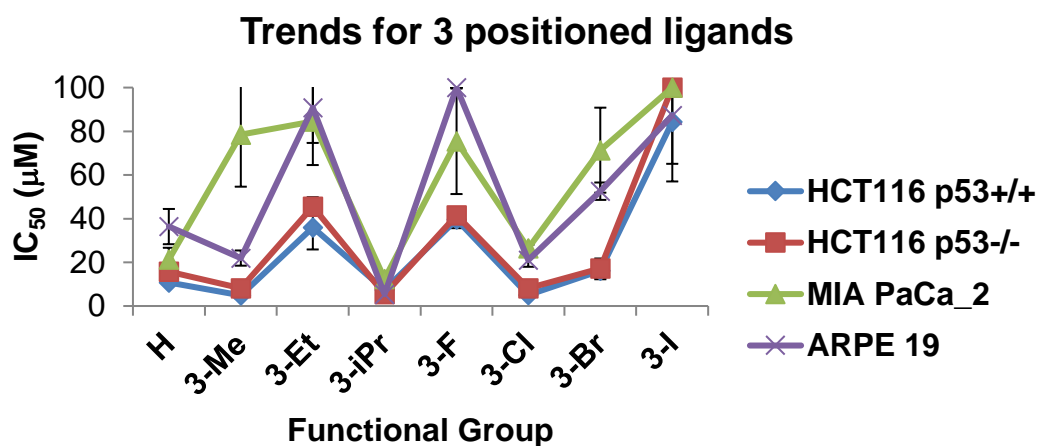


Figure 4-5: Comparison of the activity of the complexes functionalised in the position 3.

The potency of the complexes containing functional groups in the 4th position converge when the substituent is 4-^tBu. This means, the smaller the EDG and the bigger the EWG the higher the IC₅₀ against all cell lines, this potency is enhanced by increasing the bulkiness of the EDG and by decreasing the size of the EWG, as shown in **Figure 4-6**.

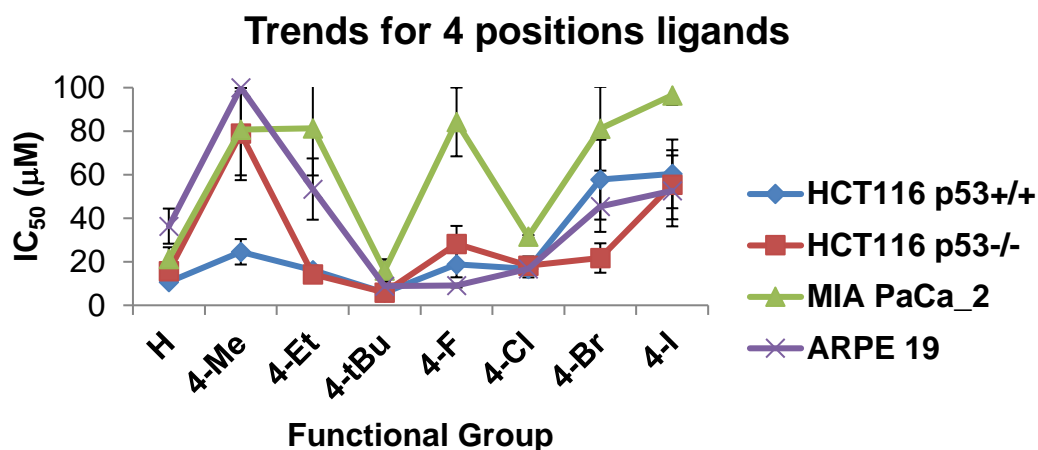


Figure 4-6: Comparison of the activity of the complexes functionalised in the position 4.

The di-substituted bisquinaldamide complexes decrease their activity when replacing di-fluoro for di-chloro, but when R is 2,4-diBr (**3.36**), the anticancer activity shows a three-fold increase in activity than the 2,4-diF, as shown in **Figure 4-7**. When comparing the 2,5-disubstituted, the activity increases when replacing 2,5-diF for 2,5-diCl. These complexes show low IC₅₀ values against the cancerous cells and high IC₅₀ values against a non-cancerous cell line favouring the selectivity ratio, which is a parameter discussed in section (4.3.3).

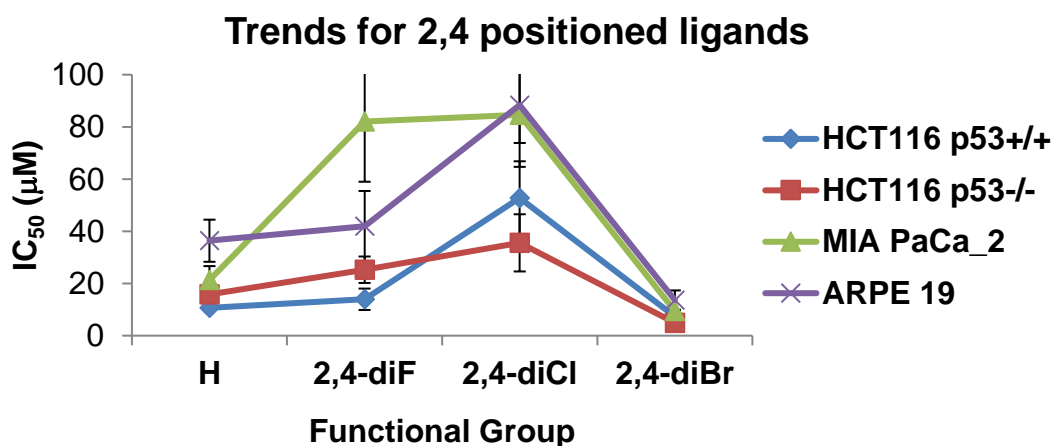


Figure 4-7: Comparison of the activity of the complexes functionalised in the position 2 and 4.

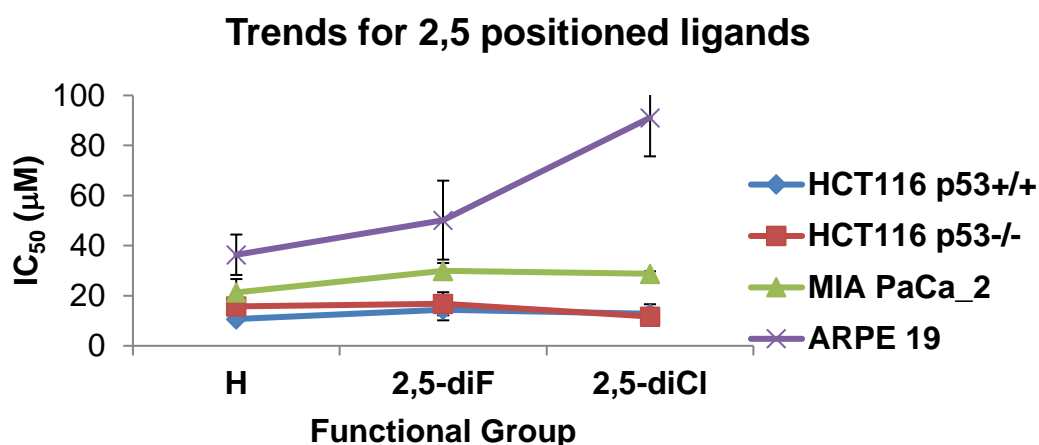


Figure 4-8: Comparison of the activity of the complexes functionalised in the position 2 and 5.

The final set of compounds that shows a remarkable variation are substituted in position 2 and 6. Compound **3.15** is constituted by two isopropyl groups (2,6-diⁱPr) and compound **3.16** is constituted by one methyl and one isopropyl (2-Me-6-ⁱPr). Interestingly, **3.15** shows not effect at all, whereas **3.16** is classified as one of the most active compounds, as shown in (Figure 4-9).

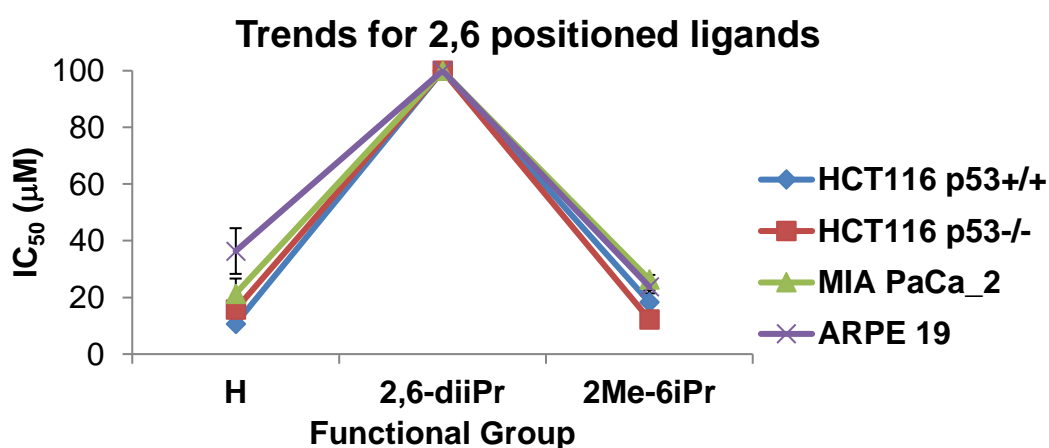


Figure 4-9: Comparison of the activity of the complexes functionalised in the position 2 and 6.

Determining the cytotoxicity values exposes the potency of the complexes against the different cell lines, and also shows how chemical modifications can affect the preference towards cancerous cell lines. Importantly, these molecules showed less toxicity against non-cancerous cells. This characteristic is very interesting in bioinorganic medicinal chemistry as, in general, most of the metal-based compounds that affect cancerous cells are equipotent or more toxic

towards healthy cell lines. However, after proving that not many trends can be outlined by using a chemical approach, the next step is to understand the anticancer activity from a biological point of view.

4.3.3 Selectivity of the ruthenium complexes

There is a well-established parameter called selectivity factor (s. f.) used to obtain the Lead Compounds apart from analysing the IC₅₀ values and the chemical structures. This factor is defined as the IC₅₀ value of the non-cancerous cell lines divided by the IC₅₀ value of the cancerous cells. The outcome is a unit-less number which should be higher than one and the current chemotherapeutic drugs (cisplatin, carboplatin and oxaliplatin). In terms of phenotypic outcome, the selectivity shows the preference of the compounds towards cancerous cell lines causing little damage to healthy cells. In other words, the dose of the drugs can be increased to eradicate the tumour mass while avoiding side effects.

All the selectivity factor (s. f.) values for the *trans*-dichloride bisquinaldamide ruthenium (III) complexes tested can be found in **Table 4-5** and **Table 4-6**, and the selectivity factor values for the current chemotherapeutic compounds (cisplatin, carboplatin and oxaliplatin) are reported in **Table 4-7**. After 96 hours of drug exposure, the clinical platinum-based compounds drop significantly in selectivity. The colour code follows the same rationale as the IC₅₀, highly selective complexes in green (s. f. < 3), moderate selectivity highlighted in blue (2 < s. f. < 3), moderately active highlighted in orange (1 < s. f. < 2) and no highlighted when s. f. < 1. When plotting selectivity (s. f.) versus the functional groups (R) (**Figure 4-10**), it is very clear the compounds are mainly selective towards the human colorectal carcinoma cell lines both dependent and independent on the tumour suppressor gene p53. The platinum drugs do not show much selectivity against the HCT 116 cell lines. Across the panel of complexes tested, compounds bearing 2-ⁱPr (**3.12**), 3-ⁱPr (**3.13**), 2,6-diⁱPr (**3.15**), 2-Me-6-ⁱPr (**3.16**), 2-^tBu (**3.17**), 4-^tBu (**3.18**), 4-F (**3.25**), 4-Cl (**3.30**), 2-Br (**2.33**), 3-I (**2.39**) and 4-I (**2.40**) show no selectivity against any cancer cell lines. Some of the compounds (R = H (**3.1**), 2-F (**3.23**), 2,5-diF (**3.37**), 2,5-diCl (**3.32**) and 2,4-diBr (**3.36**)) target the pancreatic adenocarcinoma cells but with less potency. However, from the thirty compounds tested, there is one which its substituent is the 2,5-diCl group (complex **3.32**) that has a remarkable selectivity. When compared against the current chemotherapeutic benchmarks, it increases up to four times against the

colorectal cell lines after 72 hours exposure and the potency is double against oxaliplatin and carboplatin. Cisplatin shows a good selectivity against the pancreatic cell line which drops before reaching 96 hours of exposure when it becomes extremely toxic towards non-cancerous cell lines. Opposed to this selectivity, if R is a 4-F (complex **3.25**) the damage to non-cancerous cells is higher than to the cancerous cell lines.

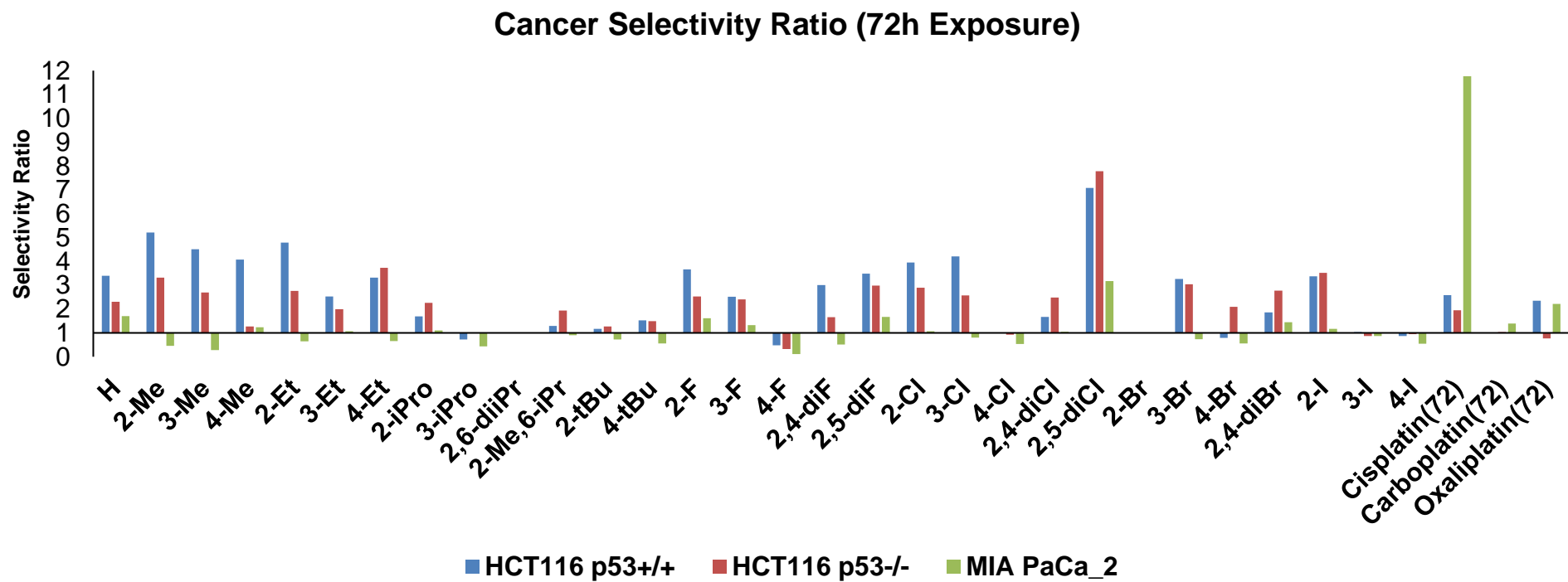


Figure 4-10: Selectivity ratio bar-chart of all the complexes after 72h drug exposure.

Table 4-5: Selectivity factor (s. f) values for the compounds 3.1 – 3.24

Complex	R	HCT 116 p53 (+/+)	HCT 116 p53 (-/-)	MIA PaCa_2
3.1	H	3.4	2.3	1.7
3.5	2-Me	5.2	3.3	0.5
3.6	3-Me	4.5	2.7	0.3
3.7	4-Me	4.1	1.3	1.2
3.9	2-Et	4.7	2.8	0.6
3.10	3-Et	2.5	2.0	1.1
3.11	4-Et	3.3	3.7	0.7
3.12	2- ⁱ Pr	1.6	2.3	1.1
3.13	3- ⁱ Pr	0.7	1.0	0.4
3.15	2,6-di ⁱ Pr	1.0	1.0	1.0
3.16	2-Me-6- ⁱ Pr	1.3	1.9	0.9
3.17	2- ^t Bu	1.2	1.3	0.7
3.18	4- ^t Bu	1.5	1.5	0.6
3.23	2-F	3.7	2.5	1.6
3.24	3-F	2.5	2.4	1.3

Table 4-6: Selectivity factor (s. f) values for the compounds **3.25 – 3.40**

Complex	R	HCT 116 p53 (+/+)	HCT 116 p53 (-/-)	MIA PaCa_2
3.25	4-F	0.5	0.3	0.1
3.26	2,4-diF	3.0	1.7	0.5
3.27	2,5-diF	3.5	3.0	1.6
3.28	2-Cl	3.9	2.9	1.1
3.29	3-Cl	4.2	2.6	0.8
3.30	4-Cl	1.0	0.9	0.5
3.31	2,4-diCl	1.7	2.5	1.0
3.32	2,5-diCl	7.1	7.8	3.2
3.33	2-Br	1.0	1.0	1.0
3.34	3-Br	3.3	3.0	0.7
3.35	4-Br	0.8	2.1	0.6
3.36	2,4-diBr	1.9	2.8	1.4
3.38	2-I	3.4	3.5	1.2
3.39	3-I	1.0	0.9	0.9
3.40	4-I	0.9	0.9	0.5

Table 4-7: Selectivity factor (s. f.) values of the current chemotherapeutic drugs (cisplatin, carboplatin and oxaliplatin) after 72 hours exposure

Complex	HCT 116 p53 (+/+)	HCT 116 p53 (-/-)	MIA PaCa_2
Cisplatin	2.6	1.9	0.5
Carboplatin	1.0	1.0	11.8
Oxaliplatin	2.3	0.8	2.2

In order to choose Lead Compounds of this family, the following factors were considered: selectivity, IC₅₀ values, functional group and comparison against bench marks after 72 hours drug exposure. To validate the activity of the most promising drug candidates, compounds with very poor selectivity were added to the list in order to establish activity structure relationships when molecules are constituted with different EDG and EWG. Finally, eight complexes were chosen as Lead Compounds and further biological analysed; they are formed by the following functional groups: H (**3.1**); 3-ⁱPr (**3.13**); 4-^tBu (**3.18**); 2-F (**3.23**); 3-Cl (**3.29**); 2,5-diCl (**3.32**); 2,4-diBr (**3.36**) and 2-I (**3.38**). The summary of the IC₅₀ values lie within the standard error (**Figure 4-11**) and the selectivity (**Figure 4-12**) of the Lead Compounds are shown. In the literature, it is well described how ligand functionality plays a big role and having a slight alteration of both the electronics and the steric hindrance of the R groups affects profoundly the anticancer activity. **Figure 4-2** shows the general structure of the compounds and the discussion crystal structures in **Chapter 3**.

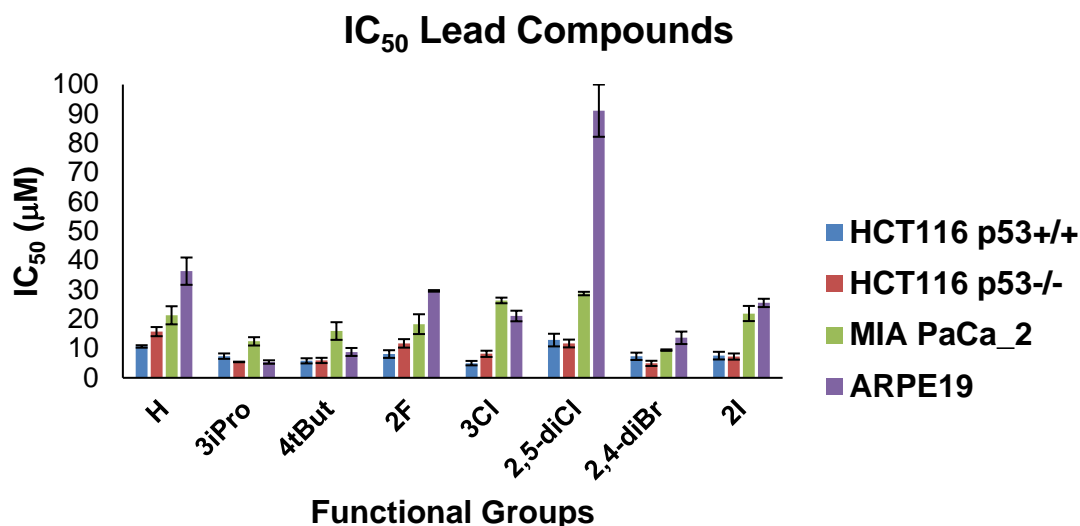


Figure 4-11: Bar-chart summary of the IC₅₀ ± S E. values of the Lead Compounds analysing the colorectal cell lines HCT 116 p53 (+/+), HCT 116 p53 (-/-) and MIA PaCa_2 after 72h drug exposure.

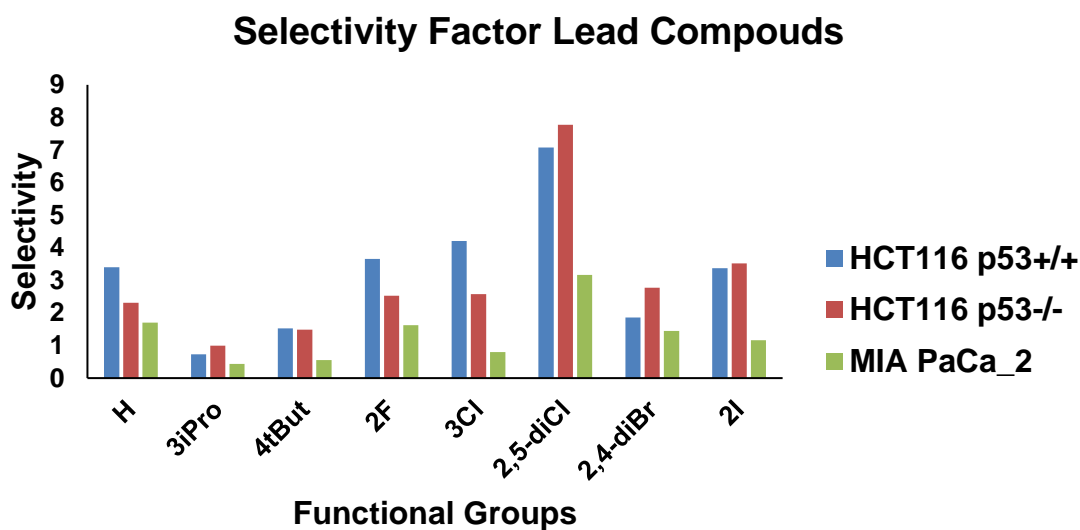


Figure 4-12: Bar-chart summary of the selectivity factor of the Lead Compounds analysing the colorectal cell lines HCT 116 p53 (+/+), HCT 116 p53 (-/-) and MIA PaCa_2 after 72h drug exposure.

4.3.4 Expansion of the cancer cell panel

As a general trend, the compounds tested showed more cytotoxicity against colorectal cancers (CRC) than the pancreatic cell line (MIA PaCa_2), thus further tests were carried out on the 'Lead Compounds' to investigate the potency against other colorectal cell lines. In this case, the cell line chosen was the

colorectal HCT 116, but targeting a different gene. The proto-oncogene Kras, formed by two alleles, is the antagonist of the tumour suppressor p53. Once cells start to mutate, Kras gets activated by replacement of one amino acid in one allele, which is the oncogene responsible for tumour/cancer growth.¹⁶ Due to scarcity of the complexes, 2,4-diBr and 2-I were not evaluated. Due to logistics, (five compounds per plate), the ruthenium control complex **3.1** (R = H) was not evaluated either. The remaining five Lead Compounds were tested against three isogenic human colorectal cancer cell lines: HCT 116 Kras parent, HCT 116 Kras Wild Type and HCT 116 Kras mutant. In order of relevancy, Kras parent resembles the regulated proportion of the proto-oncogene in normal cells (one wild-type allele and one mutant allele), Kras mutant has no wild-type allele and one mutant, whereas the Kras WT or (+) shows the wild-type allele and no mutant allele.¹⁶ In simple terms, compounds that have a preferential activity against the cell line HCT 116 Kras mutant would be desirable, as this is the stage when the cancer is being more aggressive.

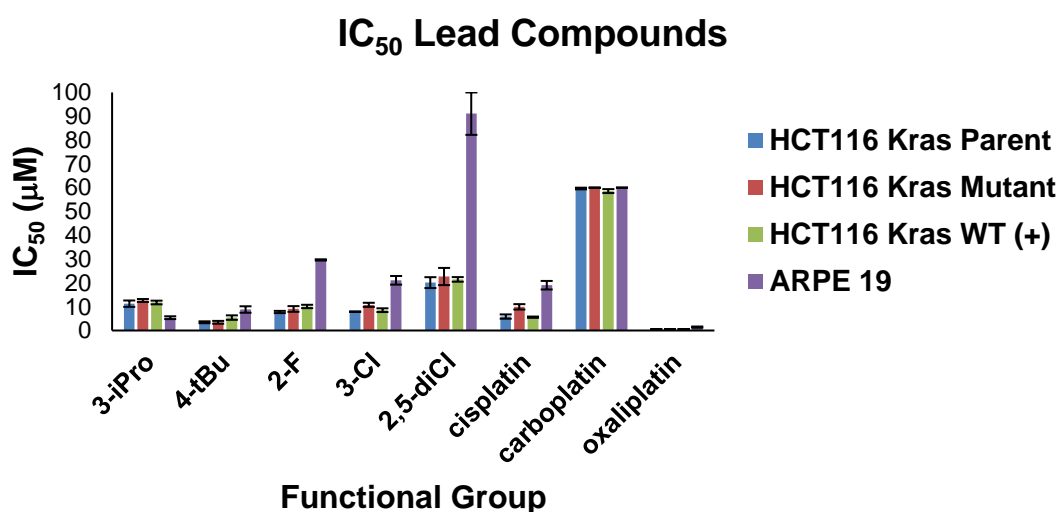


Figure 4-13: Bar-chart summary of the IC₅₀ values of the compounds **3.13**, **3.18**, **3.23**, **3.29**, **3.32**, cisplatin, carboplatin and oxaliplatin tested against the Kras oncogene family, and the non-cancerous cell line ARPE-19.

Table 4-8 shows all the IC₅₀ values with their respective standard errors. The values for ARPE-19 were shown previously in **Table 4-2** and **Table 4-3**. From the plot, IC₅₀ against functional group, (**Figure 4-13**), all compounds apart from the 4-tBu complex, display similar potency against the three isogenic cancerous cell lines. The complex bearing the substituent 4-tBu (**3.18**) shows more potency against the inactivated and activated proto-oncogene family. Overall, excluding

the complex with R = 2,5-diCl, the compounds exhibit greater potency than cisplatin and carboplatin. In terms of selectivity (**Figure 4-14**), complexes 2-F (**3.23**) and 2,5-diCl (**3.32**) show more selectivity than the platinum benchmarks.

Table 4-8: IC₅₀ ± S.E. values (μM) of compounds **3.13**, **3.18**, **3.23**, **3.29**, **3.32**, cisplatin, carboplatin and oxaliplatin against the Kras oncogene family

Complex	R	Kras Parent	Kras WT	Kras Mutant
3.13	3- ⁱ Pr	11.27 ± 1.33	11.77 ± 0.77	12.60 ± 0.61
3.18	4- ^t Bu	3.46 ± 0.40	5.43 ± 0.93	3.45 ± 0.59
3.23	2-F	7.78 ± 0.47	10.09 ± 0.70	9.05 ± 1.18
3.29	3-Cl	7.91 ± 0.13	8.54 ± 0.78	10.79 ± 0.85
3.32	2,5-diCl	20.11 ± 2.29	21.47 ± 0.96	22.67 ± 3.62
Cisplatin		5.86 ± 0.89	5.59 ± 0.26	9.94 ± 1.13
Carboplatin		59.64 ± 0.35	58.56 ± 0.83	>60
Oxaliplatin		0.48 ± 0.06	0.59 ± 0.04	0.59 ± 0.02

Selectivity of Lead Compounds

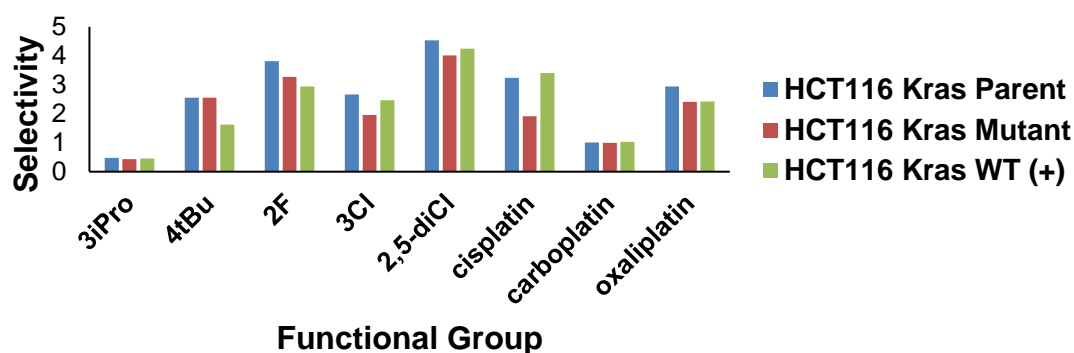


Figure 4-14: Bar-chart summary of the selectivity of the Lead Compounds and platinum compounds against HCT 116 with mutated Kras oncogene family.

Table 4-9: Selectivity factor (s. f.) values of **3.13**, **3.18**, **3.23**, **3.29**, **3.32**, cisplatin, carboplatin and oxaliplatin against the Kras colorectal cell lines

Complex	R	Kras Parent	Kras WT	Kras Mutant
3.13	3- ⁱ Pr	0.47	0.46	0.43
3.18	4- ^t Bu	2.55	1.62	2.56
3.23	2-F	3.81	2.94	3.27
3.29	3-Cl	2.66	2.47	1.95
3.32	2,5-diCl	4.53	4.24	4.02
Cisplatin		3.24	3.40	1.91
Carboplatin		1.01	1.02	2.41
Oxaliplatin		2.94	2.42	2.41

4.3.5 Gene Preference of the ruthenium metal complexes

The selectivity or preferential activity of the ruthenium metal complexes was focused on tumour suppressor gene p53 (-/-) or knockdown/mutant and the oncogene Kras mutant. These two genes are antagonists to each other, the tumour suppressor gene p53, in cancerous cells, is inhibited and the gene Kras oncogene is overexpressed. In terms of impact, the cell lines constituted by these genes show more resistance and potential cancer relapse, making them more challenging to eradicate.

The selectivity is determined by the division of the IC₅₀ of the natural occurrence gene and the mutant, yielding a unit-less number. If the value is more than one means preference towards the mutant variant and *vice versa*. For the tumour suppressor gene this means IC₅₀ of HCT 116 p53 (+/+) divided by IC₅₀ of HCT 116 p53 (-/-). **Figure 4-15** shows that few complexes display some preference towards the p53(-/-) being compound **3.35** (R = 4-Br) the most selective showing a selectivity factor of 2.66. Generally, the compounds are slightly more toxic towards HCT 116 p53 (+/+) inferring the complexes are equipotent against both cell lines. Results are colour coded in **Table 4-10**, blue highlighted means compounds are selective towards p53 (-/-) and compound **3.35** in green as is the most selective.

Table 4-10: Preferential activity values towards the colonic cancer cell line HCT 116 p53 (-/-)

Complex	R	p53	Complex	R	p53
3.1	H	0.68	3.25	4-F	0.67
3.5	2-Me	0.64	3.26	2,4-diF	0.55
3.6	3-Me	0.60	3.27	2,5-diF	0.86
3.7	4-Me	0.31	3.28	2-Cl	0.73
3.9	2-Et	0.58	3.29	3-Cl	0.61
3.10	3-Et	0.79	3.30	4-Cl	0.92
3.11	4-Et	1.13	3.31	2,4-diCl	1.48
3.12	2- ⁱ Pr	1.34	3.32	2,5-diCl	1.10
3.13	3- ⁱ Pr	1.36	3.33	2-Br	1.00
3.15	2,6-di ⁱ Pr	1.00	3.34	3-Br	0.93
3.16	2-Me-6- ⁱ Pr	1.50	3.35	4-Br	2.66
3.17	2- ^t Bu	1.09	3.36	2,4-diBr	1.49
3.18	4- ^t Bu	0.98	3.38	2-I	1.04
3.23	2-F	0.69	3.39	3-I	0.84
3.24	3-F	0.96	3.40	4-I	1.09
Cisplatin		0.75			
Carboplatin		1.03			
Oxaliplatin		0.33			

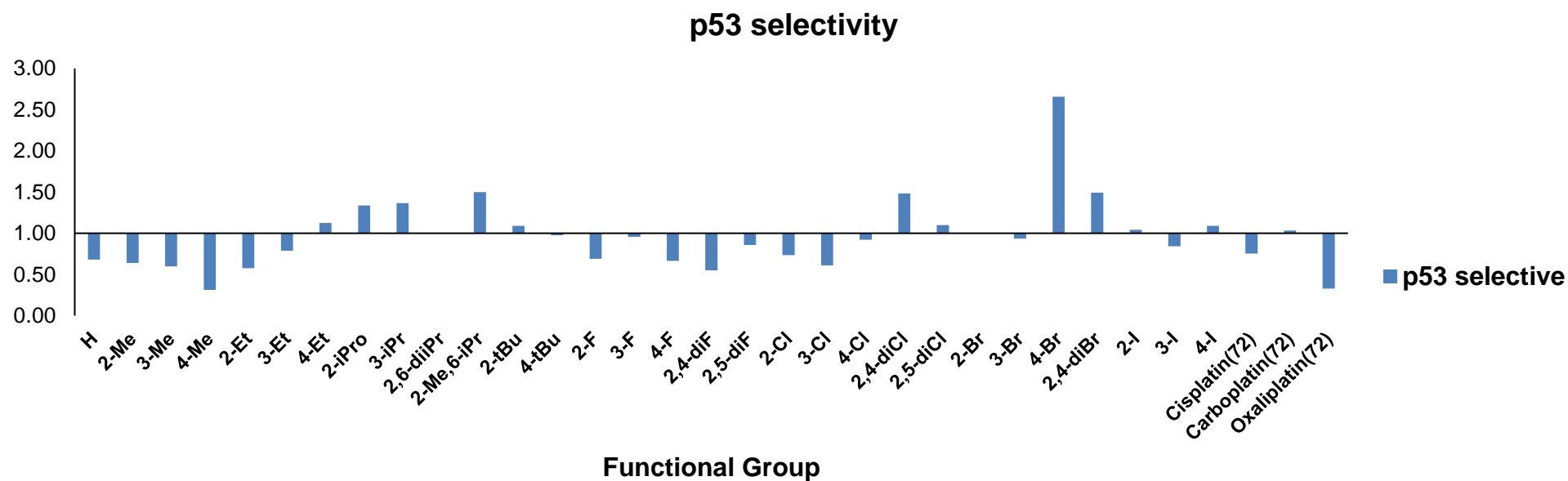


Figure 4-15: Bar-chart of the ruthenium complexes preferential activity for the tumour suppressor gene p53.

For the activated proto-oncogene Kras is translated to the IC₅₀ of HCT Kras WT or (+) divided by the IC₅₀ of HCT Kras mutant. **Figure 4-16** shows that complex **3.29** (R = 3-Cl), highlighted in green, is more potent towards the mutated cell line which is the more difficult to defeat, and also, it can participate in cancer relapse. In terms of p53 selectivity, compound **3.29** has preference for the HCT 116 p53 (+/+) gene. Interestingly, complexes **3.32** (2,5-diCl) and **3.13** (R = 3-ⁱPro) shows a preference for both HCT p53 (-/-) and HCT 116 Kras mutant. These is a very positive result as, potentially, it could be establish that compounds substituted in position 3 could interact at different levels with the proto-oncogene Kras.

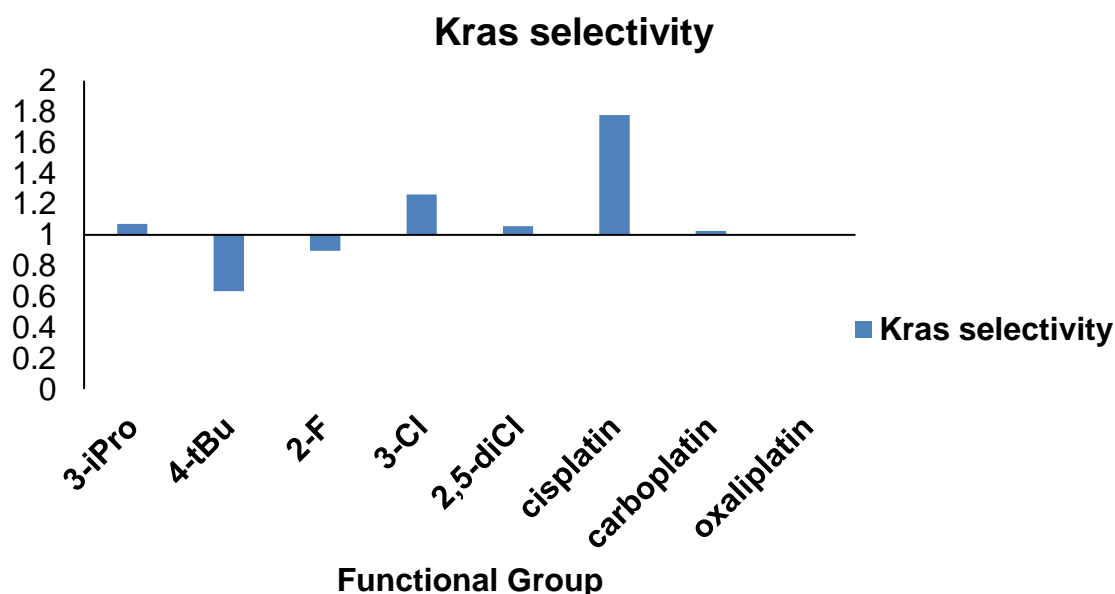


Figure 4-16: Bar-chart of the ruthenium Lead Compounds preferential activity for the oncogene Kras.

Table 4-11: Preferential activity values towards the colonic cancer cell line HCT 116 Kras Mutant. In green highlighted shows the most selective and blue highlighted means the selectivity factor is above 1

Complex	R	Kras
3.13	3- ⁱ Pr	1.07
3.18	4- ^t Bu	0.64
3.23	2-F	0.89
3.29	3-Cl	1.26
3.32	2,5-diCl	1.05
Cisplatin		1.78
Carboplatin		1.02
Oxaliplatin		1.00

4.3.6 Summary of the normoxia cytotoxicity cell work

Thirty compounds were tested against three cancerous cell lines (HCT 116 p53 (+/+), HCT 116 p53 (-/-) and MIA PaCa_2) and one non-cancerous cell line (ARPE-19). The variety of IC₅₀ values ranging from over 100 μM to 5 μM proved challenging to obtain the Lead Compounds, hence the introduction of the selectivity factor based on how preferable a drug is toxic against tumorigenic/tumoral cells. Eight Lead Compounds were identified after obtaining the selectivity, comparing them to the current chemotherapeutic drugs and considering additional factors previously discussed. However, only five compounds were tested against a wider panel of colorectal cancer cell lines differing from the first ones on the gene mutated, (in the first ones, the target was a tumour suppressor gene, and the panel expansion considers three isogenic cell lines based on the proto-oncogene Kras, non-activated and activated) showing activities between 20 μM and 4 μM. **Figure 4-17** and **Figure 4-18** shows that the compounds substituted with electron-donating groups show low IC₅₀ values but less selectivity. Complexes **3.23** and **3.29**, the IC₅₀ values are generally below 10 μM for the colorectal cell lines and between 15 – 30 μM for the pancreatic cell lines. When analysing complex **3.32** (R = 2,5-diCl), the IC₅₀ values rise when compared to complexes **3.23** and **3.29**. In terms of gene

preference, the compound bearing the 4-Br substituent (complex **3.34**) has the best selectivity towards the knockdown tumour suppressor gene p53, whereas the compound bearing 3-Cl (complex **3.13**) has a preference towards the oncogene Kras mutant.

Summary of IC₅₀ Lead Compounds

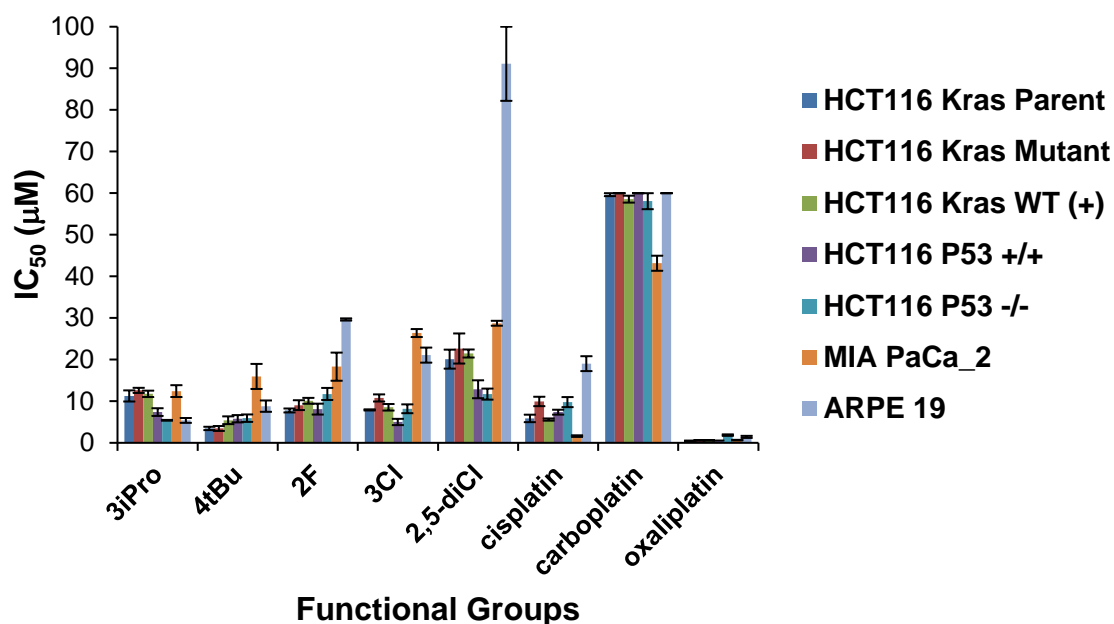


Figure 4-17: Bar chart of IC₅₀ values of compounds **3.13**, **3.18**, **3.23**, **3.29**, **3.32**, cisplatin, carboplatin and oxaliplatin.

Summary of Selectivity Factors Lead Compounds

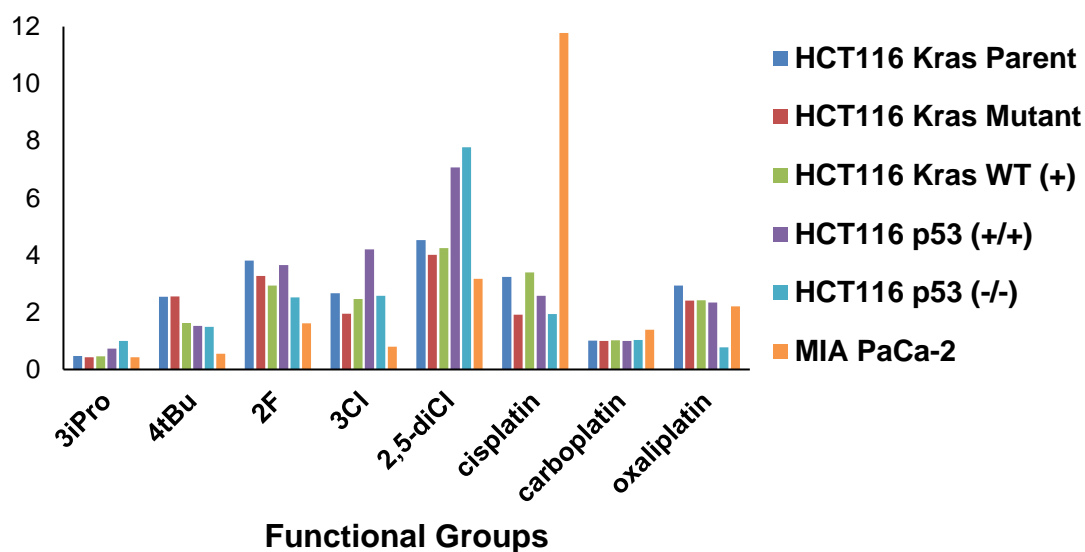


Figure 4-18: Summary of the selectivity factors of **3.13**, **3.18**, **3.23**, **3.29**, **3.32**, cisplatin, carboplatin and oxaliplatin.

4.4 Hypoxia cytotoxic studies of *trans*-dichloride bisquinaldamide Ruthenium complexes

Hypoxic cells are considered to be resistant to several chemotherapeutic drugs.¹⁷ Healthy mammalian tissues need to regulate the homeostasis of molecular oxygen (O₂) for cell survival and to maintain intracellular energy, typically existing between values of 2–9% oxygen known as *normoxia*. The difference in percentage is accounted depending on the blood vessel network and metabolism. The pioneering work lead by Peter Vaupel has shown that tumours larger than 1 mm³ are characterised by areas containing very low concentration of oxygen and containing a more reducing environment due to the overexpression of the sulphur containing tripeptide, glutathione. This inner sphere is known as hypoxic region. When healthy cells start to behave wrongly, they clamp together forming spheres divided into two sections: the outer sphere behaving like a regular healthy cell and the inner sphere which is a thick mass that does not allow molecular oxygen to diffuse through, creating a gradient of oxygen concentration. These hypoxia environments can exist at $\leq 2\%$ oxygen and severe hypoxia (anoxia) as $\leq 0.02\%$ oxygen, which is cell line dependent.^{18,19}

The survival of tumours depends on a process call angiogenesis where cancerous cells use host cell vessels to create a network of new ones. Such a quick process comes with disadvantages, forming abnormal vessels that disrupt the correct blood supply, hence restricting the normal oxygen diffusion.²⁰ This explains how cancer can metastasise so quickly and how easy is to invade healthy cells by creating a fascinating new vascular system. Recently, it was reported that cancerous cells survive their hypoxic state through activation of hypoxia-inducible factor-1 (HIF-1). This transcription factor is constituted by the heterodimeric subunits: α and β . In normoxic conditions, the α subunit is degraded by a cytosolic proteasome, whereas under hypoxic conditions, the specific enzyme is inhibited, thus the α -subunits accumulate.^{18,21,24} The intact HIF-1 can bind to the hypoxia responsive element (HRE) and upregulate the transcription of a number of genes involved in cell survival such as coding-genes for proteins involved in glycolysis, angiogenesis and the inflammatory response.^{25,26} HIF-1 is implicated in a number of cancers and there is also a

strong correlation between HIF-1 overexpression and the tumour grade and vascularisation.²⁵ An overview of HIF-1 regulation is shown in **Figure 4-19**.

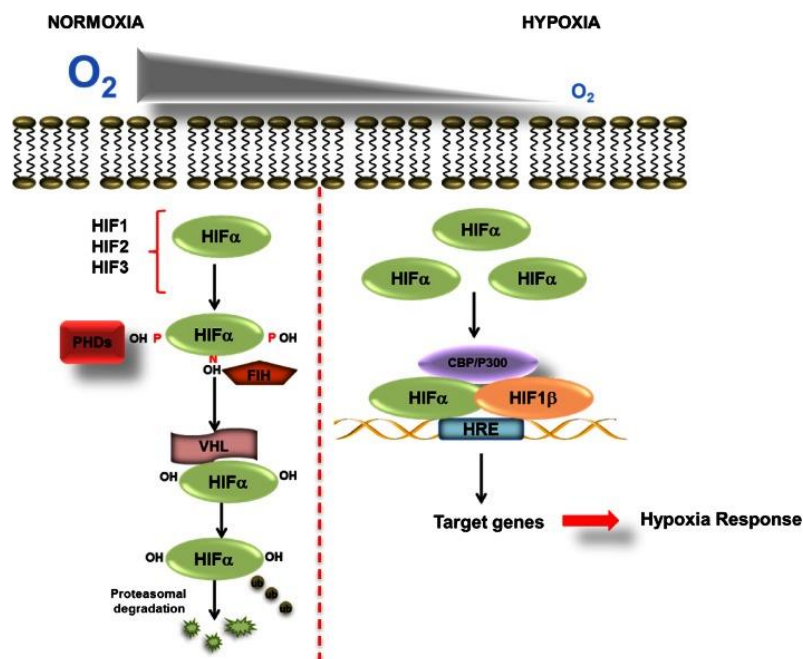


Figure 4-19: Mechanism of HIF-1 α regulation within the cell.²⁷

Hypoxic tumours are a strong prognostic factor for many cancers. The bigger the hypoxic mass (tumour) the more reduced the chemotherapeutic drug delivery, the more cancer inherent resistance to radiotherapy, the more neovascularisation, the greater metastatic capacity and the increase of apoptotic resistance. The depletion of oxygen in the hypoxic environment of cells can lead to upregulation of genes involved in drug resistance and promotion of cancerous cell growth.²⁰ Furthermore, the more reducing environment of hypoxic cancerous cells is thought to help the stabilisation of HIF- α when compared to healthy cells. This provides the potential of targeting the centre of hypoxic cancer cells selectively.

Nowadays, the chemotherapeutic resistance of hypoxic cells to cancer therapies is targeted by using bio-reductive prodrugs or hypoxia activated drugs. These drugs possess the unique property of getting activated once entered in the reducing environment. For such a feature, metal-based drugs perfectly suit such a strategy, due to the variations in coordination number, geometry and accessible oxidation states.²⁸ This activation was proposed as follows, a prodrug get activated by one-electron enzymatic reaction yielding a radical anion. In normoxia, molecular oxygen will react with it deactivating the drug, but in hypoxia

this radical is slightly more stabilised and spontaneously fragmented or further reduced yielding cytotoxic species. It is known that DNA alkylation and kinase inhibition occur through the last process.²⁸⁻³⁰



Figure 4-20: Mechanism proposed for pro-drug activation by hypoxia.³¹

4.4.1 Hypoxia cytotoxic results

The five Lead Compounds (**Figure 4-21**) were tested against the main three cancerous cell lines, HCT116 p53 (+/+), HCT116 p53 (-/-) and MIA PaCa_2. The studies were performed in a Whitley H35 Hypoxystation where the oxygen level is set to 0.1%. This is the level which yields drug resistance in both radiotherapy and chemotherapy activating the HIF-1 complex under physiological cancerous conditions. Cells were cultured in 96-well plates, allowed to adhere for 24 hours under normoxia conditions, and for other 24 hours to acclimatise to the hypoxic conditions. They were exposed to different concentrations of the Lead Compounds ranging from 60 μM till 0.468 μM and incubated for 72 hours. IC_{50} values were calculated after analysing the MTT readings after 3 hours.

The biological evaluation of these compounds will show if they are good candidates to develop new hypoxia scaffolds.

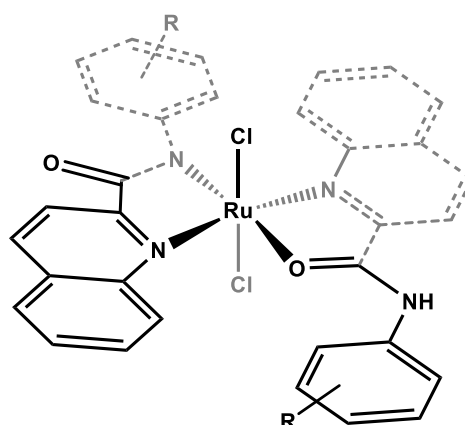


Figure 4-21: General structure of complexes: **3.13** (R = 3-ⁱPr), **3.18** (R = 4-^tBu), **3.23** (R = 2-F), **3.29** (R = 3-Cl) and **3.23** (R = 2,5-diCl)

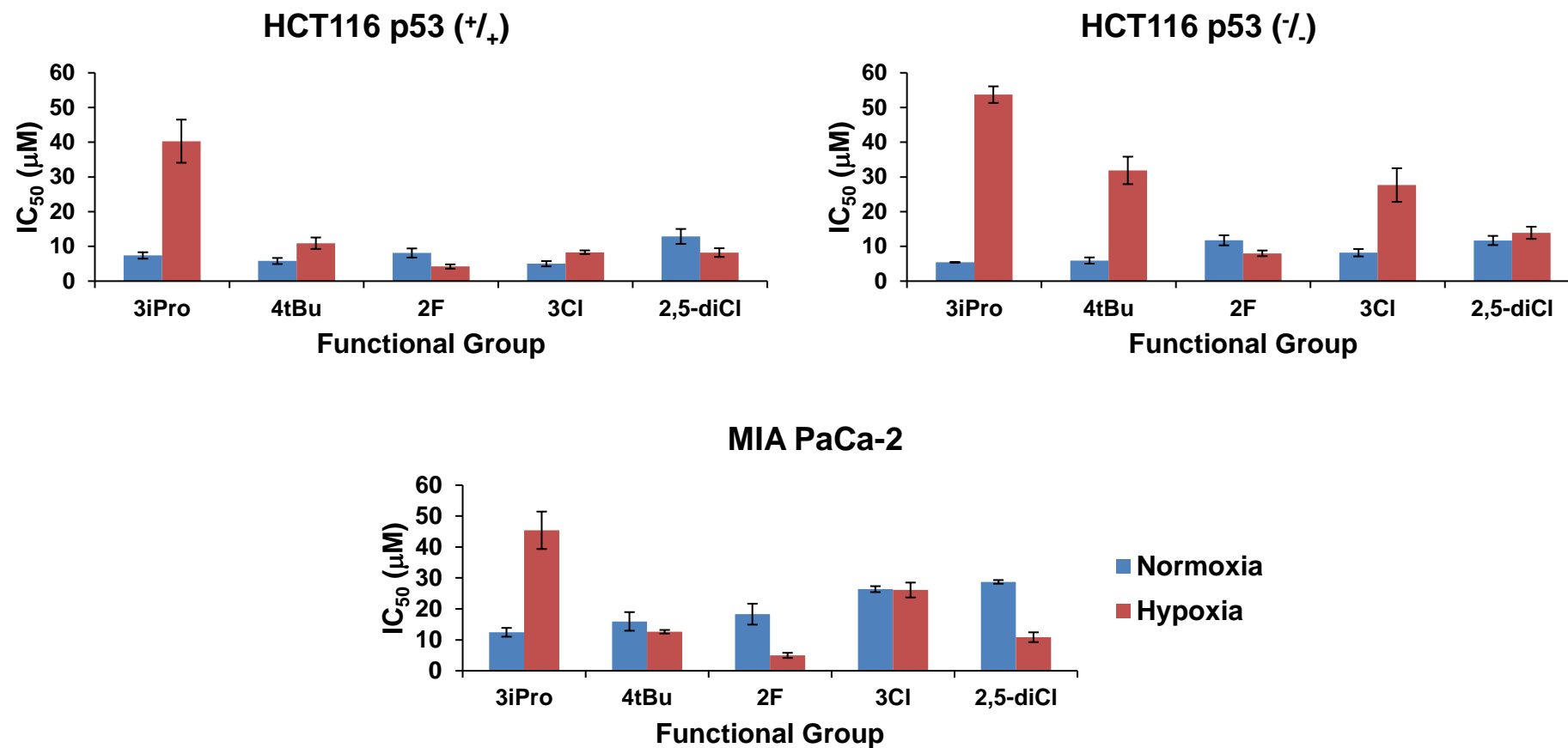


Figure 4-22: Bar-chart of compounds **3.13** (R= 3-ⁱPr), **3.18** (R = 4-^tBu), **3.23** (R = 2-F), **3.29** (R = 3-Cl) and **3.23** (R = 2,5-diCl) tested against HCT 116 p53(+/+), HCT 116 p53 (-/-) and MIA PaCa₂. Normoxia results highlighted in blue hypoxia results in red.

Figure 4-22 (top left chart) shows the potency of the compounds under normoxic and hypoxic conditions against the colorectal cell line HCT 116 p53 (+/+). Compound **3.13** (R = 3-ⁱPr) shows a decrease in activity of almost six times lower than the normoxia result. When the R group is 4-^tBu (complex **3.18**), the compound loses its activity from 5.79 μ M to 10.92 μ M. Compound **3.29** (R = 3-Cl) shows the same trend as the previous one increasing the IC₅₀ value from 5.01 μ M to 8.32 μ M. On the other hand, compounds with R = 2,5-diCl and 2-F the activity increases from 12.87 μ M to 8.22 μ M, and from 8.10 μ M to 4.21 μ M, respectively. This feature is consistent with the already published compounds within the McGowan group³² showing that the *trans*-dihalide ruthenium scaffold can be a relevant strategy to tackle hypoxic cancerous cells.

Figure 4-22 (top right chart) shows the comparison between normoxic and hypoxic results against the colorectal cell line HCT 116 p53 (-/-). In this case, compounds **3.13** (R = 3-ⁱPr), **3.18** (R = 4-^tBu) and **3.29** (R = 3-Cl) show the same trend as the potency against HCT 116 p53 (+/+), however with a bigger increase of drug deactivation. Compound **3.32** (R = 2,5-diCl) shows equipotent activity as under normoxic conditions. Interestingly, compound **3.23** (R = 2-F) increases its activity from 11.75 μ M to 8.00 μ M, although it is not as effective as against the HCT 116 p53 (+/+). This suggest that compounds **3.32** (R = 2,5-diCl) and **3.23** (R = 2-F) are good candidates for further biological studies.

Figure 4-22 (bottom chart) shows the normoxia and hypoxia IC₅₀ values against the pancreatic adenocarcinoma cell line MIA PaCa_2. Only compound **3.13** (R = 3-ⁱPr) decreases its activity under hypoxic conditions. Complexes **3.18** (R = 4-^tBu) and **3.29** (R = 3-Cl) show similar potency within the standard errors as the normoxic studies. Remarkably, compounds **3.32** (R = 2,5-diCl) and **3.23** (R = 2-F) show a threefold increase and four fold increase in potency under hypoxic conditions, respectively. The IC₅₀ value of complex **3.32** (R = 2,5-diCl) decreases from 28.74 μ M to 10.85 μ M, and compound **3.23** (R = 2-F) decreases from 18.30 μ M to 4.97 μ M. In terms of IC₅₀ intervals, these compounds go from active to be highly active under hypoxic conditions.

Table 4-12: Summary of the IC₅₀ under hypoxic conditions of complexes **3.13**, **3.18**, **3.23**, **3.29** and **3.32**. (Blue highlighted show compounds anticancer activity under these conditions)

Complex	R	p53 (+/+)	p53 (-/-)	MIA PaCa_2
3.13	3- ⁱ Pr	40.31 ± 10.76	53.71 ± 4.13	45.41 ± 10.48
3.18	4- ^t Bu	10.92 ± 2.86	31.89 ± 6.85	12.62 ± 1.01
3.23	2-F	4.21 ± 1.07	8.00 ± 1.42	4.97 ± 1.44
3.29	3-Cl	8.32 ± 0.91	27.67 ± 8.39	26.11 ± 4.18
3.32	2,5-diCl	8.22 ± 2.17	13.92 ± 3.03	10.85 ± 2.74

4.4.2 Hypoxia Cytotoxicity Ratio

The IC₅₀ value of the drug in normoxia divided by the IC₅₀ value in hypoxic conditions against a given cell line yields a unit-less number that expresses the preference of drug to target the oxygen depleted cells or the normoxia cells. The purpose of this ratio is to show if the compounds tested could potentially be used in 3D cancer models. This means that cells clump together forming the inside of the tumour and the outside behaves like a normal cell based on spheroids and mammospheres.

Figure 4-23 shows compounds **3.13** (R = 3-ⁱPr), **3.18** (R = 4-^tBu) and **3.29** (R = 3-Cl) display no enhancement unless for complex **3.18** (R = 4-^tBu) against MIA PaCa-2. Compound **3.32** (R = 2,5-diCl) increases activity against HCT 116 p53 (+/+) and MIA PaCa_2 but decreases for HCT 116 p53 (-/-). Finally, compound **3.23** (R = 2-F) shows increase cytotoxicity in hypoxic conditions against all cell lines. Overall, compounds **3.32** (R = 2,5-diCl) and **3.23** (R = 2-F) display better activity being the best candidates for further analysis in 3D models.

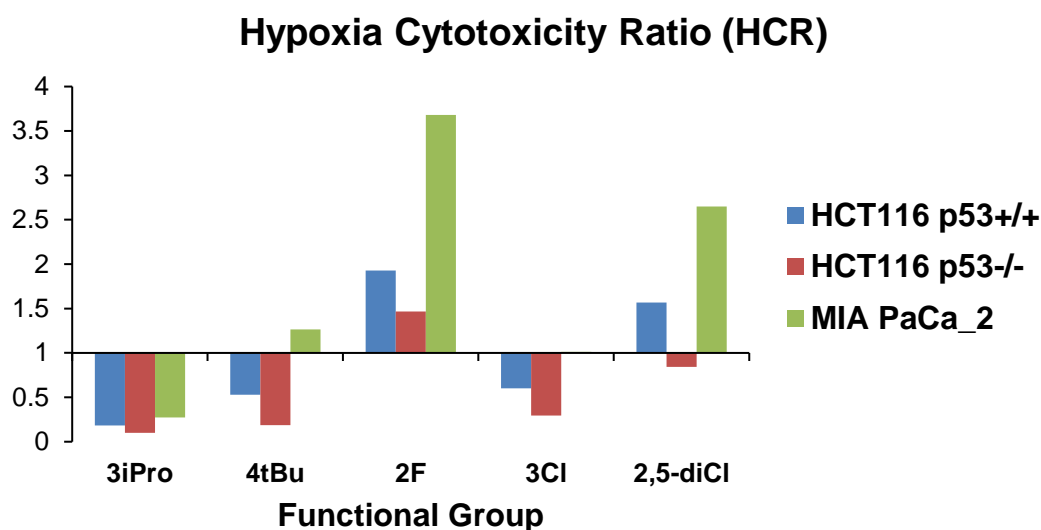


Figure 4-23: Hypoxia cytotoxicity ratio (HCR) bar-chart of compounds **3.13** (R= 3-*i*Pr), **3.18** (R = 4-*t*Bu), **3.23** (R = 2-F), **3.29** (R = 3-Cl) and **3.23** (R = 2,5-diCl).

4.4.3 Hypoxia Enhancement Ratio

The 'Hypoxia Enhancement Ratio' is defined by the IC₅₀ value of a healthy cell line divided by the IC₅₀ value of a cancerous cell line. The outcome represents the selectivity of the compounds towards cancerous cells. **Figure 4-24** shows the hypoxia enhancement ratios for each compound and only compounds **3.23** (R = 2-F) and **3.32** (R = 2,5-diCl) have shown more selectivity towards cancerous cells under hypoxic conditions. **Figure 4-25** compares both the hypoxic and normoxic results.

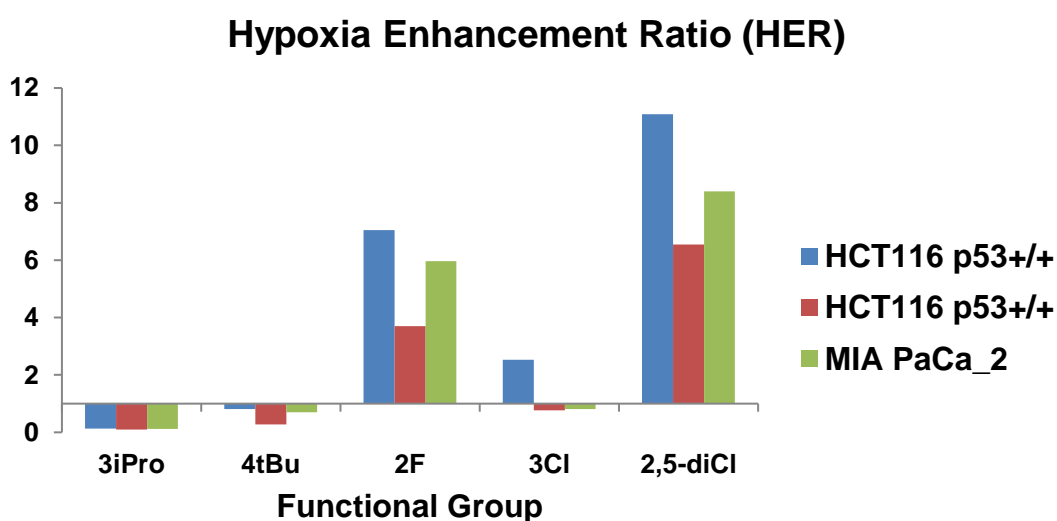


Figure 4-24: Bar-chart of the hypoxia enhancement ratio (HER) of the Lead compounds tested.

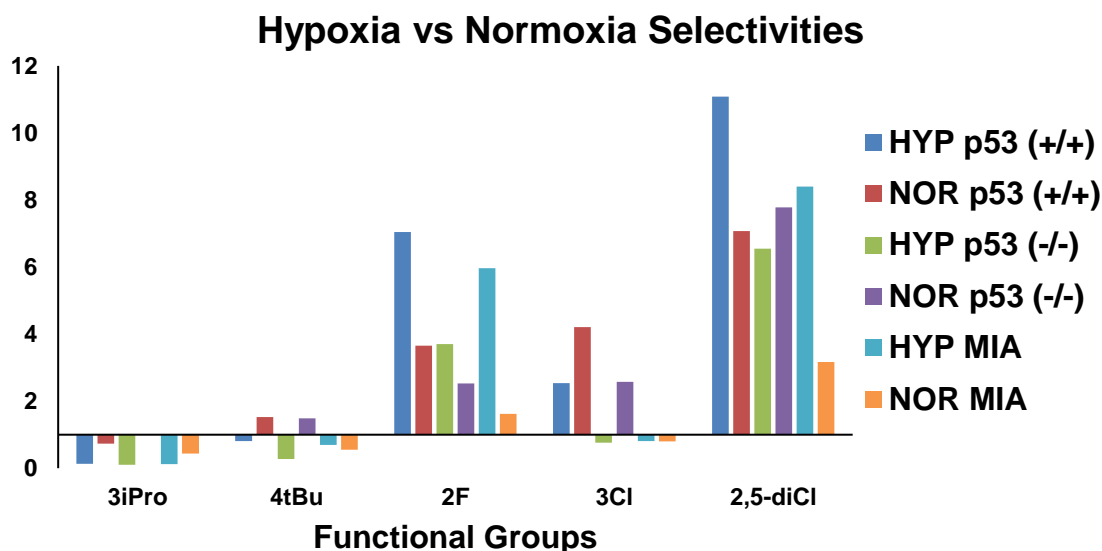


Figure 4-25: Bar-chart comparison of the hypoxia enhancement ratio and the selectivity under normoxic conditions for **3.13** (R= 3-ⁱPr), **3.18** (R = 4-^tBu), **3.23** (R = 2-F), **3.29** (R = 3-Cl) and **3.32** (R = 2,5-diCl) against the cell lines tested.

4.4.4 Summary of the hypoxia cytotoxicity cell work

From the normoxia cell work (4.3) eight Lead Compounds were identified after obtaining the selectivity, comparing them to the current chemotherapeutic drugs and considering additional factors previously discussed. Five compounds were tested under hypoxic conditions against HCT 116 p53 (+/+), HCT 116 p53 (-/-) and MIA PaCa-2. From those five compounds, **3.13** (R = 3-ⁱPr), **3.18** (R = 4-^tBu), **3.29** (R = 3-Cl), **3.23** (R = 2-F) and **3.32** (R = 2,5-diCl) only two showed better IC₅₀ under hypoxic conditions, and those are **3.23** (R = 2-F) and **3.32** (R = 2,5-diCl).

4.5 Cell recovery

One of the many challenges in medicinal chemistry for both inorganic and biology is understanding if the potential drugs show cytotoxic or cytostatic properties. This means, if a cell is exposed to a drug, it has three modes to react against it: the drug does nothing to the cells, the drug affects the cells, but they recover after exposure (cytostatic) or the drug kills the cells and there is no recovery (cytotoxic). The advantage of a compound to be cytotoxic, it means that the drug exposure can be lower which avoids non-cancerous cell damage.

The two Lead Compounds **3.23** (2-F) and **3.32** (2,5-diCl) were tested for the cytotoxicity or cytostatic properties. This can be done by carrying out the MTT

assay, explained at the beginning of the chapter. However, the main changes are on how long the drug exposure is left for, and the recovery period which is left until 72 hours to match the cytotoxic normoxic results discussed previously within this chapter (4.3). This drug exposure periods were set at 1 hour and 24 hours with a recovery period of 71 hours and 48 hours respectively. Then, MTT is added and incubated for a further of three hours and the IC₅₀ values were obtained.

Figure 4-26 shows the different potencies of the two Lead Compounds tested against HCT 116 p53 (+/+), HCT 116 p53 (-/-) and MIA PaCa_2. In **Table 4-13** all the values are shown with their respective standard deviations. The two compounds show similar activity against the cancerous cell lines, there is no recovery of the cells proving that they are cytotoxic complexes, and, they also exhibit their anticancer activity is time-dependent. Compound **3.23** (2-F) shows the quickest cytotoxic effects, however it is not very selective. Compound **3.32** (2,5-diCl) only shows quicker cytotoxic activity against MIA PaCA_2 after 1h of exposure without compromising its selectivity.

Figure 4-26 (top left HCT 116 p53(+/+) chart) shows that compound **3.23** (2-F) has its cytotoxic effect after 1h of exposure which enhances after 72h drug treatment. Compound **3.32** (2,5-diCl) increases its activity after prolonged times. The complex bearing 2-F is surprisingly interesting as, showing its cytotoxicity after one hour meaning the selectivity towards the cancerous cells is greater than after 72h and it can be removed to not cause any damage to healthy cell lines.

Figure 4-26 (top right HCT 116 p53(-/-) chart) shows both compounds displaying similar behaviour where their activity increases with time and there is no cell recovery. Complex **3.23** (R = 2-F) shows faster cytotoxicity after 24h than complex **3.32** (R = 2,5-diCl).

Figure 4-26 (bottom left MIA PaCa_2 chart) shows both compounds increase their anticancer activity with longer exposure times. However, compound **3.32** (2,5-diCl) displays a better cytotoxicity after 1h exposure stabilising the toxicity after 24h.

Figure 4-26 (bottom right ARPE-19 chart) shows the compound **3.23** (R = 2-F) increases its cytotoxicity with time, which translates to potential decrease of selectivity. Conversely, the IC₅₀ values for compound **3.32** (R = 2,5-diCl) are similar at different time exposure. This is greatly appreciated for *in vivo* assays or

clinical trials, as this means, exposure of this drug could be done more frequently and for longer periods of time.

Figure 4-27 shows the selectivity ratios of the complexes after 1h, 24h and 72h and all values can be found in **Table 4-14**. The complexes show opposite trends, complex **3.23** (R = 2-F) decreases its selectivity with longer time drug exposures, whereas complex **3.32** increases after longer time treatments.

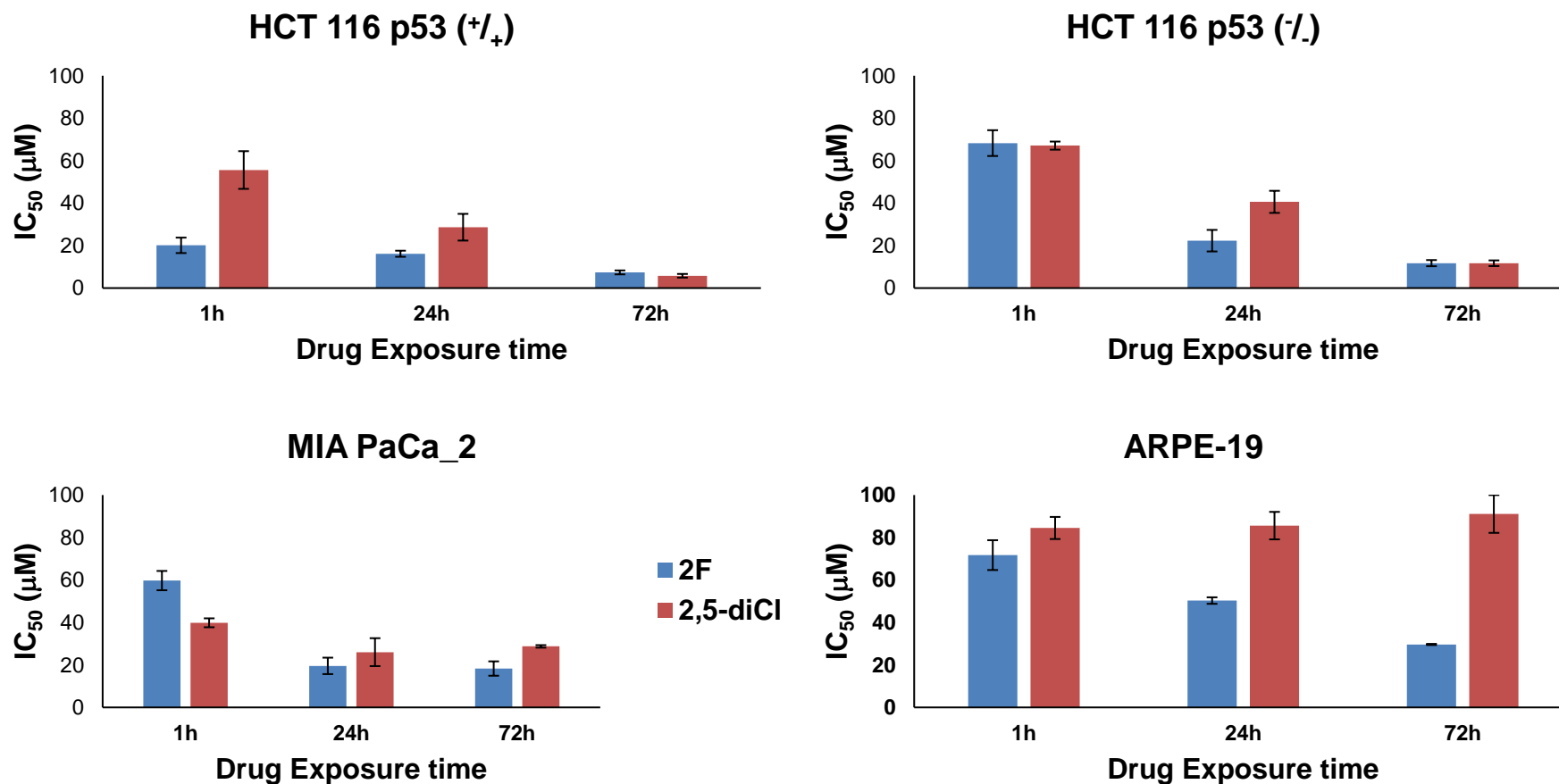


Figure 4-26: Bar-chart of compounds **3.23** (R = 2-F in blue) and **3.32** (R = 2,5-diCl in red) for the different time exposure cytotoxic assays against HCT 116 p53(+/+), HCT 116 p53 (-/-), MIA PaCa_2 and ARPE-19.

Table 4-13: IC₅₀ values (μM) of compounds **3.23** (R = 2-F) and **3.32** (R = 2,5-diCl) for the different time exposure cytotoxic assays against HCT 116 p53(+/+), HCT 116 p53 (-/-), MIA PaCa_2 and ARPE-19.

		Cell Line							
		HCT 116 p53(+/+)		HCT 116 p53(-/-)		MIA PaCa_2		ARPE-19	
Time		3.23 (2-F)	3.32 (2,5-diCl)						
1h		20.12 \pm 3.63	55.59 \pm 8.87	68.27 \pm 6.08	67.08 \pm 1.91	59.71 \pm 4.54	39.84 \pm 2.10	71.71 \pm 7.02	84.49 \pm 5.20
24h		16.18 \pm 1.43	28.67 \pm 6.28	22.32 \pm 5.07	40.60 \pm 5.21	19.55 \pm 3.87	26.02 \pm 6.57	50.31 \pm 1.54	85.60 \pm 6.47
72h		8.10 \pm 1.30	12.87 \pm 2.15	11.74 \pm 1.44	11.71 \pm 1.32	18.30 \pm 3.38	28.73 \pm 0.58	29.64 \pm 0.26	91.09 \pm 8.90

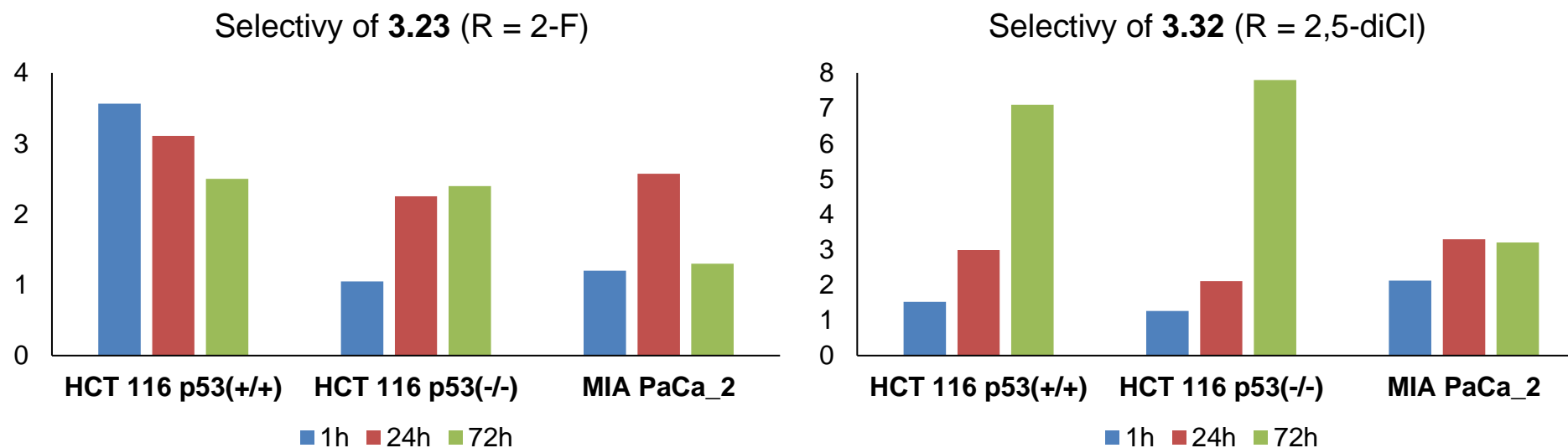


Figure 4-27: Selectivity ratios of (*left*) complex 3.23 and (*right*) complex 3.32 at different time points.

Table 4-14: Selectivity values of compounds **3.23** (R = 2-F) and **3.32** (R = 2,5-diCl) for the different time exposure cytotoxic assays against HCT 116 p53(+/+), HCT 116 p53 (-/-) and MIA PaCa_2.

	Cell Line					
	HCT 116 p53(+/+)		HCT 116 p53(-/-)		MIA PaCa_2	
Time	3.23 (2-F)	3.32 (2,5-diCl)	3.23 (2-F)	3.32 (2,5-diCl)	3.23 (2-F)	3.32 (2,5-diCl)
1h	3.6	1.5	1.1	1.3	1.2	2.1
24h	3.1	3.0	2.25	2.1	2.6	3.3
72h	2.5	7.1	2.40	7.8	1.3	3.2

4.6 Cell viability and cycle analysis

Once the compounds are evaluated and validated, the next step in the process of drug development is understanding/elucidating the mechanism of action.¹ Anticancer drugs are divided into cytotoxic or cytostatic drugs. A cytotoxic drug induces cancer cell death (cisplatin) and a cytostatic drug inhibits the proliferation (tamoxifen). Cell imaging techniques like the ones based on fluorescence imaging have revolutionised the way to analyse samples (flow cytometry). These techniques can discriminate between if a drug is cytotoxic or cytostatic.³³⁻³⁵ In section 4.5, it was proven there was no cell recovery, being the compound **3.23** (2-F) cytotoxic towards the pancreatic and epithelial cell lines tested, whereas compound **3.32** (2,5-diCl) is only cytotoxic towards the pancreatic cancer, showing great selectivity.

Eukaryotic cells have two representative processes: cell cycle and cell division. Cell division is the final step of a sequence of events that a cell goes through, also known as cell cycle (**Figure 4-28**). It is divided in four stages: mitosis (M phase), gap-1 (G1 phase), synthesis (S phase) and gap-2 (G2 phase). Normal non-dividing cells are quiescent (G0 phase); once within the cell cycle they enter in G1 phase (cells increasing in size), followed by the phase when DNA is replicated (S phase). A further short period of cell growth called G2 phase, follows the final M phase (mitosis) producing two identical daughter cells. During the oncogenic phase of a cell, this sequential cycle is disrupted in different pathways that regulate the process.^{36,37}



Figure 4-28: The eukaryotic cell cycle.³⁸

Chapter 4 Biological Investigations

Depending on the phase of the cell cycle, different drugs target the S phase, the M phase or all of them. Alkylating agents and cytotoxic antibiotics damage the DNA at all phases, e.g. cisplatin and mitomycin-C respectively. Anti-metabolites replace normal metabolites at the S phase interfering with the DNA replication, e.g. 5-fluorouracil. Topoisomerase inhibitor operate at S phase as well, but are involved with the DNA unwinding, e.g. etoposide. Lastly, mitotic inhibitors prevent the formation of the binding between tubulin subunits and the mitotic spindle, hence interfering in the M phase.^{39,40}

The two Lead Compounds **3.23** (2-F) and **3.32** (2,5-diCl) were analysed further by determining their effects on both, the cell viability and the cell cycle of two different cell lines, one cancerous, the pancreatic MIA PaCa_2, and one non-cancerous, the epithelial ARPE-19. Due to time constraint, only two runs were carried out and a third one is needed in order to validate the results. These assays were carried out by the author under the supervision of Professor Roger M. Phillips at The University of Huddersfield. The complexes, at a given concentration (18 μ M), were incubated with the different cell lines at 37°C, 5% CO₂ and analysed for 24h, 48h and 72h. For cell viability, single cell suspensions of 1 mL were prepared and loaded into a Via1-Cassette™. The inside of these cassettes is coated with two different dyes, Acridine Orange stains all the cell population and DAPI (4'-6-diamino-2-phenylindole) stains the non-viable cells that possess permeable cell membranes. The outcome is a number in percentage units that shows the number of viable cells. For cell cycle analysis, cell suspensions were centrifuged, treated with an acidic lysis buffer, and stained with DAPI for 5 min at 37°C. After, a neutraliser basic buffer was added, and the cellular fluorescence was quantified by using a NC-Slide 8™ and the NucleoCounter® NC-3000™. The outcome is a spectrum analysed using the software NucleoView™ software, that, after using the markers it will show if the compounds interact with the cell cycle at any stage.³⁸

Table 4-15 summarises the cell viability results for the experiments carried out using the healthy cell line, ARPE-19, for the control experiments, after treatment with complex **3.23** (2-F) and complex **3.32** (2,5-diCl) respectively. These experiments are carried out using the same concentration for the complexes (18 μ M) in order to observe the effect of the drugs after 24h, 48h and 72h.

For the control and the treatment with complex **3.23** (2-F) there is a reduction in the number of total cells after 72 hours and there is almost no reduction in the percentage of viable cells. Whereas for treatment with complex **3.32** (2-5-diCl) there is an increase in the number of total cells, however, there is a slight decrease the cell viability percentage. If a drug shows a cytotoxic behaviour, the number of total cells and the percentage should decrease, whereas if the drugs behave as cytostatic, the cell proliferation will be impeded without changing the percentage of cells viable. These suggest that both complexes show a cytostatic behaviour when using the ARPE-19 cells. These feature is consistent with the IC_{50} values against the ARPE-19 cell lines as the IC_{50} values are quite high, making these two complexes the most selective out of the thirty compounds tested.

In **Figure 4-29**, it can be seen the optical images of the cells before analysing the cell viability and cell cycle. All the images are very similar apart from the 3rd row. The last row of **Figure 4-29**, involves the treatment of the cells with complex **3.32** (R = 2,5-diCl). Interestingly, it was observed a series of needles attached to the cells and the walls of the T25 flasks (**Figure 4-30**). Several attempts were made in order to get some of the crystals and analyse them by x-ray crystallography, but, unfortunately, these crystals are very tiny and very fragile. Different crystallisations were set up under the same conditions as the treatment of the cells, but no crystals were formed. This suggests that in order to obtain the crystals the cells might play an important role. This could potentially be attributed to the cytostatic properties.

Table 4-15: ARPE-19 cell viability summary for control, complexes **3.23** and **3.32** after 24h, 48h and 72h (* = Not determined)

ARPE-19	Time (Control)			Time (3.23 (2-F))			Time (3.32 (2,5-diCl))		
	24h	48h	72h	24h	48h	72h	24h	48h	72h
Total Cells	3.68×10^5	9.40×10^5	6.87×10^5	2.93×10^5	6.24×10^5	2.34×10^5	1.91×10^5	8.16×10^5	2.57×10^6
Cell viability / %	98.1	98.1	94.8	98.4	97.5	94.7	98.9	98	91.9
Cell diameter / μm	16.4 ± 7.9	$>20 \pm *$	16.0 ± 8.3	16.7 ± 8.1	17.5 ± 8.7	17.0 ± 8.7	17.1 ± 8.2	17.1 ± 8.3	13.7 ± 9.5
Aggregates of >5 cells	0	4	15	11	1	3	5	2	71



Figure 4-29: Representative optical microscopy images (x10) of ARPE-19 cells after 24h, 48h and 72h in: (*top*) control experiment, (*medium*) treatment with complex **3.23** (2-F) and (*bottom*) treatment with complex **3.32** (2,5-diCl).

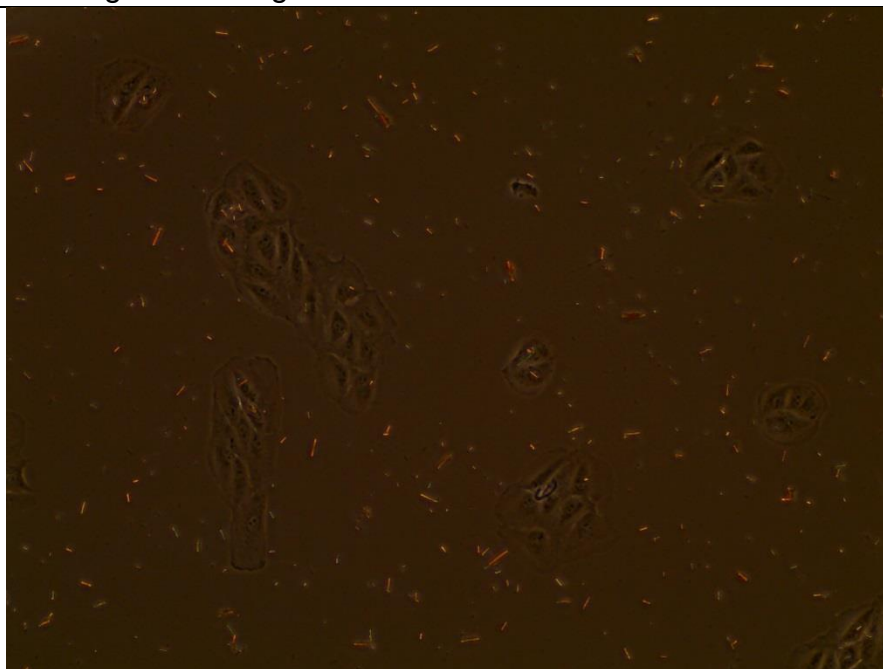


Figure 4-30: Optical image (x10) of ARPE-19 treated with the complex **3.32** (2,5-diCl) after 48h. Several needle-like crystals can be seen when using polarised light.

Table 4-16 collects all the data for the cell cycle analysis for ARPE-19. After 24h of drug exposure, cell cycle analysis shows two different behaviours for the complexes. Complex **3.23** (R = 2-F) an increase of 10% in the number sub G₁ cells. The phase G₀/G₁ decreases in 30% and showing increased values the remaining both phases, S and G₂/M. However, and as expected from the very high IC₅₀ value, complex **3.32** (2,5-diCl) shows similar percentages as the control meaning little affect towards the healthy cell line.

After 48h of drug exposure, cell cycle analysis displays, again, two different behaviours for the complexes. Complex **3.23** (R = 2-F) shows an increase of 30% in the number sub G₁ cells. The phase G₀/G₁ decreases from 89.1% to a 30% showing increased values for both phase, S and G₂/M. For S-phase, the percentage increases in 10 units and for G₂/M, the final result is 22.8 % that corresponds with almost a 20% increase. Complex **3.32** (2,5-diCl) displays similar percentages as the control.

After 72h of drug exposure, cell cycle analysis shows the same patterns in the cell cycle for the cells treated compared to the untreated cells. In this case, complex **3.23** (R = 2-F) shows an increase of nearly 35% in the number sub G₁ cells. The phase G₀/G₁ decreases from 80.9% to a 27.3% showing increased

values of 10% for the S phase with a final value of 20%, and an increase of 10% for the G₂/M with a final value of 15.1%. Complex **3.32** (2,5-diCl) displays similar percentages as the control.

Figure 4-31 is a bar-chart representation of the different percentages of the cell cycle analysis for the different time experiments (duplicate). It can be seen that, only complex **3.32** (2-F) shows an increase in the Sub G₁ phase (black highlighted in the plot). This phase is attributed to the leaching of DNA from the cell which is related to cell death. To corroborate this effect, another experiment using 18 μ M should be done in order to finish the triplicates. To prove the compound selectively increases the Sub G₁ phase, another set of experiments should be carried out at higher concentration, to understand completely if this complex induces apoptosis, the following assays could be done: Annexin V assay, Caspase assay or Mitochondrial Potential assay.⁴¹

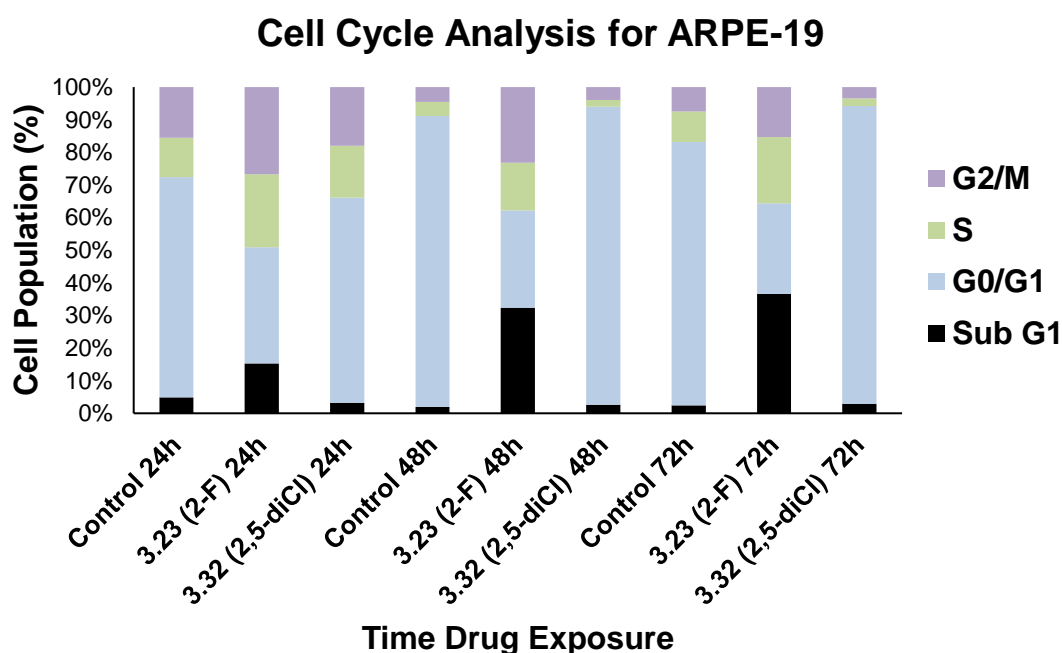


Figure 4-31: Bar chart representing the proportions of the cell cycle for the cell line ARPE-19 after 24h, 48h and 72h, including the drug exposure experiments.

The ruthenium complexes NAMI-A and KP-1019 were proved by cell cycle arrest assays, that both complexes alter the cycle in the phase G₂/M which involves two processes: mitosis when the chromosomes condense and pulled to the sides of the cells by spindle fibres, and cytokinesis involving the formation of a ring which will divide the parent cell into two daughters.^{42,43}

Chapter 4 Biological Investigations

In 2014, a *cis*-tetraammine(oxolato) ruthenium (III) dithionate complex was analysed against leukaemia cells showing that the cell cycle arrest was attributed to the sub G₁ phase.⁴⁴ The results against the ARPE-19 cells described in this section give an indicative that these compounds interact in a similar way to the complex dithionate complex. However, little it is known about the *trans*-dihalide arrangement of the chloride labile ligands when coordinated to a metal, hence further analysis should be done to understand the mechanism of action of this novel family.

Table 4-16: ARPE-19 cell cycle analysis after 24h, 48h and 72h, showing the control, drug treatment with complex **3.23** (2-F) and complex **3.32** (2,5-diCl) at a concentration of 18 μ M

Cell cycle phase ARPE-19	Time (Cell Population (%)) Control)			Time (Cell Population (%))3.23 (2-F))			Time (Cell Population (%))3.32 (2,5-diCl))		
	24h	48h	72h	24h	48h	72h	24h	48h	72h
Sub G₁	4.9	1.9	2.4	14.9	31.8	36.0	3.2	2.6	2.9
G₀/G₁	67.2	89.1	80.9	34.7	29.4	27.3	61.9	91.2	91.1
S	12.0	4.3	9.3	21.8	14.4	20.0	15.6	2.1	2.3
G₂/M	15.5	4.5	7.5	26.0	22.8	15.1	17.7	3.9	3.5

Table 4-17 contains the cell viability results for the experiments carried out using the cancerous cell line, MIA PaCa_2, for the control experiments, after treatment with complex **3.23** (2-F) and complex **3.32** (2,5-diCl) respectively. These experiments were carried out using the same concentration for the complexes (18 μ M) in order to observe the effect of the drugs after 24h, 48h and 72h.

For the control experiment, the total number of cells and viability increases with time showing a normal behaviour. When the cells are treated with complex **3.23** (2-F) there is a reduction in the number of total cells after 72 hours and a clear reduction in the percentage of viable cells what means this is a clear cytotoxic behaviour. Whereas after treatment with complex **3.32** (2-5-diCl) there is a decrease in the total number of cells with a substantial decrease in the percentage of cell viability after 48h, however, after 72h there is an increase in the number of total cells, as well as for the cell viability percentage, reaching similar values to the ones obtained for the control. This suggests that compound **3.32** (2-5-diCl) has two potential modes of action, a cytotoxic behaviour before 48h and cytostatic properties thereafter. However, this result is slightly contradictory to the cell recovery assay, as it was proved that pancreatic cells did not recover after drug exposure of 24h.

Figure 4-32 shows the different drug exposure optical images of the cells before analysing the cell viability and cell cycle. Apart from the 3rd row, all the images are very similar showing a decrease in cell population. **Figure 4-33** involves the treatment of the cells with complex **3.32** (R = 2,5-diCl). Interestingly, it was observed a series of needles attached to the cells and the walls of the T25 flasks. These crystals are very tiny and very fragile, with unsuccessful attempts to synthesise them for x-ray crystallography. The attempts made did not involve cells what suggests they might play an important role which could potentially be related to the mode of action of compound **3.32**.

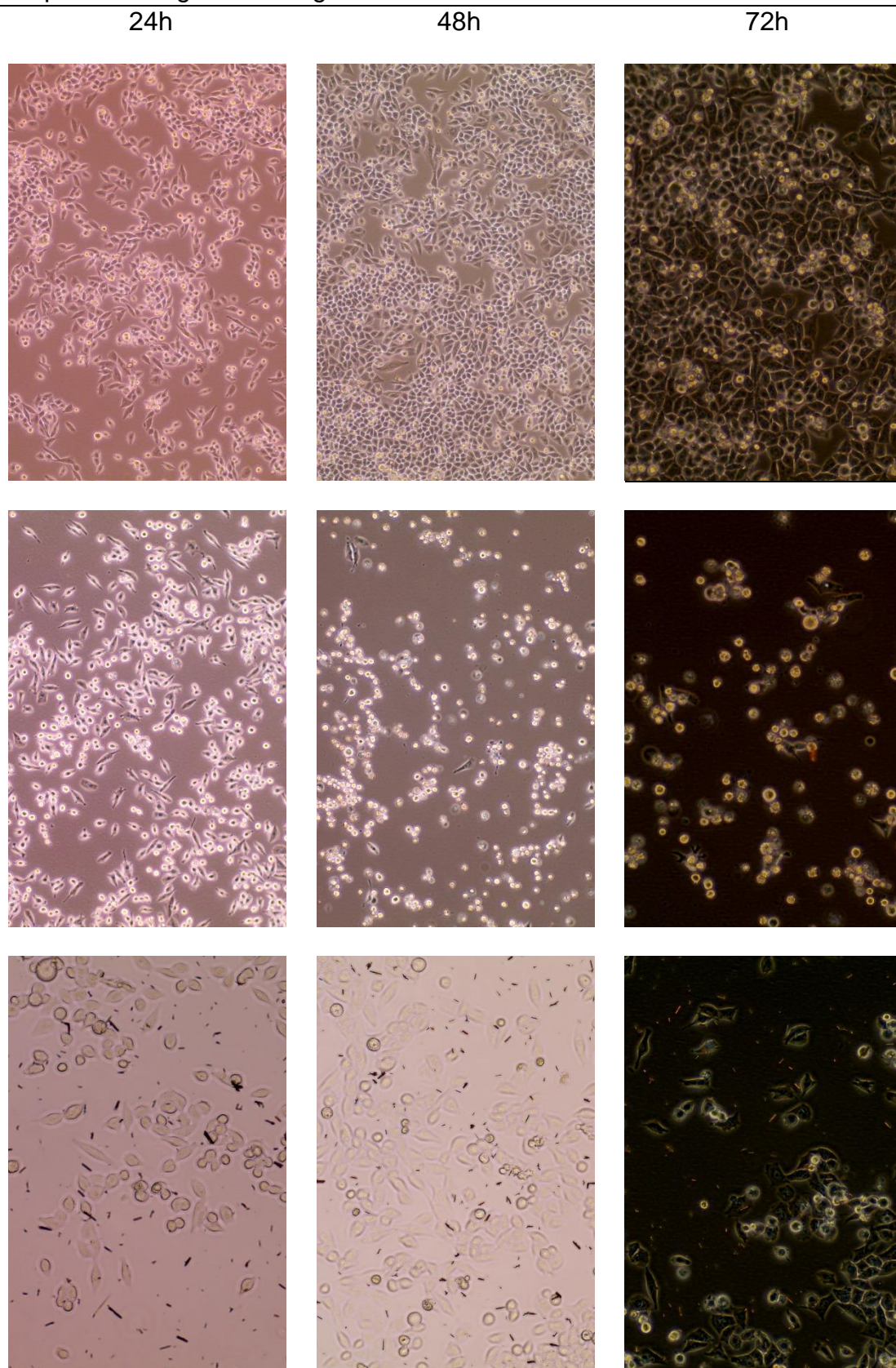


Figure 4-32: Representative optical microscopy images (x10) of MIA PaCa₂ cells after 24h, 48h and 72h in: (*top*) control experiment, (*medium*) treatment with complex **3.23** (2-F) and (*bottom*) treatment with complex **3.32** (2,5-diCl).

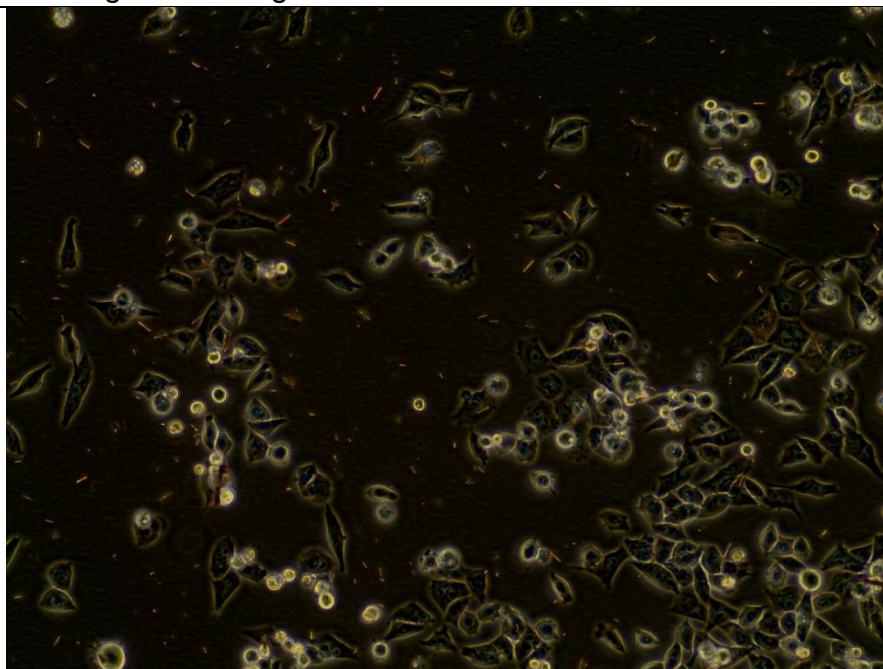


Figure 4-33: Optical image (x10) of MIA PaCa_2 treated with the complex **3.32** (2,5-diCl) after 48h. Several needle-like crystals can be seen when using polarised light, displaying three different colours: blue, red and green.

Table 4-17: MIA PaCa_2 cell viability summary for control, complexes **3.23** and **3.32** after 24h, 48h and 72h (* = Not determined)

MIA PaCa_2	Time (Control)			Time (3.23 (2-F))			Time (3.32 (2,5-diCl))		
	24h	48h	72h	24h	48h	72h	24h	48h	72h
Total Cells	1.11 x 10 ⁶	8.91 x 10 ⁵	1.69 x 10 ⁶	1.35 x 10 ⁶	1.32 x 10 ⁶	6.34 x 10 ⁵	1.10 x 10 ⁶	9.63 x 10 ⁵	2.10 x 10 ⁶
Cell viability / %	77.0	64.7	90.2	79.6	67.2	48.6	94.6	81.0	92.4
Cell diameter / μm	16.7 ± 9.9	15.1 ± 10.1	16.1 ± 10.5	16.5 ± 10.9	12.9 ± 10.0	15.1 ± 10.1	16.9 ± 9.6	15.6 ± 10.4	16.1 ± 10.9
Aggregates of >5 cells	59	43	63	62	41	32	73	58	75

Table 4-18 collects all the data for the cell cycle analysis for MIA PaCa_2. After 24h of drug exposure, cell cycle analysis shows two different behaviours for the complexes. Complex **3.23** (R = 2-F) shows a decrease of 10% in the number of G₀/G₁ cell phase and an increase of 10% in the S phase. However, complex **3.32** (2,5-diCl) shows a 22% decrease in the G₀/G₁ phase which was almost evenly distributed between the other three phases. From the untreated cells, Sub G₁, S and G₂/M show values of 7.6, 11.7 and 12.3, whereas for the treated cells it was 14.6, 17.2 and 20.5, respectively.

After 48h of drug exposure, cell cycle analyses have displayed two different behaviours for the complexes. Surprisingly, complex **3.23** (R = 2-F) shows an increase of 30% in the number sub G₁ cells, 50% decrease in G₀/G₁ phase and 10% decrease for both S phase and G₂/M phase. Conversely to the 24h results, for complex **3.32** (2,5-diCl) shows no variation when compared to the untreated cells or control.

After 72h of drug exposure, cell cycle analysis shows that complex **3.23** (R = 2-F) has an increase of nearly 30% in the number sub G₁ cells. The phase G₀/G₁ decreases from 71.2% to 34.9% showing increased values of 8% for both the S phase and the G₂/M with final values of 17.8% and 15.1%, respectively. Complex **3.32** (2,5-diCl) shows a 10% increase in the Sub G₁, a decrease of the G₀/G₁ phase of 35%; and increases of 12% and 13% for the S-phase and the G₂/M phase, respectively.

Figure 4-34 is a bar-chart representation of the different percentages of the cell cycle analysis for the different time experiments (duplicate). Both complexes show a significantly change in the phase Sub G₁ (black highlighted in the plot). This is consistent with the results obtained for the ARPE-19 cell cycle analyses. This phase is attributed to cell death. However, to corroborate this effect, another experiment using 18 µM should be done in order to finish the triplicates. The results obtained for complex **3.32** (2,5-diCl) after 48h seem odd as they do not follow a trend when compared to the 24h. To prove the compound selectively increases the Sub G₁ phase for both complexes, experiments inducing apoptosis should be carried out.

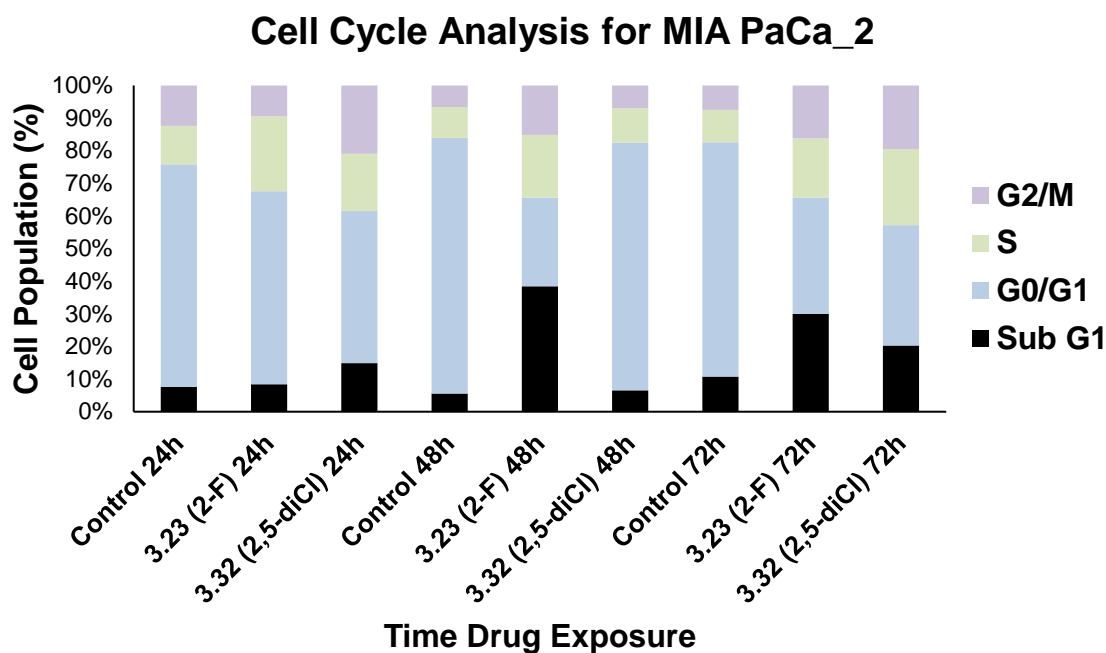


Figure 4-34: Bar chart representing the proportions of the cell cycle for the cell line MIA PaCa_2 after 24h, 48h and 72h, including the drug exposure experiments.

4.6.1 Summary of Cell viability and Cell cycle assay

After determining the Lead compounds, complex **3.23** (2-F) and **3.32** (2,5-diCl) were proved to be the best candidates for further analysis. Cell viability was determined and proven there is no recovery after 1h and 24h drug treatment, suggesting these compounds have cytotoxic properties. Cell cycle arrest analyses proven that only complex **3.23** (2-F) shows cytotoxic effects against ARPE-19 at the Sub G₁ phase (suggesting that this compound might induce cell programme death or apoptosis). When analysing the cell cycle arrest data against the MIA PaCa_2 cell line, both compounds showed a remarkable increase of the cell population in the Sub G₁ phase. As this phase is linked to cell death, further analyses should be done in order to determine the mechanism of action, such as apoptosis assays or MTT assays with inhibitors.

Table 4-18: MIA PaCa_2 cell cycle analysis after 24h, 48h and 72h, showing the control, drug treatment with complex **3.23** (2-F) and complex **3.32** (2,5-diCl) at a concentration of 18 μ M

Cell cycle phase ARPE-19	Time (Cell Population (%)) Control)			Time (Cell Population (%))3.23 (2-F))			Time (Cell Population (%))3.32 (2,5-diCl))		
	24h	48h	72h	24h	48h	72h	24h	48h	72h
Sub G₁	7.6	5.5	10.7	8.1	38.1	29.4	14.6	6.5	19.8
G₀/G₁	67.9	77.9	71.2	56.8	27.0	34.9	45.6	75.4	36.1
S	11.7	9.3	9.9	22.	19.1	17.8	17.2	10.5	22.9
G₂/M	12.3	6.6	7.4	9.1	15.0	15.9	20.5	6.9	19.0

4.7 Anti-bacterial activity

Nowadays, modern medicine is facing a critical stage of bacterial resistance. There are two classes of bacteria: Gram-negative and Gram-positive meaning the bacteria lacks or possessed an external wall, respectively; and some pathogens that have shown resistance in hospital-based infections. This combination of pathogens is called ESKAPE. This family is known for be resistant to several drugs and it is formed by: *Enterococcus faecium*, *Staphylococcus aureus*, *Klebsiella pneumoniae*, *Acinetobacter baumannii*, *Pseudomonas aeruginosa* and *Enterobacter* species.⁴⁵ This resistance to current drugs is due to the ability of bacteria of rapid proliferation and the transfer of genes both between generations (vertically) or in the same generation (horizontally). It can be active which results when bacteria counter-attack or passive when, for example, the bacteria develop a non-specific barrier against the drug.⁴⁶ New antibiotics are modifications of the pre-existing ones, but this is not a solution and they are not very successful. In 1950s, Rubbo *et al.* proved that complexation of oxine (sanitizer) to copper and iron ions improved its antibiotic properties.^{47,48} Hence, the introduction of metal-based complexes as potential drugs which will approach the biocidal approach through different mechanism of action.⁴⁹ The reported metal complexes contain an existing antibacterial compound in order to merge the antimicrobial activity and proved to increase its activity.⁵⁰ The most successful family of ruthenium compounds were developed by Dwyer *et al.* are focused on ruthenium (II) polypyridyl complexes showing great activity against Gram-positive, Gram-negative and acid-fast bacteria.⁵¹

Recently, more focus is given to ruthenium (III) complexes constituted by chelating ligands which are derived from polypyridyl units, base Schiff ligands or thiourea building blocks and two dichloride labile ligands.⁵²⁻⁵⁴ The ruthenium (III) polypyridyl charged complexes have been proven to be more active than the ruthenium (II) neutral complexes derived by Dwyer. The biocidal activity of the former increases when one of the chlorides is substituted by guanide (**Figure 4-35**). This feature was attributed to the Overtone's concept of cell permeability were the more liposoluble the drug the better the antibacterial activity,⁵⁵ and Tweedy's chelation theory which states that the polarity of the metal ion is reduced due to the overlap of the ligand orbital and partially sharing the

metal ion charge increasing the delocalization of p-electrons what enhances the penetration of the metal complexes in lipid membranes (Overtone's concept) blocking the metal binding sites on enzymes of the microorganisms.⁵⁶

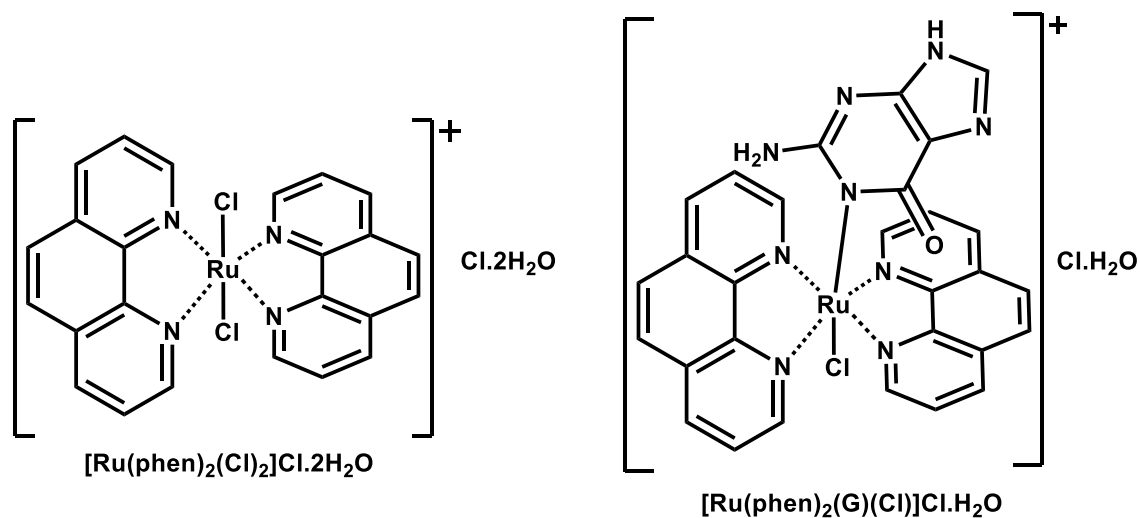


Figure 4-35: Chemical structures of the ruthenium (III) polypyridyl complexes (*left*) dichloride complex and (*right*) its Guanide (G) derivative.

Ruthenium (III) bearing amide ligands have not yet been exploited nor any literature could be found to date. In this work, *trans*-dichloride ruthenium (III) bis-quinaldamide neutral complexes are proposed as candidates for selective antibacterial studies.

Complexes were screened (**Figure 4-36**) for their anti-bacterial activity against two types of bacteria classified depending on the absence (Gram negative) or presence (Gram positive) of bacteria cell wall; *Escherichia coli* (E. c.), *Klebsiella pneumoniae* (K. p.), *Acinetobacter baumannii* (A. b.), *Pseudomonas aeruginosa* (P. a.) and *Staphylococcus aureus* (S. a.) by The Community for Antimicrobial Drug Discovery (CO-ADD) at The University of Queensland. The complexes at a single concentration of 32 $\mu\text{g}/\text{mL}$, were incubated with the bacterial strains at 37°C for 18 hours without shaking. All growth inhibition assays were performed in duplicate. Growth inhibition was determined by measuring absorbance at 600 nm. Complexes with growth inhibition greater than 80% are classed as active, complexes in the range of 50-80% are considered partially active and below 50% are considered inactive.

Antibacterial screening results for the *trans*-dichloride ruthenium (III) bisquinaldamide neutral complexes are summarised in **Table 4-19** from

Chapter 4 Biological Investigations

complexes **3.1 – 3.24**, and **Table 4-20** for complexes **3.25 – 3.40**. The results are highlighted for ease of understanding. Green means greater than 80% and subject to further analysis by the same institution. Orange means between 50-80%.

From the results obtained, almost half of the complexes tested have shown a preferential activity against *Staphylococcus aureus* (S. a.); being selective towards this bacterial strain and with any other biocidal activity against the remaining ones. Compounds **3.5** (2-Me), **3.9** (2-Et), **3.26** (2,4-diF), **3.32** (2,5-diCl), **3.39** (3-I) and **3.40** (4-I) are classified as moderately active with MIC values ranging between 52.48% until 79.08%. Compounds **3.12** (2-ⁱPr), **3.28** (2-Cl), **3.30** (4-Cl), **3.33** (2-Br), **3.34** (3-Br), **3.35** (4-Br) and **3.38** (2-I) classified as active antibacterial drugs with values ranging between 81.83% until 98.72%; they were analysed further by the same institution and discussed later in this chapter.

Interestingly, both series of compounds show that the 2-substituted complexes have an effect on this selective biocidal activity against *Staphylococcus aureus*. Compounds with electron-donating groups show a MIC in the moderately active region, whereas, apart for the complex substituted with R = 2-ⁱPr, when the functional groups are electron-withdrawing groups the activity falls in the region of active compounds. Surprisingly, compounds with fluoro groups did not show an effect that falls in this activity range, however when conversion to Cl, Br and I the MIC rises to near 98% of activity. The size of these EWG have a clear effect as well as the position, when the functional group of the ligand is Cl, only positions 2 and 4 show activity; if the ligand is I, only position 2 shows potency and if the ligand is monofunctionalised with Br, positions 2, 3 and 4 show activity. From these results, it is very clear that position is a crucial factor being position 2 of the ligands the most relevant. In terms of functional group, only when the functionalised ligand is Br, it shows activity independently of the position, what makes bromide a key factor in the selectivity and potency.

The ruthenium benchmark (complex **3.1** with R = H) shows no activity at all. In contrast with the anticancer activity, this compound shows that aryl modifications are important in order to increase the activity of the compounds. It also shows that this sort of *trans*-dichloride disposition effects selectivity. Unfortunately, the similar family published within the group³² was not tested against any bacteria

Chapter 4 Biological Investigations

strains. Nonetheless, there is some work done (*unpublished*) in cobalt metal complexes having picolinamide ligands as functional groups and their antibacterial studies. The outcome was that the bispicolinamide cobalt complexes with different labile ligands showed no activity against the same bacterial strains used for this thesis. This shows that ruthenium metal complexes are good candidates as antibacterial agents, as it was seen for the Ru(III) polypyridyl complexes, and, also that they can be fine-tuned to be selective and very potent when the ligands are bulky amides.

It is important to highlight that: the complexes tested have a *trans*-dichloride arrangement and, to date, little it is known about this metal-amide based scaffolds in terms of antibacterial activity neither there is a comparison between *trans* or *cis* labile ligands

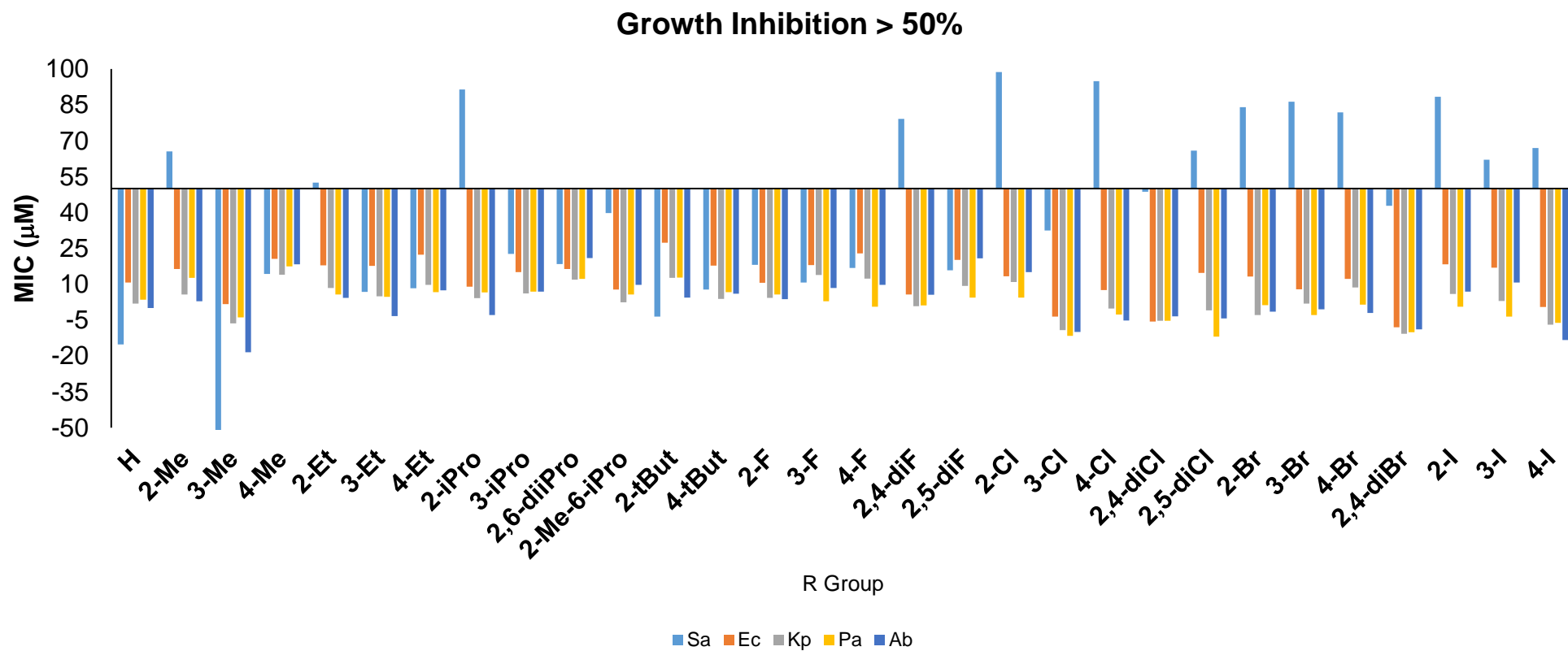


Figure 4-36: Bar-chart summary of the growth inhibition (%) of the ruthenium complexes against the different bacterial strains tested by the Community for Antimicrobial Drug Discovery.

Table 4-19: Growth inhibition of *trans*-dichloride ruthenium bisquinaldamide **3.1 – 3.24** complexes against bacterial strains expressed in %

Complex	R	S. a.	E. c.	K. p.	P. a.	A. b.
3.1	H	-15.17	10.74	1.85	3.57	0
3.5	2-Me	65.53	16.37	5.71	12.67	2.91
3.6	3-Me	-51.18	1.69	-6.4	-3.88	-18.4
3.7	4-Me	14.25	20.61	14.01	17.4	18.35
3.9	2-Et	52.48	17.88	8.41	5.75	4.26
3.10	3-Et	6.83	17.63	4.95	4.73	-3.33
3.11	4-Et	8.34	22.32	9.77	6.64	7.49
3.12	2- ⁱ Pr	91.42	8.96	4.16	6.58	-2.86
3.13	3- ⁱ Pr	22.64	15.05	6.18	6.92	6.94
3.15	2,6-di ⁱ Pr	18.41	16.32	11.89	12.2	20.9
3.16	2-Me-6- ⁱ Pr	39.8	7.76	2.47	5.67	9.72
3.17	2- ^t Bu	-3.54	27.31	12.72	12.81	4.37
3.18	4- ^t Bu	7.79	17.82	3.9	6.71	6
3.23	2-F	18.09	10.59	4.32	5.75	3.78
3.24	3-F	10.69	18.01	13.86	2.93	8.46

Table 4-20: Growth inhibition of *trans*-dichloride ruthenium bisquinaldamide **3.25 – 3.40** complexes against bacterial strains expressed in %

Complex	R	S. a.	E. c.	K. p.	P. a.	A. b.
3.25	4-F	16.84	22.87	12.33	0.64	9.68
3.26	2,4-diF	79.08	5.7	0.81	1.16	5.6
3.27	2,5-diF	15.79	20.16	9.33	4.35	20.86
3.28	2-Cl	98.76	13.27	10.97	4.35	15.08
3.29	3-Cl	32.44	-3.51	-9.15	-11.54	-10
3.30	4-Cl	94.93	7.51	-0.15	-2.66	-5.14
3.31	2,4-diCl	48.63	-5.6	-5.29	-5.31	-3.44
3.32	2,5-diCl	65.88	14.75	-0.95	-11.87	-4.35
3.33	2-Br	84.07	13.26	-2.93	1.26	-1.43
3.34	3-Br	86.28	7.88	1.92	-2.87	-0.53
3.35	4-Br	81.83	12.27	8.6	1.41	-1.97
3.36	2,4-diBr	42.81	-8.05	-10.71	-10.08	-8.86
3.38	2-I	88.35	18.27	5.87	0.64	6.9
3.39	3-I	62.04	16.86	3.02	-3.58	10.71
3.40	4-I	66.95	0.52	-6.88	-6.17	-13.29

Chapter 4 Biological Investigations

Complexes showing antibacterial activity (**3.12**, **3.28**, **3.30 – 3.35** and **3.38**) and classed as active were tested further, undergoing the hit confirmation process, which yields a number called minimum inhibitory concentration (MIC). MIC refers to the lowest drug concentration which displays visible growth of a given pathogen; the five antibacterial strains in this case, focusing on *Staphylococcus aureus*. This hit confirmation assay was carried by the same institution (CO-ADD) at The University of Queensland. The active *trans*-dichloride bisquinaldamide ruthenium (III) complexes were incubated, at eight concentrations, with the cells suspensions of the bacteria strains at 35 °C for 18 hours without shaking. All growth inhibition assays were performed in duplicate. Inhibition of bacterial growth was determined by measuring the absorbance at 600 nm. The MIC was determined as the lowest concentration at which the growth was fully inhibited, defined by an inhibition greater than 80%. Complexes with MIC values less than 32 µg/mL are classed as confirmed active hits.

In order to determine if these complexes are toxic to humans, they were also tested for their cytotoxicity against a non-cancerous cell line HEK 293 which is a human embryonic kidney. The cells were incubated with the complexes (eight different concentrations) at 37 °C for 20 hours in an atmosphere of 5% CO₂. In this case, the cytotoxicity was not measured by the addition of MTT, but after 3 hours incubation of the addition of resazurin (excitation wavelength of 560 nm and emission of 590 nm), under the same conditions as the assay was carried out. In this case, a value called CC₅₀ is obtained and is defined as the concentration of drug required to kill 50% of cells.

Haemolysis assays were also carried out using human blood. The active complexes, at different concentrations, were shaken with the cells for then minutes prior to incubation at 37 °C for one hour. The degree of haemolysis was determining by measuring the absorbance of the supernatant at 405 nm of the centrifuged samples, then it is expressed in term of HC₁₀. The HC₁₀ is a number that expressed the amount of the drug required to cause 10% haemolysis.

The antibacterial MIC values, cytotoxicity and haemolysis results for complexes **3.12** (2-*i*Pr), **3.28** (2-Cl), **3.30** (4-Cl), **3.33** (2-Br), **3.34** (3-Br), **3.35** (4-Br) and **3.38** (2-I) are summarised in **Table 4-21**.

Table 4-21: Antibacterial toxicity (MIC), cytotoxicity (CC₅₀) and haemolysis (HC₁₀) of **3.12**, **3.28**, **3.30**, **3.33 – 3.35** and **3.38**, all data expressed in $\mu\text{g/ml}$ (μM)

Complex	R	MIC					CC ₅₀	HC ₁₀
		S. a.	E. c.	K. p.	P. a.	A. b.	HEK	Hm
3.12	2- ⁱ Pr	16	>32	>32	>32	>32	12.62	>32
3.28	2-Cl	>32	>32	>32	>32	>32	>32	>32
3.30	4-Cl	>32	>32	>32	>32	>32	>32	>32
3.33	2-Br	>32	>32	>32	>32	>32	>32	>32
3.34	3-Br	8	>32	>32	>32	>32	13.46	>32
3.35	4-Br	>32	>32	>32	>32	>32	>32	>32
3.38	2-I	32	>32	>32	>32	>32	>32	>32

The first screening showed that the complexes **3.12**, **3.28**, **3.30 – 3.35** and **3.38** possessed a positive growth inhibition against *Staphylococcus aureus*, however only two complexes **3.12** (R = 2-ⁱPro) and **3.34** (R = 3-Br) display sufficient activity to be completely classed as active hits, showing MIC values of 16 $\mu\text{g/mL}$ and 8 $\mu\text{g/mL}$, respectively. Interestingly, only these two complexes showed cytotoxicity values towards the non-cancerous cell line HEK 293, showing CC₅₀ values of 12.62 μM for complex **3.12** (R = 2-ⁱPro) and 13.46 μM **3.34** (R = 3-Br). These values are actually very interesting when compared to the IC₅₀ values obtained for the non-cancerous cell ARPE-19 (retinal pigmented epithelium). This suggest that non-cancerous cell lines should be expanded as well as the cancerous ones. The fact that the two hit Lead Compounds show CC₅₀ against kidney cells suggest this family of *trans*-dichloride ruthenium complexes could be nephrotoxic. On the other hand, haemolysis results showed that the selection of active compounds are non-toxic to human blood under 32 μM .

4.8 Anti-fungal activity

Fungal infections can be classified as superficial or invasive, being the latter life-threatening. The pathogens which cause invasive infections are *Candida albicans*, *Cryptococcus neoformans* and *Aspergillus fumigates*.⁵⁷ There are only four classes of drugs based on organic molecules: polyenes, azoles, allylamines and echinocandins.

Modern medicine has evolved very quickly in terms of surgery and treatment of different illness. However, these advantages sometimes compromise the immunological system. Surgical procedures that involve transplantation, and treatments against cancer or HIV/AIDS are linked to the weakness of the immune system making patients to be vulnerable against fungal infections.⁵⁸ Furthermore, these infections have increased with a worrying mortality rate.⁵⁹

Organometallic and coordination metal complexes are slowly proving to be excellent candidates in terms of anticancer agents. Recently, the applications of those metal complexes have shifted to the antibiotic field, however, there are not many publications on the use of ruthenium (III) metal complexes as antifungal agents.

The main complexes proved to show anti-fungal activities are based on the metals of the first row, and generally it was found that their activity is dose dependant, the higher the dose concentration the better the activity. Historically, Schiff bases were the first ligands used as organic moieties that showed an increase in activity when complexed to metals, especially copper.⁶⁰ However, little it is known about the use of a bigger metal like ruthenium. Ruthenium (III) complexes are not as well studied as, for example, the piano-stool ruthenium (II) complexes. It can be found that the ligands bound to the ruthenium (III) centre are based on cycle Schiff bases⁶¹ acyclic hydrazones,⁶² catecholamine⁶³ or sulfur derivatives.⁶⁴

The trans-dichloride bisquinaldamide ruthenium complexes will expand another functionality, the amide bond coordinated to the ruthenium (III) as novel anti-fungal family.

Complexes were screened for their anti-fungal activity against *Candida albicans* (C. a.) and *Cryptococcus neoformans* (C. n.) by CO-ADD at the University of

Queensland. The complexes were tested at single concentration of 32 µg/mL, incubated with the fungal strains at 35 °C for 24 hours without shaking. All growth inhibition assays were performed by duplicate. Growth inhibition of *Candida albicans* was determined by measuring the absorbance at 530 nm. Growth inhibition of *Cryptococcus neoformans* was determined by measuring the difference in absorbance between 580 nm and 600 nm following the addition of resazurin and incubation at 35 °C for a further two hours. Complexes are divided in active is inhibition is higher than 80% or moderately active if the inhibition ranges between 50% and 80%.

Antifungal screening results for the complexes are summarised in **Table 4-22** and the compounds are highlighted in orange if moderately active and in green if active.

Only one complex possesses some activity against one of the fungal strains screened, *Candida albicans*; all other complexes were inactive or helped to proliferate the strains. Complex **3.26** (R = 2,4-diF) was moderately active and very selective against *Candida albicans*, showing an inhibition growth of 67.35%. Any alteration on the position of the substituents and on the number of them would affect dramatically. This disposition seems to be fundamental to show the moderate but selective antifungal activity. Haemolysis analysis have shown that these compounds are potentially not toxic to humans.

Table 4-22: Growth inhibition of *trans*-dichloride ruthenium bisquinaldamide **3.1 – 3.40** complexes against fungal strains expressed in %

Complex	R	C. a.	C. n.	Complex	R	C. a.	C. n.
3.1	H	-0.57	21.8	3.25	4-F	21.1	1.62
3.5	2-Me	7.39	-6.61	3.26	2,4-diF	67.35	-33.47
3.6	3-Me	-7.75	0.32	3.27	2,5-diF	7.75	-0.53
3.7	4-Me	7.46	-5.09	3.28	2-Cl	9.38	-7.26
3.9	2-Et	12.16	-11.58	3.29	3-Cl	9.67	-21.14
3.10	3-Et	29.01	-12.03	3.30	4-Cl	2.7	-3.5
3.11	4-Et	43.45	-7.33	3.31	2,4-diCl	-6.1	-14.98
3.12	2- ⁱ Pr	29.58	-12	3.32	2,5-diCl	39.48	9
3.13	3- ⁱ Pr	46.58	-12.22	3.33	2-Br	46.23	-8.35
3.15	2,6-di ⁱ Pr	35.89	-1.16	3.34	3-Br	24.39	-11.37
3.16	2-Me-6- ⁱ Pr	37.55	0.95	3.35	4-Br	11.62	-19.65
3.17	2- ^t Bu	4.26	23.75	3.36	2,4-diBr	32.3	-26.67
3.18	4- ^t Bu	17.44	10.95	3.38	2-I	8.25	-10.94
3.23	2-F	36.68	3.14	3.39	3-I	27.73	-14.13
3.24	3-F	13.72	2.71	3.40	4-I	-8.89	-30.28

4.9 Conclusions

Thirty ruthenium (III) *trans*-dichloride bis-quinaldamide complexes were tested for anti-cancer potency. Eight complexes were classified as Lead Compounds targeting two isogenic colorectal cancer cell lines based on tumour suppressor genes and one pancreatic cell line. Five of the Lead Compounds were studied further by expanding the colorectal cell line panel, targeting a proto-oncogene family. This work represents the first time a wide library of pure *trans*-dihalide complexes have a great potency under normoxic studies targeting several isogenic cell lines. The Lead Compounds were also screened under hypoxic conditions observing that compounds **3.23** (R = 2-F) and **3.32** (R = 2,5-diCl) enhance their activity. The two aforementioned compounds were studied further to understand their mechanism of action against the pancreatic cell line. Short time drug exposure showed the compounds are cytotoxic and cell cycle analysis proved that compounds arrest in the Sub G1 DNA phase.

All complexes were screened for their anti-fungal and anti-bacterial properties, showing that the complexes bearing the functional group in position 2 are toxic towards *Staphylococcus aureus* and only compound **3.26** displayed a moderate activity against *Candida albicans*.

4.10 References

- ¹ Lee, J.; Bogoyo, M.; *Curr. Opin. Chem. Biol.*, **2013**, 1 (1),1-22.
- ² Andrade, E. L.; Bento, A. F.; Cavalli, J.; Oliveira, S. K.; Freitas, C. S.; Marcon, R.; Schwanke, R. C.; Siqueira, J. M.; Calixto, J. B.; *Braz. J. Med. Biol. Res.*, **2016**, 49, 11, e5644.
- ³ Hann, M. M.; Leach, A. R.; Harper, G.; *J. Chem. Inf. Comp. Sci.*, **2001**, 41, 856-864.
- ⁴ Hughes, J. P.; Rees, S.; Kalindjian, S. B.; Philpott, K. L.; *Brit. J. Pharmacol.*, **2011**, 162, 1239-1249
- ⁵ Koehn, F. E.; Carter, G. T.; *Nat. Rev. Drug Discov.*, **2005**, 4, 206-220.
- ⁶ Mosmann, T.; *J. Immunol. Methods*, **1983**, 65, 55-63.
- ⁷ Lee, J.;Bogoyo, M.; *Curr. Opin. Chem. Biol.*, **2013**, 17(1), 118-126.
- ⁸ Sylvester, P. W.; Drug Design Discovery, **2011**, e-ISBN: 978-1-61779-012-6, 157-168.
- ⁹ Stockert, J. C.; Blázquez-Castro, A.; Cañete, M.; Horobin, R. W.; and Villanueva, Á., *Acta Histochem.*, **2012**, 114, 785-796.
- ¹⁰ Gerlier, D.; Thomasset, N.; *J. Immunol. Methods*, **1986**, 94, 57-63.
- ¹¹ www.cancerresearchuk.org/health-professional/cancer-statistics/statistics-by-cancer-type/bowel-cancer#heading-Four
- ¹² www.lgcstandards-atcc.org/products/all/CCL-247.aspx#generalinformation
- ¹³ www.cancerresearchuk.org/health-professional/cancer-statistics/statistics-by-cancer-type/pancreatic-cancer
- ¹⁴ www.lgcstandards-atcc.org/products/all/CRL-1420.aspx
- ¹⁵ www.lgcstandards-atcc.org/products/all/CRL-2302.aspx
- ¹⁶ So-Young, L.; Jae-Cheong, L.; Eun-Ha, C.; Sung-Hee, J.; *Radiochim. Acta*, **2016**, 104, 1, 59-65.
- ¹⁷ Brown, J. M.; *Methods in Enzymology, academic Press 2007*, vol. 435 pp 295-321
- ¹⁸ Bertout, J. A.; Mishra, A.; Ali, A.; Adhikari, J. S.; Verma, A. K.; Gupta, R.; *J. Biol. Inorg. Chem.*, **2012**, 17, 1217-1230.
- ¹⁹ Hunter, F. W.; Wouters, B. G.; Wilson, W. R., *Brit J. Cancer*, **2016**, 114, 1071-1077.
- ²⁰ Brown, J. M.; Wilson, W. R.; *Nat. Rev. Cancer*, **2004**, 4, 437-447.

- ²¹ Maxwell, P. H.; Pugh, C. W.; Ratcliffe, P. J.; *Curr. Opin. Genet. Dev.*, **2001**, 11, 293-299.
- ²² Michiels, C.; *Am. J. Pathol.*, **2004**, 164, 1875-1882.
- ²³ Weidemann, A.; Johnson, R. S.; *Cell Death Differ.*, **2008**, 15, 621-627.
- ²⁴ Ziello, E. J.; Jovin, I. S.; Huang, Y.; *Yale Journal of Biology and Medicine*, 2007, 80, 51-60.
- ²⁵ Michiels, C.; *American Journal of Pathology*, 2004, 164, 1875-1882.
- ²⁶ Ziello, E. J.; Jovin, I. S.; Huang, Y.; *Yale J. Biol. Med.*, **2007**, 80, 51-60.
- ²⁷ Ortmann, B.; Druker, J.; Rocha, S.; *Cell. Mol. Life Sci.*, **2014**, 71, 3569.
- ²⁸ Graf, N.; Lippard, S. J.; *Adv. Drug Deliv. Rev.*, **2012**, 64, 993-1004.
- ²⁹ Wilson, W. R.; Hay, M. P.; *Nat. Rev. Cancer*, **2011**, 11, 393-410.
- ³⁰ Fricker, S. P.; *Dalton Trans.*, **2007**, 0, 4903-4917
- ³¹ Denny, W. A.; *Eur. J. Med. Chem.*, **2001**, 36, 577-595.
- ³² Basri, A. M.; Lord, R. M.; Allison, S. J.; Rodriguez-Barzano, A.; Lucas, S. J.; Janeway, F. D.; Shepherd, H. J.; Pask, C. M.; Phillips, R. M.; McGowan, P. C. *Chem. Eur. J.*, **2017**, 23 (26). 6341-6356.
- ³³ Riss, T. L.; Moravec, R. A.; Niles, A. L.; Duellman, S.; Benink, H. A.; Worzella, T. J.; Minor, L.; *Assay guidance manual, Edition edn.*, **2013**.
- ³⁴ Heathman, T. R. J.; Glyn, V.A. M.; Picken, A.; Rafiq, Q. A.; Coopman, K.; Nienow, A. W.; Kara, B.; Hewitt, C. J.; *Biotechnol. Bioeng.*, **2015**, 112, 8, 1696-1707.
- ³⁵ Heathman, T. R.; Stolzing, A.; Fabian, C.; Rafiq, Q. A.; Coopman, K.; Nienow, A. W.; Kara, B.; Hewitt, C. J.; *Cytotherapy*, **2015**, 17, 11, 1524-1535.
- ³⁶ Blagosklonny, M. V.; Pardee, A. B.; *Cell cycle*, **2002**, 1, 103-110.
- ³⁷ Lapenna, S.; Giordano, A.; *Nat. Rev. Drug discov.*, 2009, 8, 547-566.
- ³⁸ Chemometec.com/cell-counting-assays/cell-cycle-analysis/ accessed 11/12/18
- ³⁹ Isoldi, M. C.; Visconti, M. A.; Castrucci, A. M.; *Mini-Rev. Med. Chem.*, **2005**, 5, 7, 685-689.
- ⁴⁰ Shah, M. A.; Schwartz, G. K.; *Clin. Cancer Res.*, **2001**, 7, 2168-2181.
- ⁴¹ <https://chemometec.com/cell-counters/nc3000-cell-analyzer-image-cytometer/>
- ⁴² Trondl, R.; Heffeter, P.; Kowol, C. R.; Jakupec, M. A.; Berker, W.; Keppler, B. K.; *Chem. Sci.*, **2014**, 5, 2925-2932.

- ⁴³ Bergamo, A.; Gagliardi, R.; Scarcia, V.; Furlani, A.; Alessio, E.; Sava, G.; *J. Pharma. Exp. Ther.*, **1999**, 289, 1, 559-564.
- ⁴⁴ Pereira, F. C.; Pereira de Lima, A.; Vilanova-Costa, C. A. S. T.; Pires, W. C.; Ribeiro, A. S. B. B.; Pereira, L. C. G.; Pavanin, L. A.; Santos, W. B.; Silveira-Lacerda, P.; SpringerPlus, **2014**, 3, 301-311.
- ⁴⁵ Pendleton, J. N.; Gorma, S. P.; Gilmore, B. F.; *Expert Rev. Anti Infect. Ther.*, **2013**, 11, 297-308.
- ⁴⁶ Wright, G. D.; *Adv. Drug Deliv. Rev.*, **2005**, 57, 1451-1470.
- ⁴⁷ Rubbo, S.; Albert, A.; Gibson, M. I.; *Br. J. Exp. Pathol.*, **1950**, 31, 425-441.
- ⁴⁸ Albert, A.; Gibson, M.; Rubbo, S.; *Br. J. Exp. Pathol.*, **1953**, 34, 119-130.
- ⁴⁹ Patra, M.; Gasser, G.; Metzler-Nolte, *Dalton Trans.*, **2012**, 41, 6350-6358.
- ⁵⁰ Sekhon, B. S.; *J. Pharm. Educ. Res.*, **2010**, 1, 1-20.
- ⁵¹ Dwyer, F.; Gyarfás, E. C.; Rogers, W.; Koch, J. H.; *Nature*, **1952**, 170, 190-191
- ⁵² Abebe, A.; Hailemariam, T.; *Bioinorg. Chem. Appl.*, **2016**, ID: 3607924
- ⁵³ Vadivel, T.; Dhamoradan, M.; *Int. J. Biol. Macromol.*, **2016**, 90, 44-52.
- ⁵⁴ Terbouche, A.; Ait-Ramdane-Terbouche, C.; Bendjilali, Z.; Berriah, H.; Lakhdari, H.; Lerari, D.; Bachari, K.; Mezaoui, D.; El Houda Bensiradj, N.; Guegan, J. P.; Hauchard, D.; *Spectrochim. Acta A*, **2018**, 205, 146-159.
- ⁵⁵ Anjaneyulu, Y.; Rao, R. P.; *Synth. React. Inorg. Met-Org. Chem.*, **1986**, 16, 257-272
- ⁵⁶ Tweedy, B. G. *Phytopathology*, **1964**, 55, 910-914.
- ⁵⁷ Liu, N.; Wang, C.; Su, H.; Zhang, W.; Sheng, C.; *Future Med. Chem.*, **2016**, 8, 1435-1454.
- ⁵⁸ Perfect, J. R.; *Nat. Rev. Drug Discov.*, **2017**, 16, 603-616.
- ⁵⁹ Perfect, J. R.; *Expert Opin. Emerg. Dr.*, **2016**, 21, 129-131.
- ⁶⁰ Khan, M. I.; Khan, A.; Hussain, I.; Khan, M. A.; Gul, S.; Iqbal, M.; Inayat Ur, R and Khuda, F.; *Inorg. Chem. Comm.*, **2013**, 35, 104-109.
- ⁶¹ Arunachalam, A.; Padam Priya, N.; Saravanakumar, C.; Jayabalakrishnan, C.; Chinnusamy, V.; *J. Coord. Chem.*, **2010**, 62, 10, 1795- 1806.
- ⁶² Sharma, V. K.; Srivastava, S.; Srivastava, A.; *J. Serb. Chem. Soc.*, **2006**, 71, 917-928.
- ⁶³ Galvao da Lima, R.; Lever, A. B. P.; Ito, Y. I.; Santana da Silva, R.; *Transit. Metal Chem.*, **2003**, 28, 272-275.
- ⁶⁴ Pandey, R. N.; Gautam, K, V.; *Rasayan J. Chem.*, **2014**, 7, 2, 195-200.

**Chapter 5 Structure-Activity Relationships of the
bis-quinaldamide trans-dichloride ruthenium complexes**

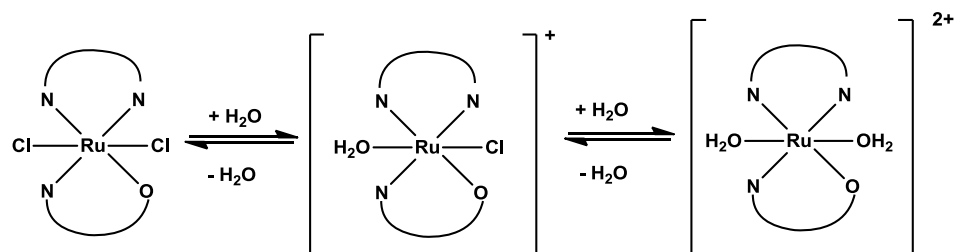
5.1 Introduction

Pharmaceutical drugs are in constant development in order to improve three features: higher potency, lower toxicity and improved selectivity. This is achieved by chemical modifications of the potential drug. To do so, the key point is understanding the relationship and behaviour between the molecular structure of a drug and its biological activity. After determining the anticancer activity of the ruthenium complexes described in **Chapter 3**, the main approaches to determine the structural-activity relationships are based on hydrolysis and hydrophobicity tests.

5.2 Hydrolysis Studies

An established mechanism of action for any anti-cancer drug with labile ligands is the activation by hydrolysis, probed for cisplatin (**Chapter 1**),^{1,2} NAMI-A (**Chapter 1**),³ and KP-1019.⁴ Once these complexes are administered intravenously into the blood plasma, they remain inert due to the high chloride concentration, what prevents the halide labile ligand attached to the metallic core. Once inside the cells, the low chloride concentration triggers the aquation reaction (inducement of hydrolysis) hence activating the molecules by replacing the halide ligand by a water molecule. It was reported that, under physiological conditions, dichloride ruthenium complexes hydrolyse yielding cationic mono-aqua or diaqua intermediates.⁵

It is assumed the *trans*-dichloride bis-quinolamide ruthenium complexes will undergo a hydrolysis reaction (proposed in **Scheme 5-1**) showing a similar aquation process to cisplatin and NAMI-A. A neutral dichloride ruthenium (III) complex undergoes a monohalide substitution with water forming a charged mono-aqua intermediate which hydrolyses further by substituting the second halide by another molecule of water yielding a 2+ charged diaqua complex. As previously discussed, the aqua derivatives are supposed to be the active species that have the potential to bind to DNA damaging its structure.⁶



Scheme 5-1: Proposed hydrolysis mechanism for the *trans*-dichloride bis-quinaldamide ruthenium complexes

Complexes **3.1**, **3.15**, **3.18**, **3.23**, **3.27**, **3.29**, **3.32** and **3.33** display different cytotoxicity ranging from highly active to inactive, hence, were selected to study their hydrolysis rate. The samples were prepared according to conditions used in hydrolysis studies previously reported in the literature and within the McGowan group for the bis-picolinamide complexes.^{7,8} The complexes were prepared in 10% DMF/90% H₂O to give a final concentration of 100 μM. These solutions were scanned using UV-vis spectrophotometry at different time points: 0 h, 1 h, 12 h, 24 h, 48 h and 72 h at 293 K to correlate with the 3-day drug incubation cytotoxic studies and cell recovery studies. After 72 h incubation, the samples were analysed by ESI-HRMS and there is no sign of any aquated species nor decomposition of the chloride ruthenium complexes. **Figure 5-1** collects the uv-vis spectra recorded from hydrolysis studies for the ruthenium *trans*-dichloride. The arrows on the graphs indicate the change of intensities of the peaks from time 0 h to 72 h. There are three different types of behaviour, in general, at 0h, each complex shows an intense absorption band in the ultraviolet region around 280 nm and two small bands between 300 and 350 nm. Compounds with electron-donating groups shows a slight decrease in intensities. There is no change in the spectra for the compounds bearing electron-withdrawing groups, except for compound **3.32** (the most selective as explained in **Chapter 5**), where there is a significant change after 1 h. The slight changes in the absorption bands suggest there are ligand substitution reactions occurring in aqueous solution.⁹ The ruthenium *trans*-dichloride complexes seem stable to hydrolysis meaning the mechanism of action would not involve a hydrolysed compound as active species. In summary, the UV-vis spectra show an intense ligand based absorbance (π-π*) at approximately 290 nm and two broad and less intense bands at 300-400 nm arising from metal-to-ligand charge transfer transitions. **Table 5.1** lists the wavelength where the maxima of each absorption bands are seen in the complexes tested.

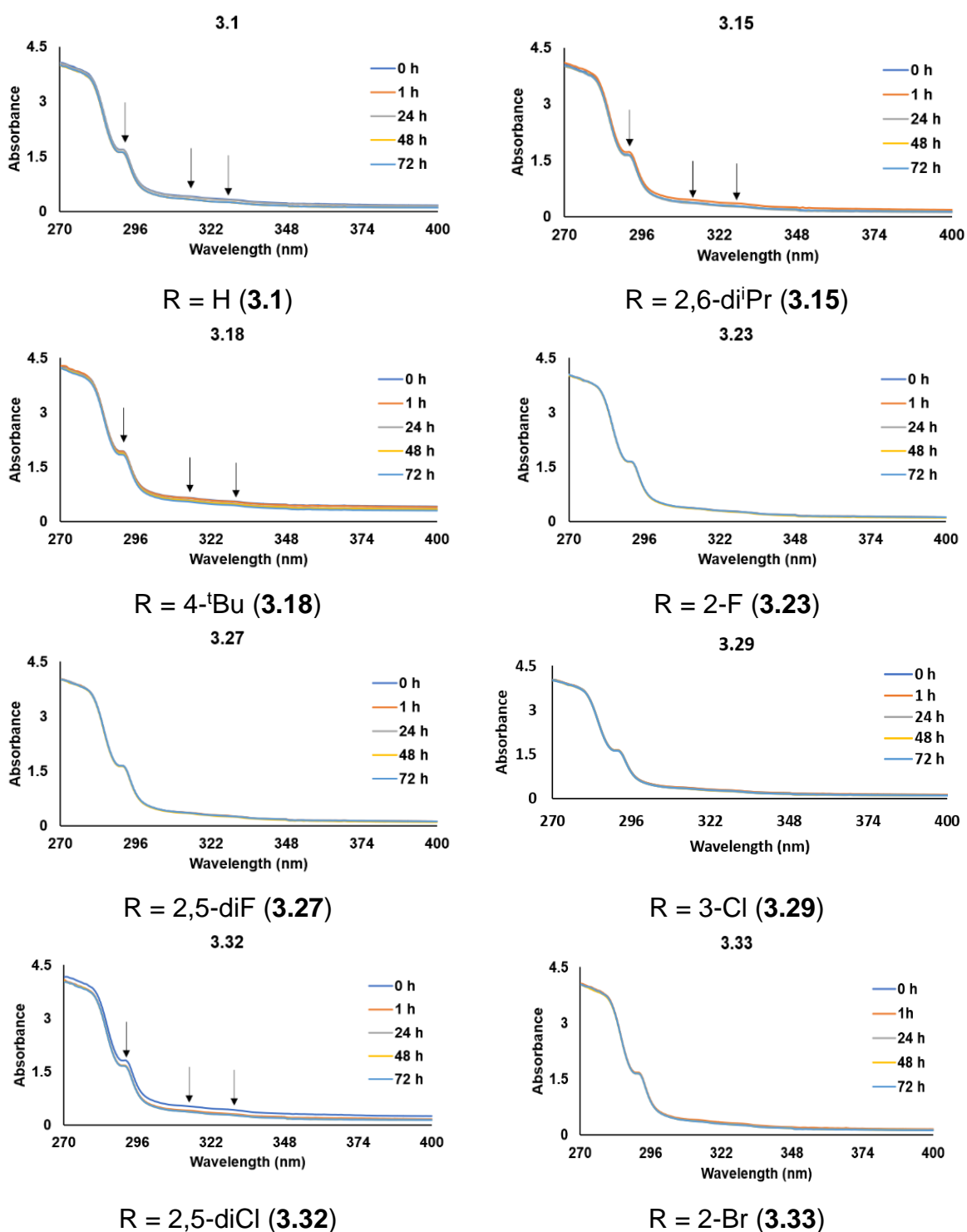


Figure 5-1: Recorded spectra for time-evolution hydrolysis studies and functional groups for the selected *trans*-dichloride Ru complexes.

Table 5.1: Absorption wavelength bands (λ_{\max}) for the Ru complexes

RuCl ₂ (L) ₂	R	λ_{\max} / nm
3.1	H	292, 315, 331
3.15	2,6-diPr	292, 314, 328
3.18	4- ^t Bu	291, 315, 332
3.23	2-F	291, 314, 330
3.27	2,5-diF	288, 313, 329
3.29	3-Cl	291, 316, 331
3.32	2,5-diCl	292, 317, 330
3.33	2-Br	289, 313, 328

Ruthenium complexes **3.1**, **3.15**, **3.18**, **3.23**, **3.27**, **3.29**, **3.32** and **3.32** follow the same trend as the *trans*-diiodide bis-picolinamide ruthenium complexes reported within the McGowan group where the anticancer activity was correlated to the less hydrolysed products. The bis-picolinamide dichloride ruthenium complexes showed that the more hydrolysed the better the anticancer activity which opposed to the trend found within this project. This outlines a new strategy in medicinal research, where a *trans* di-halide arrange can be critical to design new anticancer molecules which are less prone to hydrolysis suggesting that their integrity is not compromised when administered to the body.⁸

The equation shown below is used to estimate the final concentration in percentage of the aqua complex formed in solution. A calibration curve for each complex was used by taking the wavelength of the maximum absorbance peak to obtain the amount of complex hydrolysed after 72 h.

$$\% \text{ hydrolysed complex} = \left(\frac{[C]_{\text{initial}} - [C]_{\text{final}}}{[C]_{\text{initial}}} \right) \times 100\%$$

The percentage of hydrolysed complexes and the IC₅₀ values of the compounds tested are shown in **Table 5.2**, Hydrolysis studies have demonstrated that the ruthenium chloride complexes show no trend. The most selective compound **3.32** displays more hydrolysed product after 72 h than the remaining complexes. Although there is an striking feature, compounds tend to be stable throughout this assay but the most selective compounds shows a drop in the uv-vis spectra after between 1 h and 24 h. Finally, hydrolysis studies suggest that the mode of action

for these complexes might not be attributed to the displacement of the ligands. Additionally, these studies show this novel family is likely to be more stable under physiological conditions. The UV-vis hydrolysis samples were analysed by ESI-HRMS after 72 h to investigate if the 'aquated' ruthenium complexes can be detected. As expected, all the spectra show the main peak for each complex, but in the case of **3.23** and **3.32**, they both show a peak around 336 m/z that was absent in all the other spectra. In conclusion, the mechanism of action does not occur through hydrolysis being demonstrated by uv-vis spectroscopic and further confirmed by the absence of aqua-species of the ruthenium family.

NAMI-A and KP-1019 passed phase I clinical trials and both were demonstrated that the first step towards their activity was attributed to the displacement of two ligands arranged in a *cis* manner. McGowan *et al.* reported that *trans*-dihalide arrangement enhances the anticancer activity and, also, the less hydrolysed the compounds the lower the IC₅₀. This is challenging to prove as each cancerous cell line shows different behaviours and different mechanism of actions. It was also probed that the anticancer properties of the *trans*-dihalide complexes increases under hypoxic conditions for colorectal and breast cancer. That is also true for this family of compounds, what means the compounds could be possible prone to hydrolyse once the Ru(III) is reduced to Ru(II) being the latter more likely to react with water. Finally, this behaviour breaks the following rule: complexes with *trans* geometry could lead to an increase in toxicity due to kinetic instability, which was proposed by Rosenberg,¹⁰ Cleare and Hoeschele.^{11,12}

Table 5.2: IC₅₀ values against the cell lines tested and percentage of hydrolysed ruthenium complexes tested

Complexes	IC ₅₀ / μ M							% hydrolysed
	p53 ^{+/+}	p53 ^{-/-}	Kras Mutant	Kras WT	Kras Parent	MIA PaCa-2	ARPE-19	
3.1	10.69 \pm 0.42	15.75 \pm 1.56	-	-	-	21.32 \pm 3.08	36.37 \pm 4.65	5.06
3.15	>100	>100	-	-	-	>100	>100	5.08
3.18	5.79 \pm 0.87	5.93 \pm 0.89	3.45 \pm 0.59	5.43 \pm 0.93	3.46 \pm 0.40	15.95 \pm 3.01	8.82 \pm 1.35	4.65
3.23	8.10 \pm 1.30	11.74 \pm 1.44	9.05 \pm 1.18	10.09 \pm 0.70	7.78 \pm 0.47	18.30 \pm 3.38	29.64 \pm 0.26	0
3.27	14.41 \pm 2.44	16.79 \pm 2.65	-	-	-	29.95 \pm 1.79	50.19 \pm 9.10	0.25
3.29	5.01 \pm 0.75	8.18 \pm 1.06	10.79 \pm 0.85	8.54 \pm 0.78	7.91 \pm 0.13	26.38 \pm 0.95	21.08 \pm 1.80	0.73
3.32	12.87 \pm 2.15	11.71 \pm 1.32	22.67 \pm 3.62	21.47 \pm 0.96	20.11 \pm 2.29	28.73 \pm 0.58	91.09 \pm 8.90	9.50
3.33	>100	>100	-	-	-	>100	>100	1.51

5.3 Hydrophobicity

Drug resistance is a big milestone that needs to be overcome. It is believed that the decrease in cellular uptake of drugs is one of the main factors cause tumours to be resistant against chemotherapeutic drugs promoting cancer relapse.¹³ Cells possess a bilipid membrane which is hydrophobic in nature, hence, if compounds hydrophobic the easier they can enter the cells by passive diffusion.¹⁴ A way to make a drug more potent is by increasing its optimising liposolubility. Increasing the hydrophobicity of the drug will facilitate the cellular uptake, hence increasing their cytotoxicity. Furthermore, hydrophobicity has an optimum range, as a drug must be soluble in aqueous media and be able to cross the cell membrane, otherwise it decreases its potency.

The hydrophobicity of the ruthenium compounds was determined by the shake-flask method of octanol-water partition coefficient to obtain log P values.¹⁵ Deionised water containing 300 mM of NaCl was used to prevent the hydrolysis of the complexes during the study. Complexes **3.1**, **3.15**, **3.18**, **3.23**, **3.27**, **3.29**, **3.32** and **3.33** were dissolved in water-saturated octanol to be shaken with octanol-saturated water for 4 hours to ensure equilibrium. The organic layer of the samples before and after the experiment were analysed by uv-vis obtaining the concentration of the complex. Using pre-calibration curve of the respective complex, it was possible to calculate the concentration of the compounds hence determining the Log P values by using the following formula,

$$\text{Log } P = \text{Log} \left(\frac{[C]_{org}}{[C]_{aq}} \right)$$

The organic phase in a shake-flask method models the hydrophobic layers of the cell membrane. A complex is defined as hydrophobic when the concentration in the organic phase is higher than in the aqueous phase, what yields a positive Log P value. If log P is negative it means the drug concentration in the aqueous phase is higher, like cisplatin. The Log P values for the *trans*- dichloride ruthenium complexes selected are as shown in **Figure 5-1**. The complexes tested are found to be hydrophobic with their partition coefficients preferentially in the organic layer with values between 0.78 – 1.79. Lipinski's 'rule of five' were developed to understand what the requirements are for a molecule to be a successful chemotherapeutic drug, stating that poor absorption can be expected when the molecular weight is over 500 Da, Log P value is greater than 5, number of H-

bond donors is more than 5, and number of H-bond acceptors is more than 10.¹⁶ The bisquinaldamide ruthenium complexes are more hydrophobic – as expected – than the complexes previously published within the McGowan group, due to the extra fused ring in the ligand.⁸ Generally, transition metal drugs have proved to break some of the Lipinski's rules, as many compounds tend to weight more than stated. As hydrophobicity is concerned, complementing Lipinski rule, the Hansch's principle of minimum hydrophobicity states that a Log P should be lower than 2.0 to avoid related side effects with the central nervous system (CNS).¹⁷ The two lead ruthenium *trans*-dichloride compounds **3.23** and **3.32** have log P values of 1.50 and 1.79 respectively are the two most hydrophobic in the series. The remaining complexes do not follow really a trend but that can be explained as not all the complexes were tested for hydrophobicity. The compounds with moderate to none anticancer activity fall in the region between 1 and 1.25, and the compounds with some activity tend to be less hydrophobic.

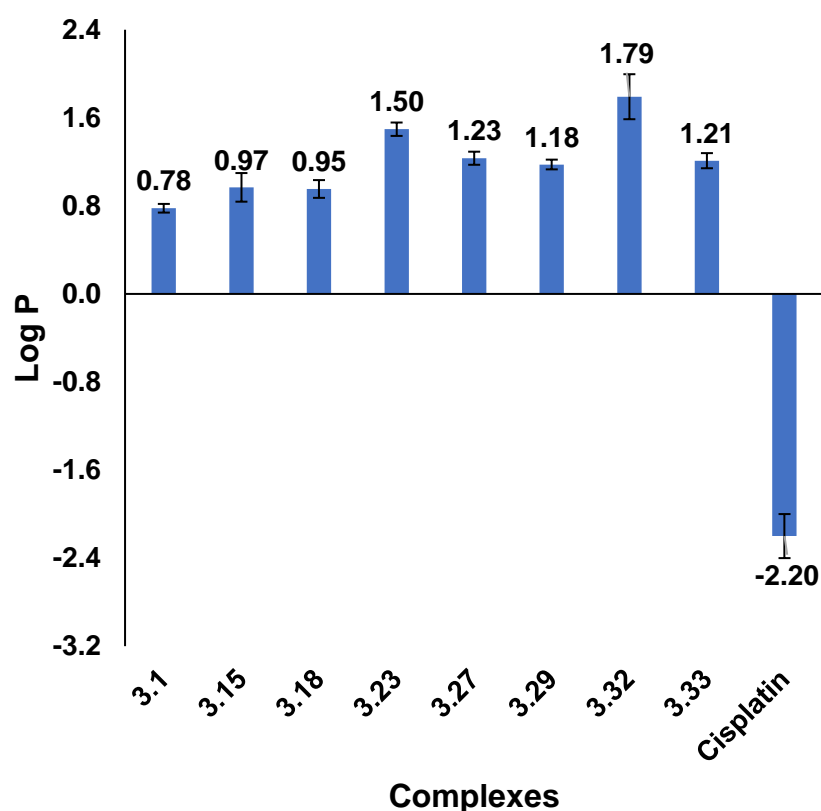


Figure 5-2: Log P values of the *trans*-dichloride bis-quinaldamide ruthenium complexes and cisplatin from the average of six independent experiments

Some platinum complexes have shown that by increasing their hydrophobicity correlates with the increase in their anti-cancer activity, unless for cisplatin.¹⁸

Figure 5-3 shows the correlation between the cytotoxicity values and Log P values of the selected trans-dichloride ruthenium complexes against all the cell lines. There are some interesting correlations, the complexes that have been tested against HCT 116 Kras (mutant, WT and parent) show a quasi-linear relationship. The compounds that have high IC₅₀ for the non-cancerous cell line follow a nice linear trend, but half of the complexes are outliers from the correlation (given by R²) and have showed irregularities of Log P values in the order of their cytotoxic activity.

The observations suggest that these hydrophobic complexes can easily enter the cells by passive diffusion. The correlations seen between the partition coefficient values and some cancerous cell lines suggest that these compounds have more preference to get into colorectal cell lines with the overexpression of oncogenes. Although, with only few correlations seen between their cytotoxicity and log P values, their cellular uptake mechanism may not influence their anti-cancer activity to these specific cell lines tested. Studies have shown the cellular uptake of KP-1019 occurs *via* overexpressed protein transferrin receptor within the cancer cell membrane.¹⁹ As ruthenium is in the same group as iron, it could be these family of ruthenium dichloride complexes may bind to a specific transporter, thus relating their anti-cancer activity to active cellular uptake.

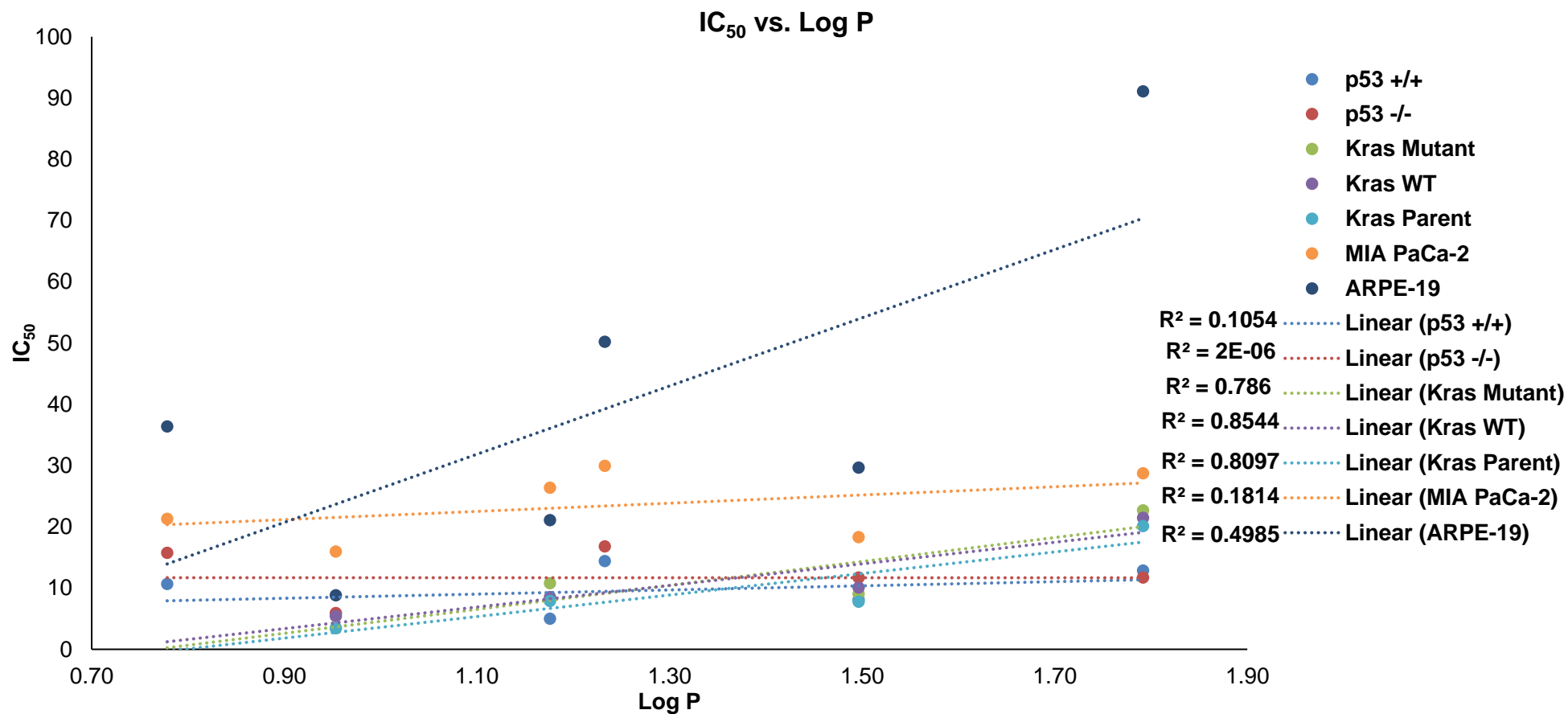


Figure 5-3: Representation of IC₅₀ values and Log P of the complexes analysed

5.4 References

- ¹ Jakupec, M. A.; Galanski, M.; Keppler, B. K.; *Rev. Physiol. Biochem. Pharmacol.*, Springer Berlin Heidelberg, **2003**, pp. 1-53.
- ² Brabec, V.; Kasparkova, J.; *Drug Resist. Updates*, **2005**, 8, 131-146.
- ³ Bouma, M.; Nuijen, B.; Jansen, M. T.; Sava, G.; Flaibani, A.; Bult, A.; Beijnen, J. H.; *Int. J. Pharm.*, **2002**, 248, 239-246.
- ⁴ Mestroni, G.; Alessio, E.; Sava, G.; Pacor, S.; Coluccia, M.; Boccarelli, A.; *Met. Based Drugs*, **1994**, 1, 41-63.
- ⁵ Roy, S.; Maheswari, P. U.; Golobič, A.; Kozlevčar, B.; Reedijk, J.; *Inorg. Chim. Acta*, **2012**, 393, 239-245.
- ⁶ Guo, Z.; Sadler, P. J.; *Angew. Chem. Int. Ed.*, **1999**, 38, 1512-1531.
- ⁷ Liu, Z.; Romero-Canelón, I.; Qamar, B.; Hearn, J. M.; Habtemariam, A.; Barry, N. P. E.; Pizarro, A. M.; Clarkson, G. J.; Sadler, P. J.; *Angew. Chem. Int. Ed.*, **2014**, 53, 3941-3946.
- ⁸ Basri, A. M.; Lord, R. M.; Allison, S. J.; Rodríguez-Bárcano, A.; Lucas, S. J.; Janeway, F. D.; Shepherd, H. J.; Pask, C. M.; Phillips, R. M.; McGowan, P. C.; *Chem. Eur. J.*, **2017**, 23, 26, 6341-3656.
- ⁹ Betanzos-Lara, S.; Habtemariam, A.; Clarkson, G. J.; Sadler, P. J.; *Eur. J. Inorg. Chem.*, **2011**, 3257-3264.
- ¹⁰ Rosenberg, B.; Van Camp, L.; Grimley, E. B.; Thomson, A. J.; *J. Biol. Chem.*, **1967**, 242, 1347-1352.
- ¹¹ Cleare, M. J.; Hoeschele, J. D.; *J. Bioinorg. Chem*, **1973**, 2, 187-210.
- ¹² Cleare, M. J.; Hoeschele, J. D.; *Plat. Metals Rev.*, **1973**, 17, 2.
- ¹³ Loh, S. Y.; Mistry, P.; Kelland, L. R.; Abel, G.; Harrap, K. R.; *Br. J. Cancer*, **1992**, 66, 1109-1115.
- ¹⁴ Ratain MJ, in *Holland-Frei Cancer Medicine*, ed. R. E. P. Donald W Kufe, Ralph R Weichselbaum, Robert C Bast, Jr, Ted S Gansler, James F Holland, and Emil Frei, III, BC Decker, Hamilton, 2003.
- ¹⁵ Concepcion, J. J.; Jurss, J. W.; Templeton, J. L.; Meyer, T. J.; *Proc. Natl. Acad. Sci.*, **2008**, 105, 17632-17635.
- ¹⁶ Lipinski, C. A.; Lombardo, F.; Dominy' B. W.; Feeney, P. J.; *Adv. Drug Delivery Rev.*, **1997**, 23, 3-25.
- ¹⁷ Hansch, C.; Bjorkroth, J. P.; Leo, A.; *J. Pharm. Sci.*, **1987**, 76, 663-687.

¹⁸ Platts, J. A.; Hibbs, D. E.; Hambley, T. W.; Hall M. D.; *J. Med. Chem.*, **2000**, 44, 472-474.

¹⁹ Heffeter, P.; Pongratz, M.; Steiner, E.; Chiba, P.; Jakupec, M. A.; Elbling, L.; Marian, B.; Korner, W.; Sevela, F.; Micksche, M.; Keppler, B. K.; Berger, W.; *J. Pharmacol. Exp. Ther.*, **2005**, 312, 281-289.

Chapter 6 Experimental

6.1 General Experimental Procedures

All ligands and complexes are air stable and all reactions were carried out in air. Chemicals were obtained from Sigma-Aldrich Chemical Co., Acros Organics, Alfa Aesar, Fisher Chemicals and FluoroChem and were all used as supplied. Deuterated NMR solvents were purchased from Sigma-Aldrich Chemical Co. or Argos Organics.

6.2 Characterisation techniques and Instrumentation

6.2.1 IR spectroscopy

Infra-red spectra were recorded using a Bruker platinum-ATR FT-IR spectrophotometer on a crystal plate. The samples were analysed using the software OPUS.

6.2.2 Mass spectrometry

High resolution mass spectrometry data were collected on a Bruker Daltonics (microTOF) instrument using positive and negative ion electrospray as ionization technique. Samples of 1 μ g/mL were directly injected and acquired over an m/z range of 50 – 1500. The HRMS measurements are accurate within 5ppm.

6.2.3 NMR spectroscopy

^1H spectra were recorded on a Bruker DPX300 spectrometer, where the operating frequency was 300.1MHz for ^1H and 75MHz for ^{13}C . $^{13}\text{C}\{^1\text{H}\}$ spectra were recorded on a Bruker Avance500 spectrometer where the operating frequency was 500.13 MHz for ^1H and 125.80 MHz for ^{13}C . $^{19}\text{F}\{^1\text{H}\}$ spectra were recorded on a Bruker AscendTM400 spectrometer whose operating frequency was 400.13 for ^1H and 376.46 MHz for ^{19}F . All spectra were recorded at 300 K in deuterated solvents (see individual experiment). Chemical shift values (δ) are quoted in parts per million (ppm) and the coupling constants (J) are quoted in Hertz (Hz).

6.2.4 Elemental Analysis

Microanalyses were acquired by Mr. Stephen Boyer at the London Metropolitan University Elemental Analysis Service using a Carlo Erba 1108 Elemental Analyser instrument being the value the average of two independent measurements.

6.2.5 Magnetic Susceptibility

Magnetic susceptibility measurements were determined by using a Sherwood Scientific Susceptibility at room temperature.

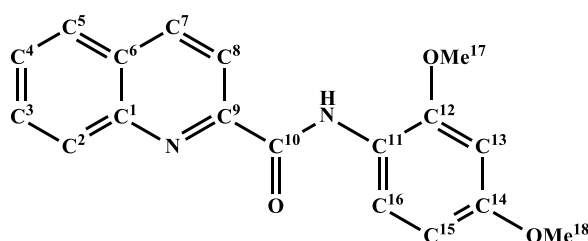
6.2.6 X-Ray Crystallography

Single crystal X-ray diffraction data for the neutral *trans*-dichloride complexes were collected by Dr. Christopher Pask, the positively charged complex by Dr. Matthew Allison, and the novel ligands by the author. An Agilent SuperNova diffractometer fitted with an Atlas CCD detector with Mo-K α radiation ($\lambda = 0.71073 \text{ \AA}$) or Cu-K α radiation ($\lambda = 1.54184 \text{ \AA}$) was used. For a general procedure, a suitable crystal was selected, immersed in an inert oil and mounted under Fomblin on nylon loops. The experiments were run at 120K using an Oxford Cryosystems low temperature device¹ during both unit cell determination and data collection. The full data set was recorded and the images processed using CrysAlis Pro². Structure solution by direct methods was achieved by using SHELXT³ program, and the structure model refined by full matrix least squares on F^2 using ShelXL. Molecular graphics were plotted using Olex2-1.2⁴. Editing of CIFs and construction of tables of bond lengths and angles were achieved using Olex2-1.2. Unless stated, hydrogen atoms were placed using idealised geometric positions (with free rotation for methyl groups) and allowed to move alongside with the atom adjacent. The overall structures were refined anisotropically.

6.3 Preparation of Arene Functionalised Quinaldamide Ligands

Some of the ligands synthesised were previously reported and were prepared using the same synthetic route, however some alterations were made from the published procedure by Bhattacharya *et al.*⁵ Ligands **2.8**, **2.12-2.14**, **2.22** & **2.40** can be found in the database Scifinder, however, all the analytical data, spectra and properties are predicted.

6.3.1 N-(2,4-dimethoxyphenyl)quinoline-2-carboxamide, (2.3)

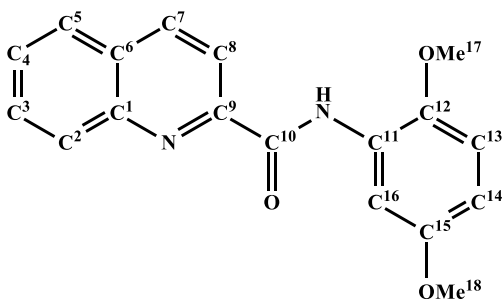


2,4-Dimethoxyaniline (1 eq., 5 mmol, 0.7659 g) was added to a solution of 2-quinolinecarboxylic acid (1 eq., 5 mmol; 0.8659 g) in pyridine (4 mL) and warmed for 15 minutes. While

warming, triphenylphosphite (1 eq., 5 mmol; 1.31 mL) was added. The reaction was heated overnight at 110°C and cooled to room temperature. Addition of water (20 mL) yielded a precipitate, which was filtered and washed with distilled water and methanol. The product was recrystallised from chloroform.

Yield: 73%; **¹H NMR (CDCl₃, 300 MHz, 300 K):** δ 10.54 (bs, 1H, NH), 8.46 (d, 1H, ³J(¹H-¹H)= 9.3 Hz, H¹⁶), 8.33 (d, 1H, ³J(¹H-¹H)= 8.5 Hz, H⁸), 8.28 (d, 1H, ³J(¹H-¹H)= 8.7 Hz, H⁷), 8.14 (d, 1H, ³J(¹H-¹H)= 8.9 Hz, H²), 7.84 (dd, 1H, ³J(¹H-¹H)= 8.2 Hz, 0.9 Hz, H⁵), 7.72 (ddd, 1H, ³J(¹H-¹H)= 6.9 Hz, 1.5 Hz, H³), 7.57 (ddd, 1H, ³J(¹H-¹H)= 6.9 Hz, 1.4 Hz, H⁴), 6.51 (d, 1H, ⁴J(¹H-¹H)= 2.4 Hz, H¹⁵), 6.49 (d, 1H, ⁴J(¹H-¹H)= 2.7 Hz, H¹³), 3.92 (s, OMe¹⁸), 3.75 (s, OMe¹⁷); **¹³C{¹H} NMR: (CDCl₃, 126 MHz 300 K):** δ 161.8 (C¹⁰), 156.7 (C¹), 150.4 (C⁶), 150.3 (C¹⁴), 146.4 (C¹²), 137.6 (C⁷), 130.1 (C²), 130.0 (C³), 129.3 (C⁹), 127.9 (C⁴), 127.8 (C⁵), 121.3 (C¹¹), 120.6 (C¹⁶), 118.8 (C⁸), 103.8 (C¹⁵), 98.9 (C¹³), 56.0 (OMe¹⁸), 55.6 (OMe¹⁷); **IR (cm⁻¹):** 3364 (s) 3100-2785 (m), 1681 (s), 1630-1400 (m), 1300-1000 (m), 920 (s), 850-400 (m); **H.R.M.S. [ESI⁺] (m/z)** in MeOH (Theoretical/ Found) **[M+H]⁺:** 309.1234/309.1242.

6.3.2 N-(2,5-dimethoxyphenyl)quinoline-2-carboxamide, (2.4)

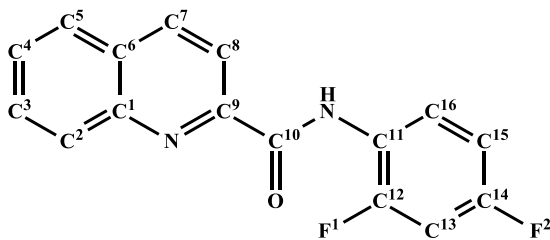


2,5-Dimethoxyaniline (1 eq., 5 mmol, 0.7659 g) was added to a solution of 2-quinolinecarboxylic acid (1 eq., 5 mmol; 0.8659 g) in pyridine (4 mL) and warmed for 15 minutes. While warming, triphenylphosphite (1 eq., 5 mmol; 1.31 mL)

was added. The reaction was heated overnight at 110°C, then cooled to room temperature. Addition of water (20 mL) yielded a precipitate, which was filtered and washed with distilled water and methanol. The product was recrystallised from chloroform.

Yield: 86%; **¹H NMR (CDCl₃, 300 MHz, 300 K):** δ 10.84 (bs, 1H, NH), 8.40 (d, 1H, ³J(¹H-¹H)= 3.1 Hz, H¹⁶), 8.37 – 8.34 (m, 2H, H^{7/8}), 8.21 (dt, 1H, ³J(¹H-¹H)= 8.5 Hz, 0.5 Hz, H²), 7.90 (dd, 1H, ³J(¹H-¹H)= 8.2 Hz, 0.9 Hz, H⁵), 7.80 (ddd, 1H, ³J(¹H-¹H)= 8.4 Hz, 6.9 Hz, 1.5 Hz, H³), 7.64 (ddd, 1H ³J(¹H-¹H)= 8.9 Hz, 6.9 Hz, 1.2 Hz, H₄), 6.89 (d, 1H, ³J(¹H-¹H)= 8.9 Hz, H₁₄), 6.65 (dd, 1H, ³J(¹H-¹H)= 8.9 Hz, 3.0 Hz, H¹³), 3.98 (s, OMe¹⁸), 3.86 (s, OMe¹⁷); **¹³C{¹H} NMR (CDCl₃, 126 MHz 300 K):** δ 162.3 (C¹⁰), 154.0 (C¹), 150.0 (C⁶), 146.4 (C¹⁵), 143.2 (C¹²), 137.7 (C⁷), 130.2 (C²), 130.0 (C³), 129.4 (C⁹), 128.3 (C⁴), 128.1 (C⁵), 127.8 (C¹¹), 118.8 (C¹⁶), 111.2 (C⁸), 109.2 (C¹⁴), 105.8 (C¹³), 56.6 (OMe¹⁸), 55.9 (OMe¹⁷); **IR (cm⁻¹):** 3336 (s) 3005-2831 (m), 1680 (s), 1599 (s), 1561-1476 (m), 1338 (s), 1277-1199 (m), 1164 (s), 1140 (s), 913-443 (m); **H.R.M.S. [ESI⁺] (m/z)** in methanol (Theoretical/ Found) **[M+H]⁺:** 309.1234/309.1244.

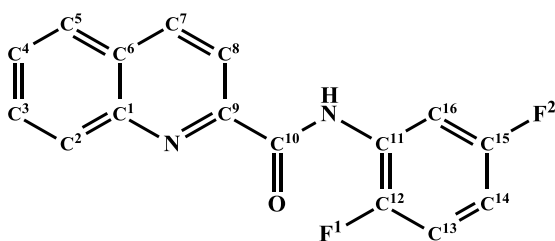
6.3.3 N-(2,4-difluorophenyl)quinoline-2-carboxamide, (2.26)



2,4-Difluoroaniline (1 eq., 5 mmol, 0.51 mL) was added to a solution of 2-quinolinecarboxylic acid (1 eq., 5 mmol; 0.8659 g) in pyridine (4 mL) and warmed for 15 minutes. While warming, triphenylphosphite (1 eq., 5 mmol; 1.31 mL) was added. The reaction was heated overnight at 110°C, then cooled to room temperature. Addition of water (20 mL) yielded a white precipitate, which was filtered and washed with distilled water and methanol. The product was recrystallised from chloroform.

Yield: 32%; **¹H NMR (CDCl₃, 300 MHz, 300 K):** δ 10.38 (bs, 1H, NH), 8.51 (ddd, 1H, ³J(¹H-¹H)= 9.1 Hz, 6.0 Hz, H¹³), 8.31 (s, 2H, H^{7/8}), 8.14 (d, 1H, ³J(¹H-¹H)= 8.5 Hz, H²), 7.85 (ddd, 1H, ³J(¹H-¹H)= 8.1 Hz, 1.4 Hz, 0.6 Hz, H⁵), 7.75 (ddd, 1H, ³J(¹H-¹H)= 8.5 Hz, 6.9 Hz, 1.5 Hz, H³), 7.60 (ddd, 1H, ³J(¹H-¹H)= 8.1 Hz, 6.9 Hz, 1.2 Hz, H⁴), 6.94 – 6.83 (m, 2H, H^{14/16}); **¹³C{¹H} NMR (CDCl₃, 126 MHz, 300 K):** δ 162.3 (C¹⁰), 159.7 (C¹), 157.8 (C⁶), 149.0 (C¹⁴), 146.4 (C¹²), 137.9 (C⁷), 130.4 (C²), 129.9 (C³), 129.5 (C⁹), 128.4 (C⁴), 127.8 (C⁵), 122.9 (C¹¹), 122.2 (dd, ²J(¹³C-¹⁹F)= 9.1 Hz, 2.3 Hz, C¹⁶), 118.6 (C⁸), 111.3 (dd, ²J(¹³C-¹⁹F)= 21.6 Hz, 3.77 Hz, C¹⁵), 103.8 (dd, ²J(¹³C-¹⁹F)= 26.6 Hz, C¹³); **¹⁹F{¹H} NMR (CDCl₃, 376 MHz, 300 K):** δ -115.14 (d, 1F, F²), -125.85 (d, 1F, F¹); **IR (cm⁻¹):** 3326 (s) 3076-3017 (m), 1682 (s), 1607 (s), 1534 (s), 1504 (s), 1423 (s), 1284-1086 (m), 962-689 (m), 537 (s); **H.R.M.S. [ESI⁺] (m/z)** in methanol (Theoretical/Found) **[M+H]⁺:** 285.0834/285.0847.

6.3.4 N-(2,5-difluorophenyl)quinoline-2-carboxamide, (2.27)

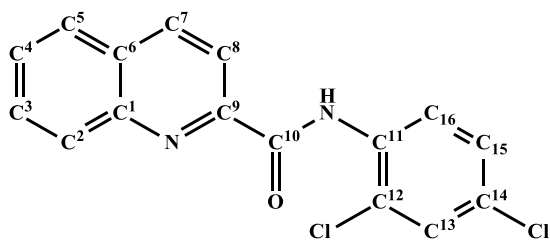


2,5-Difluoroaniline (1 eq., 5 mmol, 0.50 mL) was added to a solution of 2-quinolinecarboxylic acid (1 eq., 5 mmol; 0.8659 g) in pyridine (4 mL) and warmed for 15 minutes. While

warming, triphenylphosphite (1 eq., 5 mmol; 1.31 mL) was added. The reaction was heated overnight at 110°C, then cooled to room temperature. Addition of water (20 mL) yielded a precipitate, which was filtered and washed with distilled water and methanol. The product was recrystallised from chloroform.

Yield: 69%; **¹H NMR (CDCl₃, 300 MHz, 300 K):** δ 10.61 (bs, 1H, NH), 8.52-8.42 (m, 1H, H¹³), 8.42 - 8.34 (m, 2H, H^{7/8}), 8.21 (d, 1H, ³J(¹H-¹H)= 8.1 Hz, H²), 7.92 (dd, 1H, ³J(¹H-¹H)= 8.2 Hz, 0.8 Hz, H⁵), 7.82 (ddd, 1H, ³J(¹H-¹H)= 8.5 Hz, 6.9 Hz, 1.4 Hz, H³), 7.72 - 7.63 (m, 1H, H⁴), 7.13 (ddd, ³J(¹H-¹H)= 10.3 Hz, 9.1 Hz, 4.9 Hz 1H, H¹⁴), 6.83 - 6.73 (m, 1H, H¹⁶); **¹³C{¹H} NMR (CDCl₃, 126 MHz, 300 K):** δ 162.4 (C¹⁰), 159.7 (C¹), 157.8 (C⁶), 149.0 (C¹⁵), 146.4 (C¹²), 138.0 (C⁷), 130.5 (C²), 130.0 (C³), 129.6 (C⁹), 128.5 (C⁴), 127.8 (C⁵), 127.4 (C¹¹), 118.6 (C⁸), 115.3 (dd, ²J(¹³C-¹⁹F)= 21.7 Hz, 9.76 Hz, C¹⁴), 110.2 (dd, ²J(¹³C-¹⁹F)= 24.7 Hz, 7.8 Hz, C¹³), 108.4 (d, ²J(¹³C-¹⁹F)= 30.1 Hz, C¹⁶); **¹⁹F{¹H} NMR (CDCl₃, 376 MHz, 300 K):** δ -116.07 (d, 1F, F²), -136.49 (d, 1F, F¹); **IR (cm⁻¹):** 3338 (s), 3103-3057 (m), 1697 (s), 1632 (s), 1530 (s), 1503-1442 (m), 1246 (s), 1159 (s), 1124 (s), 969-686 (m); **H.R.M.S. [ESI⁺] (m/z)** in methanol (Theoretical/Found) **[M+H]⁺**: 285.0834/285.0848

6.3.5 N-(2,4-dichlorophenyl)quinoline-2-carboxamide, (2.31)

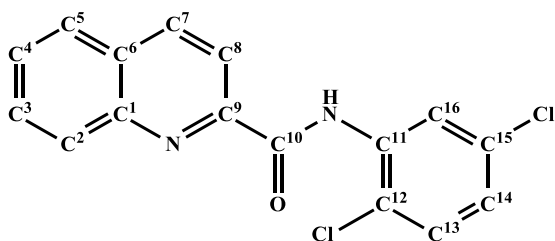


2,4-Dichloroaniline (1 eq., 5 mmol, 0.8101 g) was added to a solution of 2-quinolinecarboxylic acid (1 eq., 5 mmol; 0.8659 g) in pyridine (4 mL) and warmed for 15 minutes. While

warming, triphenylphosphite (1 eq., 5 mmol; 1.31 mL) was added. The reaction was heated overnight at 110°C, then cooled to room temperature. Addition of water (20 mL) yielded a precipitate, which was filtered and washed with distilled water and methanol. The product was recrystallised from chloroform.

Yield: 67%; **¹H NMR (CDCl₃, 300 MHz, 300 K)** δ 10.87 (bs, 1H, NH), 8.59 (d, 1H, ³J(¹H-¹H)= 8.9 Hz, H¹⁶), 8.34 - 8.23 (m, 2H, H^{7/8}), 8.11 (d, 1H, ³J(¹H-¹H)= 8.4 Hz, H²), 7.83 (d, 1H, ³J(¹H-¹H)= 8.1 Hz, H⁵), 7.78 – 7.68 (m, 1H, H³), 7.59 (dd, 1H, ³J(¹H-¹H)= 11.0 Hz, 4.0 Hz, H⁴), 7.38 (d, 1H, ³J(¹H-¹H)= 2.3 Hz, H¹⁵), 7.23 (dt, 1H, ³J(¹H-¹H)= 10.2 Hz, 5.1 Hz, H¹³); **¹³C{¹H} NMR (CDCl₃, 126 MHz, 300 K):** δ 162.3 (C¹⁰), 153.7 (C¹), 149.1 (C⁶), 146.3 (C¹⁴), 138.0 (C¹²), 133.6 (C⁷), 130.4 (C²), 130.0 (C³), 129.6 (C⁹), 129.0 (C⁴), 128.4 (C⁵), 127.9 (C¹¹), 127.7 (C¹³), 124.0 (C¹³), 121.6 (C¹⁵), 118.6 (C¹⁶); **IR (cm⁻¹)** 3293 (s), 3098-3038 (m), 1695 (s), 1591-1099 (m), 953-830 (m), 766 (s), 730-552 (m); **H.R.M.S. [ESI⁺] (m/z)** in methanol (Theoretical/Found) **[M+H]⁺** 317.0243/317.0252.

6.3.6 N-(2,5-dichlorophenyl)quinoline-2-carboxamide, (2.32)

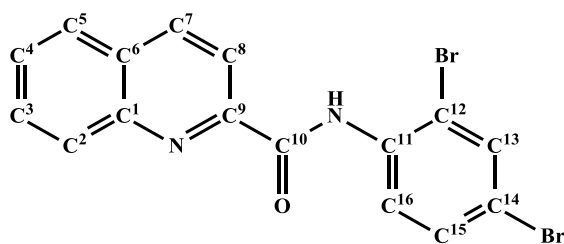


2,5-Dichloroaniline (1 eq., 5 mmol, 0.53 mL) was added to a solution of 2-quinolinecarboxylic acid (1 eq., 5 mmol; 0.8659 g) in pyridine (4 mL) and warmed for 15 minutes. While

warming, triphenylphosphite (1 eq., 5 mmol; 1.31 mL) was added. The reaction was heated overnight at 110°C and cooled to room temperature. Addition of water (20 mL) yielded a precipitate, which was filtered and washed with distilled water and methanol. The product was recrystallised from chloroform.

Yield: 55%; **EA** (Theoretical/Found)(%): **C** (60.59/60.60), **H** (3.18/3.20) & **N** (8.83/8.50); **¹H NMR (CDCl₃, 300 MHz, 300 K):** δ 11.01 (bs, 1H, NH), 8.81 (d, 1H, ³J(¹H-¹H)= 2.5 Hz, H¹³), 8.45 - 8.36 (m, 2H, H^{7/8}), 8.21 (d, 1H, ³J(¹H-¹H)= 8.5 Hz, H²), 7.93 (dd, 1H, ³J(¹H-¹H)= 8.2 Hz, 0.8 Hz, H⁵), 7.82 (ddd, 1H, ³J(¹H-¹H)= 8.5 Hz, 6.9 Hz, 1.5 Hz, H³), 7.68 (ddd, 1H, ³J(¹H-¹H)= 8.1 Hz, 6.9 Hz, 1.2 Hz, H⁴), 7.38 (d, 1H, ³J(¹H-¹H)= 8.6 Hz, H¹⁴), 7.08 (dd, 1H, ³J(¹H-¹H)= 8.6 Hz, 2.5 Hz, H¹⁶); **¹³C{¹H} NMR (CDCl₃, 126 MHz, 300 K):** δ 162.4 (C¹⁰), 149.1 (C¹), 146.3 (C⁶), 138.0 (C¹⁴), 135.7 (C¹²), 133.6 (C⁷), 130.5 (C²), 130.1 (C³), 129.9 (C⁹), 129.6 (C⁴), 128.5 (C⁵), 127.8 (C¹¹), 124.5 (C¹³), 121.6 (C¹³), 120.8 (C¹⁵), 118.7 (C¹⁶); **IR (cm⁻¹)** 3304-3288 (d), 3098-3039 (m), 1694 (s), 1589-1204 (m), 1122-1050 (m), 913-841 (m), 766 (s), 730-525 (m); **H.R.M.S. [ESI⁺] (m/z)** in methanol (Theoretical/ Found) **[M+H]⁺** 317.0243/317.0246

6.3.7 N-(2,4-dibromophenyl)quinoline-2-carboxamide, (2.36)

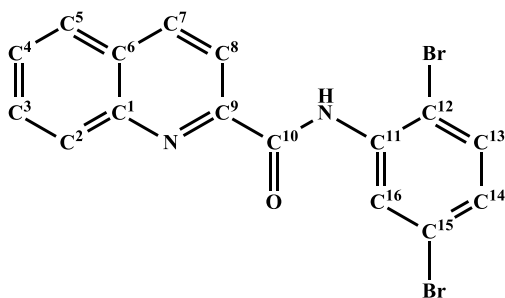


2,4-Dibromoaniline (1 eq., 5 mmol, 1.2546 g) was added to a solution of 2-quinolinecarboxylic acid (1 eq., 5 mmol, 0.8659 g) in pyridine (4 mL) and warmed for 15 minutes. While

warming, triphenylphosphite (1 eq., 5 mmol, 1.31 mL) was added. The reaction was heated overnight at 110°C, then cooled to room temperature. Addition of water (20 mL) yielded a precipitate, which was filtered and washed with distilled water and methanol. The product was recrystallised from chloroform.

Yield: 54%; **¹H NMR:** (CDCl₃, 300 MHz, 300 K) δ 11.00 (bs, 1H, NH), 8.62 (d, 1H, ³J(¹H-¹H)= 8.9 Hz, H¹³), 8.38 (d, 2H, ³J(¹H-¹H)= 1.9 Hz, H^{7/8}), 8.21 (d, 1H, ³J(¹H-¹H)= 8.5 Hz, H²), 7.93 (d, 1H, ³J(¹H-¹H) = 8.2 Hz, H⁵), 7.86 – 7.79 (m, 1H, H³), 7.78 (d, 1H, ³J(¹H-¹H)= 2.2 Hz, H¹⁶), 7.68 (dd, 1H, ³J(¹H-¹H)= 11.1 Hz, 4.0 Hz, H⁴), 7.52 (dd, 1H, ³J(¹H-¹H)= 8.8 Hz, 2.2 Hz, H¹⁵); **¹³C{¹H} NMR (CDCl₃, 126 MHz, 300 K):** δ 163.0 (C¹⁰), 149.5 (C¹), 146.3 (C⁶), 138.0 (C¹⁴), 135.3 (C¹²), 134.7 (C⁷), 131.5 (C²), 130.5 (C³), 130.1 (C⁹), 128.5 (C⁴), 127.8 (C⁵), 122.1 (C¹¹), 118.6 (C¹³), 118.1 (C⁸), 116.6 (C¹⁵), 111.1 (C¹⁶); **IR (cm⁻¹)** 3288 (s), 3101-2961 (m), 1690 (s), 1585-1205 (m), 1124-1079 (m), 914-545 (m); **H.R.M.S. [ESI⁺] (m/z)** in methanol (Theoretical/ Found) **[M+H]⁺** 406.9233/406.9215

6.3.8 N-(2,5-dibromophenyl)quinoline-2-carboxamide, (2.37)

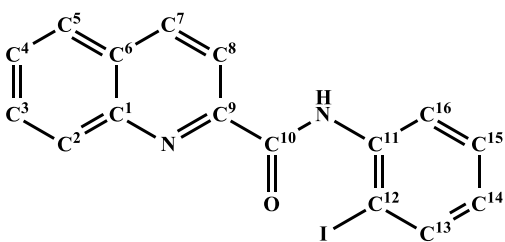


2,5-Dibromoaniline (1 eq., 5 mmol, 1.2546 g) was added to a solution of 2-quinolinecarboxylic acid (1 eq., 5 mmol, 0.8659 g) in pyridine (4 mL) and warmed for 15 minutes. While warming, triphenylphosphite (1 eq., 5 mmol, 1.31

mL) was added. The reaction was heated overnight at 110°C, then cooled down to room temperature; addition of water (20 mL) yielded to a precipitate, which was filtered and washed with distilled water and methanol. The product was recrystallised from chloroform.

Yield: 42%; **¹H NMR (CDCl₃, 300 MHz, 300 K):** δ 11.01 (bs, 1H, NH), 8.93 (d, 1H, ³J(¹H-¹H)= 2.3 Hz, H¹³), 8.44 – 8.32 (m, 2H, H^{7/8}), 8.21 (dd, 1H, ³J(¹H-¹H)= 8.0 Hz, 0.5 Hz, H²), 7.93 (dd, 1H, ³J(¹H-¹H)= 8.2 Hz, 0.9 Hz, H⁵), 7.85 – 7.78 (m, 1H, H³), 7.68 (ddd, 1H, ³J(¹H-¹H)= 8.1 Hz, 6.9 Hz, 1.2 Hz, H⁴), 7.48 (d, 1H, ³J(¹H-¹H)= 8.5 Hz, H¹⁴), 7.16 (d, 1H, ³J(¹H-¹H)= 8.5 Hz, 2.4 Hz, H¹⁶); **¹³C{¹H} NMR (CDCl₃, 126 MHz, 300 K):** δ 162.4 (C¹⁰), 149.1 (C¹), 146.4 (C⁶), 138.0 (C¹⁵), 137.1 (C¹²), 133.4 (C⁷), 130.5 (C²), 130.1 (C³), 129.6 (C⁹), 128.5 (C⁴), 128.0 (C⁵), 127.8 (C¹¹), 123.9 (C¹³), 122.1 (C⁸), 118.62 (C¹⁴), 112.3 (C¹⁶); **IR (cm⁻¹)** 3299 (s), 3105-3056 (m), 1699 (s), 1578-1425 (m), 1401-1205 (m), 1124-850 (m), 767 (s), 763-452 (m); **H.R.M.S. [ESI⁺] (m/z)** in methanol (Theoretical/ Found) **[M+H]⁺** 406.9233/406.9214

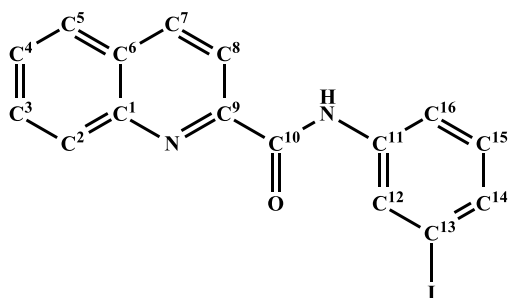
6.3.9 N-(2-iodophenyl)quinoline-2-carboxamide, (2.38)



2-Iodoaniline (1 eq., 5 mmol, 1.0951 g) was added to a solution of 2-quinolinecarboxylic acid (1 eq., 5 mmol; 0.8659 g) in pyridine (4 mL) and warmed for 15 minutes. While warming, triphenylphosphite (1 eq., 5 mmol; 1.31 mL) was added. The reaction was heated overnight at 110°C, then cooled to room temperature. Addition of water (20 mL) yielded a precipitate, which was filtered and washed with distilled water and methanol. The product was recrystallised from chloroform.

Yield: 60%; **¹H NMR (CDCl₃, 300 MHz, 300 K):** δ 10.78 (bs, 1H, NH), 8.52 (dd, 1H, ³J(¹H-¹H)= 8.3 Hz, 1.5 Hz, H¹³), 8.30 (s, 2H, H^{7/8}), 8.16 (d, 1H, ³J(¹H-¹H)= 8.4 Hz, H²), 7.84 (dd, 1H, ³J(¹H-¹H)= 8.2 Hz, 0.8 Hz, H⁵), 7.80 (dd, 1H, ³J(¹H-¹H)= 7.9 Hz, 1.4 Hz, H¹⁶), 7.73 (ddd, 1H, ³J(¹H-¹H)= 8.4 Hz, 6.9 Hz, 1.4 Hz, H¹⁴), 7.58 (ddd, 1H, ³J(¹H-¹H)= 11.0 Hz, 6.1 Hz, 2.6 Hz, H³), 7.40 – 7.28 (m, 1H, H⁴), 6.89 – 6.70 (m, 1H, H¹⁵); **¹³C{¹H} NMR (CDCl₃, 126 MHz, 300 K):** δ 162.5 (C¹⁰), 149.4 (C¹), 146.3 (C⁶), 139.2 (C¹²), 137.9 (C⁷), 130.3 (C²), 130.1 (C³), 129.6 (C⁹), 129.5 (C⁴), 129.3 (C⁵), 128.3 (C¹¹), 127.7 (C¹³), 125.8 (C⁸), 121.1 (C¹⁴), 118.62 (C¹⁵), 89.7 (C¹⁶); **IR (cm⁻¹)** 3299 (s), 3057 (s), 1679 (s), 1574-1424 (m), 1298-835 (m), 766-690 (m), 670-447 (m); **H.R.M.S. [ESI⁺] (m/z)** in methanol (Theoretical/ Found) **[M+H]⁺** 374.9989/374.9995

6.3.10 N-(3-iodophenyl)quinoline-2-carboxamide, (2.39)

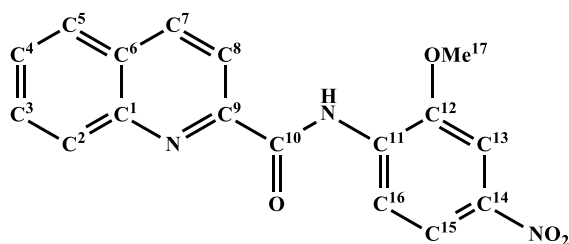


3-Iodoaniline (1 eq., 5 mmol, 0.60 mL) was added to a solution of 2-quinolinecarboxylic acid (1 eq., 5 mmol; 0.8659 g) in pyridine (4 mL) and warmed for 15 minutes. While warming, triphenylphosphite (1 eq., 5 mmol;

1.31 mL) was added. The reaction was heated overnight at 110°C, then cooled to room temperature. Addition of water (20 mL) yielded a precipitate, which was filtered and washed with distilled water and methanol. The product was recrystallised from chloroform.

Yield: 81%; **¹H NMR (CDCl₃, 300 MHz, 300 K):** δ 10.85 (bs, 1H, NH), 8.63 (d, 1H, ³J(¹H-¹H)= 8.2 Hz, H¹²), 8.45 (s, 2H, H^{7/8}), 8.25 (d, 1H, ³J(¹H-¹H)= 7.9 Hz, H²), 8.12 (dd, 1H, ³J(¹H-¹H)= 8.3 Hz, 1.0 Hz, H⁵), 7.99 (ddd, 1H, ³J(¹H-¹H)= 8.2 Hz, 2.0 Hz, 0.9 Hz, H⁴), 7.93 (ddd, 1H, ³J(¹H-¹H)= 8.5 Hz, 6.9 Hz, 1.5 Hz, H³), 7.76 (ddd, 1H, ³J(¹H-¹H)= 8.1 Hz, 6.9 Hz, 1.2 Hz, H¹⁴), 7.51 (ddd, 1H, ³J(¹H-¹H)= 7.8 Hz, 1.6 Hz, 0.9 Hz, H¹⁶), 7.21 (dd, 1H, ³J(¹H-¹H)= 8.0 Hz, H¹⁵); **¹³C{¹H} NMR (CDCl₃, 126 MHz, 300 K):** δ 168.2 (C¹⁰), 154.9 (C¹), 151.1 (C⁶), 145.0 (C¹³), 143.5 (C¹²), 137.7 (C⁷), 136.0 (C²), 135.9 (C³), 134.5 (C⁹), 134.2 (C⁴), 133.7 (C⁵), 133.42 (C¹¹), 124.8 (C¹²), 124.0 (C⁸), 103.84 (C¹⁴), 99.71 (C¹⁵); **IR (cm⁻¹)** 3331 (s), 3150-3063 (m), 1673 (s), 1581-1380 (m), 1290-816 (m), 773-679 (m), 658-581 (m); **H.R.M.S. [ESI⁺] (m/z)** in methanol (Theoretical/ Found) **[M+H]⁺** 374.9989/375.0008

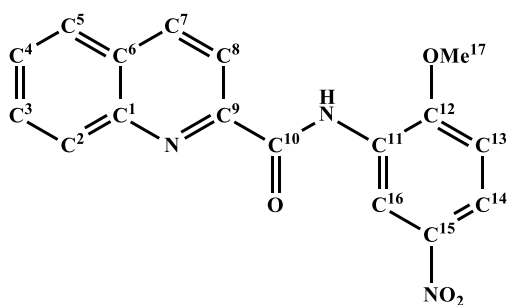
6.3.11 N-(2-methoxy-4-nitrophenyl)quinoline-2-carboxamide, (2.41)



2-Methoxy-4-nitroaniline (1 eq., 5 mmol, 0.8408 g) was added to a solution of 2-quinolinecarboxylic acid (1 eq., 5 mmol; 0.8659 g) in pyridine (4 mL) and warmed for 15 minutes.

While warming, triphenylphosphite (1 eq., 5 mmol; 1.31 mL) was added. The reaction was heated overnight at 110°C, then cooled to room temperature. Addition of water (20 mL) yielded a precipitate, which was filtered and washed with distilled water and methanol. The product was recrystallised from chloroform. (Yield: 25%; $^1\text{H NMR}$ (CDCl_3 , 300 MHz, 300 K): δ 11.09 (bs, 1H, NH), 8.84 (d, 1H, $^3\text{J}(\text{H}^7\text{H}^8) = 9.0$ Hz, H¹⁶), 8.39 (s, 2H, H^{7/8}), 8.22 (d, 1H, $^3\text{J}(\text{H}^1\text{H}^2) = 8.5$ Hz, H¹⁵), 8.00 (d, 1H, $^3\text{J}(\text{H}^1\text{H}^2) = 9.0$ Hz, 2.4 Hz, H²), 7.93 (dd, 1H, $^3\text{J}(\text{H}^1\text{H}^2) = 8.2$ Hz, 0.9 Hz, H⁵), 7.87 – 7.80 (m, 1H, H³), 7.68 (ddd, 1H, $^3\text{J}(\text{H}^1\text{H}^2) = 8.1$ Hz, 6.9 Hz, 1.2 Hz, H⁴), 4.14 (s, OMe¹⁷); $^{13}\text{C}\{^1\text{H}\}$ NMR (CDCl_3 , 126 MHz, 300 K): δ 162.8 (C¹⁰), 149.2 (C¹), 148.5 (C⁶), 146.4 (C¹⁴), 143.3 (C¹²), 138.0 (C⁷), 133.8 (C²), 130.5 (C³), 130.0 (C⁹), 129.6 (C⁴), 128.5 (C⁵), 127.9 (C¹¹), 118.7 (C¹⁶), 118.3 (C⁸), 117.8 (C¹⁵), 106.4 (C¹³), 56.6 (OMe¹⁷); IR (cm^{-1}) 3320 (s), 3090-2926 (m), 1641 (s), 1613-1514 (m), 1128-1032 (m), 895-585 (m); H.R.M.S. [ESI⁺] (m/z) in methanol (Theoretical/ Found) [M+H]⁺ 324.0979/324.0984.

6.3.12N-(2-methoxy-5-nitrophenyl)quinoline-2-carboxamide, (2.42)

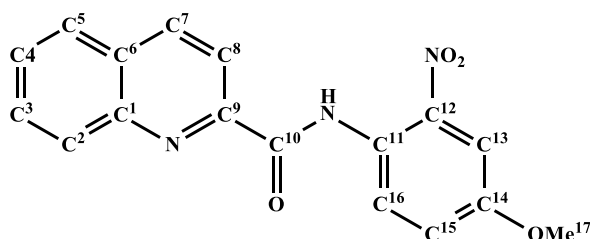


2-Methoxy-5-nitroaniline (1 eq., 5 mmol, 0.8408 g) was added to a solution of 2-quinolinecarboxylic acid (1 eq., 5 mmol, 0.8659 g) in pyridine (4 mL) and warmed for 15 minutes. While warming, triphenylphosphite (1 eq., 5 mmol; 1.31

mL) was added. The reaction was heated overnight at 110°C and cooled to room temperature. Addition of water (20 mL) yielded a precipitate, which was filtered and washed with distilled water and methanol. The product was recrystallised from chloroform.

Yield: 58%; **¹H NMR (CD₃CN, 300 MHz, 300 K):** δ 10.73 (bs, 1H, NH), 9.32 (d, 1H, ³J(¹H-¹H)= 2.8 Hz, H¹³), 8.39 (d, 1H, ³J(¹H-¹H)= 7.9 Hz, H²), 8.19 (d, 1H, ³J(¹H-¹H)= 8.5 Hz, H⁸), 8.08 (d, 1H, ³J(¹H-¹H)= 8.5 Hz, H⁷), 7.94 - 7.88 (m, 1H, H¹⁴), 7.74 (t, 1H, ³J(¹H-¹H)= 7.8 Hz, H³), 7.58 (t, 1H, ³J(¹H-¹H)= 7.0, H⁴), 7.07 (d, 1H, ³J(¹H-¹H)= 9.2 Hz, H⁵), 4.00 (s, OMe¹⁷); **¹³C{¹H} NMR (CDCl₃, 100.6 MHz, 300 K):** δ 162.5 (C¹⁰), 153.4 (C¹), 149.4 (C⁶), 146.4 (C¹⁵), 141.2 (C¹²), 138.0 (C⁷), 130.4 (C²), 129.9 (C³), 129.6 (C⁹), 128.4 (C⁴), 128.0 (C⁵), 127.9 (C¹¹), 120.1 (C¹⁶), 118.8 (C⁸), 115.0 (C¹⁴), 109.3 (C¹³), 56.7 (OMe¹⁷); **IR (cm⁻¹)** 3316 (s), 3100-2946 (m), 1681 (s), 1615-1424 (m), 1328-1022 (m), 897-565 (m); **H.R.M.S. [ESI⁺] (m/z)** in methanol (Theoretical/ Found) **[M+H]⁺** 324.0979/324.0983

6.3.13N-(4-methoxy-2-nitrophenyl)quinoline-2-carboxamide, (2.43)



4-Methoxy-2-nitroaniline (1 eq., 5 mmol, 0.8408 g) was added to a solution of 2-quinolinecarboxylic acid (1 eq., 5 mmol, 0.8659 g) in pyridine (4 mL) and warmed for 15 minutes.

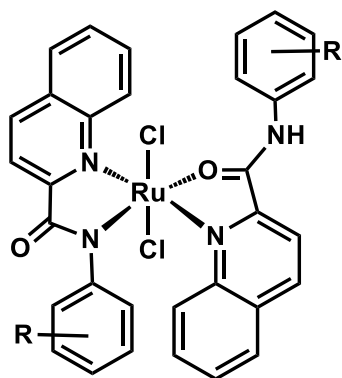
While warming, triphenylphosphite (1 eq., 5 mmol; 1.31 mL) was added. The reaction was heated overnight at 110°C, then cooled to room temperature. Addition of water (20 mL) yielded a precipitate, which was filtered and washed with distilled water and methanol. The product was recrystallised from chloroform.

Yield: 36%; **¹H NMR (CDCl₃, 300 MHz, 300 K):** δ 10.19 (bs, 1H, NH), 8.36 (s, 2H, H^{7/8}), 8.25 (dd, 1H, ³J(¹H-¹H)= 1.8 Hz, H¹³), 8.17 (d, 1H, ³J(¹H-¹H)= 8.5 Hz, H¹⁶), 7.94 - 7.84 (m, 1H, H²), 7.87 - 7.78 (m, 1H, H⁵), 7.65 (ddd, 1H, ³J(¹H-¹H)= 8.1 Hz, 6.9 Hz, 1.2 Hz, H⁴), 7.49 (ddd, 1H, ³J(¹H-¹H)= 7.9 Hz, 1.5 Hz, 1.0Hz, H³), 7.13 (dd, 1H, ³J(¹H-¹H)= 8.0 Hz, H¹⁵), 3.75 (s, OMe¹⁷); **¹³C{¹H} NMR (CDCl₃, 76 MHz, 300 K):** δ 162.2 (C¹⁰), 155.4 (C¹²), 149.2 (C¹), 146.3 (C¹⁴), 143.3 (C⁶), 139.0 (C⁷), 133.3 (C²), 130.6 (C³), 134.0 (C⁹), 130.0 (C⁴), 129.5 (C⁵), 128.4 (C¹¹), 128.3 (C¹⁶), 127.85 (C¹³), 118.9 (C⁸), 118.7 (C¹⁵), 94.3 (OMe¹⁷); **IR (cm⁻¹)** 3277 (s), 3107-3058 (m), 1679 (s), 1563-1345 (m), 1263-1014 (m), 920-547 (m); **H.R.M.S. [ESI⁺] (m/z)** in methanol (Theoretical/ Found) **[M+H]⁺** 324.0979/324.0981.

6.4 Preparation of *trans*-dichloride bis-quinaldamide ruthenium (III) neutral complexes

As explained in **Chapter 3**, following the protocol established within the McGowan group⁶ the final product was a mixture of different complexes. Hence, the focus is given to the synthesis that yielded to the neutral complexes, otherwise it will be stated in the protocol.

6.4.1 Synthesis and Characterisation of *trans*-dichloride bis-quinaldamide ruthenium (III) complexes



The procedure was as follows: a functionalised quinaldamide ligand (R) (2 eq., 0.765 mmol) was dissolved in 20 mL of ethanol. The solution was heated up to 80°C until the ligand was completely dissolved. After 30 min, the functionalised ligand was added to a solution of RuCl₃·3H₂O (1 eq., 0.382 mmol, 0.1 g) in 5 mL of ethanol and left to reflux overnight. The reaction was cooled down to 65°C and filtered immediately. A reddish solid (general structure shown on the left) was isolated which recrystallised from DMF or DMSO, and the mother liqueurs were left to crystallise.

6.4.2 Bis-(N-phenylquinaldamide) ruthenium dichloride, C₃₂H₂₃O₂N₄RuCl₂, (3.1)

Ligand **2.1** (2 eq., 0.765 mmol, 0.1886 g) was dissolved in 20 mL of ethanol. The solution was heated up to 60°C until the ligand was completely dissolved. After 30 min, it was added to a solution of RuCl₃·3H₂O (1 eq., 0.382 mmol, 0.1 g) in 5 mL of ethanol and left to reflux overnight. The reaction was cooled down to 65°C and filtered immediately. A red solid was isolated, recrystallised from DMF, and the mother liqueurs were left to crystallise.

Yield: 0.1507 g, 0.23 mmol, 59 %; $\mu_{\text{eff}} = 1.85$.; **EA** (Theoretical/Found)(%): **C** (56.66/56.54), **H** (3.89/3.68) & **N** (8.01/7.88) [**3.1+0.5H₂O+0.5EtOH**]; **IR** (cm⁻¹) 3277 (s), 3107-3058 (m), 1679 (s), 1563-1345 (m), 1263-1014 (m), 920-547 (m); **H.R.M.S.** [ESI⁺] (m/z) in methanol (Theoretical/ Found) [**M+H**]⁺ 668.0302/668.0306.

6.4.3 Bis-(N-2-Methoxyphenylquinaldamide) ruthenium dichloride, $C_{34}H_{27}O_4N_4RuCl_2$, (3.2)

Ligand **2.2** (2 eq., 0.765 mmol, 0.2129 g) was dissolved in 20 mL of ethanol. The solution was heated up to 80°C until the ligand was completely dissolved. After 30 min, the functionalised ligand was added to a solution of $RuCl_3 \cdot 3H_2O$ (1 eq., 0.382 mmol, 0.1 g) in 5 mL of ethanol and left to reflux overnight. The reaction was cooled down to 65°C and filtered immediately. A violet powder was isolated, recrystallised from DMF and the mother liqueurs were left to crystallise. (Not tested for anticancer properties)

Yield: 0.0626 g, 0.09 mmol, 24 %; $\mu_{eff} = 1.76$; **EA** (Theoretical/Found)(%): **C** (52.24/52.20), **H** (4.75/3.88) & **N** (6.77/6.93) [**3.2+3H₂O+EtOH**]; **IR** (cm^{-1}), 3207-2858 (m), 1635 (s), 1563-1345 (m), 764 (s); **H.R.M.S. [ESI⁺]** (m/z) in methanol (Theoretical/ Found) [**M+H**]⁺ 728.0526/728.0522.

6.4.4 Bis-(N-2,4-diMethoxyphenylquinaldamide) ruthenium dichloride, $C_{36}H_{31}O_6N_4RuCl_2$, (3.3)

Ligand **2.3** (2 eq., 0.765 mmol, 0.2358 g) was dissolved in 20 mL of ethanol. The solution was heated up to 80°C until the ligand was completely dissolved and then $N(Et)_3$ was added (1 eq., 0.382 mmol, 0.053 mL). After 30 min, the functionalised ligand was added to a solution of $RuCl_3 \cdot 3H_2O$ (1 eq., 0.382 mmol, 0.1 g) in 5 mL of ethanol and left to reflux overnight. The reaction was filtered immediately isolating a black powder. The mother liqueurs were left to crystallise. (Characterisation on going)

Yield: 0.0245 g, 0.031 mmol, 8 %; **H.R.M.S. [ESI⁺]** (m/z) in methanol (Theoretical/ Found) [**M+H**]⁺ 788.0737/not found.

6.4.5 Bis-(N-2,5-diMethoxyphenylquinaldamide) ruthenium dichloride, $C_{36}H_{31}O_6N_4RuCl_2$, (3.4)

Ligand **2.4** (2 eq., 0.765 mmol, 0.2358 g) was dissolved in 20 mL of ethanol. The solution was heated up to 80°C until the ligand was completely dissolved and then $N(Et)_3$ was added (1 eq., 0.382 mmol, 0.053 mL). After 30 min, the functionalised ligand was added to a solution of $RuCl_3 \cdot 3H_2O$ (1 eq., 0.382 mmol, 0.1 g) in 5 mL of ethanol, and left to reflux overnight. The reaction was filtered

immediately, and a black powder was isolated which recrystallised from DMF, and the mother liqueurs were left to crystallise. (Characterisation ongoing)

Yield: 0.0374 g, 0.047 mmol, 12 %; **IR (cm⁻¹)** -; **H.R.M.S. [ESI⁺] (m/z)** in methanol (Theoretical/ Found) **[M+H]⁺** 788.0737/787.0737.

6.4.6 Bis-(N-2-Methylphenylquinaldamide) ruthenium dichloride, C₃₄H₂₇O₂N₄RuCl₂, (3.5)

Ligand **2.5** (2 eq., 0.765 mmol, 0.2006 g) was dissolved in 20 mL of ethanol. The solution was heated up to 70°C until the ligand was completely dissolved. After 30 min, the functionalised ligand was added to a solution of RuCl₃·3H₂O (1 eq., 0.382 mmol, 0.1 g) in 5 mL of ethanol and left to reflux overnight. The reaction was cooled down to 65°C and filtered immediately. A reddish solid was isolated which recrystallised from DMF or DMSO, and the mother liqueurs were left to crystallise.

Yield: 0.1235 g, 0.18 mmol, 47 %; $\mu_{\text{eff}} = 1.74$; **EA** (Theoretical/Found)(%): **C** (55.82/55.80), **H** (4.27/3.57) & **N** (7.66/7.72) [**3.5+2H₂O**]; **IR (cm⁻¹)** 3277 (s), 3107-3058 (m), 1679 (s), 1563-1345 (m), 1263-1014 (m), 920-547 (m); **H.R.M.S. [ESI⁺] (m/z)** in methanol (Theoretical/ Found) **[M+H]⁺** 696.0627/696.0630.

6.4.7 Bis-(N-3-Methylphenylquinaldamide) ruthenium dichloride, C₃₄H₂₇O₂N₄RuCl₂, (3.6)

Ligand **2.6** (2 eq., 0.765 mmol, 0.2006 g) was dissolved in 20 mL of ethanol. The solution was heated up to 80°C until the ligand was completely dissolved. After 30 min, the functionalised ligand was added to a solution of RuCl₃·3H₂O (1 eq., 0.382 mmol; 0.1 g) in 5 mL of ethanol and left to reflux overnight. The reaction was cooled down to 65°C and filtered immediately. A reddish solid was isolated which recrystallised from DMF and the mother liqueurs were left to crystallise.

Yield: 0.0856 g, 0.12 mmol, 32 %; $\mu_{\text{eff}} = 1.78$; **EA** (Theoretical/Found)(%): **C** (57.23/57.34), **H** (4.10/3.79) & **N** (7.85/7.91) [**3.6+1H₂O**]; **IR (cm⁻¹)** 3059-2873 (m), 1629-1509 (m), 1370-1335 (m), 764 (s); **H.R.M.S. [ESI⁺] (m/z)** in methanol (Theoretical/ Found) **[M+H]⁺** 696.0627/696.0631.

6.4.8 Bis-(N-4-Methylphenylquinaldamide) ruthenium dichloride, $C_{34}H_{27}O_2N_4RuCl_2$, (3.7)

Ligand **2.7** (2 eq., 0.765 mmol, 0.2006 g) was dissolved in 20 mL of ethanol. The solution was heated up to 80°C until the ligand was completely dissolved. After 30 min, the functionalised ligand was added to a solution of $RuCl_3 \cdot 3H_2O$ (1 eq., 0.382 mmol; 0.1 g) in 5 mL of ethanol and left to reflux overnight. The reaction was cooled down to 65°C and filtered immediately. A reddish solid was isolated and the mother liqueurs were left to crystallise.

Yield: 0.1046 g, 0.15 mmol, 39 %; $\mu_{eff} = 1.77$; **EA** (Theoretical/Found)(%): **C** (55.82/55.87), **H** (4.27/3.74) & **N** (7.66/7.67) [**3.7+2H₂O**]; **IR** (cm^{-1}) 3139-2852 (b), 1616 (s), 1571-1510 (m), 1409-1372 (m), 764 (s); **H.R.M.S. [ESI⁺] (m/z)** in methanol (Theoretical/ Found) [**M+H**]⁺ 696.0627/696.0612.

6.4.9 Bis-(N-2,4,6-triMethylphenylquinaldamide) ruthenium dichloride, $C_{38}H_{35}O_2N_4RuCl_2$, (3.8)

Ligand **2.8** (2 eq., 0.765 mmol, 0.2218 g) was dissolved in 20 mL of ethanol. The solution was heated up to 80°C until the ligand was completely dissolved. After 30 min, the functionalised ligand was added to a solution of $RuCl_3 \cdot 3H_2O$ (1 eq., 0.382 mmol; 0.1 g) in 5 mL of ethanol and left to reflux overnight. The reaction was cooled down to 65°C and filtered immediately. A reddish solid was isolated which recrystallised from DMSO, and the mother liqueurs were left to crystallise. (E.A. impure, more characterisation on going)

Yield: 0.0788 g, 0.105 mmol, 27 %; $\mu_{eff} = 1.78$; **H.R.M.S. [ESI⁺] (m/z)** in methanol (Theoretical/ Found) [**M+H**]⁺ 752.1253/752.1256.

6.4.10 Bis-(N-2-Ethylphenylquinaldamide) ruthenium dichloride, $C_{36}H_{31}O_2N_4RuCl_2$, (3.9)

Ligand **2.9** (2 eq., 0.765 mmol, 0.2114 g) was dissolved in 20 mL of ethanol. The solution was heated up to 60°C until the ligand was completely dissolved. After 30 min, the functionalised ligand was added to a solution of $RuCl_3 \cdot 3H_2O$ (1 eq., 0.382 mmol, 0.1 g) in 5 mL of ethanol and left to reflux overnight. The reaction was cooled down to 65°C and filtered immediately. A red powder was isolated which recrystallised from DMF and the mother liqueurs were left to crystallise.

Yield: 0.2011 g, 0.28 mmol, 73 %; $\mu_{\text{eff}} = 1.69$; **EA** (Theoretical/Found)(%): **C** (56.92/56.78), **H** (4.64/4.22) & **N** (7.38/7.45) [**3.9+2H₂O**]; **IR** (**cm⁻¹**) 3132-2875 (m), 1611-1507 (m), 760 (s); **H.R.M.S. [ESI⁺] (m/z)** in methanol (Theoretical/ Found) [**M+H**]⁺ 726.0916/726.0947.

6.4.11 Bis-(N-3-Ethylphenylquinaldamide) ruthenium dichloride, C₃₆H₃₁O₂N₄RuCl₂, (3.10)

Ligand **2.10** (2 eq., 0.765 mmol, 0.2114 g) was dissolved in 20 mL of ethanol. The solution was heated up to 60°C until the ligand was completely dissolved. After 30 min, the functionalised ligand was added to a solution of RuCl₃·3H₂O (1 eq., 0.382 mmol, 0.1 g) in 5 mL of ethanol and left to reflux overnight. After the reaction was cooled down to 65°C, it was filtered immediately. A reddish solid was isolated which recrystallised from DMF and the mother liqueurs were left to crystallise.

Yield: 0.0973 g, 0.13 mmol, 35 %; $\mu_{\text{eff}} = 1.70$; **EA** (Theoretical/Found)(%): **C** (59.75/59.53), **H** (4.32/4.24) & **N** (7.74/7.65) [**3.10**]; **IR** (**cm⁻¹**) 3277 (s), 3107-3020 (m), 2957-2869 (m), 1627-1513 (m), 760 (s); **H.R.M.S. [ESI⁺] (m/z)** in methanol (Theoretical/ Found) [**M+H**]⁺ 726.0916/726.0936.

6.4.12 Bis-(N-4-Ethylphenylquinaldamide) ruthenium dichloride, C₃₆H₃₁O₂N₄RuCl₂, (3.11)

Ligand **2.11** (2 eq., 0.765 mmol, 0.2114 g) was dissolved in 20 mL of ethanol. The solution was heated up to 70°C until the ligand was completely dissolved. After 30 min, the functionalised ligand was added to a solution of RuCl₃·3H₂O (1 eq., 0.382 mmol, 0.1 g) in 5 mL of ethanol and left to reflux overnight. The reaction was cooled down to 75°C and filtered immediately. A red solid was isolated which recrystallised from DMF and the mother liqueurs were left to crystallise.

Yield: 0.150 g, 0.21 mmol, 55 %. $\mu_{\text{eff}} = 1.80$; **EA** (Theoretical/Found)(%): **C** (59.75/59.62), **H** (4.32/4.24) & **N** (7.74/7.66) [**3.11**]; **IR** (**cm⁻¹**) 3052 (s), 2961-2836 (m), 1601 (s), 1574-1511 (m), 1370-1337 (m), 764 (s); **H.R.M.S. [ESI⁺] (m/z)** in methanol (Theoretical/ Found) [**M+H**]⁺ 724.0940/724.0922.

6.4.13 Bis-(N-2-ⁱPropylphenylquinaldamide) ruthenium dichloride, C₃₈H₃₅O₂N₄RuCl₂, (3.12)

Ligand **2.12** (2 eq., 0.765 mmol, 0.2221 g) was dissolved in 20 mL of ethanol. The solution was heated up to 50°C until the ligand was completely dissolved. After 30 min, the functionalised ligand was added to a solution of RuCl₃·3H₂O (1 eq., 0.382 mmol; 0.1 g) in 5 mL of ethanol and left to reflux overnight. The reaction was cooled down to 65°C and filtered immediately. A red powder was isolated which recrystallised from DMF and the mother liquors were left to crystallise.

Yield: 0.2078 g, 0.28 mmol, 73 %; $\mu_{\text{eff}} = 1.68$; **EA** (Theoretical/Found)(%): **C** (55.41/55.45), **H** (5.26/4.52) & **N** (6.80/6.60) [**3.12+4H₂O**]; **IR** (cm⁻¹) 3420 (s), 3159-2867 (m), 1611-1545 (m), 754 (s); **H.R.M.S. [ESI⁺] (m/z)** in methanol (Theoretical/ Found) [**M+H**]⁺ 752.1073/752.1249.

6.4.14 Bis-(N-3-ⁱPropylphenylquinaldamide) ruthenium dichloride, C₃₈H₃₅O₂N₄RuCl₂, (3.13)

Ligand **2.13** (2 eq., 0.765 mmol, 0.2221 g) was dissolved in 20 mL of ethanol. The solution was heated up to 50°C until the ligand was completely dissolved. After 30 min, the functionalised ligand was added to a solution of RuCl₃·3H₂O (1 eq., 0.382 mmol, 0.1 g) in 5 mL of ethanol and left to reflux overnight. The reaction was cooled down to 65°C and filtered immediately. A dark green solid was isolated which recrystallised from DMF and the mother liquors were left to crystallise.

Yield: 0.0206 g, 0.03 mmol, 7 %; $\mu_{\text{eff}} = 1.69$; **EA** (Theoretical/Found)(%): **C** (54.11/55.45), **H** (5.79/4.18) & **N** (6.31/6.07) [**3.13+5H₂O+EtOH**]; **IR** (cm⁻¹) 3239-3189 (m), 3136-3016 (m), 2955-2865 (m), 1607-1558 (m), 1490 (s), 762 (s); **H.R.M.S. [ESI⁺] (m/z)** in methanol (Theoretical/ Found) [**M+H**]⁺ 752.1073/752.1250.

6.4.15 Bis(N-4-ⁱPropylphenylquinaldamide) ruthenium dichloride, C₃₈H₃₅O₂N₄RuCl₂, (3.14)

Ligand **2.14** (2 eq., 0.765 mmol, 0.2221 g) was dissolved in 20 mL of ethanol. The solution was heated up to 80°C until the ligand was completely dissolved. After 30 min, the functionalised ligand was added to a solution of RuCl₃·3H₂O

(1 eq., 0.382 mmol; 0.1 g) in 5 mL of ethanol and left to reflux overnight. The reaction was cooled down to 65°C and filtered immediately. A reddish solid was isolated which recrystallised from DMF or DMSO, and the mother liqueurs were left to crystallise. (Analytically impure)

Yield: 0.1331 g, 0.177 mmol, 46 %; **H.R.M.S. [ESI⁺] (m/z)** in methanol (Theoretical/ Found) **[M+H]⁺** 752.1073/324.0981.

6.4.16 Bis-(N-2,6-diⁱPropylphenylquinaldamide) ruthenium dichloride, C₄₄H₄₇O₂N₄RuCl₂, (3.15)

Ligand **2.15** (2 eq., 0.765 mmol, 0.2543 g) was dissolved in 20 mL of ethanol. The solution was heated up to 60°C until the ligand was completely dissolved. After 30 min, the functionalised ligand was added to a solution of RuCl₃·3H₂O (1 eq., 0.382 mmol; 0.1 g) in 5 mL of ethanol and left to reflux overnight. The reaction was cooled down to 65°C and filtered immediately. A reddish solid was isolated which recrystallised from DMF and the mother liqueurs were left to crystallise.

Yield: 0.0739 g, 0.09 mmol, 23 %; $\mu_{\text{eff}} = 1.65$; **EA** (Theoretical/Found)(%): **C** (59.99/60.19), **H** (5.95/5.31) & **N** (6.36/6.58) [**3.15+2.5H₂O**]; **IR (cm⁻¹)**, 3143-2478 (b), 3139 (s), 3012 (s), 2957 (s), 2929 (s), 2868 (s), 1601 (s), 748 (s); **H.R.M.S. [ESI⁺] (m/z)** in methanol (Theoretical/ Found) **[M+H]⁺** 836.2012/836.2204.

6.4.17 Bis-(N-2-Methyl-6-ⁱPropylphenylquinaldamide) ruthenium dichloride, C₄₀H₃₉O₂N₄RuCl₂, (3.16)

Ligand **2.16** (2 eq., 0.765 mmol, 0.2329 g) was dissolved in 20 mL of ethanol. The solution was heated up to 80°C until the ligand was completely dissolved. After 30 min, the functionalised ligand was added to a solution of RuCl₃·3H₂O (1 eq., 0.382 mmol, 0.1 g) in 5 mL of ethanol and left to reflux overnight. The reaction was filtered immediately. A reddish solid was isolated which recrystallised from DMF and the mother liqueurs were left to crystallise.

Yield: 0.2172 g, 0.28 mmol, 73 %; $\mu_{\text{eff}} = 1.70$; **EA** (Theoretical/Found)(%): **C** (52.01/51.82), **H** (6.34/4.75) & **N** (5.78/5.76) [**3.16+8H₂O+EtOH**]; **IR (cm⁻¹)** 3496 (s), 3226-3142 (m), 2962 (s), 2928 (s), 1582-1537 (m), 767 (s); **H.R.M.S. [ESI⁺] (m/z)** in methanol (Theoretical/ Found) **[M+H]⁺** 780.1566/780.1569.

**6.4.18 Bis-(N-2-^tButylphenylquinaldamide) ruthenium dichloride,
C₄₀H₃₉O₂N₄RuCl₂, (3.17)**

Ligand **2.17** (2 eq., 0.765 mmol, 0.231 g) was dissolved in 20 mL of ethanol. The solution was heated up to 80°C until the ligand was completely dissolved. After 30 min, the functionalised ligand was added to a solution of RuCl₃·3H₂O (1 eq., 0.382 mmol; 0.1 g) in 5 mL of ethanol, and left to reflux overnight. The reaction was cooled down to 65°C and filtered immediately. A reddish solid was isolated which recrystallised from DMF, and the mother liqueurs were left to crystallise.

Yield: 0.0293 g, 0.04 mmol, 10 %. $\mu_{\text{eff}} = 1.85$; **EA** (Theoretical/Found)(%): **C** (58.59/58.71), **H** (5.31/5.42) & **N** (6.87/7.02) [**3.17+2H₂O**]; **IR** (cm⁻¹) 3428 (b), 3159-3059 (m), 1606 (s), 1586-1504 (m), 1258 (s), 772-762 (d); **H.R.M.S. [ESI⁺]** (**m/z**) in methanol (Theoretical/ Found) [**M+H**]⁺ 780.1556/780.1620.

**6.4.19 Bis-(N-4-^tButylphenylquinaldamide) ruthenium dichloride,
C₄₀H₃₉O₂N₄RuCl₂, (3.18)**

Ligand **2.18** (2 eq., 0.765 mmol, 0.231 g) was dissolved in 20 mL of ethanol. The solution was heated up to 80°C until the ligand was completely dissolved. After 30 min, the functionalised ligand was added to a solution of RuCl₃·3H₂O (1 eq., 0.382 mmol; 0.1 g) in 5 mL of ethanol and left to reflux overnight. The reaction was cooled down to 65°C and filtered immediately. A reddish solid was isolated which recrystallised from DMF or DMSO, and the mother liqueurs were left to crystallise.

Yield: 0.0372 g, 0.048 mmol, 13 %. $\mu_{\text{eff}} = 1.90$; **EA** (Theoretical/Found)(%): **C** (60.22/60.26), **H** (5.18/4.6) & **N** (7.02/7.20) [**3.18+H₂O**]; **IR** (cm⁻¹) 3420 (b), 3172-3070 (m), 1610 (s), 1576-1524 (m), 1268 (s), 776-763 (d); **H.R.M.S. [ESI⁺]** (**m/z**) in methanol (Theoretical/ Found) [**M+H**]⁺ 780.1556/780.2360.

**6.4.20 Bis-(N-2-triFluoromethylphenylquinaldamide) ruthenium
dichloride, C₃₄H₂₁O₂N₄F₆RuCl₂, (3.19)**

Ligand **2.19** (2 eq., 0.765 mmol, 0.2419 g) was dissolved in 20 mL of ethanol. The solution was heated up to 80°C until the ligand was completely dissolved. After 30 min, the functionalised ligand was added to a solution of RuCl₃·3H₂O (1 eq., 0.382 mmol; 0.1 g) in 5 mL of ethanol and left to reflux overnight. The

reaction was cooled down to 65°C and filtered immediately. A reddish solid was isolated which recrystallised from DMF, and the mother liqueurs were left to crystallise.

Yield: 0.0151 g, 0.018 mmol, 5 %; **IR (cm⁻¹)** 3240 (s), 3059 (s), 1612-1574 (m), 762 (s); **H.R.M.S. [ESI⁺] (m/z)** in methanol (Theoretical/ Found) **[M+H]⁺** 804.0062/804.0069.

6.4.21 Bis-(N-3-triFluoromethylphenylquinaldamide) ruthenium dichloride, C₃₄H₂₁O₂N₄F₆RuCl₂, (3.20)

Ligand **2.20** (2 eq., 0.765 mmol, 0.2419 g) was dissolved in 20 mL of ethanol. The solution was heated up to 80°C until the ligand was completely dissolved. After 30 min, the functionalised ligand was added to a solution of RuCl₃·3H₂O (1 eq., 0.382 mmol, 0.1 g) in 5 mL of ethanol and left to reflux overnight. The reaction was cooled down to 65°C and filtered immediately. A green powder was isolated, and the mother liqueurs were left to crystallise.

Yield: 0.0283 g, 0.04 mmol, 9 %; **IR (cm⁻¹)** 3249 (s), 3210 (s), 3067 (s), 1611-1594 (m), 763 (s); **H.R.M.S. [ESI⁺] (m/z)** in methanol (Theoretical/ Found) **[M+H]⁺** 804.0062/804.0064.

6.4.22 Bis-(N-4-triFluorophenylquinaldamide) ruthenium dichloride, C₃₄H₂₁O₂N₄F₆RuCl₂, (3.21)

Ligand **2.21** (2 eq., 0.765 mmol, 0.2419 g) was dissolved in 20 mL of ethanol. The solution was heated up to 80°C until the ligand was completely dissolved. After 30 min, the functionalised ligand was added to a solution of RuCl₃·3H₂O (1 eq., 0.382 mmol, 0.1 g) in 5 mL of ethanol and left to reflux overnight. The reaction was cooled down to 65°C and filtered immediately. A green solid was isolated which recrystallised from DMF, and the mother liqueurs were left to crystallise.

Yield: 0.0590 g, 0.073 mmol, 19 %; **H.R.M.S. [ESI⁺] (m/z)** in methanol (Theoretical/ Found) **[M+H]⁺** 804.0062/804.0084.

6.4.23 Bis-(N-3,5-difluoromethylphenylquinaldamide) ruthenium dichloride, C₃₆H₁₉O₂N₄F₁₂RuCl₂, (3.22)

Ligand **2.22** (2 eq., 0.765 mmol, 0.2940 g) was dissolved in 20 mL of ethanol. The solution was heated up to 80°C until the ligand was completely dissolved. After 30 min, the functionalised ligand was added to a solution of RuCl₃·3H₂O (1 eq., 0.382 mmol, 0.1 g) in 5 mL of ethanol and left to reflux overnight. The reaction was cooled down to 65°C and filtered immediately. A green solid was isolated which recrystallised from DMF or DMSO, and the mother liquors were left to crystallise.

Yield: 0.0409 g, 0.044 mmol, 12 %; **H.R.M.S. [ESI⁺] (m/z)** in methanol (Theoretical/ Found) **[M+H]⁺** 939.9810/939.9820.

6.4.24 Bis-(N-2-Fluorophenylquinaldamide) ruthenium dichloride, C₃₂H₂₁O₂N₄F₂RuCl₂, (3.23)

Ligand **2.23** (2 eq., 0.765 mmol, 0.2037 g) was dissolved in 20 mL of ethanol. The solution was heated up to 55°C until the ligand was completely dissolved. After 30 min, the functionalised ligand was added to a solution of RuCl₃·3H₂O (1 eq., 0.382 mmol, 0.1 g) in 5 mL of ethanol and left to reflux overnight. The reaction was cooled down to 65°C and filtered. A reddish solid was isolated which recrystallised from DMF and the mother liquors were left to crystallise.

Yield: 0.0926 g, 0.13 mmol, 34 %; $\mu_{\text{eff}} = 1.9$; **EA** (Theoretical/Found)(%): **C** (53.27/53.37), **H** (3.21/2.62) & **N** (7.77/7.72) **[3.23+H₂O]**; **IR (cm⁻¹)** 3148 (s), 3025 (s), 2785 (s), 1611 (s), 1580-1503 (m), 753 (s); **H.R.M.S. [ESI⁺] (m/z)** in methanol (Theoretical/ Found) **[M+H]⁺** 704.0126/704.0227.

6.4.25 Bis-(N-3-Fluorophenylquinaldamide) ruthenium dichloride, C₃₂H₂₁O₂N₄F₂RuCl₂, (3.24)

Ligand **2.24** (2 eq., 0.765 mmol, 0.2037 g) was dissolved in 20 mL of ethanol. The solution was heated up to 50°C until the ligand was completely dissolved. After 30 min, the functionalised ligand was added to a solution of RuCl₃·3H₂O (1 eq., 0.382 mmol, 0.1 g) in 5 mL of ethanol and left to reflux overnight. The reaction was cooled down to 65°C and filtered immediately. A black powder was isolated which recrystallised from DMF or DMSO, and the mother liquors were left to crystallise.

Yield: 0.1725 g, 0.25 mmol, 65 % $\mu_{\text{eff}} = 1.85$; **EA** (Theoretical/Found)(%): **C** (54.63/54.50), **H** (3.01/2.99) and **N** (7.96/7.82) [3.24]; **IR** (cm^{-1}) 3334-2908 (b), 3210 (s), 3061 (s), 1640 (s), 765 (s); **H.R.M.S. [ESI⁺] (m/z)** in methanol (Theoretical/ Found) **[M+H]⁺** 704.0126/704.0120.

6.4.26 Bis-(N-4-Fluorophenylquinaldamide) ruthenium dichloride,
C₃₂H₂₁O₂N₄F₂RuCl₂, (3.25)

Ligand **2.25** (2 eq., 0.765 mmol, 0.2037 g) was dissolved in 20 mL of ethanol. The solution was heated up to 35°C until the ligand was completely dissolved. After 30 min, the functionalised ligand was added to a solution of RuCl₃·3H₂O (1 eq., 0.382 mmol, 0.1 g) in 5 mL of ethanol and left to reflux overnight. The reaction was cooled down to 65°C and filtered. A reddish solid was isolated, recrystallised from DMF and the mother liqueurs were left to crystallise.

Yield: 0.153 g, 0.217 mmol, 57 %; $\mu_{\text{eff}} = 1.94$; **EA** (Theoretical/Found)(%): **C** (54.63/54.51), **H** (3.01/3.09) and **N** (7.96/8.14) [3.25]; **IR** (cm^{-1}) 3000 (s), 3070 (s), 1619 (s), 1584-1510 (m), 792 (s), 761 (s); **H.R.M.S. [ESI⁺] (m/z)** in methanol (Theoretical/ Found) **[M+H]⁺** 704.0126/704.0115.

6.4.27 Bis-(N-2,4-diFluorophenylquinaldamide) ruthenium dichloride,
C₃₂H₂₁O₂N₄F₄RuCl₂, (3.26)

Ligand **2.26** (2 eq., 0.765 mmol, 0.2172 g) was dissolved in 20 mL of ethanol. The solution was heated up to 75°C until the ligand was completely dissolved. After 30 min, the functionalised ligand was added to a solution of RuCl₃·3H₂O (1 eq., 0.382 mmol, 0.1 g) in 5 mL of ethanol and left to reflux overnight. The reaction was filtered immediately. A dark powder was isolated which recrystallised from DMF and the mother liqueurs were left to crystallise.

Yield: 0.0467 g, 0.063 mmol, 17 %; $\mu_{\text{eff}} = 2.01$; **EA** (Theoretical/Found)(%): **C** (51.98/51.72), **H** (2.59/2.73) & **N** (7.58/7.53) [3.26]; **IR** (cm^{-1}) 3217 (b), 3066 (m), 1614 (s), 1584-1512 (m), 785-764 (m); **H.R.M.S. [ESI⁺] (m/z)** in methanol (Theoretical/ Found) **[M+H]⁺** 739.9937/739.9930.

6.4.28 Bis-(N-2,5-diFluorophenylquinaldamide) ruthenium dichloride,
C₃₂H₂₁O₂N₄F₄RuCl₂, (3.27)

Ligand **2.27** (2 eq., 0.765 mmol, 0.2172 g) was dissolved in 20 mL of ethanol. The solution was heated up to 80°C until the ligand was completely dissolved.

After 30 min, the functionalised ligand was added to a solution of $\text{RuCl}_3 \cdot 3\text{H}_2\text{O}$ (1 eq., 0.382 mmol, 0.1 g) in 5 mL of ethanol and left to reflux overnight. The reaction filtered immediately. A red solid was isolated, recrystallised from DMF and the mother liqueurs were left to crystallise.

Yield: 0.1054 g, 0.142 mmol, 37 %; $\mu_{\text{eff}} = 2.04$; **EA** (Theoretical/Found)(%): **C** (51.98/51.8), **H** (2.59/2.58) & **N** (7.58/7.41) [**3.27**]; **IR** (cm^{-1}) 3405 (s), 3063-3038 (m), 1647-1613 (d), 1586-1554 (d), 1496-1445 (m), 1341 (s) 760-728 (m); **H.R.M.S.** [**ESI**⁺] (**m/z**) in methanol (Theoretical/ Found) [**M+H**]⁺ 739.9937/739.9932.

6.4.29 Bis-(N-2-Chlorophenylquinaldamide) ruthenium dichloride, **$\text{C}_{32}\text{H}_{21}\text{O}_2\text{N}_4\text{RuCl}_4$, (3.28)**

Ligand **2.28** (2 eq., 0.765 mmol, 0.2163 g) was dissolved in 20 mL of ethanol. The solution was heated up to 60°C until the ligand was completely dissolved. After 30 min, the functionalised ligand was added to a solution of $\text{RuCl}_3 \cdot 3\text{H}_2\text{O}$ (1 eq., 0.382 mmol, 0.1 g) in 5 mL of ethanol and left to reflux overnight. The reaction was cooled down to 65°C and filtered. A reddish solid was isolated, recrystallised from DMF and the mother liqueurs were left to crystallise.

Yield: 0.1452 g, 0.20 mmol, 52 %; $\mu_{\text{eff}} = 1.97$; **EA** (Theoretical/Found)(%): **C** (52.19/51.97), **H** (2.87/2.80) & **N** (7.61/7.53) [**3.28**]; **IR** (cm^{-1}) 3371 (b), 3148-3059 (m), 1666 (s), 1594-1509 (m), 1471-1341 (m), 755 (s); **H.R.M.S.** [**ESI**⁺] (**m/z**) in methanol (Theoretical/ Found) [**M+H**]⁺ 737.4235/737.9518.

6.4.30 Bis-(N-3-Chlorophenylquinaldamide) ruthenium dichloride, **$\text{C}_{32}\text{H}_{21}\text{O}_2\text{N}_4\text{RuCl}_4$, (3.29)**

Ligand **2.29** (2 eq., 0.765 mmol, 0.2163 g) was dissolved in 20 mL of ethanol. The solution was heated up to 70°C until the ligand was completely dissolved. After 30 min, the functionalised ligand was added to a solution of $\text{RuCl}_3 \cdot 3\text{H}_2\text{O}$ (1 eq., 0.382 mmol, 0.1 g) in 5 mL of ethanol and left to reflux overnight. The reaction was cooled down to 65°C and filtered immediately. A red solid was isolated which recrystallised from DMSO, and the mother liqueurs were left to crystallise.

Yield: 0.2238 g, 0.30 mmol, 80 %. $\mu_{\text{eff}} = 2.12$; **EA** (Theoretical/Found)(%): **C** (50.95/51.24), **H** (3.07/3.14) and **N** (7.43/7.15) [**3.27+H₂O**]; **IR** (cm^{-1}) 3203 (b),

3071-2963 (m), 1568-1548 (m), 1358-1335 (d), 760 (s); **H.R.M.S. [ESI⁺] (m/z)** in methanol (Theoretical/ Found) **[M+H]⁺** 737.9511/737.9516.

**6.4.31 Bis-(N-4-Chlorophenylquinaldamide) ruthenium dichloride,
C₃₂H₂₁O₂N₄RuCl₄, (3.30)**

Ligand **2.30** (2 eq., 0.765 mmol, 0.2163 g) was dissolved in 20 mL of ethanol. The solution was heated up to 60°C until the ligand was completely dissolved. After 30 min, the functionalised ligand was added to a solution of RuCl₃·3H₂O (1 eq., 0.382 mmol, 0.1 g) in 5 mL of ethanol and left to reflux overnight. The reaction was cooled down to 65°C and filtered. A reddish solid was isolated which recrystallised from DMF and the mother liqueurs were left to crystallise.

Yield: 0.1885 g, 0.256 mmol, 67 %; $\mu_{\text{eff}} = 2.06$; **EA** (Theoretical/Found)(%): **C** (52.19/52.06), **H** (2.87/2.72) & **N** (7.61/7.53) [**3.30**]; **IR (cm⁻¹)** 3059-3012 (m), 2890-2836 (b), 1612-1535 (m), 1487-1406 (m), 791-764 (m); **H.R.M.S. [ESI⁺] (m/z)** in methanol (Theoretical/ Found) **[M+H]⁺** 737.9511/737.9514.

**6.4.32 Bis-(N-2,4-diChlorophenylquinaldamide) ruthenium dichloride,
C₃₂H₁₉O₂N₄RuCl₆, (3.31)**

Ligand **2.31** (2 eq., 0.765 mmol, 0.2423 g) was dissolved in 20 mL of ethanol. The solution was heated up to 80°C until the ligand was completely dissolved. After 30 min, the functionalised ligand was added to a solution of RuCl₃·3H₂O (1 eq., 0.382 mmol, 0.1 g) in 5 mL of ethanol and left to reflux overnight. The reaction was cooled down to 65°C and filtered immediately. A reddish solid was isolated which recrystallised from DMF or DMSO, and the mother liqueurs were left to crystallise.

Yield: 0.1226 g, 0.152 mmol, 40 %; $\mu_{\text{eff}} = 2.14$; **EA** (Theoretical/Found)(%): **C** (47.73/47.69), **H** (2.38/2.48) & **N** (6.96/6.87) [**3.31**]; **IR (cm⁻¹)** 3166-3060 (m), 1633 (s), 1593-1508 (m), 1341 (s), 767 (s); **H.R.M.S. [ESI⁺] (m/z)** in methanol (Theoretical/ Found) **[M+H]⁺** 805.8726/805.8727.

**6.4.33 Bis-(N-2,5-diChlorophenylquinaldamide) ruthenium dichloride,
C₃₂H₁₉O₂N₄RuCl₆, (3.32)**

Ligand **2.32** (2 eq., 0.765 mmol, 0.2423 g) was dissolved in 20 mL of ethanol. The solution was heated up to 80°C until the ligand was completely dissolved. After 30 min, the functionalised ligand was added to a solution of RuCl₃·3H₂O

(1 eq., 0.382 mmol, 0.1 g) in 5 mL of ethanol and left to reflux overnight. The reaction was filtered. A reddish solid was isolated, recrystallised from DMF and the mother liqueurs were left to crystallise.

Yield: 0.103 g, 0.127 mmol, 34 %. $\mu_{\text{eff}} = 2.04$; **EA** (Theoretical/Found)(%): **C** (47.73/47.85), **H** (2.38/2.43) & **N** (6.96/7.05) [**3.32**]; **IR** (cm^{-1}) 3186-3062 (m), 1638 (s), 1597-1507 (m), 1377-1341 (m), 765 (s); **H.R.M.S. [ESI⁺] (m/z)** in methanol (Theoretical/ Found) [**M+H**]⁺ 324.0979/324.0981.

6.4.34 Bis-(N-2-Bromophenylquinaldamide) ruthenium dichloride,

C₃₂H₂₁O₂N₄Br₂RuCl₂, (3.33)

Ligand **2.33** (2 eq., 0.765 mmol, 0.2503 g) was dissolved in 20 mL of ethanol. The solution was heated up to 80°C until the ligand was completely dissolved. After 30 min, the functionalised ligand was added to a solution of RuCl₃·3H₂O (1 eq., 0.382 mmol, 0.1 g) in 5 mL of ethanol and left to reflux overnight and filtered. A reddish solid was isolated which recrystallised from DMF leaving the mother liqueurs to crystallise.

Yield: 0.1035 g, 0.12 mmol, 31 %. $\mu_{\text{eff}} = 1.98$; **EA** (Theoretical/Found)(%): **C** (46.57/46.41), **H** (2.56/2.67) & **N** (6.79/6.66) [**3.33**]; **IR** (cm^{-1}) 3300-3250 (b), 3149-2961 (m), 1590-1580 (d), 754 (s); **H.R.M.S. [ESI⁺] (m/z)** in methanol (Theoretical/ Found) [**M+H**]⁺ 825.8505/825.8375.

6.4.35 Bis-(N-3-Bromophenylquinaldamide) ruthenium dichloride,

C₃₂H₂₁O₂N₄Br₂RuCl₂, (3.34)

Ligand **2.34** (2 eq., 0.765 mmol, 0.2503 g) was dissolved in 20 mL of ethanol. The solution was heated up to 85°C until the ligand was completely dissolved. After 30 min, the functionalised ligand was added to a solution of RuCl₃·3H₂O (1 eq., 0.382 mmol, 0.1 g) in 5 mL of ethanol and left to reflux overnight. The reaction was filtered immediately. A red powder was isolated which recrystallised from DMF, and the mother liqueurs were left to crystallise.

Yield: 0.2229 g, 0.27 mmol, 71 %; $\mu_{\text{eff}} = 2.21$; **EA** (Theoretical/Found)(%): **C** (46.57/46.29), **H** (2.56/2.67) and **N** (6.79/6.56) [**3.34**]; **IR** (cm^{-1}) 3250-3230 (b), 3059-2965 (m), 1594-1507 (m), 1341-1335 (m), 760 (m); **H.R.M.S. [ESI⁺] (m/z)** in methanol (Theoretical/ Found) [**M+H**]⁺ 825.8504/825.8497.

**6.4.36 Bis-(N-4-Bromophenylquinaldamide) ruthenium dichloride,
C₃₂H₂₁O₂N₄Br₂RuCl₂, (3.35)**

Ligand **2.35** (2 eq., 0.765 mmol, 0.2503 g) was dissolved in 20 mL of ethanol. The solution was heated up to 80°C until the ligand was completely dissolved. After 30 min, the functionalised ligand was added to a solution of RuCl₃·3H₂O (1 eq., 0.382 mmol, 0.1 g) in 5 mL of ethanol and left to reflux overnight. The reaction was cooled down to 65°C and filtered immediately. A reddish solid was isolated which recrystallised from DMF or DMSO, and the mother liqueurs were left to crystallise.

Yield: 0.1243 g, 0.150 mmol, 39 %; $\mu_{\text{eff}} = 2.13$. **EA** (Theoretical/Found)(%): **C** (46.57/46.75), **H** (2.56/2.66) and **N** (6.79/6.60); **IR** (cm⁻¹) 3228-3163 (m), 3059-2924 (m), 1611-1574 (m), 1537-1466 (m), 1401-1335 (m), 762 (s); **H.R.M.S.** **[ESI⁺]** (m/z) in methanol (Theoretical/ Found) **[M+H]⁺** 825.8504/825.8503.

**6.4.37 Bis-(N-2,4-diBromophenylquinaldamide) ruthenium dichloride,
C₃₂H₁₉O₂N₄Br₄RuCl₂, (3.36)**

Ligand **2.36** (2 eq., 0.765 mmol, 0.3103 g) was dissolved in 20 mL of ethanol. The solution was heated up to 80°C until the ligand was completely dissolved. After 30 min, the ligand was added to a solution of RuCl₃·3H₂O (1 eq., 0.382 mmol, 0.1 g) in 5 mL of ethanol and left to reflux overnight. Then, filtered immediately. A dark solid was isolated, recrystallised from DMF and the mother liqueurs were left to crystallise.

Yield: 0.1935 g, 0.197 mmol, 52 %; $\mu_{\text{eff}} = 2.06$. **EA** (Theoretical/Found)(%): **C** (39.10/39.27), **H** (1.95/1.83) & **N** (5.70/5.88) **[3.36]**; **IR** (cm⁻¹) 3200-3100 (b), 3139-3056 (m), 1632 (s), 1585-1507 (m), 766 (s); **H.R.M.S.** **[ESI⁺]** (m/z) in methanol (Theoretical/ Found) **[M+H]⁺** 983.6674/983.6686.

**6.4.38 Bis-(N-2,5-diBromophenylquinaldamide) ruthenium dichloride,
C₃₂H₁₉O₂N₄Br₄RuCl₂, (3.37)**

Ligand **2.37** (2 eq., 0.765 mmol, 0.3103 g) was dissolved in 20 mL of ethanol. The solution was heated up to 80°C until the ligand was completely dissolved. After 30 min, the functionalised ligand was added to a solution of RuCl₃·3H₂O (1 eq., 0.382 mmol, 0.1 g) in 5 mL of ethanol, and left to reflux overnight. The reaction was cooled down to 65°C and filtered immediately. A reddish solid was

isolated which recrystallised from DMF or DMSO, and the mother liqueurs were left to crystallise.

Yield: 0.1579 g, 0.160 mmol, 42 %; **H.R.M.S. [ESI⁺] (m/z)** in methanol (Theoretical/ Found) **[M+H]⁺** 983.6674/983.6685 (not major peak).

**6.4.39 Bis-(N-2-Iodophenylquinaldamide) ruthenium dichloride,
C₃₂H₂₁O₂N₄I₂RuCl₂, (3.38)**

Ligand **2.38** (2 eq., 0.765 mmol, 0.2862 g) was dissolved in 20 mL of ethanol. The solution was heated up to 80°C until the ligand was completely dissolved. After 30 min, the ligand was added to a solution of RuCl₃·3H₂O (1 eq., 0.382 mmol, 0.1 g) in 5 mL of ethanol, left to reflux overnight and then filtered immediately. A dark red solid was isolated, recrystallised from DMF and the mother liqueurs were left to crystallise.

Yield: 0.1053 g, 0.11 mmol, 29 %. $\mu_{\text{eff}} = 1.98$; **EA** (Theoretical/Found)(%): **C** (41.81/41.97), **H** (2.30/2.29) & **N** (6.09/6.06) [**3.38**]; **IR (cm⁻¹)** 3181-2867 (m), 1592-1558 (m), 1507-1433 (m), 1372-1335 (m), 750 (s); **H.R.M.S. [ESI⁺] (m/z)** in methanol (Theoretical/ Found) **[M+H]⁺** 919.8247/919.8239.

**6.4.40 Bis-(N-3-Iodophenylquinaldamide) ruthenium dichloride,
C₃₂H₂₁O₂N₄I₂RuCl₂, (3.39)**

Ligand **2.39** (2 eq., 0.765 mmol, 0.2862 g) was dissolved in 20 mL of ethanol. The solution was heated up to 85°C until completely dissolved. After 30 min, the functionalised ligand was added to a solution of RuCl₃·3H₂O (1 eq., 0.382 mmol, 0.1 g) in 5 mL of ethanol and left to reflux overnight. The reaction was filtered immediately. A dark solid was isolated which recrystallised from DMF and the mother liqueurs were left to crystallise.

Yield: 0.2568 g, 0.28 mmol, 74 %. $\mu_{\text{eff}} = 2.04$; **EA** (Theoretical/Found)(%): **C** (41.40/41.62), **H** (2.39/2.65) & **N** (6.04/5.88) [**3.39+0.5H₂O**]; **IR (cm⁻¹)** 3279-2963 (m), 1617-1549 (m), 1466-1333 (m), 760 (s); **H.R.M.S. [ESI⁺] (m/z)** in methanol (Theoretical/ Found) **[M+H]⁺** 921.8218/921.8240.

6.4.41 Bis-(N-4-Iodophenylquinaldamide) ruthenium dichloride, C₃₂H₂₁O₂N₄I₂RuCl₂, (3.40)

Ligand **2.40** (2 eq., 0.765 mmol, 0.2862 g) was dissolved in 20 mL of ethanol. The solution was heated up to 80°C until completely dissolved. After 30 min, the ligand was added to a solution of RuCl₃·3H₂O (1 eq., 0.382 mmol; 0.1 g) in 5 mL of ethanol, left to reflux overnight. Then, filtered immediately. A dark solid was isolated, recrystallised from DMF and the mother liquors were left to crystallise.

Yield: 0.1811 g, 0.196 mmol, 51 %; $\mu_{\text{eff}} = 1.99$; **EA** (Theoretical/Found)(%): **C** (41.81/41.715), **H** (2.30/2.09) & **N** (6.09/6.13) [**3.40**]; **IR** (cm⁻¹) 3056 (s), 3000-2870 (m), 1585-1509 (m), 1482-1398 (m), 793-763 (m); **H.R.M.S. [ESI⁺]** (m/z) in methanol (Theoretical/ Found) [**M+H**]⁺ 921.8218/921.8245.

6.5 Cell Culture Work

6.5.1 General Experimental Procedures

The *in vitro* training was performed at the University of Huddersfield under the supervision of Prof. Roger M. Phillips, Dr. Simon J. Allison and their PhD student Samantha Shepherd. The cells used were MIA PaCa-2 (human pancreatic carcinoma), HCT116 p53(+/-) and HCT116 p53(-/-) (human colorectal carcinoma with p53 upregulated and knockdown, respectively) and ARPE-19 (human retinal epithelium – non cancerous) cell lines. These were purchased from ATCC. Standard sterile techniques were used throughout this work. Unless otherwise stated, chemicals were purchased from Sigma Aldrich, consumables from Sarstedt and were used as supplied. The stock cultures were grown in T-75 flasks containing DMEM and DMEM:F12 complete cell medium (15 mL) for the cancerous and non-cancerous cell lines respectively, and incubated at 37 °C with 5.0% of CO₂. The complete media was prepared from DMEM high glucose without L-glutamine Incomplete Media (450 mL), L-Glutamine 2 mM (5 mL, 200 mM) and foetal bovine serum 10% (50 mL). The complete media was prepared from DMEM:F12 (1:1) (450 mL), L-Glutamine 2 mM (5 mL, 200 mM) and foetal bovine serum 10% (50 mL). Phosphate Buffer Saline (PBS) buffer sterile solution was used to wash the cells, Trypsin-EDTA (1x) was used to detach the cells from the flask. DMEM (complete and incomplete), DMEM:F12 (complete and incomplete), MTT (Alfa Aesar) and MTT stock solutions (5 mg/mL), trypsin-EDTA

(1x) were all stored at 4°C. L-Glutamine, foetal bovine serum and trypsin-EDTA stock solutions were stored at -20°C. All chemicals except the MTT solution were incubated in a water bath at 37°C prior to use.

6.5.2 Thawing Cells and from Cryo-Preservation

Cell stocks are kept in liquid nitrogen to preserve them. Once cells were taken from the liquid nitrogen, they were defrosted quickly in a water bath at 37°C, after that, 20 mL of culture media (dependant on the cell line) were added to dilute the amount of DMSO in the freezing medium. The suspension was centrifuged at 1500 rpm for 3 minutes forming a pellet. The media containing DMSO was carefully removed, the pellet was re-suspended in the desired media and an adequate volume of cell suspension added to the cell culture flask.

6.5.3 Sub culturing by trypsination of Monolayer Cultures

After carefully removing the media from the T-75 flasks, cells were washed with PBS buffer solution (1 x 5 mL) and carefully removed. Trypsin-EDTA (1x) (1 x 5 mL) was added and the T-75 flask was incubated for 3 min. When the cells were detached from the flask wall, if needed for cell counting, 3 mL were taken and put in a falcon tube (50 mL) and 12 mL of media (different depending on the cell line) added to the falcon tube and 13 mL to the T-75 flask to allow cells to recover and be confluent.

6.5.4 Cell Counting

Cells were detached using trypsin as above and centrifuged to 1000 rpm. for 3 minutes to form a cell pellet. Media was then carefully removed without disturbing the pellet, and depending on cell pellet size resuspended in 1-10 mL of fresh media added to make a homogenous cell suspension. From the suspension 10 µL were taken and carefully placed onto each side of the glass slide of a haemocytometer. Cells were counted under the microscope in four squares of the haemocytometer and an average was taken with units of 10⁴ cell/mL.

6.5.5 Cryo-preservation (cell stock)

After trypsination, if needed, cells were re-suspended in culture media containing 20% FBS and 10% DMSO and 1 mL of this suspension placed in pre-labelled cryo-vial. The cryo-vials were frozen by a gradient of freezing using a Nalgene ®

'Mr Frosty TM' system loaded with isopropyl alcohol. Once the cryo-vials are inserted into the 'Mr Frosty TM' container at room temperature, this was placed in a -80°C freezer overnight prior to transferring the cryo-vials into the liquid nitrogen. The exact location, number of vials, date and cell line details were entered into the liquid nitrogen storage logging system.

6.5.6 MTT stock solution

The MTT stock solution (5 mg/mL) was prepared by dissolving MTT (3-(4,5-dimethylthiazol-2-yl)-2,5-diphenyl tetrazolium bromide) 250 mg in PBS sterile (50 mL), this was then vortexed and then passing through a 0.2 µm sterile filter.

6.5.7 Validation of pipetting technique

A single cell suspension cell/mL was prepared to a final concentration of 5×10^4 . A 96 well plate was seeded at varying volumes of cell suspension and media, lane 1 had only media and lane 12 left as blank. From lane 2 to lane 11, a final volume of 200 µl remained constant decreasing the amount of cell suspension in 20 µL and increasing the cell media in 20 µl. 20 µl of MTT stock solution was immediately added and incubated for 4 hours. After 4h, the solution was carefully removed from each well to not disturb the crystals and dissolve them in 150 µL of DMSO (Fisher Scientific). The plates were read by a Tecan plate reader set at 540 nm. Finally, the mean absorbance was calculated (differing the mean of the blank) for each line and plotted against the cell number, the R value is then calculated in order to quantify the accuracy of the user pipetting technique.

6.5.8 Chemo-sensitivity MTT assays (Normoxic Conditions)

After cell counting, a suspension with a concentration of 2×10^4 cell/mL was prepared. A 96-well plate was used and 200 µL was added to a lane one, to serve as a blank. 200 µL of the diluted cell suspension was then added to lanes 2 to 12, and were incubated for 24h at 37°C in an atmosphere of 5.0% of CO₂ prior to drug exposure. The drugs to be tested were dissolved in DMSO and diluted further with media to obtain drug solutions ranging from 100 µM to 0.046 µM. The final DMSO concentration was 0.2% (v/v) which is non-toxic to cells. The second lane was left as a blank meaning no drug was added to see the effect of the anti-cancer molecules. Drug solutions were added to cells and incubated for 96h at

37°C in an atmosphere of 5% CO₂. Cell survival was determined using the MTT assay and MTT (20 µL of a 5 mg/mL stock) was added to each well and incubated for 4h at 37°C in an atmosphere of 5.0% of CO₂. The solutions were then removed and 150 µL of DMSO was added to each well plate to dissolve the formazan crystals.

6.5.9 Data Analysis

A Tecan plate reader was used to measure the absorbance at 540 nm. Lanes contained medium only and cell suspension (no drug) were used as blanks and 100% cell survival respectively. Cell survival was determined as the absorbance of treated cells divided by the true absorbance of controls and expressed as percentage. The IC₅₀ values were determined from choosing where the 50% of survival against drug concentration. Each experiment was repeated a minimum of three times, to give the mean of IC₅₀ and standard deviations.

6.5.10 Chemo-sensitivity MTT assays (Hypoxic Conditions)

The hypoxic studies were carried out in a Hypoxic chamber (Whitley H35 hypoxystation) with 0.1% of O₂, 5.0% of CO₂, 94.9% of N₂ and 81% of humidity, on MIA PaCa-2 (human pancreatic carcinoma) and HCT116 (human colon carcinoma p53 upregulated) cell lines. DMEM complete media was conditioned for at least 24h in the hypoxic chamber prior to start of the experiment in order to purge the oxygen from the media. The cells were seeded as for the 5-day cytotoxic assay in section 6.5.8 and after 24h they were moved the hypoxic chamber where the cells were exposed to the lead compounds (IC₅₀ below 20 µM) from concentrations starting at 100 µM until 0.048 µM. In this assay, it was seeded one compound per plate in order to decrease the potential cell infection. Cell survival was then determined using the MTT assay described in section 6.5.8.

6.5.11 Viability assay and drug induced Cell Cycle Arrest using the NucleoCounter (NC-3000) cytometer

The NucleoCounter (NC) 3000 is an advanced cytometer which uses fluorescence imaging to characterise cell properties. For each of the compounds selected (two Lead Compound **3.23** and **3.32**) four T-25 flasks with 1 x10⁶ cells were placed in the incubator to allow them to adhere (1 serving as a control and the other 3 for

time point experiments). The seeding density of the flasks reflected the same density as in the 96-well plate used for the MTT assay (number of cells per cm² is the same). Cells were exposed to the same IC₅₀ and the final concentration of DMSO (used to dissolve the complexes) was kept constant 0.1% v/v. The compounds were then incubated for 24h, 48h and 72h. After drug exposure, images were taken (Evos XL digital microscope) of each flask for visual comparison prior to trypsination. Then, cells were analysed using the NC3000 using the viability assay and the cell cycle arrest assay. For the two assays, the original medium was always kept and re-added prior to centrifugation to create a cell suspension with all living, apoptotic and necrotic populations present.

6.5.11.1 Viability Assay

Following the preparation of a single cell suspension, cells were drawn into the Via1-cassette by inserting the tip of the cassette into the cell suspension and pressing the piston. This cassette was pre-loaded with Acridine Orange staining the entire population and DAPI which stained only the non-viable cells. Then, the cassettes were placed in the NC3000 for analysis. The cell suspension should be in the range of 5 x10⁴-5 x10⁶ cells/mL to assure reliable results and manageable cell densities for potential further analysis. This assay not only determines the cell viability of cell suspension but provides an accurate cell count as well.

6.5.11.2 Cell Cycle Arrest Assay

To determine the degree of cell cycle arrest of a compound, a cell suspension at 1 x10⁶ cells/mL was prepared. Cells were washed twice in PBS prior to the addition of 250 µL of solution 10 (lysis buffer, Chemometec) supplemented with 10 µg/mL DAPI. The cell suspension was then incubated for 5 minutes at 37°C followed by the addition of 250 µL of solution 11 (stabilisation buffer, Chemometec). The resultant sample was analysed using A8 slides. The principle of the assay was quantifying the amount of DNA stained by DAPI. In a single population, cells are distributed among three major phases: G₁/G₀ with one set of paired chromosomes per cell, S phase where DNA is synthesised (variable in DNA content) and G₂/M phase where there are two sets of paired chromosomes per cell. Sub G₁ populations are apoptotic with higher fluorescent intensities than G₂/M phase being polyploid. DAPI intensity directly relates to DNA content.

6.5.12 Antimicrobial Studies

Antimicrobial screening was performed by CO-ADD (The Community for Antimicrobial Drug Discovery), funded by the Wellcome Trust (UK) and The University of Queensland (Australia).

6.5.13 Antibacterial Evaluation

Complexes were prepared in DMSO and water to give a final concentration of $32 \mu\text{g mL}^{-1}$ in a 384-well non-binding surface (NBS) plate. The final DMSO concentration was at a maximum of 1.0 %. All bacteria were cultured in Cation Adjusted Mueller Hinton broth (CAMHB) at 37°C overnight. A sample of each culture was diluted 40-fold in fresh broth and incubated at 37°C for 1.5 - 3 hours. The resultant mid-log phase cultures were diluted (CFU mL^{-1} measured by OD_{600}), then added to each well of the compound containing plates, giving a cell density of $5 \times 10^5 \text{ CFU mL}^{-1}$ and a total volume of $50 \mu\text{L}$. Colistin and vancomycin were used as positive bacterial inhibitor standards for Gram-negative and Gram-positive bacteria, respectively. Each standard was provided in 4 concentrations, with 2 above and 2 below its MIC or CC_{50} value, and plated into the first 8 wells of column 23 of the 384-well NBS plates. All of the plates were covered and incubated at 37°C for 18 hours without shaking. All experiments were carried out in duplicate. Inhibition of bacterial growth was determined measuring absorbance at 600 nm (OD_{600}), using a Tecan M1000 Pro monochromator plate reader. The percentage of growth inhibition was calculated for each well, using the negative control (media only) and positive control (bacteria without inhibitors) on the same plate as references. The significance of the inhibition values was determined by modified Z-scores, calculated using the median and MAD of the samples (no controls) on the same plate. Samples with inhibition value above 80 % and Z-Score above 2.5 for either replicate were classed as actives. Samples with inhibition values in the range 50 to 80 % and Z-Score above 2.5 for either replicate were classed as partial actives.

6.5.14 Antibacterial Hit Confirmation

Complexes were prepared in DMSO and water to give a final concentration of $32 \mu\text{g mL}^{-1}$ and serially diluted two fold for eight times. Each sample concentration was prepared in a 384-well non-binding surface (NBS) plate for each bacterial strain or tissue-culture treated plates for mammalian cell types. The final DMSO

concentration was at a maximum of 0.5 % DMSO. All bacteria were cultured in Cation Adjusted Mueller Hinton broth (CAMHB) at 37 °C overnight. A sample of each culture was then diluted 40-fold in fresh broth and incubated at 37 °C for 1.5-3 h. The resultant mid-log phase cultures were diluted (CFU mL⁻¹ measured by OD₆₀₀), then added to each well of the compound containing plates, giving a cell density of 5×10⁵ CFU mL⁻¹ and a total volume of 50 µL. Colistin and vancomycin were used as positive bacterial inhibitor standards for Gram-negative and Gram-positive bacteria, respectively. Each standard was provided in 4 concentrations, with 2 above and 2 below its MIC or CC₅₀ value, and plated into the first 8 wells of column 23 of the 384-well NBS plates. All the plates were covered and incubated at 37 °C for 18 h without shaking. All experiments were performed in duplicate. Inhibition of bacterial growth was determined measuring absorbance at 600 nm (OD₆₀₀), using a Tecan M1000 Pro monochromator plate reader. The percentage of growth inhibition was calculated for each well, using the negative control (media only) and positive control (bacteria without inhibitors) on the same plate as references. The MIC was determined as the lowest concentration at which the growth was fully inhibited, defined by an inhibition ≥ 80%. In addition, the maximal percentage of growth inhibition is reported as D_{Max}, indicating any compounds with partial activity. Hits were classified by MIC ≤ 16 µg mL⁻¹ or MIC ≤ 10 µM in either replicate.

6.5.15 Antifungal Evaluation

Complexes were prepared in DMSO and water to give a final concentration of 32 µg mL⁻¹ in a 384-well non-binding surface (NBS) plate. The final DMSO concentration was at a maximum of 1.0 %. Fungal strains were cultured for three days on yeast extract-peptone dextrose (YPD) agar at 30 °C. A yeast suspension of 1 × 10⁶ to 5 × 10⁶ CFU mL⁻¹ (as determined by OD₅₃₀) was prepared from five colonies. The suspension was diluted and added to each well of the compound-containing plates giving a final cell density of fungi suspension of 2.5 × 10³ CFU mL⁻¹ and a total volume of 50 µL. Fluconazole was used as a positive fungal inhibitor standard and provided in 4 concentrations, with 2 above and 2 below its MIC or CC₅₀ value, and plated into the first 8 wells of column 23 of the 384-well NBS plates. All the plates were covered and incubated at 35 °C for 36 hours without shaking. All experiments were carried out in duplicate. Growth inhibition of *C. albicans* was determined measuring absorbance at 630 nm (OD₆₃₀) and the

growth inhibition of *C. neoformans* was determined measuring the difference in absorbance between 600 and 570 nm ($OD_{600-570}$), after the addition of 0.001 % resazurin and incubation at 35 °C for an additional 2 hours. The absorbance was measured using a Biotek Synergy HTX plate reader. The percentage of growth inhibition was calculated for each well, using the negative control (media only) and positive control (fungi without inhibitors) on the same plate. The significance of the inhibition values was determined by modified Z-scores, calculated using the median and MAD of the samples (no controls) on the same plate. Samples with inhibition value above 80 % and Z-Score above 2.5 for either replicate were classed as actives. Samples with inhibition values in the range 50 to 80 % and Z-Score above 2.5 for either replicate were classed as partial actives.

6.5.16 Antifungal Hit Confirmation

Complexes were prepared in DMSO and water to give a final concentration of $32 \mu\text{g mL}^{-1}$ and serially diluted two fold for eight times. Each sample concentration was prepared in a 384-well non-binding surface plate for each fungal strain or tissue-culture treated plates for mammalian cell types. The final DMSO concentration was at a maximum of 0.5 % DMSO. Fungal strains were cultured for three days on YPD agar at 30 °C. A yeast suspension of 1×10^6 to 5×10^6 CFU mL^{-1} (as determined by OD_{530}) was prepared from five colonies. The suspension was subsequently diluted and added to each well of the compound-containing plates giving a final cell density of fungi suspension of 2.5×10^3 CFU mL^{-1} and a total volume of 50 μL . Fluconazole was used as a positive fungal inhibitor standard and provided in 4 concentrations, with 2 above and 2 below its MIC or CC_{50} value, and plated into the first 8 wells of column 23 of the 384-well NBS plates. All plates were covered and incubated at 35 °C for 36 hours without shaking. All experiments were performed in duplicate. Growth inhibition of *C. albicans* was determined measuring absorbance at 630 nm (OD_{630}) and the growth inhibition of *C. neoformans* was determined measuring the difference in absorbance between 600 and 570 nm ($OD_{600-570}$) after the addition of 0.001 % resazurin and incubation at 35 °C for 2 hours. The absorbance was measured using a Biotek Multiflo Synergy HTX plate reader. The percentage of growth inhibition was calculated for each well, using the negative control (media only) and positive control (fungi without inhibitors) on the same plate. The MIC was determined as the lowest concentration at which the growth was fully inhibited,

defined by an inhibition $\geq 80\%$ for *C. albicans* and an inhibition $\geq 70\%$ for *C. neoformans*. Due to a higher variance in growth and inhibition, a lower threshold was applied to the data for *C. neoformans*. In addition, the maximal percentage of growth inhibition is reported as D_{Max} , indicating any compounds with marginal activity. Hits were classified by $MIC \leq 16 \mu\text{g mL}^{-1}$ or $MIC \leq 10 \mu\text{M}$ in either replicate.

6.5.17 Cytotoxicity Assay (CO-ADD protocol)

To assess the cytotoxicity, HEK293 cells were counted manually in a Neubauer haemocytometer and then plated in the 384-well plates containing the compounds to give a density of 5000 cells well^{-1} in a final volume of 50 μL . Dulbecco's modified eagle medium (DMEM) supplemented with 10% FBS was used as growth media and the cells were incubated together with the compounds for 20 hours at 37°C in 5% CO_2 . Tamoxifen was used as a positive cytotoxicity standard in 8 concentrations in 2 fold serial dilutions with 50 $\mu\text{g mL}^{-1}$ highest concentration. All experiments were performed in duplicate. Cytotoxicity was measured by fluorescence with excitation at 560 nm and emission at 590 nm ($F_{560/590}$), after addition of 5 μL of resazurin (25 $\mu\text{g mL}^{-1}$) and incubation for a further 3 hours at 37°C in 5% CO_2 . The fluorescence intensity was measured using a Tecan M1000 Pro monochromator plate reader, using automatic gain calculation. CC_{50} were calculated by curve fitting the inhibition values against $\log(\text{concentration})$ using sigmoidal dose-response function, with variable fitting values for bottom, top and slope. The maximal percentage of cytotoxicity is reported as D_{Max} , indicating any compounds with partial cytotoxicity. The curve fitting was implemented using Pipeline Pilot's dose-response component. Any value with $>$ indicates a sample with no activity (low D_{Max} value) or samples with CC_{50} values above the maximum tested concentration (higher D_{Max} value). Cytotoxic samples were classified by $CC_{50} \leq 32 \mu\text{g mL}^{-1}$ or $CC_{50} \leq 10 \mu\text{M}$ in either replicate. In addition, samples were flagged as partial cytotoxic if $D_{Max} \geq 50\%$, even with $CC_{50} >$ the maximum tested concentration.

6.5.18 Haemolysis Assay

To assess blood toxicity, Human whole blood was washed three times with 3 volumes of 0.9% NaCl and then resuspended in same to a concentration of 0.5×10^8 cells mL^{-1} , as determined by manual cell count in a Neubauer

haemocytometer. The washed cells were then added to the 384-well compound-containing plates for a final volume of 50 μL . After a 10 min shake on a plate shaker the plates were then incubated for 1h at 37°C. Melittin was used as a positive haemolytic standard in 8 concentrations in 2 fold serial dilutions with 50 $\mu\text{g mL}^{-1}$ highest concentration. After incubation, the plates were centrifuged at 1000g for 10 min to pellet cells and debris, 25 μL of the supernatant was then transferred to a polystyrene 384-well assay plate. Haemolysis was determined by measuring the supernatant absorbance at 405 nm (OD_{405}). The absorbance was measured using a Tecan M1000 Pro monochromator plate reader. HC_{10} and HC_{50} (concentration at 10% and 50% haemolysis, respectively) were calculated by curve fitting the inhibition values vs. $\log(\text{concentration})$ using a sigmoidal dose-response function with variable fitting values for top, bottom and slope. In addition, the maximal percentage of haemolysis is reported as D_{Max} , indicating any compounds with partial haemolysis. The curve fitting was implemented using Pipeline Pilot's dose-response component. Any value with > indicate sample with no activity (low D_{Max} value) or samples with HC_{10} values above the maximum tested concentration (higher D_{Max} value). Haemolysis samples were classified by $\text{HC}_{10} \leq 32 \mu\text{g mL}^{-1}$ or $\text{HC}_{10} \leq 10 \mu\text{M}$ in either replicate. In addition, samples were flagged as partial haemolytic if $D_{\text{Max}} \geq 50\%$, even with $\text{HC}_{10} >$ the maximum tested concentration.

6.6 Mechanistic studies

6.6.1 Hydrolysis

A calibration curve was prepared for each complex by dissolving in 10% of DMF, and diluting it further with deionised water. The concentrations used were 100, 80, 60, 40 and 20 μM . The maximum absorbance (λ_{max}) was taken to plot the calibration curve of concentration against absorbance. Hydrolysis samples were prepared 50 μM . These aqueous solutions were scanned at different time points, 0h, 1h, 24h, 48h and 72h by UV-Visible Spectrophotometry at 293 K. The concentration of each complex from 0h to 72 hours was determined using its individual calibration curve. The following formula is used to calculate the percentage of hydrolysed complex,

$$\% \text{ hydrolysed complex} = \left(\frac{[C]_{\text{initial}} - [C]_{\text{final}}}{[C]_{\text{initial}}} \right) \times 100\%$$

6.6.2 Hydrophobicity

A calibration curve was prepared for each complex by dissolving the complexes in octanol, and diluting it further to obtain the concentrations of 100, 80, 60, 40 and 20 μM . The maximum absorbance (λ_{max}) was taken to plot the calibration curve of concentration against absorbance. Equal amounts of octanol and deionised water (containing 300 mM NaCl to prevent complexes from undergoing hydrolysis) were stirred overnight for saturation and separated to obtain water-saturated octanol and octanol-saturated water solutions. Approximately 1 mg of each complex tested was dissolved in 25 ml of water-saturated octanol as stock solution, and sonicated for complete dissolution. Six independent samples were prepared for each complex by adding 2 ml of octanol-saturated water, followed by 2 ml of the stock solution containing ruthenium complexes in each labelled 15 ml Falcon tubes. The samples were then shaken using the IKA Vibrax VXC basic shaker at 500 g/min for 4 hours. Organic (octanol) layer of the stock solution and from the six independent samples were taken for analysis on UV-Visible spectrophotometry. The concentration of each complex was determined using its individual calibration curve. The following formula is used to calculate the partition coefficient of the complexes (Log P),

$$\text{Log } P = \text{Log} \left(\frac{[C]_{org}}{[C]_{aq}} \right) ; [C]_{aq} = [C]_{org \text{ stock}} - [C]_{org}$$

6.7 References

- ¹ Cosier, J.; Glazer, A. M.; *J. App. Crystallogr.*, **1986**, 19, 105-107.
- ² Otwinowski, Z.; Minor, W., in 'DENZO and SCALEPACK programs'. **1995**.
- ³ Sheldrick, G. M.; *Acta Crystallogr. C*, **2015**, 71, 3-8.
- ⁴ Dolomanov, O. V.; Bourhis, L. J.; Gildea, R. J.; Howard, J. A.; Puschmann, H.; *J. App. Crystallogr.*, **2009**, 42, 339-341.
- ⁵ Dutta, S.; Pal, S.; Bhattacharya, P. K.; *Polyhedron*, **1999**, 18, 2157-2162.
- ⁶ Basri, A. M.; Lord, R. M.; Allison, S. J.; Rodríguez-Bárzano, A.; Lucas, S. J.; Janeway, F. D.; Shepherd, H. J.; Pask, C. M.; Phillips, R. M.; McGowan, P. C.; *Chem. Eur. J.*, **2017**, 23, 26, 6341-3656.

Chapter 7 Conclusions and Future Work

7.1 Conclusions

Amide based ligands are embedded in the field of peptide chemistry displaying key biological roles such as protein construction. Forty ligands were synthesised being twelve of them novel. Two synthetic protocols (based on amide condensation reactions) were followed. These ligands have been fully characterised by means of NMR, IR, HRMS, some by elemental analysis, and when suitable crystals were obtained, analysed for X-ray crystallography, as described in **Chapter 2**. In the solid state, these ligands opt for an almost planar configuration showing a slight twist between the quinoline and the aniline ring, allowing them to facilitate the coordination to metallic centres either by $[N,N]$ or $[N,O]$ coordination in an anionic or neutral form. .

An umbrella of novel functionalised di-chloride bis-quinaldamide ruthenium (III) complexes have been successfully synthesised. The compounds that showed pure elemental analysis (**3.1** (H), **3.5** (2-Me), **3.6** (3-Me), **3.7** (4-Me), **3.9** (2-Et), **3.10** (3-Et), **3.11** (4-Et), **3.12** (2-ⁱPr), **3.13** (3-ⁱPr), **3.15** (2,6-diⁱPr), **3.16** (2-Me,6-ⁱPr), **3.17** (2-^tBu), **3.18** (4-^tBu), **3.23** (2-F), **3.24** (3-F), **3.25** (4-F), **3.26** (2,4-diF), **3.27**, (2,5-diF), **3.28** (2-Cl), **3.29** (3-Cl), **3.30** (4-Cl), **3.31** (2,4-diCl), **3.32** (2,5-diCl), **3.33** (2-Br), **3.34** (3-Br), **3.35** (4-Br), **3.36** (2,4-diBr), **3.38** (2-I), **3.39** (3-I), and **3.40** (4-I) were fully characterised using IR, HRMS, magnetic susceptibility, X-ray powder diffraction and single crystal X-Ray diffraction, when suitable, however, only the compounds that showed relevant biological activity are described in **Chapter 3**. Several synthetic protocols were attempted, only one protocol was thoroughly discussed in this thesis which yielded the ruthenium neutral complexes recrystallised by slow evaporation of DMF or DMSO solutions. From the five potential isomers only the *trans-trans-trans* was isolated and proved by X-ray powder diffraction that the whole bulk of the sample was that only isomer. The thirty pure complexes have been tested against various cancerous and non-cancerous cell lines to assess their potential as anti-cancer agents, as reported in **Chapter 4**.

In **Chapter 3**, three further complexes were obtained as secondary products from the reactions carried in presence of a base, crystallised from mother liqueurs and from the same batch of crystallisation. These side products helped to optimise

the reaction conditions and understanding how these complexes might lose their biocidal properties. Surprisingly, following the original protocol (addition of a base to the complexation reaction) a charged complex was isolated suggesting another family of complexes type $[\text{RuCl}_2\text{L}_2]^-$ which are negatively charged but not discussed in this project.

Chapter 4 describes a library of functionalised *trans*-dichloride *bis*-quinaldamide ruthenium complexes that were tested for cytotoxicity against three cancer cell lines, HCT116 p53 $^{+/-}$ (colorectal adenocarcinoma with upregulated tumour suppressor gene), HCT 116 p53 $^{-/-}$ (colorectal adenocarcinoma with knockdown of the tumour suppressor gene) and MIA PaCa-2 (pancreatic cancer), and non-cancerous cells line ARPE-19 (retinal epithelial). Their anticancer activity was determined following a 72h drug exposure MTT assay. Longer incubation times show very low selectivity of the drug, hence 3-day incubation time was used in the assay as well as for cisplatin, carboplatin and oxaliplatin, allowing the calculation of the IC_{50} values of the drugs. The cytotoxicity of the complexes is mostly affected by the substitution of the aniline rings displaying a wide range of potency, from inactive to highly active. Only a few trends can be seen, complexes with electron withdrawing groups show more selectivity towards cancer cell lines, the *para*-substituted complexes show a general increase in activity and the compounds with double substituents in the aniline ring opt for slightly higher IC_{50} displaying selectivity ratios higher than the platinum based drugs – FDA approved. The complexes tend to be selective towards colorectal cancer cell lines being the complex **3.35** (4-Br) ($\text{IC}_{50} = 21.72 \pm 3.90 \mu\text{M}$) selective towards HCT p53 $^{-/-}$, and the complex **3.7** (4-Me) ($\text{IC}_{50} = 24.57 \pm 3.37 \mu\text{M}$) selective towards p53 $^{+/-}$, hence more cytotoxicity assays were carried out against isogenic colonic cancerous cell lines but, in this case, targeting oncogenes. Five lead compounds were tested against HCT 116 Kras cell lines (Wild type, mutant and parent). It was proven the three complexes showed equipotent activity against the oncogene cell lines, complex **3.18** (R = 4-^tBu) displayed higher activity than against the tumour suppressor gene and complex **3.32** (R = 2,5-diCl) showed lower toxicity.

The lead compounds were tested under hypoxia conditions to mimic the core of cancerous cells as the oxygen concentration is very low. Compounds with electron donating groups increased the IC₅₀ whereas the compounds with electron withdrawing groups have shown better anticancer activity when compared to their toxicity under normoxic conditions. This feature suggests that two lead compounds **3.23** and **3.32** are the two most promising anti-cancer complexes selected for further analysis.

Viability studies and cell cycle arrest studies have shown that compounds **3.23** and **3.32** disrupt the DNA in the sub G₁ phase, what means they can promote cell death by apoptosis, necrosis or necroptosis. Interestingly, compound **3.32** does not interrupt the cell cycle for healthy cells. Selected complexes (dependent on the anticancer potency) were chosen for further structural-activity relationship studies. Mechanistic studies such as hydrolysis and hydrophobicity tests have proved that compounds are not prone to hydrolysis suggesting the mechanism of action does not occur *via* aquated species. On the other hand, the compounds tend to accumulate in the octanol (organic) layer which mimics the cell membrane, suggesting the compounds get into the cell *via* passive diffusion showing acceptable Log P values according to Lipinski's rule of five and Hansch's principle of minimum hydrophobicity. The UV-vis hydrolysis study was carried at the same time points as the MTT assay in order to correlate the cytotoxicity studies. HRMS proved that there were not aquated species. It can be seen that the higher the Log P value the better the selectivity towards colonic cancer cell lines is. Although, few correlations can be observed between the cytotoxicity and Log P values these are opposed to the platinum complexes that have shown an increase in cytotoxicity when increasing hydrophobicity.

A new approach given in this research project is using these compounds as antibacterial and antifungal agents, analysed by the CO-ADD at the University of Queensland. The compounds were tested against five types of bacteria classified depending on the absence (Gram negative) or presence (Gram positive) of bacteria cell wall, showing that compounds with substituents in position 2 have better MIC values being the complex **3.12** the most active. Surprisingly, all the active compounds were selective towards the bacteria strain *Staphylococcus*

aureus. In addition, the compounds with bromo substituent in any position shows good activity across the panel of bacteria tested. In terms of antifungal activity, the compounds were tested against two fungal strains showing the compound **3.26** (R = 2,4-diF) displays good activity against the fungi *Candida albicans*.

7.2 Future Work

Further characterisation for the complexes will include Electron Paramagnetic Resonance (EPR) spectroscopy. This helps to understand the isomeric behaviour of the complexes in solution over time to elucidate if the ruthenium complexes isomerise in solution.

Further work will be investigating their cytotoxic properties in 3D models (spheroids). This will be done in the colorectal cell line HT-29 under the supervision of Prof. Roger Philips at the University of Huddersfield. Ongoing work is focused on the cytotoxic properties of these complexes against cancer stem cells (CSCs) in collaboration with Associate Professor Kogularamanan Suntharalingama at King's College/The University of Leicester as, to date, there is no literature about ruthenium-based anticancer stem cell agents. The work carried at King's College is being funded by the mobility grant awarded by the RSC. The main cell lines to work with are breast cancer (Bulk and CSCs) and the healthy breast cell line MCF10a and healthy kidney cell line HEK293T. Cellular uptake and DNA cleavage will be also studied to comprehend how these new family of complexes behave. Cellular fractionation will be helpful to determine where the drug is being accumulated within the cell (cytoplasm, cell membrane, and nucleus).

After the successful achievements, the next step is analysing *in vivo* drug accumulation in order to introduce these new family into clinical potential anti-cancer drugs. This is appropriate for complexes **3.23** (R = 2-F) and complex **3.32** (R = 2,5-diCl). The former shows great potency, selectivity and very good hypoxic enhancement ratio for pancreatic cancer (no cure to date), the latter is the most selective, although less potent than **3.23**, its enhancement properties in hypoxic conditions proves is an excellent candidate for *in vivo* studies.

Appendix: Crystallographic Data

Appendix A: Crystallographic Data

	Ligand 2.3	Ligand 2.4	Ligand 2.8
Empirical formula	C ₁₈ H ₁₅ N ₂ O ₃	C ₁₈ H ₁₆ N ₂ O ₃	C ₁₉ H ₁₈ N ₂ O
Formula weight	307.32	308.33	290.35
Temperature/K	120.3(6)	120.1(4)	119.97(12)
Crystal system	monoclinic	orthorhombic	monoclinic
Space group	C2	Pbca	C2/c
a/Å	22.7070(6)	13.4360(2)	19.3410(9)
b/Å	3.91108(9)	12.00512(19)	8.1490(4)
c/Å	16.9323(5)	19.1345(3)	19.3328(8)
α/°	90	90	90
β/°	102.619(3)	90	100.860(4)
γ/°	90	90	90
Volume/Å ³	1467.41(7)	3086.40(9)	2992.4(2)
Z	4	7	8
ρ _{calc} /cm ³	1.391	1.161	1.289
μ/mm ⁻¹	0.787	0.655	0.081
F(000)	644.0	1134.0	1232.0
Crystal size/mm ³	0.31 × 0.08 × 0.02	0.632 × 0.273 × 0.273	0.611 × 0.447 × 0.215
Radiation	CuKα (λ = 1.54184)	CuKα (λ = 1.54184)	MoKα (λ = 0.71073)
2θ range for data collection/°	7.34 to 147.56	9.244 to 147.378	6.616 to 62.434
Index ranges	-27 ≤ h ≤ 27, -4 ≤ k ≤ 4, -19 ≤ l ≤ 20	-16 ≤ h ≤ 16, -14 ≤ k ≤ 14, -22 ≤ l ≤ 23	-27 ≤ h ≤ 25, -11 ≤ k ≤ 10, -27 ≤ l ≤ 28
Reflections collected	5488	7855	10622
Independent reflections	2508 [R _{int} = 0.0299, R _{sigma} = 0.0350]	3058 [R _{int} = 0.0257, R _{sigma} = 0.0266]	4275 [R _{int} = 0.0361, R _{sigma} = 0.0477]
Data/restraints/parameters	2508/1/210	3058/0/210	4275/0/202
Goodness-of-fit on F ²	1.044	1.062	1.060
Final R indexes [I ≥ 2σ (I)]	R ₁ = 0.0327, wR ₂ = 0.0826	R ₁ = 0.0368, wR ₂ = 0.0915	R ₁ = 0.0532, wR ₂ = 0.1271
Final R indexes [all data]	R ₁ = 0.0351, wR ₂ = 0.0848	R ₁ = 0.0437, wR ₂ = 0.0967	R ₁ = 0.0677, wR ₂ = 0.1369
Largest diff. peak/hole / e Å ⁻³	0.16/-0.21	0.17/-0.18	0.34/-0.26

Appendix A: Crystallographic Data

	Ligand 2.19	Ligand 2.20	Ligand 2.41
Empirical formula	C ₁₇ H ₁₁ N ₂ OF ₃	C ₁₈ H ₁₀ F ₆ N ₂ O	C ₁₇ H ₁₃ N ₃ O ₄
Formula weight	316.28	384.28	323.31
Temperature/K	120.1(3)	120.0(2)	119.99(11)
Crystal system	monoclinic	monoclinic	monoclinic
Space group	P2 ₁ /n	Cc	P2 ₁ /n
a/Å	14.5099(6)	20.8347(15)	7.6216(3)
b/Å	5.8509(2)	4.7047(3)	19.9877(7)
c/Å	17.1616(5)	17.3675(11)	9.7135(3)
α/°	90	90	90
β/°	105.937(4)	112.427(8)	96.662(3)
γ/°	90	90	90
Volume/Å ³	1400.95(9)	1573.6(2)	1469.75(8)
Z	3	4	4
ρ _{calc} /cm ³	1.125	1.622	1.4610
μ/mm ⁻¹	0.788	0.151	0.890
F(000)	486.0	776.0	674.4
Crystal size/mm ³	0.185 × 0.129 × 0.119	0.299 × 0.13 × 0.081	0.272 × 0.104 × 0.074
Radiation	CuKα (λ = 1.54184)	MoKα (λ = 0.71073)	Cu Kα (λ = 1.54184)
2θ range for data collection/°	7.086 to 147.26	7.752 to 62.528	8.84 to 147.72
Index ranges	-16 ≤ h ≤ 18, -7 ≤ k ≤ 5, -21 ≤ l ≤ 20	-29 ≤ h ≤ 29, -6 ≤ k ≤ 5, -25 ≤ l ≤ 23	-9 ≤ h ≤ 8, -20 ≤ k ≤ 24, -8 ≤ l ≤ 11
Reflections collected	5201	10782	5632
Independent reflections	2700 [R _{int} = 0.0258, R _{sigma} = 0.0332]	4407 [R _{int} = 0.0353, R _{sigma} = 0.0418]	2888 [R _{int} = 0.0240, R _{sigma} = 0.0321]
Data/restraints/parameters	2700/0/208	4407/2/244	2888/0/217
Goodness-of-fit on F ²	1.028	1.050	0.987
Final R indexes [I ≥ 2σ (I)]	R ₁ = 0.0421, wR ₂ = 0.1028	R ₁ = 0.0666, wR ₂ = 0.1687	R ₁ = 0.0389, wR ₂ = 0.1225
Final R indexes [all data]	R ₁ = 0.0529, wR ₂ = 0.1115	R ₁ = 0.0747, wR ₂ = 0.1765	R ₁ = 0.0480, wR ₂ = 0.1345
Largest diff. peak/hole / e Å ⁻³	0.24/-0.39	0.86/-0.55	

Appendix A: Crystallographic Data

	Complex 3.1	Complex 3.5	Complex 3.6
Empirical formula	C ₃₅ H ₃₀ Cl ₂ N ₅ O ₃ Ru	C ₃₇ H ₃₄ Cl ₂ N ₅ O ₃ Ru	C ₃₇ H ₃₄ Cl ₂ N ₅ O ₃ Ru
Formula weight	740.63	768.66	768.66
Temperature/K	120.01(11)	120.01(10)	119.99(14)
Crystal system	triclinic	monoclinic	triclinic
Space group	P-1	P2 ₁ /c	P-1
a/Å	10.1760(4)	7.64577(15)	11.1744(5)
b/Å	12.4582(5)	16.1343(3)	12.0473(6)
c/Å	13.8175(5)	26.9130(5)	13.6903(6)
α/°	96.766(3)	90	109.099(4)
β/°	92.746(3)	93.8443(16)	92.921(4)
γ/°	114.018(4)	90	95.160(4)
Volume/Å ³	1580.00(11)	3312.49(10)	1728.15(15)
Z	2	4	2
ρ _{calc} /cm ³	1.5567	1.541	1.477
μ/mm ⁻¹	0.711	5.688	5.452
F(000)	752.4	1572.0	786.0
Crystal size/mm ³	0.41 × 0.38 × 0.07	0.14 × 0.08 × 0.04	0.16 × 0.08 × 0.05
Radiation	Mo Kα (λ = 0.71073)	CuKα (λ = 1.54184)	CuKα (λ = 1.54184)
2θ range for data collection/°	2.98 to 62.22	8.568 to 147.544	6.858 to 147.828
Index ranges	-14 ≤ h ≤ 12, -16 ≤ k ≤ 14, -19 ≤ l ≤ 19	-9 ≤ h ≤ 9, -19 ≤ k ≤ 13, -33 ≤ l ≤ 29	-13 ≤ h ≤ 13, -14 ≤ k ≤ 14, -15 ≤ l ≤ 17
Reflections collected	19881	13598	13885
Independent reflections	8794 [R _{int} = 0.0355, R _{sigma} = 0.0612]	6541 [R _{int} = 0.0349, R _{sigma} = 0.0469]	6508 [R _{int} = 0.0508, R _{sigma} = 0.0620]
Data/restraints/parameters	8794/20/508	6541/0/441	6508/0/437
Goodness-of-fit on F ²	1.049	1.044	1.018
Final R indexes [I >= 2σ (I)]	R ₁ = 0.0417, wR ₂ = 0.0741	R ₁ = 0.0379, wR ₂ = 0.0855	R ₁ = 0.0421, wR ₂ = 0.1049
Final R indexes [all data]	R ₁ = 0.0570, wR ₂ = 0.0821	R ₁ = 0.0514, wR ₂ = 0.0926	R ₁ = 0.0513, wR ₂ = 0.1134
Largest diff. peak/hole / e Å ⁻³	0.85/-0.76	0.74/-0.55	1.20/-1.25

Appendix A: Crystallographic Data

	Complex 3.8	Complex 3.9	Complex 3.10
Empirical formula	C ₄₄ H ₄₇ Cl ₂ N ₆ O ₄ Ru	C ₄₁ H ₄₂ Cl ₂ N ₅ O ₃ Ru	C ₃₉ H ₃₈ Cl ₂ N ₅ O ₃ Ru
Formula weight	895.84	824.76	796.71
Temperature/K	120.00(11)	120.2(5)	119.99(10)
Crystal system	triclinic	monoclinic	triclinic
Space group	P-1	P2 ₁ /c	P-1
a/Å	9.2414(8)	14.8410(9)	11.6858(6)
b/Å	10.7415(8)	16.1225(7)	11.8306(6)
c/Å	10.8201(8)	16.1394(8)	13.6476(7)
α/°	95.506(6)	90	96.853(4)
β/°	101.755(7)	104.058(6)	110.928(5)
γ/°	92.436(7)	90	90.664(4)
Volume/Å ³	1044.58(15)	3746.1(3)	1746.73(16)
Z	1	4	2
ρ _{calc} /cm ³	1.424	1.462	1.515
μ/mm ⁻¹	0.553	5.069	0.648
F(000)	463.0	1700.0	818.0
Crystal size/mm ³	0.14 × 0.06 × 0.03	0.64 × 0.04 × 0.02	0.24 × 0.15 × 0.11
Radiation	MoKα (λ = 0.71073)	CuKα (λ = 1.54184)	MoKα (λ = 0.71073)
2θ range for data collection/°	6.528 to 62.512	7.872 to 147.592	3.224 to 62.432
Index ranges	-13 ≤ h ≤ 10, -15 ≤ k ≤ 13, -15 ≤ l ≤ 13	-17 ≤ h ≤ 15, -18 ≤ k ≤ 19, -19 ≤ l ≤ 15	-13 ≤ h ≤ 17, -17 ≤ k ≤ 17, -19 ≤ l ≤ 19
Reflections collected	10768	15691	18984
Independent reflections	5842 [R _{int} = 0.0581, R _{sigma} = 0.1171]	7210 [R _{int} = 0.0674, R _{sigma} = 0.0858]	18984 [R _{int} = ?, R _{sigma} = 0.1545]
Data/restraints/parameters	5842/52/311	7210/0/475	18984/0/456
Goodness-of-fit on F ²	1.141	1.019	1.062
Final R indexes [I ≥ 2σ (I)]	R ₁ = 0.0725, wR ₂ = 0.1197	R ₁ = 0.0635, wR ₂ = 0.1625	R ₁ = 0.0710, wR ₂ = 0.1849
Final R indexes [all data]	R ₁ = 0.0938, wR ₂ = 0.1289	R ₁ = 0.0944, wR ₂ = 0.1854	R ₁ = 0.1273, wR ₂ = 0.1990
Largest diff. peak/hole / e Å ⁻³	0.93/-0.86	2.03/-1.26	3.28/-2.42

Appendix A: Crystallographic Data

	Complex 3.11	Complex 3.12	Complex 3.14
Empirical formula	C ₃₆ H ₃₁ Cl ₂ N ₄ O ₂ Ru	C ₄₁ H ₄₂ Cl ₂ N ₅ O ₃ Ru	C ₃₈ H ₃₅ Cl ₂ N ₄ O ₂ Ru
Formula weight	723.62	824.76	751.67
Temperature/K	150.01(10)	120.2(5)	150.01(10)
Crystal system	monoclinic	monoclinic	monoclinic
Space group	P2 ₁ /c	P2 ₁ /c	P2 ₁ /c
a/Å	11.7085(4)	14.8410(9)	12.6058(4)
b/Å	14.8952(4)	16.1225(7)	14.7133(4)
c/Å	18.3985(6)	16.1394(8)	18.8157(5)
α/°	90	90	90
β/°	100.220(3)	104.058(6)	102.993(3)
γ/°	90	90	90
Volume/Å ³	3157.80(17)	3746.1(3)	3400.46(17)
Z	4	4	4
ρ _{calc} /cm ³	1.522	1.462	1.468
μ/mm ⁻¹	0.706	5.069	0.659
F(000)	1476.0	1700.0	1540.0
Crystal size/mm ³	0.32 × 0.12 × 0.07	0.64 × 0.04 × 0.02	0.41 × 0.24 × 0.05
Radiation	MoKα (λ = 0.71073)	CuKα (λ = 1.54184)	MoKα (λ = 0.71073)
2θ range for data collection/°	4.5 to 62.48	7.872 to 147.592	3.55 to 62.516
Index ranges	-11 ≤ h ≤ 17, -21 ≤ k ≤ 18, -25 ≤ l ≤ 26	-17 ≤ h ≤ 15, -18 ≤ k ≤ 19, -19 ≤ l ≤ 15	-18 ≤ h ≤ 17, -20 ≤ k ≤ 16, -22 ≤ l ≤ 26
Reflections collected	23726	15691	28049
Independent reflections	9095 [R _{int} = 0.0435, R _{sigma} = 0.0674]	7210 [R _{int} = 0.0674, R _{sigma} = 0.0858]	9790 [R _{int} = 0.0462, R _{sigma} = 0.0655]
Data/restraints/parameters	9095/0/408	7210/0/475	9790/0/428
Goodness-of-fit on F ²	1.039	1.019	1.053
Final R indexes [I ≥ 2σ (I)]	R ₁ = 0.0445, wR ₂ = 0.0759	R ₁ = 0.0635, wR ₂ = 0.1625	R ₁ = 0.0447, wR ₂ = 0.0765
Final R indexes [all data]	R ₁ = 0.0654, wR ₂ = 0.0849	R ₁ = 0.0944, wR ₂ = 0.1854	R ₁ = 0.0648, wR ₂ = 0.0871
Largest diff. peak/hole / e Å ⁻³	0.82/-0.5	0.70/-0.6	0.80/-0.82

Appendix A: Crystallographic Data

	Complex 3.15	Complex 3.16	Complex 3.17
Empirical formula	C ₄₈ H ₅₉ Cl ₂ N ₄ O ₄ RuS ₂	C ₄₆ H ₅₃ Cl ₂ N ₆ O ₄ Ru	C _{45.25} H _{51.25} Cl ₂ N _{5.75} O _{3.75} Ru
Formula weight	992.08	925.91	907.64
Temperature/K	150.00(10)	120.00(13)	293(2)
Crystal system	monoclinic	monoclinic	monoclinic
Space group	P2 ₁ /n	P2 ₁	P2 ₁ /n
a/Å	9.4082(4)	9.0540(17)	9.1057(4)
b/Å	14.4854(7)	15.442(7)	29.0066(12)
c/Å	17.6893(9)	16.397(5)	16.7871(13)
α/°	90	90	90
β/°	92.648(4)	95.14(3)	97.926(5)
γ/°	90	90	90
Volume/Å ³	2408.2(2)	2283.4(13)	4391.6(4)
Z	2	2	4
ρ _{calc} /cm ³	1.368	1.347	1.373
μ/mm ⁻¹	0.570	4.240	4.392
F(000)	1034.0	962.0	1884.0
Crystal size/mm ³	0.54 × 0.04 × 0.02	0.19 × 0.09 × 0.04	0.22 × 0.02 × 0.02
Radiation	MoKα (λ = 0.71073)	CuKα (λ = 1.54184)	CuKα (λ = 1.54184)
2θ range for data collection/°	4.61 to 62.208	7.88 to 150.486	8.09 to 147.542
Index ranges	-13 ≤ h ≤ 13, -16 ≤ k ≤ 19, -25 ≤ l ≤ 16	-11 ≤ h ≤ 11, -19 ≤ k ≤ 17, -19 ≤ l ≤ 20	-11 ≤ h ≤ 11, -31 ≤ k ≤ 35, -19 ≤ l ≤ 20
Reflections collected	17439	7513	18123
Independent reflections	6786 [R _{int} = 0.0517, R _{sigma} = 0.0847]	7513 [R _{int} = ?, R _{sigma} = 0.0571]	8643 [R _{int} = 0.0796, R _{sigma} = 0.1153]
Data/restraints/parameters	6786/6/281	7513/506/543	8643/24/546
Goodness-of-fit on F ²	1.037	0.997	1.029
Final R indexes [I >= 2σ (I)]	R ₁ = 0.0659, wR ₂ = 0.1281	R ₁ = 0.0623, wR ₂ = 0.1644	R ₁ = 0.0721, wR ₂ = 0.1642
Final R indexes [all data]	R ₁ = 0.1069, wR ₂ = 0.1471	R ₁ = 0.0870, wR ₂ = 0.1804	R ₁ = 0.1154, wR ₂ = 0.1874
Largest diff. peak/hole / e Å ⁻³	1.15/-1.48	1.02/-0.79	2.25/-2.10

Appendix A: Crystallographic Data

	Complex 3.18	Complex 3.20	Complex 3.23
Empirical formula	C ₄₃ H ₄₆ N ₅ O ₃ Cl ₂ Ru	C ₄₀ H ₃₅ Cl ₂ F ₆ N ₆ O ₄ Ru	C ₃₂ H ₂₁ Cl ₂ F ₂ N ₄ O ₂ Ru
Formula weight	852.82	949.71	703.50
Temperature/K	150.00(10)	120.00(10)	119.99(15)
Crystal system	triclinic	monoclinic	monoclinic
Space group	P-1	Cc	P2 ₁ /c
a/Å	10.1238(7)	16.2080(5)	17.533(5)
b/Å	13.4444(10)	8.0049(3)	8.963(2)
c/Å	15.4499(11)	30.0705(9)	20.614(6)
α/°	107.429(7)	90	90
β/°	96.541(6)	95.556(3)	94.95(3)
γ/°	93.243(6)	90	90
Volume/Å ³	1984.1(3)	3883.1(2)	3227.3(14)
Z	2	4	4
ρ _{calc} /cm ³	1.427	1.624	1.448
μ/mm ⁻¹	0.576	0.622	5.846
F(000)	882.0	1924.0	1412.0
Crystal size/mm ³	0.14 × 0.05 × 0.03	0.26 × 0.11 × 0.05	0.05 × 0.04 × 0.01
Radiation	MoKα (λ = 0.71073)	MoKα (λ = 0.71073)	CuKα (λ = 1.54184)
2θ range for data collection/°	3.53 to 62.18	5.05 to 62.304	8.612 to 179.752
Index ranges	-14 ≤ h ≤ 11, -18 ≤ k ≤ 17, -20 ≤ l ≤ 21	-23 ≤ h ≤ 19, -10 ≤ k ≤ 11, -33 ≤ l ≤ 43	-21 ≤ h ≤ 20, -11 ≤ k ≤ 9, -23 ≤ l ≤ 20
Reflections collected	21885	12737	16704
Independent reflections	11046 [R _{int} = 0.0883, R _{sigma} = 0.2077]	7894 [R _{int} = 0.0371, R _{sigma} = 0.0725]	6454 [R _{int} = 0.1557, R _{sigma} = 0.1831]
Data/restraints/parameters	11046/18/495	7894/161/591	6454/393/364
Goodness-of-fit on F ²	1.018	1.056	0.970
Final R indexes [I ≥ 2σ (I)]	R ₁ = 0.0839, wR ₂ = 0.1191	R ₁ = 0.0571, wR ₂ = 0.1050	R ₁ = 0.1252, wR ₂ = 0.3246
Final R indexes [all data]	R ₁ = 0.1959, wR ₂ = 0.1545	R ₁ = 0.0627, wR ₂ = 0.1084	R ₁ = 0.2393, wR ₂ = 0.4601
Largest diff. peak/hole / e Å ⁻³	0.73/-0.6	1.15/-1.62	1.95/-2.45

Appendix A: Crystallographic Data

	Complex 3.24	Complex 3.25	Complex 3.26
Empirical formula	C ₃₅ H ₂₈ Cl ₂ F ₂ N ₅ O ₃ Ru	C ₃₄ H ₂₇ Cl ₂ F ₂ N ₄ O ₃ RuS	C _{34.2} H _{25.6} Cl ₂ F ₄ N ₄ O _{3.1} RuS _{1.1}
Formula weight	776.59	781.62	825.42
Temperature/K	119.99(13)	119.99(18)	119.99(10)
Crystal system	triclinic	monoclinic	monoclinic
Space group	P-1	P2 ₁ /c	P2 ₁ /c
a/Å	10.6955(13)	15.2765(4)	11.2585(5)
b/Å	12.6800(11)	8.4816(2)	20.5455(9)
c/Å	12.9715(11)	24.0986(7)	14.5593(7)
α/°	74.676(7)	90	90
β/°	82.485(8)	95.691(3)	101.760(4)
γ/°	70.882(9)	90	90
Volume/Å ³	1601.2(3)	3107.05(15)	3297.0(3)
Z	2	4	4
ρ _{calc} /cm ³	1.611	1.671	1.663
μ/mm ⁻¹	5.985	6.775	0.773
F(000)	786.0	1580.0	1661.0
Crystal size/mm ³	0.16 × 0.11 × 0.03	0.22 × 0.02 × 0.02	0.14 × 0.11 × 0.07
Radiation	CuKα (λ = 1.54184)	CuKα (λ = 1.54184)	MoKα (λ = 0.71073)
2θ range for data collection/°	7.074 to 148.528	7.374 to 146.686	6.454 to 62.602
Index ranges	-13 ≤ h ≤ 13, -15 ≤ k ≤ 15, -15 ≤ l ≤ 16	-19 ≤ h ≤ 18, -8 ≤ k ≤ 10, -29 ≤ l ≤ 26	-15 ≤ h ≤ 16, -29 ≤ k ≤ 27, -21 ≤ l ≤ 17
Reflections collected	9863	11777	22418
Independent reflections	9863 [R _{int} = ?, R _{sigma} = 0.0856]	6076 [R _{int} = 0.0383, R _{sigma} = 0.0543]	9286 [R _{int} = 0.0520, R _{sigma} = 0.0867]
Data/restraints/parameters	9863/0/436	6076/0/426	9286/38/499
Goodness-of-fit on F ²	0.937	1.034	1.038
Final R indexes [I >= 2σ (I)]	R ₁ = 0.0542, wR ₂ = 0.1282	R ₁ = 0.0403, wR ₂ = 0.0912	R ₁ = 0.0647, wR ₂ = 0.1206
Final R indexes [all data]	R ₁ = 0.0798, wR ₂ = 0.1351	R ₁ = 0.0553, wR ₂ = 0.0982	R ₁ = 0.0987, wR ₂ = 0.1358
Largest diff. peak/hole / e Å ⁻³	1.44/-1.11	1.16/-0.59	2.39/-0.79

Appendix A: Crystallographic Data

	Complex 3.27	Complex 3.28	Complex 3.29
Empirical formula	C ₃₄ H ₂₅ Cl ₂ F ₄ N ₄ O ₃ RuS	C ₃₅ H ₂₈ Cl ₄ N ₅ O ₃ Ru	C ₃₅ H ₂₈ Cl ₄ N ₅ O ₃ Ru
Formula weight	817.61	809.49	809.49
Temperature/K	120.03(18)	119.97(12)	119.99(12)
Crystal system	monoclinic	monoclinic	triclinic
Space group	P2 ₁ /c	C2/c	P-1
a/Å	17.2650(12)	17.6902(9)	10.5921(13)
b/Å	8.9406(5)	14.3662(5)	12.522(3)
c/Å	21.0198(14)	26.9972(10)	14.2189(17)
α/°	90	90	96.967(14)
β/°	97.820(6)	98.080(4)	96.459(10)
γ/°	90	90	114.707(17)
Volume/Å ³	3214.5(4)	6793.0(5)	1672.5(5)
Z	4	8	2
ρ _{calc} /cm ³	1.689	1.583	1.607
μ/mm ⁻¹	6.672	0.821	0.833
F(000)	1644.0	3272.0	818.0
Crystal size/mm ³	0.09 × 0.04 × 0.02	0.25 × 0.07 × 0.04	0.17 × 0.12 × 0.04
Radiation	CuKα (λ = 1.54184)	MoKα (λ = 0.71073)	MoKα (λ = 0.71073)
2θ range for data collection/°	8.492 to 147.492	3.844 to 62.502	6.622 to 56.56
Index ranges	-12 ≤ h ≤ 19, -10 ≤ k ≤ 9, -26 ≤ l ≤ 23	-17 ≤ h ≤ 24, -19 ≤ k ≤ 19, -39 ≤ l ≤ 27	-14 ≤ h ≤ 9, -15 ≤ k ≤ 16, -17 ≤ l ≤ 18
Reflections collected	13021	21722	8713
Independent reflections	6142 [R _{int} = 0.0804, R _{sigma} = 0.1108]	9596 [R _{int} = 0.0401, R _{sigma} = 0.0706]	8713 [R _{int} = ?, R _{sigma} = 0.1606]
Data/restraints/parameters	6142/0/444	9596/8/424	8713/404/433
Goodness-of-fit on F ²	1.032	1.049	1.099
Final R indexes [I ≥ 2σ (I)]	R ₁ = 0.0643, wR ₂ = 0.1322	R ₁ = 0.0560, wR ₂ = 0.1152	R ₁ = 0.1142, wR ₂ = 0.2653
Final R indexes [all data]	R ₁ = 0.1143, wR ₂ = 0.1574	R ₁ = 0.0772, wR ₂ = 0.1253	R ₁ = 0.1711, wR ₂ = 0.2865
Largest diff. peak/hole / e Å ⁻³	1.31/-0.89	1.80/-1.27	4.69/-1.95

Appendix A: Crystallographic Data

	Complex 3.30	Complex 3.32	Complex 3.33
Empirical formula	C ₃₅ H _{28.46} Cl ₄ N ₅ O _{3.23} Ru	C ₃₆ H ₃₃ Cl ₆ N ₄ O ₅ RuS ₂	C ₃₅ H ₂₈ Br ₂ Cl ₂ N ₅ O ₃ Ru
Formula weight	813.64	979.55	898.41
Temperature/K	120.6(10)	150.01(10)	120.00(10)
Crystal system	monoclinic	triclinic	monoclinic
Space group	P2 ₁ /n	P-1	C2/c
a/Å	11.4785(4)	12.1609(6)	17.6359(12)
b/Å	20.0177(7)	12.5357(6)	14.4253(7)
c/Å	15.2958(6)	15.0309(7)	27.0013(15)
α/°	90	74.193(4)	90
β/°	108.228(4)	78.058(4)	98.201(6)
γ/°	90	66.041(5)	90
Volume/Å ³	3338.2(2)	2002.67(17)	6798.9(7)
Z	4	2	8
ρ _{calc} /cm ³	1.619	1.624	1.755
μ/mm ⁻¹	0.836	0.943	3.014
F(000)	1645.0	990.0	3560.0
Crystal size/mm ³	0.12 × 0.06 × 0.04	0.24 × 0.21 × 0.11	0.29 × 0.15 × 0.12
Radiation	MoKα (λ = 0.71073)	MoKα (λ = 0.71073)	MoKα (λ = 0.71073)
2θ range for data collection/°	5.702 to 62.29	3.636 to 62.464	3.838 to 62.608
Index ranges	-16 ≤ h ≤ 12, -28 ≤ k ≤ 24, -21 ≤ l ≤ 20	-17 ≤ h ≤ 17, -17 ≤ k ≤ 18, -20 ≤ l ≤ 20	-24 ≤ h ≤ 16, -19 ≤ k ≤ 19, -39 ≤ l ≤ 32
Reflections collected	22990	25048	21096
Independent reflections	9366 [R _{int} = 0.0425, R _{sigma} = 0.0654]	11372 [R _{int} = 0.0451, R _{sigma} = 0.0830]	9571 [R _{int} = 0.0393, R _{sigma} = 0.0730]
Data/restraints/parameters	9366/24/442	11372/6/488	9571/9/424
Goodness-of-fit on F ²	1.035	1.045	1.044
Final R indexes [I >= 2σ (I)]	R ₁ = 0.0448, wR ₂ = 0.0784	R ₁ = 0.0523, wR ₂ = 0.1034	R ₁ = 0.0527, wR ₂ = 0.1025
Final R indexes [all data]	R ₁ = 0.0686, wR ₂ = 0.0879	R ₁ = 0.0795, wR ₂ = 0.1219	R ₁ = 0.0783, wR ₂ = 0.1135
Largest diff. peak/hole / e Å ⁻³	C ₃₅ H _{28.46} Cl ₄ N ₅ O _{3.23} Ru	1.37/-0.98	1.26/-1.23

Appendix A: Crystallographic Data

	Complex 3.34	Complex 3.35	Complex 3.38
Empirical formula	C ₃₄ H ₂₇ Br ₂ Cl ₂ N ₄ O ₃ RuS	C ₃₂ H ₂₁ Br ₂ Cl ₂ N ₄ O ₂ Ru	C ₃₅ H ₂₈ Cl ₂ I ₂ N ₅ O ₃ Ru
Formula weight	903.44	825.32	992.39
Temperature/K	119.99(13)	119.99(10)	119.99(12)
Crystal system	triclinic	monoclinic	monoclinic
Space group	P-1	P2 ₁ /c	C2/c
a/Å	8.6512(8)	11.2747(3)	17.7257(6)
b/Å	13.224(2)	14.8929(4)	14.6461(5)
c/Å	15.4719(15)	18.4091(5)	26.9124(9)
α/°	86.475(11)	90	90
β/°	73.856(9)	98.469(3)	98.602(3)
γ/°	81.339(11)	90	90
Volume/Å ³	1680.5(4)	3057.42(16)	6908.2(4)
Z	2	4	8
ρ _{calc} /cm ³	1.785	1.793	1.908
μ/mm ⁻¹	8.953	3.339	2.440
F(000)	894.0	1620.0	3848.0
Crystal size/mm ³	0.38 × 0.04 × 0.01	0.44 × 0.17 × 0.11	0.15 × 0.08 × 0.06
Radiation	CuKα (λ = 1.54184)	MoKα (λ = 0.71073)	MoKα (λ = 0.71073)
2θ range for data collection/°	6.762 to 125.054	3.532 to 62.09	3.624 to 62.37
Index ranges	-6 ≤ h ≤ 9, -15 ≤ k ≤ 15, -15 ≤ l ≤ 17	-16 ≤ h ≤ 15, -20 ≤ k ≤ 20, -26 ≤ l ≤ 18	-25 ≤ h ≤ 15, -19 ≤ k ≤ 21, -39 ≤ l ≤ 38
Reflections collected	5231	19208	22534
Independent reflections	5231 [R _{int} = ?, R _{sigma} = 0.0696]	8547 [R _{int} = 0.0345, R _{sigma} = 0.0573]	9863 [R _{int} = 0.0530, R _{sigma} = 0.0864]
Data/restraints/parameters	5231/424/448	8547/0/388	9863/83/428
Goodness-of-fit on F ²	0.980	1.028	1.077
Final R indexes [I ≥ 2σ (I)]	R ₁ = 0.0882, wR ₂ = 0.2294	R ₁ = 0.0376, wR ₂ = 0.0668	R ₁ = 0.0555, wR ₂ = 0.0956
Final R indexes [all data]	R ₁ = 0.1313, wR ₂ = 0.2524	R ₁ = 0.0542, wR ₂ = 0.0720	R ₁ = 0.0811, wR ₂ = 0.1071
Largest diff. peak/hole / e Å ⁻³	2.04/-1.17	0.81/-1.00	1.87/-1.86

Appendix A: Crystallographic Data

	Complex 3.39	Complex 3.40
Empirical formula	C ₃₅ H ₂₈ Cl ₂ I ₂ N ₅ O ₃ Ru	C ₃₂ H ₂₁ Cl ₂ I ₂ N ₄ O ₂ Ru
Formula weight	992.39	919.30
Temperature/K	120.0(2)	120.00(10)
Crystal system	monoclinic	monoclinic
Space group	P2 ₁ /c	P2 ₁ /c
a/Å	15.5339(2)	11.6666(3)
b/Å	8.55457(16)	14.8626(3)
c/Å	26.3905(4)	18.4099(6)
α/°	90	90
β/°	100.9518(14)	100.928(3)
γ/°	90	90
Volume/Å ³	3443.06(10)	3134.33(15)
Z	4	4
ρ _{calc} /cm ³	1.914	1.948
μ/mm ⁻¹	19.555	2.678
F(000)	1924.0	1764.0
Crystal size/mm ³	0.18 × 0.03 × 0.02	0.34 × 0.12 × 0.09
Radiation	CuKα (λ = 1.54184)	MoKα (λ = 0.71073)
2θ range for data collection/°	8.072 to 147.534	6.824 to 62.586
Index ranges	-19 ≤ h ≤ 14, -10 ≤ k ≤ 10, -22 ≤ l ≤ 31	-16 ≤ h ≤ 16, -21 ≤ k ≤ 21, -21 ≤ l ≤ 26
Reflections collected	14299	24810
Independent reflections	6741 [R _{int} = 0.0456, R _{sigma} = 0.0591]	8989 [R _{int} = 0.0433, R _{sigma} = 0.0593]
Data/restraints/parameters	6741/0/435	8989/0/388
Goodness-of-fit on F ²	1.022	1.044
Final R indexes [I >= 2σ (I)]	R ₁ = 0.0393, wR ₂ = 0.0916	R ₁ = 0.0383, wR ₂ = 0.0678
Final R indexes [all data]	R ₁ = 0.0517, wR ₂ = 0.0977	R ₁ = 0.0555, wR ₂ = 0.0762
Largest diff. peak/hole / e Å ⁻³	1.11/-1.02	1.20/-1.01

